MARINE MICROORGANISMS AND THEIR ENZYMES WITH BIOTECHNOLOGICAL APPLICATION

EDITED BY: Haijin Mou, Xiaoke Hu, Francesco Secundo and Benwei Zhu
PUBLISHED IN: Frontiers in Microbiology

frontiers Research Topics

ISSN 1664-8714
ISBN 978-2-88976-115-9
DOI 10.3389/978-2-88976-115-9

About Frontiers

Frontiers is more than just an open-access publisher of scholarly articles: it is a pioneering approach to the world of academia, radically improving the way scholarly research is managed. The grand vision of Frontiers is a world where all people have an equal opportunity to seek, share and generate knowledge. Frontiers provides immediate and permanent online open access to all its publications, but this alone is not enough to realize our grand goals.

Frontiers Journal Series

The Frontiers Journal Series is a multi-tier and interdisciplinary set of open-access, online journals, promising a paradigm shift from the current review, selection and dissemination processes in academic publishing. All Frontiers journals are driven by researchers for researchers; therefore, they constitute a service to the scholarly community. At the same time, the Frontiers Journal Series operates on a revolutionary invention, the tiered publishing system, initially addressing specific communities of scholars, and gradually climbing up to broader public understanding, thus serving the interests of the lay society, too.

Dedication to Quality

Each Frontiers article is a landmark of the highest quality, thanks to genuinely collaborative interactions between authors and review editors, who include some of the world's best academicians. Research must be certified by peers before entering a stream of knowledge that may eventually reach the public - and shape society; therefore, Frontiers only applies the most rigorous and unbiased reviews.
Frontiers revolutionizes research publishing by freely delivering the most outstanding research, evaluated with no bias from both the academic and social point of view. By applying the most advanced information technologies, Frontiers is catapulting scholarly publishing into a new generation.

What are Frontiers Research Topics?

Frontiers Research Topics are very popular trademarks of the Frontiers Journals Series: they are collections of at least ten articles, all centered on a particular subject. With their unique mix of varied contributions from Original Research to Review Articles, Frontiers Research Topics unify the most influential researchers, the latest key findings and historical advances in a hot research area! Find out more on how to host your own Frontiers Research Topic or contribute to one as an author by contacting the Frontiers Editorial Office: frontiersin.org/about/contact

MARINE MICROORGANISMS AND THEIR ENZYMES WITH BIOTECHNOLOGICAL APPLICATION

Topic Editors:
Haijin Mou, Ocean University of China, China
Xiaoke Hu, Yantai Institute of Coastal Zone Research, Chinese Academy of Sciences (CAS), China
Francesco Secundo, National Research Council (CNR), Italy
Benwei Zhu, Nanjing Tech University, China

Citation: Mou, H., Hu, X., Secundo, F., Zhu, B., eds. (2022). Marine Microorganisms and Their Enzymes With Biotechnological Application. Lausanne: Frontiers Media SA. doi: 10.3389/978-2-88976-115-9

Table of Contents

frontiers | Frontiers in Microbiology

EDITORIAL
published: 18 April 2022
doi: 10.3389/fmicb.2022.901161

Editorial: Marine Microorganisms and Their Enzymes With Biotechnological Application

Haijin Mou[1]*, *Francesco Secundo*[2], *Xiaoke Hu*[3] and *Benwei Zhu*[4]

[1] College of Food Science and Engineering, Ocean University of China, Qingdao, China, [2] Istituto di Scienze e Tecnologie Chimiche "Giulio Natta", CNR, Milan, Italy, [3] Yantai Institute of Coastal Zone Research, Chinese Academy of Sciences (CAS), Yantai, China, [4] College of Food Science and Light Industry, Nanjing Tech University, Nanjing, China

Keywords: marine microorganism, enzymes, biotechnological application, heterologous expression, coding gene

Editorial on the Research Topic

Marine Microorganisms and Their Enzymes With Biotechnological Application

The understanding and exploration of marine microbial resources is a new area with enormous potentialities in numerous fields of research and application. Due to the extreme and fluctuating salinity, pressure, and temperature of the marine environment, marine microorganisms are forced to develop unique metabolic pathways to adapt to this environment, producing enzymes that show different properties compared to the analogous ones obtained from terrestrial sites. Besides, being an important source of new active substances, and thanks to the disclosure of the particular the genome of marine microorganisms, as well as to the application of marine microbial engineering and enzyme engineering technologies, marine microorganisms and their enzymes show important development prospects in the agri-food industry, medicine, and other biotechnological fields. At present, the research on microbial physiology and metabolism under extreme marine conditions has made remarkable progress, and the application of this knowledge has also been applied for the restoration of the marine environment.

This Research Topic, which includes 11 original research articles and a review article, focuses on the discovery, properties, physiological characteristics, and industrial applications of new and valuable marine microbial enzymes.

Five articles focus on marine microbial hydrolases with potential application value in the preparation of functional oligosaccharides. Cao et al. described the properties of βκ-carrageenase for the degradation of hybrid carrageenan–furcellaran. Oligosaccharides from carrageenan—a group of important food carbohydrates with high sulfate content—have attracted extensive attention for their possible physiological functions. This work cloned and expressed a novel furcellaran-hydrolyzing enzyme from the marine bacterium *Wenyingzhuangia fucanilytica*. Considering the structural heterogeneity of carrageenan, this new enzyme was named as "βκ-carrageenase" instead of "furcellaranase." Liang et al. designed a consensus sequence design strategy to improve the catalytic ability of a thermostable and acidophilic β-mannanase. Based on the amino acid sequence consistency analysis compared with the reported mannanase, the authors constructed several mutants that showed 303.0, 280.4, and 210.1% increased k_{cat}/K_m and proved that this approach is an effective way to improve the performance of marine enzyme preparations. Ding et al. expressed an amylase from the marine bacterium *Saccharophagus degradans*. The recombinant enzyme can produce maltooligosaccharides with high specificity, providing a promising tool for the preparation of nutritional factors. It is worth noting that this enzyme also shows excellent cold adaptation and salt tolerance, a particularity typically observed for marine-derived enzymes. Zhou et al. characterized a new β-galactosidase from the marine

OPEN ACCESS

Edited and reviewed by:
Eric Altermann,
AgResearch Ltd, New Zealand

***Correspondence:**
Haijin Mou
mousun@ouc.edu.cn

Specialty section:
This article was submitted to Microbiotechnology, a section of the journal Frontiers in Microbiology

Received: *21 March 2022*
Accepted: *31 March 2022*
Published: *18 April 2022*

Citation:
Mou H, Secundo F, Hu X and Zhu B (2022) Editorial: Marine Microorganisms and Their Enzymes With Biotechnological Application. Front. Microbiol. 13:901161. doi: 10.3389/fmicb.2022.901161

bacterium *Bacillus* sp. BY02. The enzymatic properties show that the "Cys-Zn" motif plays an important role in the structural stability and catalytic function. Furthermore, Gal42 shows effective lactose hydrolysis activity, which makes it a potential candidate in food technology. Wang J. et al. characterized an efficient chitosanase from *Bacillus mojavensis*, which is suitable for the preparation of chitosan oligosaccharides. A high-efficiency recombinant chitosanase was obtained through homologous expression in *Pichia pastoris* X33. After 15 min of reaction, the total yield of chitosan oligosaccharides reached 92.3%, which was higher than the efficiency of most chitosanases previously reported.

In addition to enzymatic hydrolysis to produce marine characteristic carbohydrates, microbial fermentation is also considered to be a promising bioengineering technology. When extracting chitin from shrimp and crab shells, the first step is usually to remove protein and minerals. Although the widely used acid and alkali treatment method is effective, it has brought more serious environmental pollution problems. Therefore, many conventional technologies have turned to bioengineering technologies, such as the application of microbial fermentation. Xie et al. investigated the successive two-step fermentation to extract chitin from shrimp shells. Deproteination and demineralization can be effectively realized by the fermentation of a protease-producing strain, *Exiguobacterium profundum*, and a lactic acid-producing strain, *Lactobacillus acidophilus*. This work provides an environmentally friendly strategy for the industrial extraction of chitin.

Two articles focus on marine microbial lyases, including alginate lyase and hyaluronate lyases. Because many marine polysaccharides have a uronic acid scaffold, by lyases (common in marine microorganisms) it is possible to degrade them through a β-elimination mechanism, generating unsaturated disaccharides with a C_4-C_5 double bond at the non-reducing end. Wang X. et al. investigated two hyaluronate lyases from a marine bacterium *Vibrio alginolyticus* LWW-9 and proposed a model for the complete degradation of hyaluronic acid. Liu et al. expressed in *Yarrowia lipolytica* an alkaline alginate lyase that performs unique heat recovery. The enzyme mainly produces DP1–DP2 oligosaccharides, making it a potential candidate enzyme for monosaccharide and disaccharide industrial production.

One article focuses on the heterologous expression of cyclodextrin glycosyltransferase and its application in the transformation of 2-O-α-D-glucopyranosyl-L-ascorbic acid (AA-2G). Song et al. reached the maximal AA-2G yield of 28 g/L, which is particularly interesting for the industrial production of AA-2G.

Three articles are about marine ecological microorganisms and environmental bioremediation. Meyer-Cifuentes and Öztürk reported a marine mesophilic MHETase-like enzyme, which can hydrolyze polyethylene terephthalate and its intermediate degradation product, mono-2-hydroxyethyl terephthalate, to monomers. This study is of certain significance to eliminate the threat of plastics in the marine environment. In addition, Wang Y. et al. reported a mini-review to introduce the research advances in 2-haloacid dehalogenases. Changfei et al. found that the restoration of *Suaeda salsa* in coastal wetland increased bacterial taxa with the ability to degrade symbionts and aromatic compounds, which was helpful to improve the bioremediation role.

The research results collected on this Research Topic are not exhaustive. At present, marine microorganisms are considered as a novel source of new enzymes because of their genetic and biochemical diversity. Marine microorganisms produce physiological mechanisms to adapt to marine extreme environments such as cold and/or salt tolerance, surviving in harsh conditions. Compared with terrestrial homologs, marine microbial enzymes have unique structural characteristics, which show high flexibility, solubility and substrate binding ability. With the help of whole genome technology, gene recombination, rational design and synthetic microbiology, the research of marine microorganisms and enzymes is developing rapidly. A variety of enzymes with peculiar properties have been isolated from marine bacteria, actinomycetes, fungi and even bacteriophages, some of which have achieved heterologous expression and industrial application. Marine microorganisms and their enzymes will be expected to generate great industrial value, with an important impact on human life in the future.

AUTHOR CONTRIBUTIONS

All authors listed have made a substantial, direct, and intellectual contribution to the work and approved it for publication.

ACKNOWLEDGMENTS

We would like to thank all authors and reviewers who have contributed to this Research Topic.

Conflict of Interest: The authors declare that the research was conducted in the absence of any commercial or financial relationships that could be construed as a potential conflict of interest.

Publisher's Note: All claims expressed in this article are solely those of the authors and do not necessarily represent those of their affiliated organizations, or those of the publisher, the editors and the reviewers. Any product that may be evaluated in this article, or claim that may be made by its manufacturer, is not guaranteed or endorsed by the publisher.

frontiers in Microbiology

ORIGINAL RESEARCH
published: 28 May 2021
doi: 10.3389/fmicb.2021.664339

Heterologous Expression of Cyclodextrin Glycosyltransferase *my*20 in *Escherichia coli* and Its Application in 2-*O*-α-D-Glucopyranosyl-L-Ascorbic Acid Production

Kai Song[1], *Jingjing Sun*[2,3,4], *Wei Wang*[2,3,4] *and Jianhua Hao*[2,3,4]*

[1] College of Food Sciences and Technology, Shanghai Ocean University, Shanghai, China, [2] Key Laboratory of Sustainable Development of Polar Fishery, Ministry of Agriculture and Rural Affairs, Yellow Sea Fisheries Research Institute, Chinese Academy of Fishery Sciences, Qingdao, China, [3] Laboratory for Marine Drugs and Bioproducts, Qingdao National Laboratory for Marine Science and Technology, Qingdao, China, [4] Jiangsu Collaborative Innovation Center for Exploitation and Utilization of Marine Biological Resource, Lianyungang, China

OPEN ACCESS

Edited by:
Haijin Mou,
Ocean University of China, China

Reviewed by:
Jingwen Zhou,
Jiangnan University, China
Jianguo Zhang,
University of Shanghai for Science and Technology, China

***Correspondence:**
Jianhua Hao
haojh@ysfri.ac.cn

Specialty section:
This article was submitted to Microbiotechnology, a section of the journal Frontiers in Microbiology

Received: 05 February 2021
Accepted: 12 April 2021
Published: 28 May 2021

Citation:
Song K, Sun J, Wang W and Hao J (2021) Heterologous Expression of Cyclodextrin Glycosyltransferase my20 in Escherichia coli and Its Application in 2-O-α-d-Glucopyranosyl-L-Ascorbic Acid Production. Front. Microbiol. 12:664339. doi: 10.3389/fmicb.2021.664339

In this study, the cgt gene *my*20, which encodes cyclodextrin glycosyltransferase (CGTase) and was obtained by the metagenome sequencing of marine microorganisms from the Mariana Trench, was codon optimized and connected to pET-24a for heterologous expression in *Escherichia coli* BL21(DE3). Through shaking flask fermentation, the optimized condition for recombinant CGTase expression was identified as 20°C for 18 h with 0.4 mM of isopropyl β-D-L-thiogalactopyranoside. The recombinant CGTase was purified by Ni^{2+}-NTA resin, and the optimum pH and temperature were identified as pH 7 and 80°C, respectively. Activity was stable over wide temperature and pH ranges. After purification by Ni^{2+}-NTA resin, the specific activity of the CGTase was 63.3 U/mg after 67.3-fold purification, with a final yield of 43.7%. In addition, the enzyme was used to transform L-ascorbic acid into 2-*O*-α-D-glucopyranosyl-L-ascorbic acid (AA-2G). The maximal AA-2G production reached 28 g/L, at 40°C, pH 4, 24 h reaction time, 50 g/L donor concentration, and 50 U/g enzyme dosage. The superior properties of recombinant CGTase strongly facilitate the industrial production of AA-2G.

Keywords: 2-*O*-α-D-glucopyranosyl-L-ascorbic acid, cyclodextrin glucosyltransferase, *E. coli*, heterologous expression, l-ascorbic acid

INTRODUCTION

Cyclodextrin glycosyltransferase (CGTase), also called 4-α-D-(1,4-α-D-glucanol)-transferase (EC 2.4.1.19), is a member of the α-amylase family (glycosyl hydrolase family 13) (Han et al., 2014). As a multifunctional enzyme, CGTase catalyzes four types of reactions, including hydrolysis reaction and three types of transglycosylation reactions (i.e., disproportionation, cyclization, and coupling). The cyclization reaction, which is the characteristic reaction of CGTase, is used to produce

cyclodextrins. α-CD, β-CD, and γ-CD are the major structures of cyclodextrins (CD) (Leemhuis et al., 2010; Tao et al., 2020). Disproportionation and coupling reactions format glycosylated derivatives by transferring maltooligosaccharides to a variety of receptors (Fenelon et al., 2015). CGTase can produce high value-added products, such as CD and 2-*O*-α-D-glucopyranosyl-L-ascorbic acid (AA-2G). Thus, an increasing number of researchers focus on CGTase, and its demand is gradually increasing.

L-Ascorbic acid (L-AA, i.e., vitamin C) is an essential nutrient for the human body, and plays an important role in antibody and collagen syntheses, scurvy treatment, protein synthesis, and skin whitening; consequently, it has a wide application in the food, cosmetic, and pharmaceutical industries (Naidu, 2003; Han et al., 2012). However, the C2 hydroxyl group of L-AA is extremely unstable and oxidizes easily, especially in aqueous solution, thus limiting its application potential. In recent years, researchers have applied biological and chemical methods to produce a variety of L-AA derivatives that achieve better oxidation stability. Among a variety of derivatives, which include ascorbyl glucoside and ascorbyl phosphate (Mima et al., 1970; Tai et al., 2017), AA-2G has drawn enormous interest from researchers, because of its superior properties, excellent oxidation resistance, and its simple transformability to D-glucose and L-AA by α-glucosidase (Yamamoto et al., 1990). Thus, AA-2G has potential applications in the food, cosmetics, and husbandry industries. AA-2G can also enhance human immunity, as well as prevent and treat the common cold.

At present, the major method for producing AA-2G is enzymatic transglycosylation catalysis *via* several different glucosyltransferases, i.e., α-glucosidase, α-amylase, α-isomaltosyl glucosaccharide-forming enzyme, sucrose phosphatase, and CGTase (Aga et al., 1991; Bae et al., 2002; Gudiminchi and Nidetzky, 2017; Li et al., 2017). Toyoda also used the method of chemical synthesis to produce AA-2G, but the results identified the synthesis process as complicated and associated with high cost; thus, making enzymatic production unattractive (Toyoda et al., 2004). Because of the higher substrate specificity and production, CGTase is generally assumed as the most effective enzyme for AA-2G production (Jun et al., 2001). In the process of CGTase biotransformation of AA-2G by intermolecular transglycosylation, CGTase catalyzes the transfer of a glucose residue from a glucosyl donor to the C2 hydroxyl group of L-AA. Therefore, an α-configured glucoside is needed as the donor substrate in the process of enzyme reaction. Various starch-derived oligosaccharides can be used as glucosyl donor, such as cyclodextrin, starch, and maltodextrin. Currently, a number of researchers attempt to find an economic and affine glycosyl donor to synthesize AA-2G. For instance, Aga et al. (1991) used α-CD as donor and found that the conversion rate of L-AA can reach 40%; 154.8 g/L AA-2G was obtained. However, because of its high cost, α-CD is unsuitable for production of AA-2G. Therefore, Zhang et al. (2011) used β-CD as donor and achieved a AA-2G yield of 13.5 g/L. Liu et al. (2013) used maltose as donor and achieved a AA-2G yield of 1.12 g/L at optimal conditions.

Although natural CGTase is suitable for AA-2G synthesis, the conversion rates are low. To improve the conversion rate, this study applied site-directed mutagenesis to alter the glucosyl donor-binding sites of CGTases (Chen et al., 2017; Tao et al., 2019), including +1 subsite, +2 subsite, and −3 subsite. For example, Han et al. (2013) used maltose as donor and obtained higher AA-2G yield by mutant K47L, which was 64% higher than that of wild-type CGTase. In the present work, the novel recombinant CGTase MY20 was characterized and its ability to synthesize AA-2G was studied. This enzyme offers great advantages with regard to thermal stability and pH stability, which will be of great significance for the industrial production of AA-2G.

MATERIALS AND METHODS

Materials

my20 gene (GenBank accession no. MW561626) originated from the metagenome sequencing of marine microorganisms in the Mariana Trench. The gene *my20* was codon optimized, synthesized, and cloned into pET-24a(+) by Genewiz (Wuhan, China). *Escherichia coli* BL21(DE3) was used for heterologous expression. Luria–Bertani (LB) medium was used to cultivate *E. coli* strains. AA-2G was obtained from DB (Shanghai, China). Ni^{2+}-NTA HP resin was purchased from General Electric Company (United States). Other reagents were obtained from Shanghai Sinopharm Co., Ltd. (Shanghai, China).

Expression of the Recombinant CGTase

The recombinant plasmid was transformed into *E. coli* BL21(DE3) to express the protein. DNA sequencing (Sangon Biotech, Shanghai, China) confirmed that the target gene was inserted into the plasmid. The recombinant expression strain was inoculated into 5 ml LB medium with the appropriate concentration of kanamycin (37°C, 200 r/min, overnight). This seed solution was inoculated into 50 ml LB medium until the OD_{600} reached 0.6–0.8. Then, 0.2 mM of isopropyl β-D-L-thiogalactopyranoside (IPTG) was added to induce expression at 25°C and 200 r/min. The bacterial cells were obtained by centrifugation at 8,000 r/min at 4°C for 10 min and were resuspended in 20 mM PBS (pH 7.0). The cells were ultrasonically destroyed in an ice bath for 20 min. The cell disruption solution was centrifuged at 8,000 r/min at 4°C for 20 min, and the crude protein solution was obtained as the supernatant. In addition, to increase the expression of CGTase, with all of the above conditions unchanged, the IPTG concentration, induction time, and induction temperature were optimized to acquire high-level strains.

Purification and SDS-PAGE

The recombinant CGTase was purified by Ni^{2+}-NTA resin column. After loading into the column, the crude protein was washed with 20 mM phosphate-buffered saline (PBS; pH 7) and then, imidazole (0–500 mM) in 20 mM PBS (pH 7) was used to elute the target protein. The obtained protein was dialyzed overnight in 20 mM PBS solution to remove imidazole. Sodium dodecyl sulfatepolyacrylamide gel electrophoresis (SDS-PAGE, 12% gel) was used to analyze the purified recombinant protein.

Cyclodextrin Glycosyltransferase Activity Assay

The methyl orange method was used to determine the CGTase activity (Sun et al., 2015). A total of 900 μl of 4% soluble starch solution dissolved in Gly-NaOH was added to the reaction vessel, and 100 μl of enzyme solution was added to react accurately at 50°C for 10 min. Then, after the reaction was terminated with 1% HCl, 4 ml of methyl orange solution (diluted fourfold) was added. The reaction solution was kept at room temperature for 20 min, and the production of cyclodextrin was estimated at an absorbance of 502 nm. One unit of activity was defined as the amount of enzyme converting 1 μmol of cyclodextrin per min.

Biochemical Properties of the Purified Recombinant CGTase

The optimal temperature of the recombinant enzyme was determined to be 10–100°C for 10 min. The thermal stability of recombinant CGTase was measured by placing it at different temperatures (10–90°C) for 2 h, and then, the enzyme activity was determined at 80°C. The optimum activities of recombinant CGTase were set to 100%.

The optimal pH of recombinant activity was determined at 80°C for 10 min with the following buffers: NaAc–HAc buffer (pH 3–6), Na_2HPO_4–NaH_2PO_4 buffer (pH 6–8), Gly-NaOH buffer (pH 8–10), and Na_2HPO_4–NaOH (pH 10–11). To assess the pH stability, both enzyme and buffer were diluted (pH 3–11) in a proper proportion at 4°C for 12 h, and then, the enzyme activity was determined at 80°C and pH 7.

The effects of metal ions and chemical reagents on the recombinant CGTase were determined. To determine their remaining activity, the recombinant CGTase was incubated with Fe^{2+}, K^+, Ca^{2+}, Mn^{2+}, Ba^{2+}, Cu^{2+}, Mg^{2+}, Li^+, and EDTA at a final concentration of 5 mM for 2 h. The activity without metal ions and chemical reagents was used as control (100%).

Synthesis of AA-2G

The enzymatic synthesis of AA-2G followed the method described in Tao et al. (2018). Briefly, 0.5 g L-AA and β-CD were accurately weighed and dissolved into 5 ml water. Ten percent NaOH was added to adjust the pH to 5, and then, the recombinant enzyme solution was purified (enzyme solution was added according to the content of cyclodextrin) to generate AA-2G. Then, 10 g/L Na_2SO_3 was added to control oxygen. Finally, distilled water was added to 10 ml. With the above conditions unchanged (40°C and pH 5), various substrate types (α-CD, β-CD, γ-CD, and soluble starch), pH levels (3, 4, 5, 6, 7, and 8), temperatures (20, 30, 40, 50, and 60°C), enzyme concentrations (25, 50, 75, 100, and 125 U/g β-CD), donor concentrations (20, 30, 40, 50, and 60 g/L), and reaction times (6, 12, 18, 24, and 30 h) were tested to identify the optimal conditions for increasing the production of AA-2G.

An Agilent 1260 High Performance Liquid Chromatography (HPLC) system with kromasil 100-5C18 column (4.6 mm × 250 mm) was used to assess the quantity of AA-2G present in the reaction solution described above. In this work, the mobile phase was 20 mM H_3PO_4 at an 0.8-mL/min flow rate, the column temperature was 25°C, and the PDA detector used 242 nm. The peak area of the standard sample AA-2G was used to calculate the AA-2G yield.

Kinetic Parameters

The kinetic parameters for soluble starch were determined at 80°C and pH 7 with different concentrations of soluble starch. The Hanes-Woolf method was used to calculate K_m and V_{max}. The kinetic parameters of AA-2G synthesis were determined at 40°C0 and pH 5. Different concentrations of β-CD (0.5, 1, 5, 10, and 25 g/L) and L-AA (1, 5, 10, 25, and 50 g/L) were used as substrates. The detailed reaction process is the same as presented in Section "Synthesis of AA-2G". The experimental results are in accordance with the ping-pong mechanism, and the equation is as follows: $v = V_{\max} ab \div (K_{mA} b + K_{mB} a + ab)$, where V represents the reaction rate (i.e., the amount of AA-2G synthesized per milligram enzyme per minute; U/mg), V_{max} represents the maximum reaction rate (U/mg), a represents the concentration of L-AA, b represents the concentration of β-CD, A is L-AA, and B is β-CD.

RESULTS

Expression of Recombinant CGTase in *E. coli* BL21(DE3)

To increase the expression of CGTase, the culture conditions, such as induction temperature, induction time, and inducer concentration, were optimized. As shown in **Figure 1A**, the enzymatic activity reached the highest level at 20°C and decreased gradually with further increasing temperature. The optimal IPTG concentration was 0.4 mM, and both too low and too high IPTG concentration [which may be caused by cell death and protein degradation (Chu et al., 2018)] decreased the level of CGTase expression (**Figure 1B**). In addition, the key factor of induction time was tested from 6 to 24 h (**Figure 1C**). The result showed that the enzymatic activity reached the highest level after 18 h of induction. Based on the above results, the optimized conditions for CGTase expression were 20°C for 18 h with 0.4 mM of IPTG, after fermentation, and the OD_{600} reached 6.

Purification and Biochemical Properties of Recombinant CGTase

The recombinant CGTase was purified by Ni^{2+}-NTA affinity chromatography. **Table 1** shows the specific activity of CGTase at each purification step. After the production of Ni^{2+}-NTA, the specific activity of the CGTase was 63.3 U/mg after 67.3-fold purification, achieving a final yield of 43.7%. **Figure 2** shows a single band of purified recombinant enzyme on SDS-PAGE. The molecular weight of purified recombinant enzyme was about 74.3 kDa, which is consistent with the theoretical molecular mass.

Figure 3A shows that the optimal cyclization temperature of recombinant enzyme was 80°C at pH 7. At 30°C, the recombinant enzyme still exhibited more than 60% cyclization activity. The recombinant CGTase activity barely changed after treatment at a temperature range of 40–80°C for 2 h, indicating

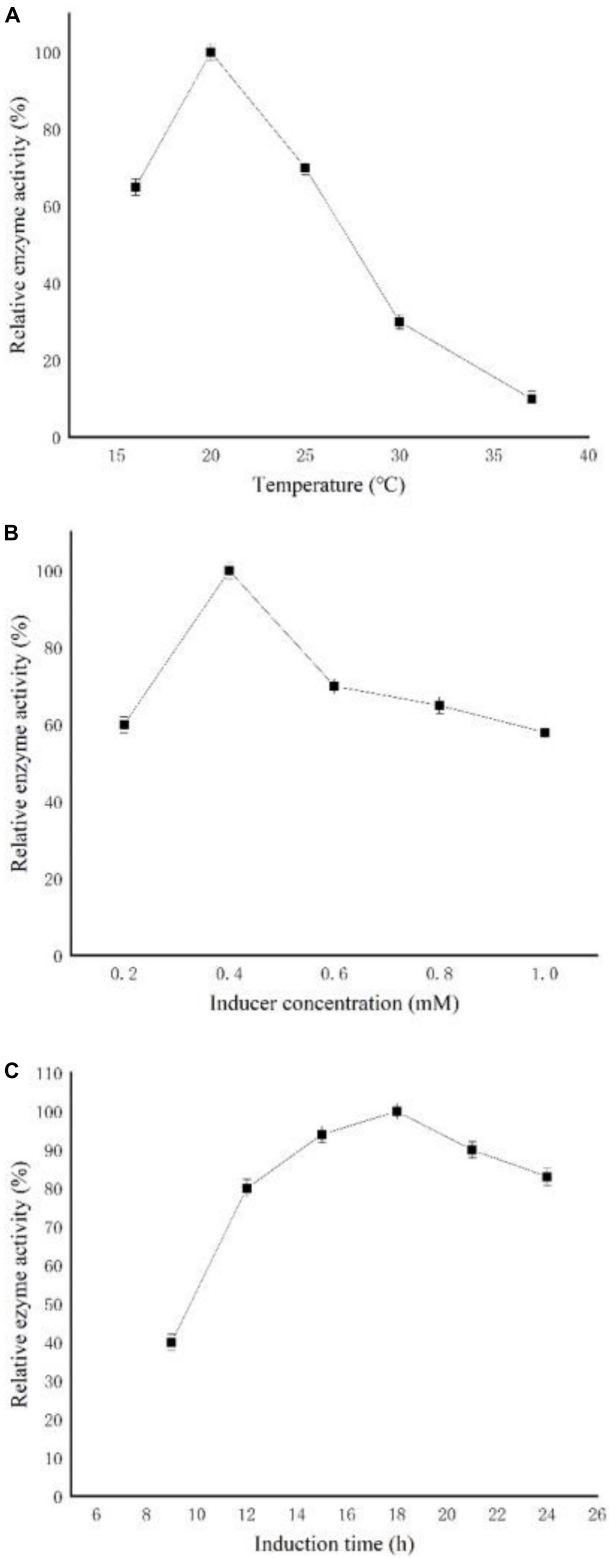

FIGURE 1 | Effects of induction conditions on the expression of recombinant cyclodextrin glycosyltransferase (CGTase). **(A)** Induction temperature, **(B)** isopropyl β-D-L-thiogalactopyranoside (IPTG) concentration, and **(C)** induction time.

TABLE 1 | Purification of recombinant cyclodextrin glycosyltransferase (CGTase).

	Total activity (U)	Protein concentration (mg/ml)	Specificity activity (U/mg)	Purification (fold)	Yield (%)
Supernatant	160	8.5	0.94	1	100
Ni^{2+}-NTA	70	0.13	63.3	67.3	43.7

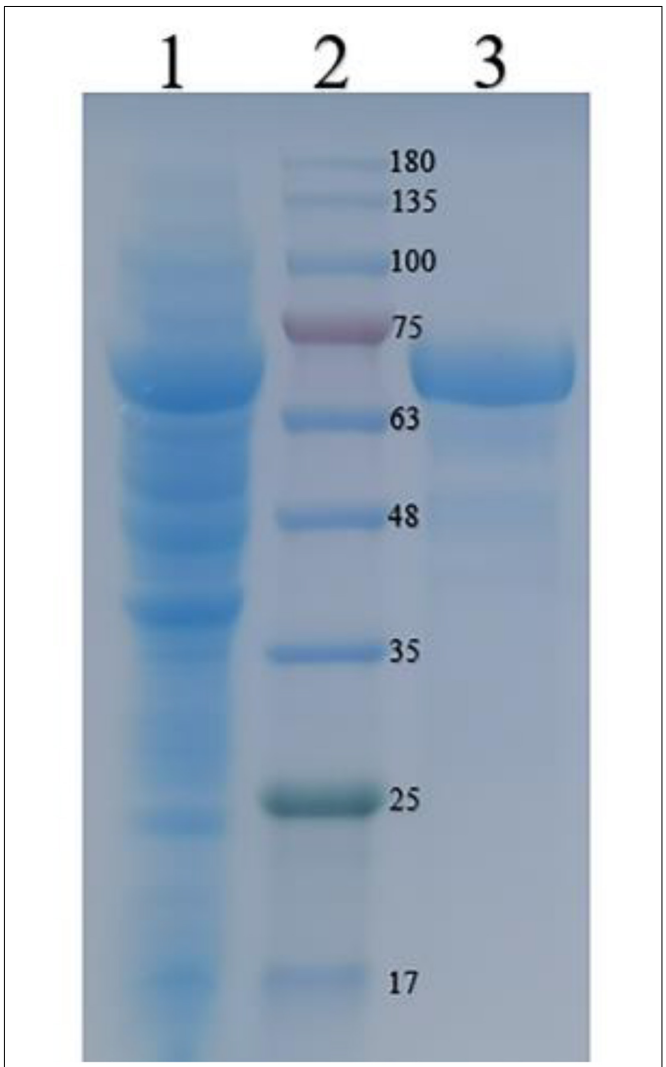

FIGURE 2 | Sodium dodecyl sulfatepolyacrylamide gel electrophoresis (SDS-PAGE) analyses of the recombinant CGTase on a 12% gel. *Lane 1* crude CGTase, *lane 2* protein marker, and *lane 3* purified CGTase.

good heat resistance. However, the recombinant enzyme retained less than 10% of its activity after treatment at 90°C (**Figure 3B**). The optimum reaction pH of the recombinant enzyme was pH 7 at optimal temperature, and the enzyme showed high activity at a range of pH levels (**Figure 3C**). However, at a pH of 11, the enzyme only retained less than 50% activity. **Figure 3D** shows the stability of cyclization activity of recombinant enzyme in the pH range of 3–11. The recombinant enzyme could still retain more than 80% enzyme activity after preservation at pH 4–10 for 12 h,

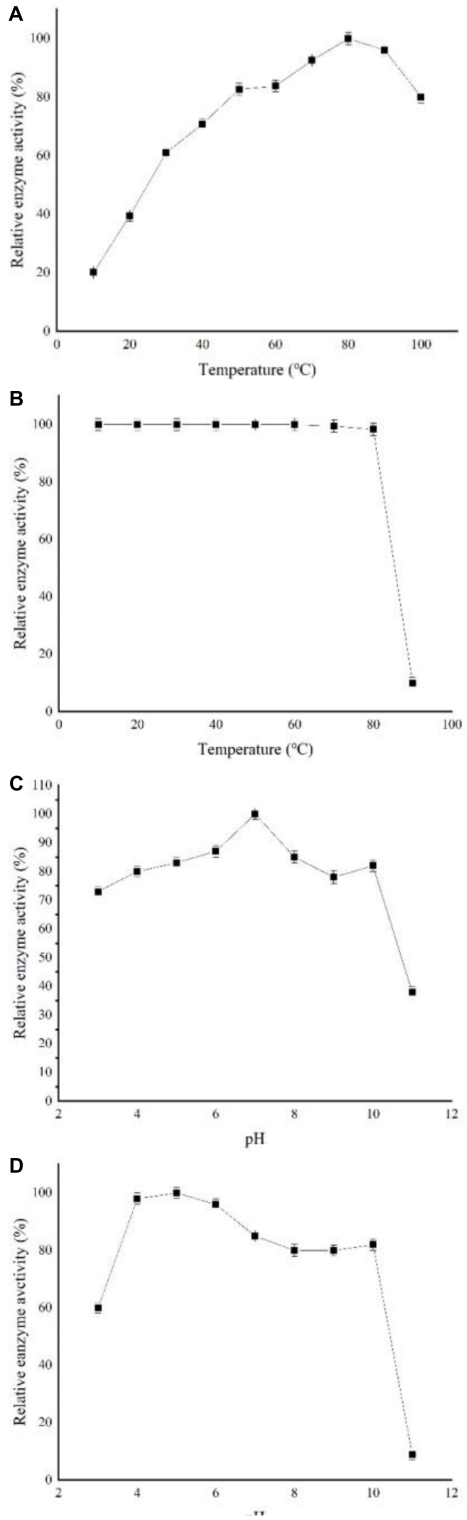

FIGURE 3 | Characterization of recombinant CGTase. **(A)** Optimum temperature, **(B)** temperature stability. Reaction mixtures contained 900 μl soluble starch and 100 μl CGTase in Na_2HPO_4-NaH_2PO_4 buffer at pH 7 from 10 to 100°C for 10 min, **(C)** optimum pH, and **(D)** pH stability. Reaction mixtures contained 900 μl soluble starch and 100 μl CGTase in different buffers at pH 3–11 and were incubated at 80°C for 10 min.

whereas its stabilities decreased clearly at pH 3 or 11, where it only retained 60 and 10% activity levels, respectively.

The effects of metal ions and chemical reagents on the activity of recombinant enzyme are shown in **Table 2**. K^+, Mg^{2+}, Ba^{2+}, Mn^{2+}, and Li^+ exerted little effect on the recombinant enzyme, whereas Fe^{2+} and Cu^{2+} inhibited the activity. In addition, 5 mM of Ca^{2+} could improve 10% of the enzyme activity of recombinant CGTase. The chemical agents of EDTA slightly activated the cyclization activity.

Biosynthesis and Analysis of AA-2G

The standard AA-2G curve with the concentrations of 100, 200, 300, 400, and 500 mg/ml was prepared with ultrapure water. The peak time of the AA-2G standard is shown in **Figure 4A**. **Figure 4B** shows that the peak position of AA-2G was 7.9 min, which was consistent with the standard sample, and the peak position of AA-2G emerged after L-AA. Recently, CGTase has been shown to be able to use numerous oligosaccharides and polysaccharides as substrates for the transformation into AA-2G. This study used the low-cost β-CD as donor and L-AA as receptor to synthesize AA-2G. Reaction conditions, including enzyme concentration, pH, temperature, time, and donor concentration, were optimized to improve the yield of AA-2G.

Figure 5 shows that the yield of AA-2G is highest when α-CD is used as substrate; however, considering its industrial cost, β-CD was selected as the substrate for subsequent research. **Figure 6A** shows the impact of the pH level on AA-2G production. At pH 4, the yield of AA-2G was highest, and the residue of L-AA was least. The low yield of AA-2G in alkaline environment may be related to the instability of L-AA. **Figure 6B** shows the effect of temperature on AA-2G production. The optimum temperature for the formation of AA-2G is 40°C. With increasing temperature, the amount of AA-2G gradually decreases. The residual amount of L-AA decreased first and then increased with increasing temperature. The effects of reaction time and donor concentration on AA-2G production are shown in **Figures 6C,D**, respectively. With increasing reaction time, the yield of AA-2G gradually increased, and when the reaction time reached 24 h, the highest yield of AA-2G was obtained. The residual amount of L-AA decreased gradually and remained stable after 24 h. The best donor concentration of β-CD was 50 with 50 g/L VC, as shown in **Figure 6D**. With increasing β-CD, the yield of AA-2G also increased. This demonstrated that increased donor substrate concentration drove the overall synthesis toward the oligoglucosylation of AA-2G (Xiong et al., 2015; Gudiminchi et al., 2016). When the substrate concentrations continued to increase, the yield of AA-2G decreased. As shown in **Figure 6E**, the optimal enzyme dosage was 75 U/g, and with increasing amount of enzyme, the yield of AA-2G decreased gradually. When the production of AA-2G was highest, the consumption of L-AA was also highest. In conclusion, the highest yield of AA-2G was 28 g/L and was achieved at 40°C, pH 4, 75 U/g enzyme dosage, 50 g/L donor concentration, and 24 h reaction time.

Kinetic Parameters

The kinetic parameters of soluble starch were calculated as follows: V_{max} = 0.62 ± 0.04 μmol/min, K_m = 5.1 ± 0.09 g/L,

TABLE 2 | Effects of metal ions and chemical reagents on CGTase activity.

Metal ions and chemical reagents	Control	K^+	Ca^{2+}	Mn^{2+}	Ba^{2+}
Relative activity (%)	100	94.4 ± 1.2	110.3 ± 2.3	96 ± 3.5	96 ± 2.7
Metal ions and chemical reagents	Fe^{2+}	Mg^{2+}	Li^+	Cu^{2+}	EDTA
Relative activity (%)	73.9 ± 3.0	98.5 ± 1.7	98.1 ± 1.6	63.6 ± 4.3	106.7 ± 3.1

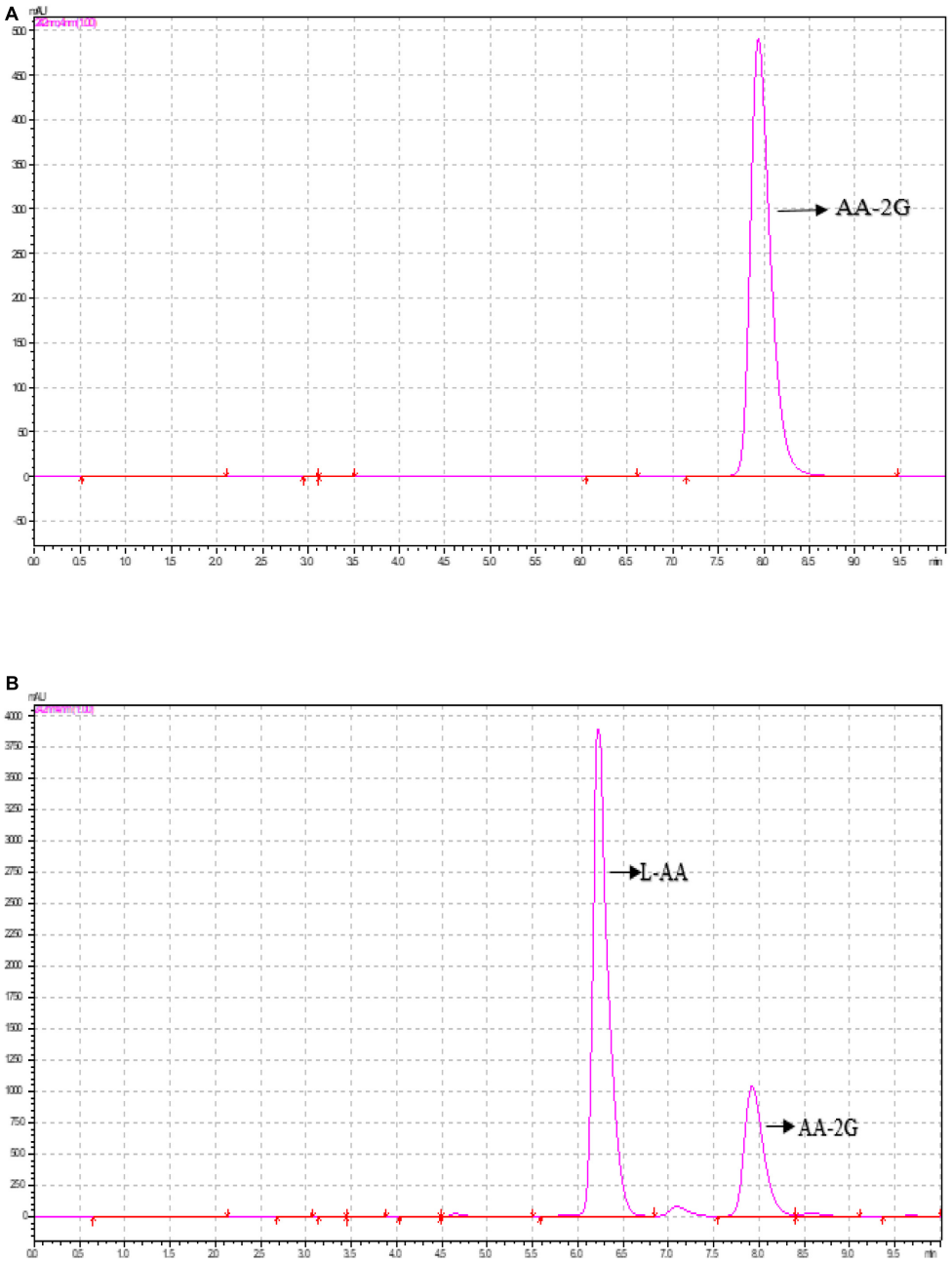

FIGURE 4 | HPLC analysis of 2-*O*-α-D-glucopyranosyl-L-ascorbic acid (AA-2G) production by the recombinant CGTase. **(A)** Standard sample of AA-2G, **(B)** reaction mixture.

and K_{cat} = 28.5 s^{-1}. The kinetic parameters of AA-2G synthesis by recombinant CGTase were studied. As shown in **Figure 7**, the effects of L-AA and β-CD concentrations on the synthesis of AA-2G by recombinant CGTase were explored. The experimental data were fitted to a ping-pong mechanism, which is consistent with the experimental results of Tao et al. (2018). The kinetic

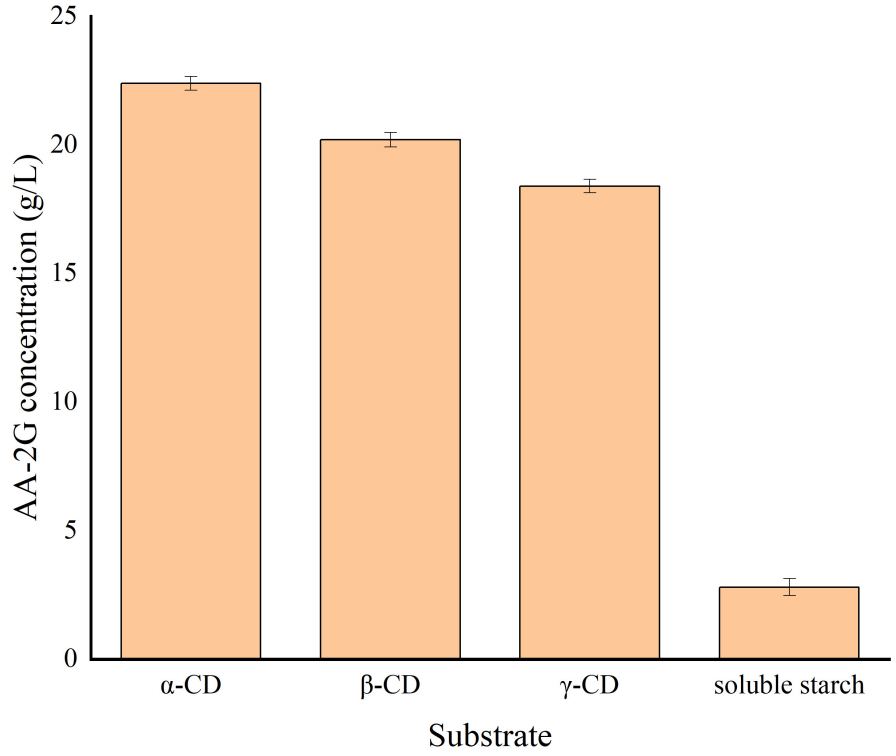

FIGURE 5 | Influence of substrate species on AA-2G synthesis.

parameters of the recombinant enzyme were calculated as follows: V_{max} = 21.6 ± 0.13 U/mg, K_{mA} = 9.2 ± 0.06 g/L, K_{mB} = 6.9 ± 0.04 g/L, and K_{cat} = 99,105 h^{-1}.

DISCUSSION

Fermentation conditions such as induction time, inducer concentration, and induction temperature affect the expression of foreign protein (Berry, 1996; Fakruddin et al., 2013; Jaliani et al., 2014). To reduce the formation of inclusion bodies, the induction temperature mostly ranges between 15 and 25°C (Song et al., 2012), which is consistent with the results of the present study. A too low inducer concentration will lead to insufficient induction, which will reduce protein expression (Pan and Malcolm, 2000; Mora et al., 2012; Gupta and Shukla, 2016). However, excessive IPTG will lead to the formation of inclusion bodies and have toxic effects on cells (Graslund et al., 2008; Jia and Jeon, 2016); therefore, it is necessary to avoid excessive IPTG accumulation. However, the recombinant enzyme is an intracellular enzyme that needs to be broken. Its use in industrial production will increase the cost. Therefore, the yeast expression system or the *Bacillus subtilis* expression system will be considered to secrete the enzyme into the medium in future research.

The recombinant enzyme was purified by Ni^{2+} column. The specific activity of the recombinant enzyme was 66.3 U/mg, which was higher than that of a number of reported CGTases, such as *Bacillus* sp. 8SB, *Bacillus* sp., *alkalophilic Bacillus* sp. g-825-6. The specific activities were 48, 2.24, and 5.57 U/mg, respectively (Hirano et al., 2006; Kitayska et al., 2011; Mora et al., 2012). The molecular weight of the recombinant enzyme is similar to that of other CGTases, such as *Bacillus* sp. Y112 (74 kD), *Bacillus megaterium* (66 kD), and *Bacillus pseudoalcaliphilus* (75 kD) (Vazquez et al., 2016; Zhang et al., 2017; Li et al., 2020).

The recombinant enzyme achieved good physical and chemical properties, which proved that the enzyme has promising industrial application value. The properties of CGTase from different sources are listed in **Table 3**. With regard to thermal stability, the optimal temperatures of a number of reported CGTases range between 40 and 60°C. The optimal temperature of the recombinant CGTase encoded by the *my*20 gene is 80°C. The most important property of the enzyme is its thermal stability. The activity of most CGTases will decrease or even be completely inactivated when the temperature exceeds 50°C for a period of time. The stability of the recombinant CGTase encoded by the *my20* gene is much better than these recombinant CGTases. Because of the good thermal stability of the recombinant enzyme, the application of the recombinant enzyme for industrial production will extend its working time, reduce the pollution risk, and improve the solubility of the substrate (Zhang et al., 2018). Therefore, the recombinant enzyme will have great potential in the industrial production of CD and AA-2G. As shown in **Table 3**, the optimal pH of CGTase reported in this study ranged from 6 to 8. However, a number of CGTase exist whose optimum pH is

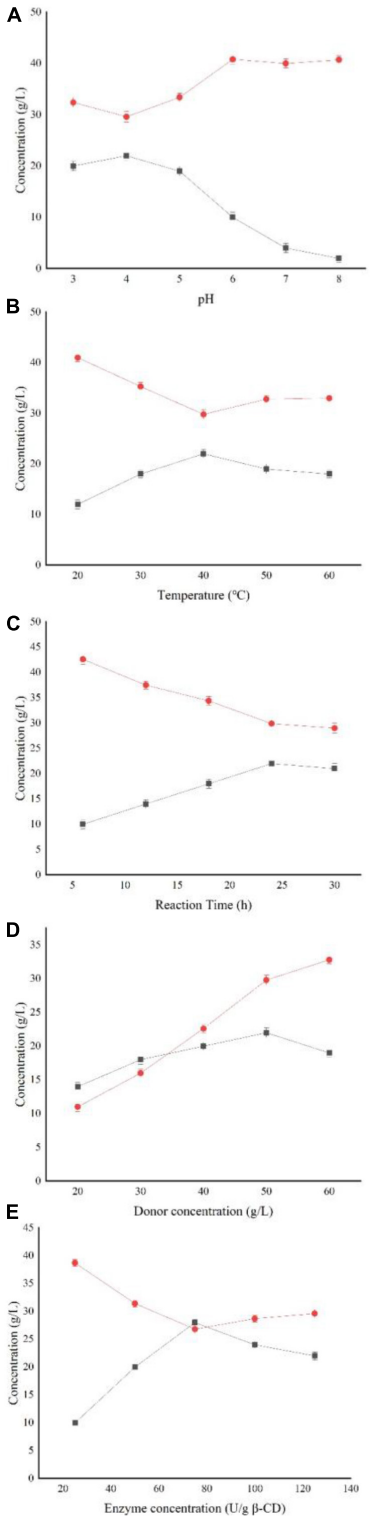

FIGURE 6 | Effect of reaction conditions on AA-2G synthesis. **(A)** Influence of pH on AA-2G synthesis, **(B)** influence of temperature on AA-2G synthesis, **(C)** influence of reaction time on AA-2G synthesis, **(D)** influence of donor concentration on AA-2G synthesis, and **(E)** influence of enzyme concentration on AA-2G synthesis. AA-2G production (*filled squares*), L-AA residual content (*filled circles*).

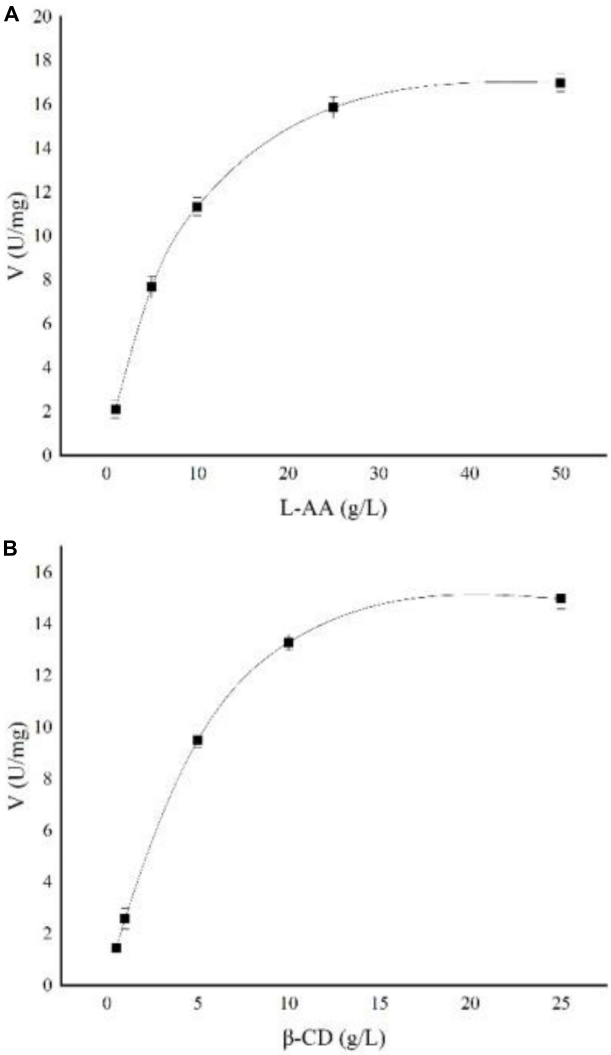

FIGURE 7 | Nonlinear regression of AA-2G synthesis by recombinant CGTase. **(A)** L-AA, **(B)** β-CD.

alkaline, such as *Bacillus* sp. Y112 with an optimum pH of 10 (Li et al., 2020). In the present study, the optimum pH was 7, and the CGTase encoded by MY20 achieved better pH stability than the enzyme (**Table 3**). When CGTase (**Table 3**) is exposed to pH 4–5 for a certain period of time, its activity will be greatly decreased. When CGTase was used for the production of AA-2G, the yield of AA-2G may be reduced, because most of the experimental data show that the recombinant CGTase can produce more AA-2G in an acidic environment. However, the recombinant CGTase encoded by MY20 showed good acid tolerance. Therefore, because of its good thermal and pH stabilities, the recombinant enzyme will have great significance for guiding the industrial production of AA-2G. With regard to the tolerance to metal ions, Ca^{2+} could increase the activity of recombinant enzyme, which is consistent with the results of *Paenibacillus illinois* ZY-08 (Lee et al., 2013). The results of *Paenibacillus pabuli* US132

TABLE 3 | Properties of CGTase from different strains.

Strain	Source	Optimal temperature	Optimal pH	K_m (g/L)	References
Paenibacillus illinoisensis ZY-08	Soil in China	40°C	pH 7	0.48	Lee et al., 2013
Paenibacillus pabuli US132	Tunisian soil	60°C	pH 6.5	8.62	Jemli et al., 2007
Alkaliphilic Bacillus sp. SD5	Lake Salda in Burdur Province	50°C	pH 6	13.59	Kabacaoglu and Karakas, 2017
Bacillus pseudalcaliphilus 8SB	Soil from Sapareva Bania region	60°C	pH 6	Not mentioned	Kitayska et al., 2011
Bacillus lehensis CGII	Wastewater samples from a cassava flour mill in Brazil.	55°C	pH 8	Not mentioned	Blanco et al., 2014
*my*20	Mariana trench	80°C	pH 7	5.1	This study

TABLE 4 | Optimum reaction conditions of 2-*O*-α-D-glucopyranosyl-L-ascorbic acid (AA-2G) synthesis by CGTase from different strains.

Strain	Temperature (°C)	pH	Donor substrate	AA-2G concentration (g/L)	References
Paenibacillus macerans	37	5	β-CD	15	Zhang et al.
Paenibacillus macerans	36	6.5	Maltose	1.12	Liu et al.
Thermoanaerobacter sp.	50	4.5	α-CD	143	Gudiminchi et al., 2016
Paenibacillus sp.	37	6.5	γ-CD	1.7	Jun et al.
P. macerans JFB05-01	40	5	α-CD	9.1	Jiang
my20	40	4	β-CD	28	This study

also showed that Fe^{2+} and Cu^{2+} could reduce the enzyme activity (Jemli et al., 2007).

As generally accepted, a smaller K_m implies a higher affinity of enzyme to substrate. In this study, where soluble starch was used as substrate, the K_m value of recombinant enzyme was 5.1 g/L, which was lower than that of CGTase from *Bacillus lehensis* CGII and *alkaliphilic Bacillus* sp. SD5, as shown in **Table 3**.

2-*O*-α-D-glucopyranosyl-L-ascorbic acid, as the best substitute of L-AA, has received wide interest of researchers. In recent years, reports on the synthesis of AA-2G by CGTase are becoming more numerous, as shown in **Table 4**. Many studies have shown that cyclodextrins (α-CD, β-CD, and γ-CD), soluble starch, and maltose can be used as donor substrates for the synthesis of AA-2G. Although the achieved yield of AA-2G is very high, using α-CD as donor is expensive and therefore, not suitable for industrial production. When using γ-CD and soluble starch as substrate, the yield of AA-2G is low and the price of γ-CD is also high. The experimental results of the present study are consistent with those of Jiang et al. (2018). They used soluble starch as substrate and the achieved AA-2G yield was 61% lower than that of α-CD, and 36% lower than that of β–CD (Jiang et al., 2018). Therefore, in this study, β-CD was selected as the donor substrate to synthesize AA-2G. The optimum pH for AA-2G production is pH 4–6, which is consistent with the results of the present study. However, there is also a CGTase from *Bacillus* sk 13.002, with an optimal pH for AA-2G synthesis of ∼8 (Eibaid et al., 2014). However, the yield of AA-2G synthesis of the recombinant CGTase encoded by MY20 decreased significantly at pH 8. This may be caused by the instability of L-AA aqueous solution in the alkaline environment. The optimum temperature for synthesis of AA-2G is mostly between 36 and 50°C, which is consistent with the results of the present study. When the reaction temperature increased, the yield of AA-2G decreased. This may be due to the unstable oxidative decomposition of L-AA at high temperature (Teng et al., 2018), or the decrease of coupling activity and disproportionation activity of recombinant enzyme at high temperature. In this study, the optimal reaction time of AA-2G synthesis is 24 h, which is consistent with the results of Gudiminchi et al. (2016). They used α-CD as substrate, and the yield of AA-2G did not increase after 24 h (Gudiminchi et al., 2016). In summary, under optimal reaction conditions, the recombinant CGTase encoded by MY20 can produce 28 g/L AA-2G, which is higher than the amount of AA-2G synthesized by many other CGTases, as shown in **Table 4**. Moreover, because of the good thermal and pH stabilities, the recombinant enzyme can transform L-AA to produce more AA-2G; therefore, the recombinant enzyme will have great economic value in the industrial production of AA-2G. Current experiments show that the site-directed mutagenesis of CGTase +1 and CGTase +2 can improve the yield of AA-2G. Therefore, subsequent experiments will assess the use of site directed mutagenesis to further improve the yield of AA-2G.

This study showed that the recombinant enzyme encoded by *my*20 gene offers great advantages in pH and temperature stabilities. On the one hand, high optimum temperature and good thermal stability are helpful to prolong the working time and increase the solubility of the substrate. On the other hand, the recombinant enzyme has strong acid resistance, which is helpful for the production of AA-2G. Therefore, the recombinant enzyme will have great application prospects for the industrial production of AA-2G.

DATA AVAILABILITY STATEMENT

The raw data supporting the conclusions of this article will be made available by the authors, without undue reservation.

AUTHOR CONTRIBUTIONS

KS: conceptualization, methodology, writing-original draft, and writing–review and editing. JS: formal analysis and writing-original draft. WW: data curation and methodology. JH: funding acquisition and writing–review and editing. All authors have read and agreed to the published version of the manuscript.

FUNDING

This research was funded by the National Key Research and Development Program of China (No. 2018YFC0311106), the Provincial Key Research and Development Program of Shandong (No. 2019GHY112030), the Central Public-interest Scientific Institution Basal Research Fund, CAFS (No. 2020TD67), and the Shinan Science and Technology Plan of Qingdao (No. 2018-4-002-ZH).

SUPPLEMENTARY MATERIAL

The Supplementary Material for this article can be found online at: https://www.frontiersin.org/articles/10.3389/fmicb.2021.664339/full#supplementary-material

REFERENCES

Aga, H., Yoneyama, M., Sakai, S., Yamamoto, I. (1991). Synthesis of 2-O-α-D-gluconotransferase from *Bacillus stearothermophilus*. *Agric. Biol. Chem*. 55, 1751–1756. doi: 10.1080/00021369.1991.10870856

Bae, H. K., Lee, S. B., Park, C. S., Shim, J. H., Lee, H. Y., and Kim, M. J. (2002). Modification of ascorbic acid using transglycosylation activity of *Bacillus stearothermophilus* maltogenic amylase to enhance its oxidative stability. *Agric. Food Chem*. 50, 3309–3316. doi: 10.1021/jf011550z

Berry, A. (1996). Improving production of aromatic compounds in *Escherichia coli* by metabolic engineering. *Trends Biotechnol*. 14, 250–256. doi: 10.1016/0167-7799(96)10033-0

Blanco, K. C., Moraes, F. F., Bernardi, N. S., Vettori, M. H., Monti, R., and Contiero, J. (2014). Cyclodextrin production by *Bacillus lehensis* isolated from Cassava starch: characterisation of a Novel Enzyme. *Czech. J. Food Sci*. 32, 48–53. doi: 10.17221/432/2012-CJFS

Chen, S., Xiong, Y. J., Su, L. G., Wang, L., and Wu, J. (2017). Position 228 in *Paenibacillus macerans* cyclodextrin glycosyltransferase in critical for 2-O-α-glucopyranosyl L-ascorbic acid synthesis. *J. Biotechnol*. 247, 18–24. doi: 10.1016/j.jbiotec.2017.02.011

Chu, C., Zhang, W. Q., Li, J. L., and Wan, Y. (2018). A single codon optimization enhances recombinant human TNF-α vacxine expression in *Escherichia coli*. *Biomed. Res. Int* 2018:3025169. doi: 10.1155/2018/3025169

Eibaid, A., Miao, M., and Bashari, M. (2014). Biosynthesis of 2-O-α-D-glucopyranosyl-L-ascorbic acid from maltose catalyzed by cyclodextrin glucanotransferase from *Bacillus sp*. Sk13.002. *J. Food Nutr Res. Slov*. 2, 19–28. doi: 10.12691/jfnr-2-4-10

Fakruddin, M., Mohamm, R., Chowdhury, A., and Hossain, M. N. (2013). Critical factors affecting the success of cloning, expression, and mass production of enzymes by recombinant *E.coli*. *ISRN Biotechnol.* 2013:590587. doi: 10.5402/2013/590587

Fenelon, V. C., Aguiar, M. F. A., Miyoshi, J. H., Martinez, C. O., and Matioli, G. (2015). Ultrafiltration system for cyclodextrin production in repetitive batches by CGTase from *Bcillus firmus* strain 37. *Bioprocess. Biosyst. Eng*. 38, 1291–1301. doi: 10.1007/s00449-015-1369-8

Graslund, S., Nordlund, P., Weigelt, J., Bray, J., Hallberg, B. M., and Gileadi, O. (2008). Protein production and purification. *Nat. Methods*. 5, 135–146. doi: 10.1038/nmeth.f.202

Gudiminchi, R. K., and Nidetzky, B. (2017). Walking a fine line with sucrose phosphorylase: efficient single-step biocatalytic production of L-ascorbic acid 2-glucoside from sucrose. *Chembiochem* 18, 1387–1390. doi: 10.1002/cbic.201700215

Gudiminchi, R. K., Towns, A., Varalwar, S., and Nidetzky, B. (2016). Enhanced synthesis of 2-O-alpha-D-glucopyranosyl-L-ascorbic acid from alpha cyclodextrin by a highly disproportionating CGTase. *ACS. Catal*. 6, 1606–1615. doi: 10.1021/acscatal.5b02108

Gupta, S. K., and Shukla, P. (2016). Advanced technologies for improved expression of recombinant proteins in bacteria: perspectives and applications. *Crit. Rev. Biotechnol*. 36, 1089–1098. doi: 10.3109/07388551.2015.1084264

Han, R., Liu, L., Li, J., and Chen, J. (2012). Functions, applications, and production of 2-O-D-glucopyranosyl-L-ascorbic acid. *Appl. Microbiol. Biotechnol*. 95, 313–320. doi: 10.1007/s00253-012-4150-9

Han, R. Z., Li, J. H., Shin, H. D., Chen, R. R., Du, G. C., and Liu, L. (2014). Recent advances in discovery, heterologous expression, and molecular engineering of cyclodextrin glycosyltransferase for versatile applications. *Biotechnol. Adv*. 32, 415–428. doi: 10.1016/j.biotechadv.2013.12.004

Han, R. Z., Liu, L., Shin, H. D., Chen, R. R., Du, G. C., and Chen, J. (2013). Site-saturation engineering of lysine 47 in cyclodextrin glycosyltransferase from *Paenibacillus macerans* to enhance substrate specificity towards maltodextrin for enzymatic synthesis of 2-O-D-glucopyranosyl-L-ascorbic acid(AA-2G). *Appl. Microbiol. Biotechnol.* 97, 5851–5860.

Hirano, K., Ishihara, T., Ogasawara, S., Maeda, H., Nakajima, T., and Yamagata, Y. (2006). Molecular cloning and characterization of a novel gamma-CGTase from alkalophilic *Bacillus sp*. *Appl. Microblol. Biotechnol.* 70, 193–201. doi: 10.1007/s00253-005-0041-7

Jaliani, H. Z., Farajnia, S., Safdari, Y., Talebi, S., and Barzegar, A. (2014). Optimized condition for enhanced soluble expression of recombinant mutant anabaena variabilis phenylalanine ammonia lyase. *Adv. Pharm. Bull.* 4, 261–266. doi: 10.5681/apb.2014.038

Jemli, S., Ben, E., Ayad, D., Naili, B., Khemakhem, B., and Bejar, S. (2007). A beta-cyclodextrin glycosyltransferase from a newly isolated *Paenibacillus pabuli* US 132 strain: purification, properties and potential use in bread-making. *Biochem. Eng. J*. 34, 44–50.

Jia, B., and Jeon, C. (2016). High-throughput recombinant protein expression in *Escherichia coli*: current status and future perspectives. *Open Biol*. 6:160196. doi: 10.1098/rsob.160196

Jiang, Y. J., Zhou, J., Wu, R. F., and Jiang, M. (2018). Heterologous expression of cyclodextrin glycosyltransferase from *Paenibacillus macerans* in *Escherichia coli* and its application in 2-O-α-D-glucopyranosyl-L-ascorbic acid production. *BMC Biotechnol.* 18:53. doi: 10.1186/s12896-018-0463-9

Jun, H. K., Bae, K. M., and Kim, S. K. (2001). Production of 2-O-α-D-glucopyranosyl L-ascorbic acid using cyclodextrin glucanotransferase from *Paenibacillus sp*. *Biotechnol. Lett*. 23, 1793–1797. doi: 10.1023/A:1012413301061

Kabacaoglu, E., and Karakas, B. (2017). Heterologous expression of beta-gamma-type cyclodextrin glycosyltransferase of newly isolated alkaliphilic *Bacillus sp* SD5 in Pichia pastoris. *Starch Starke*. 69, 9–10. doi: 10.1002/star.201600365

Kitayska, T., Petrova, P., Ivanova, V., and Tonkova, A. I. (2011). Purification and properties of a new thermostable cyclodextrin glucanotransferase from *Bacillus pseudalcaliphilus* 8SB. *Appl. Biochem. Biotechnol*. 165, 1285–1295. doi: 10.1007/s12010-011-9346-4

Lee, Y. S., Zhou, Y., Park, D. J., and Yong, J. C. (2013). β-cyclodextrin production by the cyclodextrin glucanotransferase from *Paenibacillus illinoisensis* ZY-08: cloning, purification, and properties. *World J. Microbiol. Biotechnol*. 29, 865–873. doi: 10.1007/s11274-012-1241-9

Leemhuis, H., Kelly, R., and Dijkhuizen, L. (2010). Engineering of cyclodextrin glucanotransferases and the impact for biotechnological applications. *Appl. Microbiol. Biotechnol*. 85, 823–835. doi: 10.1007/s00253-009-2221-3

Li, X., Sun, J., Wang, W., Guo, J., Song, K., and Hao, J. (2020). Site-saturation mutagenesis of proline 176 in Cyclodextrin Glucosyltransferase from *Bacillus*

sp. Y112 effects product specificity and enzymatic properties. *Process Biochem.* 94, 180–189. doi: 10.1016/j.procbio.2020.04.024

Li, Z. J., Han, H. J., Wang, B., Gao, J. J., Zhu, B., and Peng, R. (2017). Transglucosylation of ascorbic acid to ascorbic acid 2-glucoside by a truncated version of α-glucosidase from *Aspergillus niger*. *Food. Biochem.* 41:e12432. doi: 10.1111/jfbc.12432

Liu, L., Han, R. Z., Shin, H. D., Li, J. H., Du, G. C., and Chen, J. (2013). Biosynthesis of 2-O-D-glucopyranosyl-L-ascorbic acid from maltose by an engineered cyclodextrin glycosyltransferase from *Paenibacillus macerans*. *Carbohyd. Res.* 382, 101–107. doi: 10.1016/j.carres.2013.04.028

Mima, H., Nomura, H., Jmai, Y., and Takashima, H. (1970). Chemistry and application of ascorbic acid phosphate. *Vitamins* 41, 387–398.

Mora, M. M., Sanchez, K. H., Santana, R. V., Rojas, A. P., Ramirez, H. L., and Torres, J. J. (2012). Partial purification and properties of cyclodextrin glycosiltransferase (CGTase) from alkalophilic *Bacillus species*. *SpringerPlus* 1:61. doi: 10.1186/2193-1801-1-61

Naidu, K. A. (2003). Vitamin C in human health and disease is still a mystery. an overview. *Nutr. J.* 2:7. doi: 10.1186/1475-2891-2-7

Pan, S. H., and Malcolm, B. A. (2000). Reduced background expression and improved plasmid stability with pET vectors in BL21(DE3). *Biotechniques* 29, 1234–1238. doi: 10.2144/00296st03

Song, J. M., An, Y. J., Kang, M. H., Lee, Y. H., and Cha, S. S. (2012). Cultivation at 6-10 degrees C is an effective strategy to overcome the insolubility of recombinant proteins in *Escherichia coli*. *Protein Expr. Purif.* 82, 297–301. doi: 10.1016/j.pep.2012.01.020

Sun, X. L., Hao, J. H., and Sun, M. (2015). Optimized fermentation of a cyclomaltodextrin glucanotransferase producing strain. *Chin. J. Mar. Drugs* 34, 63–70.

Tai, A., Iomori, A., and Ito, H. (2017). Structural evidence for the DPPH radical-scavenging mechanism of 2-O-alpha-d-glucopyranosyl-l-ascorbic acid. *Bioorg. Med. Chem.* 25, 5303–5310. doi: 10.1016/j.bmc.2017.07.044

Tao, X. M., Su, L. Q., Wang, L., Chen, X. X., and Wu, J. (2018). Enhanced 2-O-α-D-glucopyranosyl-L-ascorbic acid synthesis through lterative saturation mutagenesis of acceptor subsite residues in *Bacillus stearothermopilus* NO2 cyclodextrin glycosyltransferase. *J. Agr. Food Chem.* 34, 9052–9060. doi: 10.1021/acs.jafc.8b03080

Tao, X. M., Su, L. Q., and Wu, J. (2019). Current studies on the enzymatic preparation 2-O-α-D-glucopyranosyl-Lascorbic acid with cyclodextrin glycosyltransferase. *Crit. Rev. Biotechnol.* 39, 249–257. doi: 10.1080/07388551.2018.1531823

Tao, X. M., Su, L. Q., and Wu, J. (2020). Improved production of cyclodextrin glycosyltransferase from *Bacillus stearothermophilus* NO2 in *Escherichia coli* via directed evolution. *Appl. Microbiol. Biotechnol.* 104, 173–185. doi: 10.1007/s00253-019-10249-8

Teng, J., Pourmand, A., and Mazer, M. A. (2018). Vitamin C: the next step in sepsis management. *Crit. Care* 48, 230–234. doi: 10.1016/j.jcrc.2017.09.031

Toyoda, Y., Maeda, M., Nakao, M., Yoshimura, M., and Fukami, H. (2004). 2-O- (beta-D-Glucopyranosyl) ascorbic acid, a novel ascorbic acid analogue isolated from Lycium fruit. *J. Agr. Food Chem.* 52, 2092–2096. doi: 10.1021/jf035445w

Vazquez, M. B., Alquicira, E. P., Fornue, E. D., Godínez, G. D., and Santos, J. S. (2016). Integral use of amaranth starch to obtain cyclodextrin glycosyltransferase by *Bacillus megaterium* to Produce β-Cyclodextrin. *Front. Microbiol* 7:1513. doi: 10.3389/fmicb.2016.01513

Xiong, Y. J., Wang, L., and Wu, J. (2015). The study of 2-O-α-D-glucopyranosyl-L-ascorbic acid synthesis by cyclodextrin glucosyltransferase. *Acta Microbiol. Sin.* 55, 27–32.

Yamamoto, I., Muto, N., Murakami, K., Suga, S., and Yamaguchi, H. (1990). L-ascorbic acid alpha-glucoside formed by regioselective transglucosylation with rat intestinal and rice seed alpha-glucosidases: its improved stability and structure determination. *Chem. Pharm. Bull.* 38, 3020–3023. doi: 10.1248/cpb.38.3020

Zhang, J., Li, M., and Zhang, Y. (2018). Enhancing the thermostability of recombinant cyclodextrin glucanotransferase via optimized stabilizer. *Process Biochem.* 67, 64–70. doi: 10.1016/j.procbio.2018.02.006

Zhang, J. G., Zhang, Y., and Li, M. L. (2017). High-level secretion and characterization of cyclodextrin glycosyltransferase in recombinant *Komagataella phaffii*. *J. Biotechnol.* 259, 126–134. doi: 10.1016/j.jbiotec.2017.07.031

Zhang, Z. C., Li, J. H., Liu, L., Sun, J., Hua, Z. Z., and Chen, J. (2011). Enzymatic transformation of 2-O-α-D-glucopyranosyl-L-ascorbic acid by α-cyclodextrin glucanotransferase from recombinant *Escherichia coli*. *Biotechol. Bioproc. E.* 16, 107–113. doi: 10.1007/s12257-010-0161-5

Conflict of Interest: The authors declare that the research was conducted in the absence of any commercial or financial relationships that could be construed as a potential conflict of interest.

frontiers in Microbiology

ORIGINAL RESEARCH
published: 10 June 2021
doi: 10.3389/fmicb.2021.696096

Characterization of a Hyaluronic Acid Utilization Locus and Identification of Two Hyaluronate Lyases in a Marine Bacterium *Vibrio alginolyticus* LWW-9

Xiaoyi Wang[1,2], Ziwei Wei[1,2], Hao Wu[1,2], Yujiao Li[1,2], Feng Han[1,2] and Wengong Yu[1,2]**

[1]*Shandong Provincial Key Laboratory of Glycoscience and Glycoengineering, School of Medicine and Pharmacy, Ocean University of China, Qingdao, China,* [2]*Laboratory for Marine Drugs and Bioproducts, Qingdao National Laboratory for Marine Science and Technology, Qingdao, China*

Hyaluronic acid (HA) is a negatively charged and linear polysaccharide existing in the tissues and body fluids of all vertebrates. Some pathogenic bacteria target hyaluronic acid for adhesion and/or infection to host cells. *Vibrio alginolyticus* is an opportunistic pathogen related to infections of humans and marine animals, and the hyaluronic acid-degrading potential of *Vibrio* spp. has been well-demonstrated. However, little is known about how *Vibrio* spp. utilize hyaluronic acid. In this study, a marine bacterium *V. alginolyticus* LWW-9 capable of degrading hyaluronic acid has been isolated. Genetic and bioinformatic analysis showed that *V. alginolyticus* LWW-9 harbors a gene cluster involved in the degradation, transport, and metabolism of hyaluronic acid. Two novel PL8 family hyaluronate lyases, VaHly8A and VaHly8B, are the key enzymes for the degradation of hyaluronic acid. VaHly8A and VaHly8B have distinct biochemical properties, reflecting the adaptation of the strain to the changing parameters of the aquatic habitats and hosts. Based on genomic and functional analysis, we propose a model for the complete degradation of hyaluronic acid by *V. alginolyticus* LWW-9. Overall, our study expands our knowledge of the HA utilization paradigm within the *Proteobacteria*, and the two novel hyaluronate lyases are excellent candidates for industrial applications.

Keywords: hyaluronate lyase, hyaluronic acid, polysaccharide utilization loci, *Vibrio*, *Proteobacteria*

OPEN ACCESS

Edited by:
Benwei Zhu,
Nanjing Tech University, China

Reviewed by:
Damao Wang,
Southwest University, China
Yayue Wang,
Shangqiu Normal University, China

****Correspondence:***
Feng Han
fhan@ouc.edu.cn
Wengong Yu
yuwg66@ouc.edu.cn

Specialty section:
This article was submitted to Microbiotechnology, a section of the journal Frontiers in Microbiology

Received: *16 April 2021*
Accepted: *17 May 2021*
Published: *10 June 2021*

Citation:
Wang X, Wei Z, Wu H, Li Y, Han F and Yu W (2021) Characterization of a Hyaluronic Acid Utilization Locus and Identification of Two Hyaluronate Lyases in a Marine Bacterium Vibrio alginolyticus LWW-9. Front. Microbiol. 12:696096. doi: 10.3389/fmicb.2021.696096

INTRODUCTION

Animal cells are in close interaction with extracellular matrices (ECM), which function as a physical scaffold for organs and tissues, regulate various cellular functions and maintain homeostasis (Theocharis et al., 2016). Hyaluronic acid (HA), a significant constituent of ECM, is a linear polysaccharide consisting of repeating units of glucuronic acid and N-acetylglucosamine *via* a β-1,4 linkage. HA is involved in various physiological and pathological processes of the biological system, such as cell migration, adhesion, growth and differentiation, embryogenesis, cancer, inflammation, and damage repair (Volpi et al., 2009). Due to its excellent physicochemical characteristics, HA has a variety of applications in the pharmaceutical industry, such as orthopedics, ophthalmology, and aesthetic dermatology (Sudha and Rose, 2014).

Some pathogenic bacteria, such as *streptococci* and *streptobacillus*, produce extracellular or cell-surface hyaluronate lyase to depolymerize HA, facilitating the invasion of the host (Li and Jedrzejas, 2001; Oiki et al., 2017). Hyaluronate lyases degrade HA by β-elimination mechanism, generating unsaturated disaccharides with a C_4-C_5 double bond at the non-reducing end (Wang et al., 2017). Hyaluronate lyases are categorized into four polysaccharide lyase (PL) families, PL8, PL16, PL30, and PL33, in the Carbohydrate-Active Enzymes (CAZy) database according to primary structures (Lombard et al., 2014).

The utilization of HA requires multiple proteins, such as PLs, glycoside hydrolases (GHs), sugar transporters, and transcriptional factors. These genes often cluster in a polysaccharide utilization loci (PUL), orchestrating sensing, enzymatic digestion, transport, and metabolism of a specific polysaccharide (Martens et al., 2009; Grondin et al., 2017). There are some reports on the polysaccharide utilization locus of hyaluronic acid (PUL$_{HA}$) in *Firmicutes* and *Fusobacteria*, but few reports on the PUL$_{HA}$ in *Proteobacteria* (Kawai et al., 2018; Oiki et al., 2019a,b). Although several hyaluronate lyases of *Proteobacteria* have been characterized in detail, the pathway for HA utilization in *Proteobacteria* remains largely opaque (Han et al., 2014; Peng et al., 2018).

Members of the genus *Vibrio* are pathogenic bacteria that cause serious infections to aquatic animals and humans, called vibriosis (Austin, 2010). Vibriosis is one of the most common bacterial diseases posing a threat to cultured fish, shellfish, and shrimp, which has a negative effect on the development of the global aquaculture industry (Ina-Salwany et al., 2019). *Vibrio* infections occur when humans expose to contaminated water or consume raw or undercooked contaminated seafood, causing many diseases, such as gastroenteritis, and wound infections and septicemia (Dechet et al., 2008). *Vibrio* strains could degrade hyaluronic acid to facilitate host invasion; however, little is known about how they utilize hyaluronic acid.

In this study, we isolated a hyaluronate lyase-producing bacterium, *Vibrio alginolyticus* strain LWW-9. A PUL$_{HA}$ was found in the draft genome of *V. alginolyticus* LWW-9 by genome analysis. In particular, two novel hyaluronate lyases in PUL$_{HA}$, VaHly8A, and VaHly8B, were characterized. VaHly8A and VaHly8B showed distinct biochemical properties, which revealed their adaption to the living environment. Finally, we provided a model for how *V. alginolyticus* strain LWW-9 utilizes the HA. These results presented here not merely extend our understanding of the HA utilization paradigm within the *Proteobacteria* but also may contribute to the elucidation of bacterial physiology and pathogenicity.

MATERIALS AND METHODS

Materials

Hyaluronic acid was obtained from Macklin (Shanghai, China). The pET-28a (+) plasmid and *Escherichia coli* BL21(DE3) were obtained from Takara (Dalian, China). DNA polymerase was obtained from Vazyme (Nanjing, China). Restriction enzymes and T_4 DNA ligase were purchased from Takara (Dalian, China). Pageruler unstained protein ladder was obtained from Thermo Scientific (Wilmington, United States). All other chemicals were purchased from Sinopharm (Beijing, China).

Isolation of Marine Hyaluronate Lyase-Producing Bacteria

Seawater was collected from Zhanqiao, Qingdao, China. A selective medium supplemented with HA as the sole carbon source was used to isolate hyaluronate lyase-producing bacteria from seawater. The medium consisted of 0.3% (w/v) KH_2PO_4, 0.7% (w/v) $K_2HPO_4{\cdot}3H_2O$, 0.2% (w/v; $(NH_4)_2SO_4$, 0.01% (w/v) $MgSO_4$, 0.01% (w/v) $FeSO_4{\cdot}7H_2O$, 3% NaCl, 0.05% (w/v) HA, and 1.5% (w/v) agar (pH 7.0). After microorganisms had grown at 25°C for 48 h, the plates were soaked with Gram's iodine for 1 min (Patil and Chaudhari, 2017). Clones with distinct clearance zones were detected as HA-degrading strains. They were picked up and purified on the fresh selective medium plates for three times. The pure cultured strains were incubated at 25°C and 160 r/min for 48 h in 100 ml marine broth 2216, and the hyaluronate lyase activity in the culture supernatant was determined. The strain LWW-9 that exhibited the highest hyaluronate lyase activity was obtained and used in the following experiment.

Identification of the Strain LWW-9

The 16S rDNA of strain LWW-9 was amplified by PCR using the universal primers 27F (5'-AGAGTTTGATCCTGGCTCAG-3') and 1492R (5'-TACGGTTACCTTGTTACGACTT-3'). A colony of strain LWW-9 was used as the template. The PCR product was purified, and sequenced by Ruibiotech Co., Ltd. (Beijing, China). The sequence analysis was conducted using Blast program[1] to search for sequences with high identity in GenBank database. The phylogenetic analysis was performed by MEGA X using the neighbor-joining method (Kumar et al., 2018).

Prediction of PUL$_{HA}$ in *Vibrio alginolyticus* Strain LWW-9

The genomic DNA of strain LWW-9 was prepared using Tianamp bacteria DNA kit (Tiangen, China). The draft genome of strain LWW-9 was sequenced using Roche 454 FLX Titanium technologies (Margulies et al., 2005). The genome annotation was performed online in the Rapid Annotation using Subsystem Technology (RAST) server.[2] Cazymes were further identified using pfam (Finn et al., 2014) and dbCAN Hidden Markov model (Zhang et al., 2018). Homologs searches of predicted protein sequences were carried out using Blatsp against NCBI PDB and nr databases. The gene cluster involved in the utilization of HA was identified as a potential PUL$_{HA}$. If genes adjacent to hyaluronate lyases encoded proteins dedicated to the utilization of HA, including Cazymes, sugar transporters, and transcription factors, the boundary of PUL$_{HA}$ was extended. When five continuous genes were not annotated as HA utilization proteins, the last gene with related function was regarded as the putative boundary of PUL$_{HA}$.

[1]http://blast.ncbi.nlm.nih.gov/Blast.cgi
[2]https://rast.nmpdr.org/

Sequence Analysis of VaHly8A and VaHly8B

The online Blastp algorithm was used to perform similarity searches against NCBI PDB and nr databases. Protein modules and domains were analyzed using Conserved Domain (CD) Search.[3] A neighbor-joining tree based on the protein sequence alignment was constructed using MEGA X (Kumar et al., 2018). Amino acid alignment with other enzymes of the PL8 family was carried out using ESPrit 3.0 (Robert and Gouet, 2014). The physical and chemical parameters of proteins, such as molecular weight (Mw) and isoelectric point (*pI*) were predicted by the ProtParam tool on the ExPASy server.[4] The existence and pattern of signal peptides were identified using SignalP 5.0 server.[5]

Heterologous Expression and Purification of VaHly8A and VaHly8B

The *vahly8B* and *vahly8B* were amplified by PCR using the genomic DNA of strain LWW-9 as the template. The primers for VaHly8A were 5'-GGAATTCCATATGAATAAATTTAATATTTCAA-3' and 5'-CCGCTCGAGTTCCTTAATGCGTTTAAC-3'. The primers for VaHly8B were 5'-GGAATTCCATATGAAACCTCTGAAACTCAC-3' and 5'-CCGCTCGAGCTCTTTTACCAAAGAGAAGG-3'. The PCR products were recovered from the agarose gel, digested with *Nde* I and *Xho* I, and ligated into the expression plasmid pET-28a(+). The recombinant plasmids, pET28a(+)-VaHly8A and pET28a(+)-VaHly8B, were transformed into *E. coli* BL21(DE3) cells, respectively.

Escherichia coli BL21(DE3) cells harboring pET28a(+)-VaHly8A and pET28a(+)-VaHly8B were incubated in Luria-Bertani (LB) medium at 37°C until the OD_{600} reached 0.4–0.6, then induced with 0.02 mM isopropyl β-D-thiogalactoside at 18°C for 24 h. The cells were harvested by centrifugation, resuspended in 20 mM Na_2HPO_4-NaH_2PO_4 buffer (pH 7.4) containing 500 mM NaCl, and disrupted by sonication. The cell lysate was centrifuged, and the recombinant hyaluronate lyase with N-terminal and C-terminal $(His)_6$ tags was purified from the supernatant by Histrap column (GE Healthcare, United States). The purity and Mw of the proteins were determined by sodium dodecyl sulfate-polyacrylamide gel electrophoresis (SDS-PAGE) on a 10% (w/v) resolving gel. Protein concentration was measured by the BCA protein assay kit (NCM Biotech, China).

Enzyme Activity Assay

The enzyme activity was measured in a 1 ml reaction system under the optimal reaction condition. First, 0.1 ml enzyme (0.18 U/ml) was added to 0.9 ml 0.2% (w/v) HA substrate solution. After incubation for 10 min at the optimal temperature, the reaction was terminated by boiling for 10 min, and then the absorbance of the solution was measured at 232 nm by a UH5300 UV visible spectrophotometer (HITACHI, Japan). One unit of enzyme activity was defined as the amount of the protein required to produce 1 μmol unsaturated oligosaccharides using the molecular extinction coefficient value of 5,500 M^{-1} cm^{-1} at 232 nm (Lin et al., 1994).

Biochemical Characterization of VaHly8A and VaHly8B

The optimal temperature was determined in 50 mM Tris-HCl buffer (pH 7.05) at different temperatures ranging from 0 to 70°C. The optimal pH was measured in the following buffers with various pH values: 50 mM Na_2HPO_4-Citrate buffer (pH 3.0–8.0), 50 mM NaH_2PO_4-Na_2HPO_4 buffer (pH 6.0–8.0), 50 mM Tris-HCl buffer (pH 7.05–8.95), and 50 mM Glycine-NaOH buffer (pH 8.6–10.6). To determine the thermostability of the enzyme, it was incubated for 1 h under temperatures ranging from 0 to 50°C, and the residual activities were determined at the optimal temperature and pH. To determine the pH stability of the enzyme, it was incubated for 6 h in buffers with varying pH values from 3.0 to 10.6 at 0°C, and the residual activities were determined at the optimal temperature and pH. The effect of NaCl was investigated by examining the enzyme activities in Tris-HCl buffer (pH 7.05) containing various concentrations of NaCl ranging from 0 to 1.0 M at the optimal temperature and pH. The effects of metal ions and surfactants were investigated by examining the enzyme activities in Tris-HCl buffer (pH 7.05) containing various compounds (1 mM) at the optimal temperature and pH.

Kinetic Parameters of VaHly8A and VaHly8B

To investigate the kinetic parameters of VaHly8A and VaHly8B, 0.1–8.0 mg/ml HA were used as the substrate. 0.1 ml enzyme (0.36 U/ml) was added to 0.9 ml substrate solution. After incubation at the optimal temperature for 3 min, the absorbance of the solution was measured at 232 nm. K_m and V_{max} values were determined using the Michaelis-Menten equation and the curve fitting program by non-linear regression analysis using Graphpad Prism 8.

Analysis of Degradation Pattern and Final Product

To investigate the degradation pattern and final product of HA by VaHly8A and VaHly8B, 0.2% (w/v) HA was digested by the purified enzyme (0.15 U/ml) at 20°C for VaHly8A and 30°C for VaHly8B. The reaction mixture was incubated for different time intervals ranging from 0 to 12 h. Samples were inactivated at 100°C for 10 min and centrifuged at 12,000 r/min for 10 min. The supernatant was then analyzed on a Superdex™ Peptide 10/300 GL column (GE Health, United States) by monitoring the absorbance at 232 nm. The mobile phase and flow rate were 0.2 M ammonium bicarbonate and 0.2 ml/min, respectively.

The exact Mw of final product was detected by negative ion electrospray ionization-mass spectroscopy (ESI-MS, Thermo Fisher Scientific, United States) with the mass acquisition range of 100–2,000. The ESI-MS analysis was carried out under the following conditions: sheath gas flow rate, 10 arb; spray voltage, 2.5 kV; tube lens, 35 V; capillary voltage, 16 V; and capillary temperature, 275°C.

[3]https://www.ncbi.nlm.nih.gov/Structure/cdd/wrpsb.cgi
[4]https://web.expasy.org/protparam/
[5]http://www.cbs.dtu.dk/services/SignalP/

RESULTS

Identification of Strain LWW-9

The 16S rDNA of strain LWW-9 was sequenced and submitted to GenBank under the accession number MW396717. The Blast search analysis against GenBank database revealed that strain LWW-9 showed 99% identity with multiple *Vibrio* strains. *Vibrio alginolyticus* strain Va-X15 (MH298577.1) showed the highest identity of 99.23%. Sixteen type strains in *Vibrio* were selected for phylogenetic analysis, and the result showed that strain LWW-9 was closest to *V. alginolyticus* strain ATCC 17749 (NR_118258.1) in the phylogenetic tree (**Figure 1**). Therefore, strain LWW-9 was identified as *V. alginolyticus*.

Model of HA Utilization in *V. alginolyticus* LWW-9

Genes related to the utilization of HA in *V. alginolyticus* LWW-9 were clustered in a ~19,600 bp genomic region, which suggested that this genetic cluster could be a PUL$_{HA}$. The PUL$_{HA}$ encodes two PL8 family hyaluronate lyases (VN1760 and VN1761), one GH88 family unsaturated glucuronyl hydrolase (VN1754), four enzymes involved in the metabolism of HA monosaccharides (VN1747, VN1748, VN1749, and VN1752), and one sugar transporter glucose phosphotransferase system (PTS) composed of four components (VN1755, VN1756, VN1757, and VN1758; **Figure 2A**). Despite the lack of *susC/susD* pairs in PUL$_{HA}$, TonB-dependent transporter (TBDT) encoded elsewhere in the genome may enable the oligosaccharides sensing and transport, similar to the SusC/SusD system of *Bacteroides* (Blanvillain et al., 2007).

A pathway for the metabolism of HA in *V. alginolyticus* LWW-9 has been proposed (**Figure 2B**). HA is degraded to unsaturated disaccharides by extracellular and cell-surface hyaluronate lyases. Unsaturated disaccharides are first transported to the periplasm by TBDT and then imported to the cytoplasm by PTS. They are degraded to unsaturated uronates and N-acetyl-D-glucosamines by GH88 through hydrolysis of β-1,4 linkages in the cytoplasm. Unsaturated uronates are converted to 4-deoxy-L-*threo*-5-hexosulose-uronate (DHU) by nonenzymatic reactions. DHU was ultimately metabolized to pyruvate and glyceraldehyde-3-phosphate by consecutive reactions of isomerase, dehydrogenase, kinase, and aldolase (Maruyama et al., 2015).

Sequence Analysis of VaHly8A and VaHly8B

The putative gene *vahly8A* was 2,385 bp in length and encoded VaHly8A consisting of 794 amino acid residues. The theoretical Mw and *pI* of VaHly8A are 88.1 kDa and 5.40, respectively. According to SignalP 5.0, VaHly8A has a type I signal peptide of 26 amino acid residues at its N-terminus. CD Search indicated that VaHly8A contained a Lyase_8 module (Trp^{49}-Ile^{381}) and a GAG lyase superfamily module (Phe^{42}-Pro^{740}). Blastp searches showed that VaHly8A shared the identity with HCLase (39%) from *Vibrio* sp. FC509 (Han et al., 2014), HAase-B (31%) from *Bacillus* sp. A50 (Guo et al., 2014), and XalA (30%) from *Paenibacillus alginolyticus* XL-1 (Ruijssenaars et al., 1999).

The putative gene *vahly8B* was 2,373 bp in length and encoded VaHly8B composed of 790 amino acid residues. The theoretical Mw and *pI* of VaHly8B are 86.5 kDa and 4.90, respectively. According to SignalP 5.0, VaHly8B has a type II signal peptide of 19 amino acid residues at its N-terminus. CD Search indicated that VaHly8A contained a Lyase_8 module (Trp^{54}-Lys^{373}) and a GAG_lyase superfamily module (Arg^{51}-Ser^{736}). Balstp searches showed that VaHly8B shared the identity with HCLase (41%)

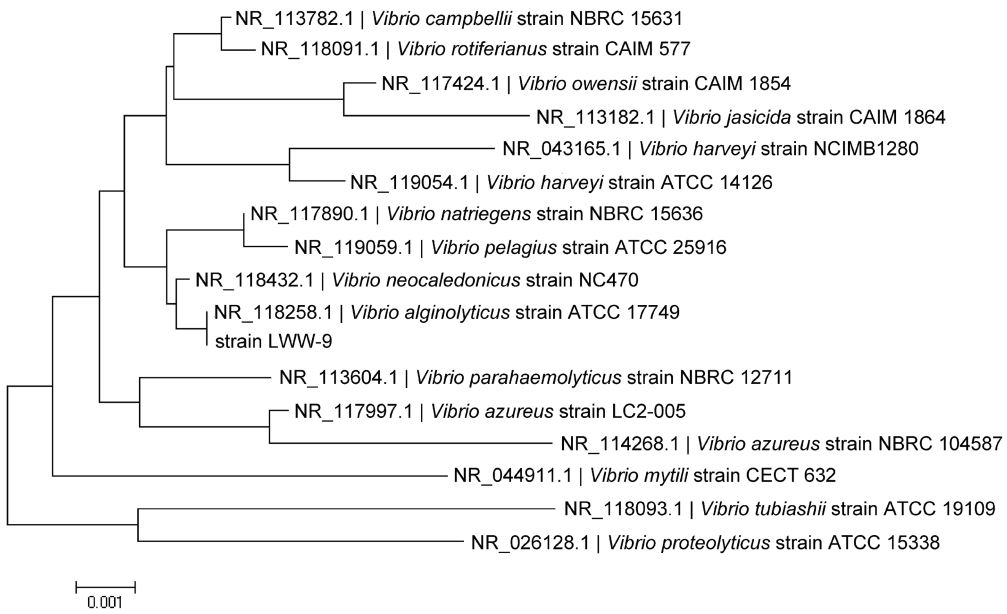

FIGURE 1 | Phylogenetic tree of strain LWW-9 based on 16S rRNA sequences. The phylogenetic tree was generated by MEGA X using the neighbor-joining method.

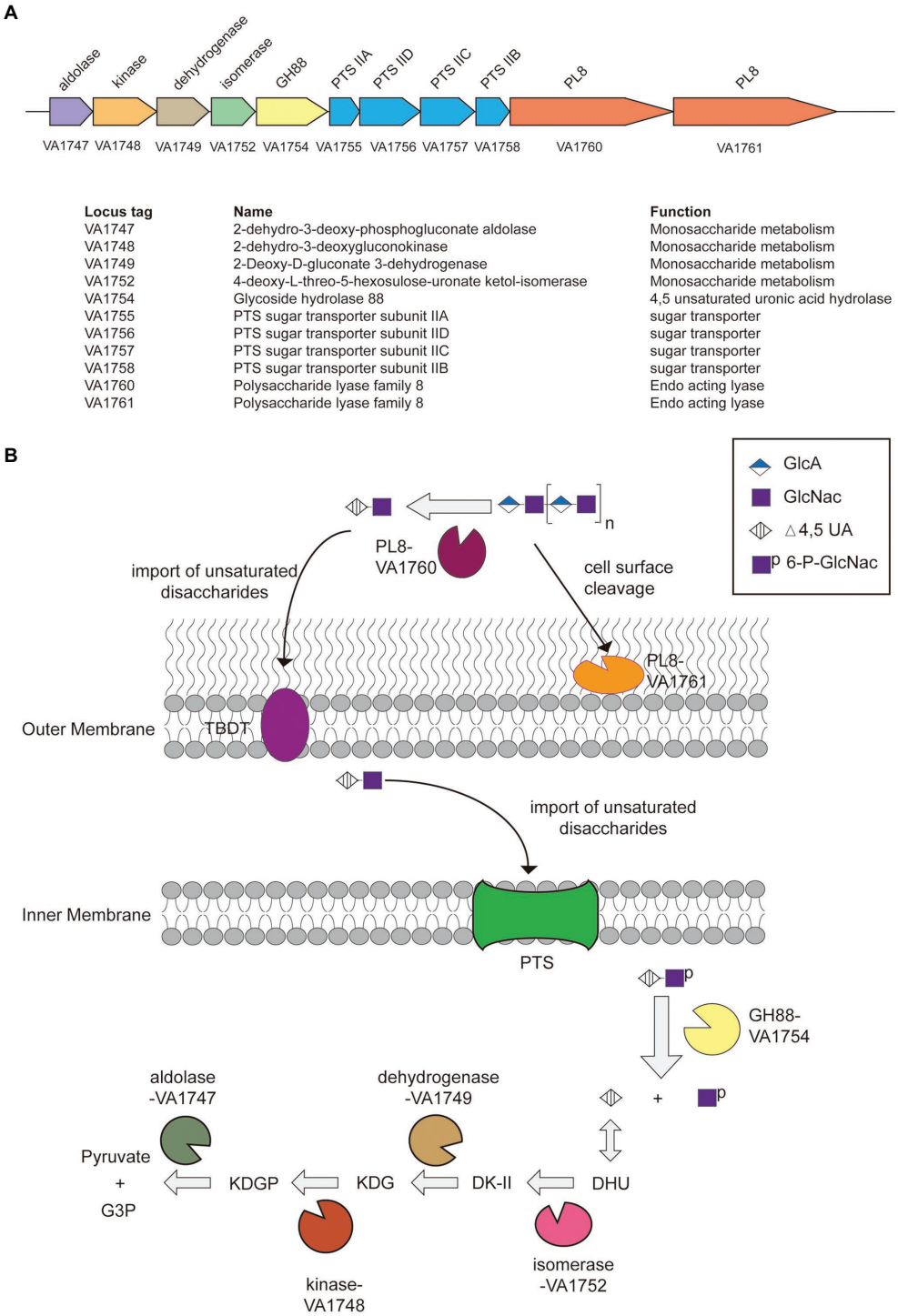

Locus tag	Name	Function
VA1747	2-dehydro-3-deoxy-phosphogluconate aldolase	Monosaccharide metabolism
VA1748	2-dehydro-3-deoxygluconokinase	Monosaccharide metabolism
VA1749	2-Deoxy-D-gluconate 3-dehydrogenase	Monosaccharide metabolism
VA1752	4-deoxy-L-threo-5-hexosulose-uronate ketol-isomerase	Monosaccharide metabolism
VA1754	Glycoside hydrolase 88	4,5 unsaturated uronic acid hydrolase
VA1755	PTS sugar transporter subunit IIA	sugar transporter
VA1756	PTS sugar transporter subunit IID	sugar transporter
VA1757	PTS sugar transporter subunit IIC	sugar transporter
VA1758	PTS sugar transporter subunit IIB	sugar transporter
VA1760	Polysaccharide lyase family 8	Endo acting lyase
VA1761	Polysaccharide lyase family 8	Endo acting lyase

FIGURE 2 | The paradigm of hyaluronic acid (HA) utilization by *Vibrio alginolyticus* LWW-9. **(A)** Predicted polysaccharide utilization locus of hyaluronic acid (PUL_{HA}) in *V. alginolyticus* LWW-9. **(B)** Schematic of the cellular location, activity, and specificity of the PUL_{HA}-encoded enzymes. DHU, 4-deoxy-L-*threo*-5-hexosulose-uronate; DK-II, 3-deoxy-D-*glycero*-2,5-hexodiulosonate; KDG, 2-keto-3-deoxy-D-gluconate; KDGP, 2-keto-3-deoxy-6-phosphogluconate; and G3P, glyceraldehyde-3-phosphate.

from *Vibrio* sp. FC509 (Han et al., 2014), XalA (33%) from *Paenibacillus alginolyticus* XL-1 (Ruijssenaars et al., 1999), and HAase-B (32%) from *Bacillus* sp. A50 (Guo et al., 2014).

The amino acid alignment of VaHly8A, VaHly8B, and identified PL8 family enzymes showed that VaHly8A and VaHly8B contained the conserved catalytic residues of PL8

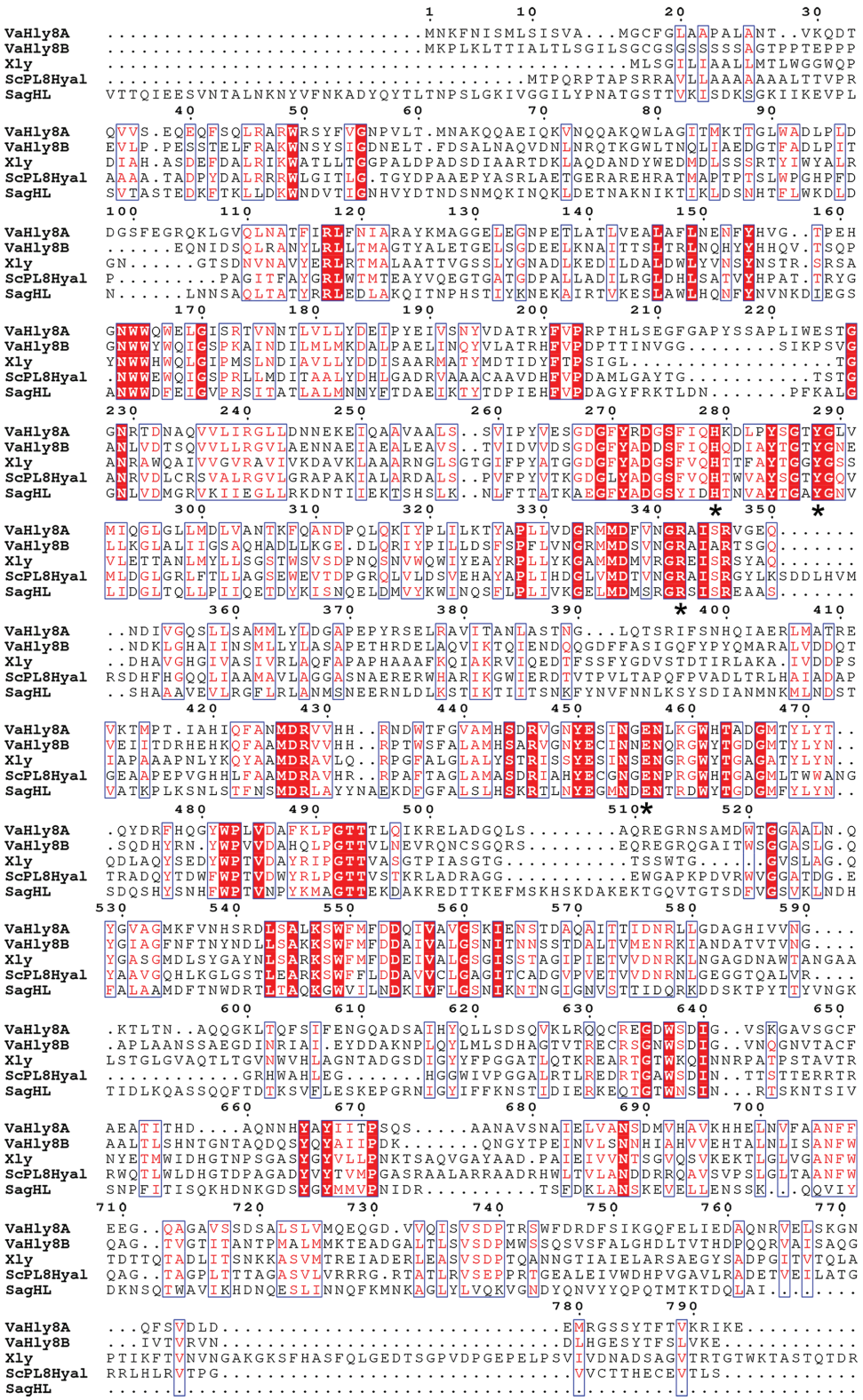

FIGURE 3 | Protein sequence alignment of VaHly8A and VaHly8B to the identified enzymes of the PL8 family. Red background represents the same amino acid residues and blue frames indicate amino acid residues with identity > 70%. The critical catalytic residues were highlighted by asterisks below them. Xly, from *Bacillus* sp. GL1, Genbank: BAB21059.1; ScPL8Hyl, from *Streptomyces coelicolor* A3(2), Genbank: CAA19982.1; SagHL, from *Streptococcus agalactiae* NEM316, Genbank: CAD46929.1.

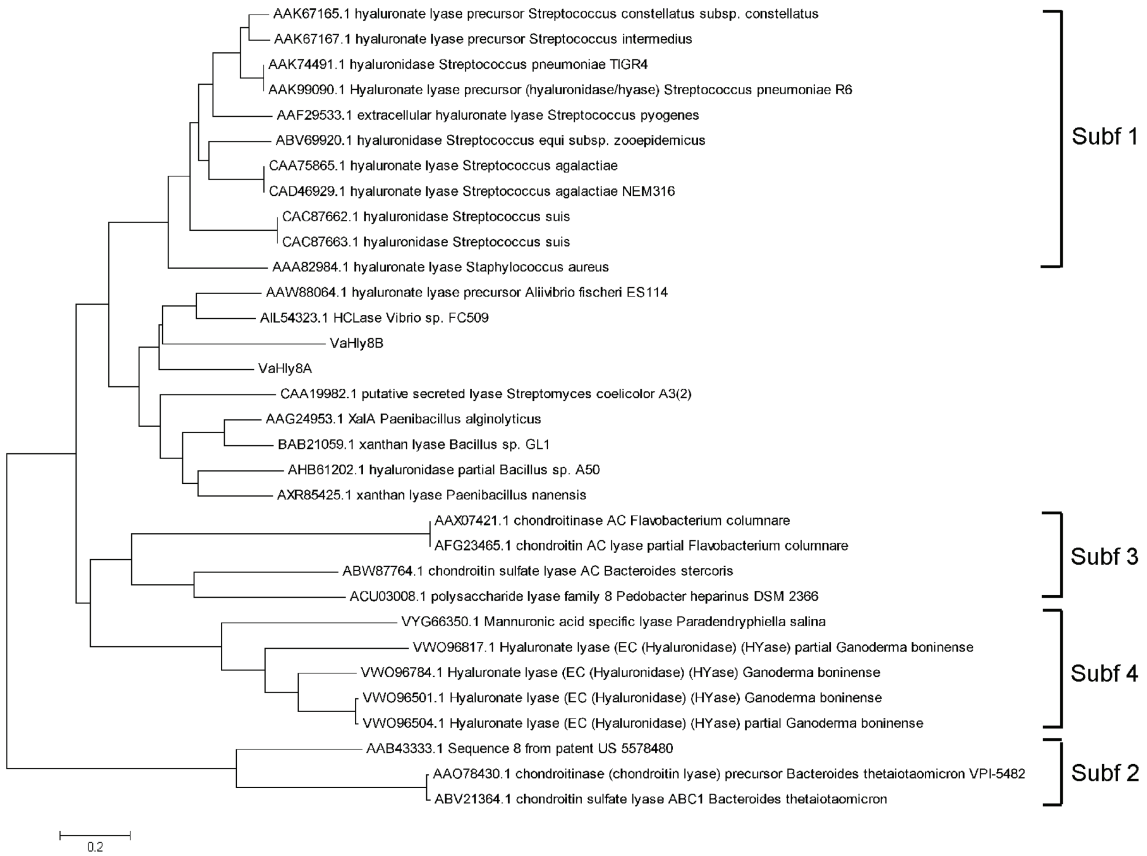

FIGURE 4 | Phylogenetic tree of VaHly8A, VaHly8B and other enzymes of the PL8 family. The phylogenetic tree was constructed by MEGA X using the neighbor-joining method.

family (His^{279}, Tyr^{288}, Arg^{342}, and Glu^{456} in VaHly8A; His^{271}, Tyr^{280}, Arg^{333}, and Glu^{451} in VaHly8B; **Figure 3**). Phylogenetic tree was constructed and the result (**Figure 4**) revealed that VaHly8A and VaHly8B were new members of the PL8 family.

Heterologous Expression of VaHly8A and VaHly8B in *E. coli*

The genes *vahly8A* and *vahly8B* were heterologously expressed in pET-28a (+)/*E. coli* BL21(DE3) system and successfully purified by Ni-affinity chromatography. SDS-PAGE showed that VaHly8A (**Figure 5A**) and VaHly8B (**Figure 5B**) purified to homogeneity with Mw of approximately 83 and 87 kDa, respectively, which had no significant difference with the predicted Mw. The specific activity of VaHly8A and VaHly8B were 223.65 and 26.38 U/mg, respectively.

Biochemical Properties of VaHly8A and VaHly8B

VaHly8A exhibited the maximal activity at 30°C (**Figure 6A**) and maintained over 90% original activity after incubation at temperatures from 0 to 20°C for 1 h (**Figure 6C**). VaHly8B showed the highest activity at 50°C (**Figure 6A**) and retained over 90% original activity after incubation at temperatures from 0 to 30°C for 1 h (**Figure 6C**). Compared with VaHly8B, VaHly8A had a lower optimal temperature and thermostability. The optimal pH of VaHly8A and VaHly8B was 7.05 in Tris-HCl buffer (**Figure 6B**). VaHly8A retained over 70% original activity after incubation at pH ranging from 5.0 to 10.6 for 6 h (**Figure 6D**). VaHly8B maintained over 70% original activity after incubation at pH ranging from 3.6 to 10.6 for 6 h. Despite the same optimal pH of VaHly8A and VaHly8B, VaHly8B showed higher activity and stability than VaHly8A under acidic conditions. The activity of VaHly8A was inhibited in the presence of NaCl (**Figure 6E**). However, VaHly8B is more tolerant of NaCl than VaHly8A, and the activity of VaHly8B reached the maximum when the concentration of NaCl was 100 mM. Mn^{2+}, Co^{2+}, and Ni^{2+} showed significantly stimulating effects on VaHly8B with 126.8, 134.5, and 142.0% of relative activity, respectively (**Figure 6F**). The activity of VaHly8A was not obviously enhanced by these metal ions, but inhibited by Co^{2+} and Ni^{2+}. The activities of both VaHly8A and VaHly8B were strongly inhibited by SDS. Besides, the activity of VaHly8A was strongly inhibited by Zn^{2+}. Other tested chemicals had no significant effect on both VaHly8A and VaHly8B. Overall, VaHly8B had higher resistance to metal ions than VaHly8A. As shown in **Table 1**, the K_m and k_{cat} of VaHly8A toward HA were 1.21 μM and 477.93 s^{-1}, respectively. The K_m and k_{cat} of VaHly8B toward HA were 0.78 μM and 54.59 s^{-1}, respectively.

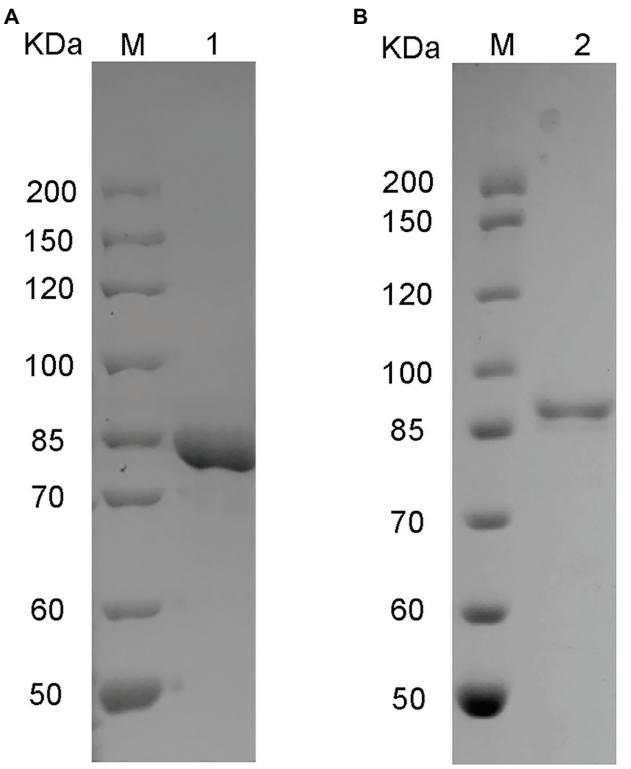

FIGURE 5 | Sodium dodecyl sulfate-polyacrylamide gel electrophoresis (SDS-PAGE) of purified recombinant VaHly8A **(A)** and VaHly8B **(B)**. Lane M, unstained protein molecular weight marker; lane 1, purified VaHly8A; and lane 2, purified VaHly8B.

Degradation Patterns and End Products of VaHly8A and VaHly8B

To investigate the degradation patterns of VaHly8A and VaHly8B, reaction products incubated for different time intervals were analyzed by the Superdex™ peptide 10/300 gel filtration column. The appearance of unsaturated oligosaccharides was detected using the absorbance at 232 nm. At the beginning of the reaction, products with high degree of polymerization were produced (**Figures 7A,B**). As the reaction continues, smaller oligomers continuously accumulated. The HA was completely digested after 6 h by VaHly8A and 12 h by VaHly8B (**Figures 7C,D**). These results indicated that both VaHly8A and VaHly8B acted in an endolytic manner.

To further obtain the exact molecular weight of the final products, the negative-ion ESI-MS was used (**Figures 7E,F**). Both main peaks in mass spectra were 378.10 m/z, corresponding to the molecular weight of unsaturated disaccharides. Therefore, VaHly8A and VaHly8B degraded HA to unsaturated disaccharides as the final products.

DISCUSSION

Hyaluronic acid-degrading bacteria are common in the marine ecosystem: a few studies previously reported hyaluronate lyase-encoding *bacilli* (Kurata et al., 2015) and *gammaproteobacterial* (Han et al., 2014; Peng et al., 2018). In this study, a hyaluronate lyase-producing marine bacterium, *V. alginolyticus* LWW-9, was isolated from seawater.

Based on the bioinformatic analysis, we discovered an enzymatic HA degradation system in *V. alginolyticus*. The organization of PUL_{HA} of *V. alginolyticus* closely resembles the HA PULs in *Firmicutes* and *Fusobacteria* (Oiki et al., 2017, 2019b; Kawai et al., 2018). However, compared with archetypal PULs of *Bacteroides*, PUL_{HA} lacks *susC/susD* pairs encoding a TBDT and a glycan-binding lipoprotein, respectively (Tancula et al., 1992; Reeves et al., 1997). SusC/SusD-like proteins are considered as the hallmark of PUL and have been used to identify PULs in the genomes of *Bacteroides*. In the genome of *V. alginolyticus*, no protein showing similarity with SusD was detected. Similar to other bacteria in *Proteobacteria*, *V. alginolyticus* contains TBDT proteins in the genome, which is the counterpart of SusC/SusD pairs in *Proteobacteria* (Blanvillain et al., 2007; Neumann et al., 2015). Blastp searches revealed that none of TBDTs identified in *V. alginolyticus* genome displayed high similarity with SusC. These results strongly support Blanvillain's opinion that TBDTs related to glycan uptake evolved independently in *Proteobacteria* and *Bacteroidetes* (Blanvillain et al., 2007).

The combination of genomic studies and biochemical characterizations of individual CAZymes can enhance our knowledge of the functions of PULs in microbial communities. Here, two hyaluronate lyases in the PUL_{HA}, VaHly8A, and VaHly8B, were heterologously expressed, purified, and characterized. VaHly8A has a type I signal peptide, whereas VaHly8B has a type II signal peptide, suggesting their different subcellular localization in the bacterial cells. Hence, VaHly8A is an extracellular enzyme, whereas VaHly8B is an outer membrane enzyme. Moreover, they show distinct biochemical properties. The survival and colonization of vibrios depend on their adaption to variable parameters of the aquatic habitats and respective hosts. From the perspective of evolution, the generation of these two hyaluronate lyases is the result of the strain's adaptation to environmental changes.

VaHly8A and VaHly8B exhibited the highest activity at 30 and 50°C, respectively. By contrast, the optimal temperatures of most identified enzymes of PL8 are 37–45°C (**Table 2**). VaHly8A was a cold-adapted hyaluronate lyase with lower optimal temperature and thermostability, which can conserve energy and reduce the risk of environmental contamination. Furthermore, it can be inactivated selectively by increasing the temperature slightly. Owing to these properties, the enzymatic reaction can be easily terminated and the product can be conveniently separated from the reaction mixture. Both VaHly8A and VaHly8B are most active at neutral pH, which is different from most characterized hyaluronate lyases from the PL8 family with the highest activity at acidic conditions (**Table 2**). VaHly8B retained about 70% activity at pH 3.6–10.6. Compared with most identified enzymes of PL8 (**Table 2**), VaHly8B was stable over a wider pH range. This property is advantageous for the storage of the enzyme preparation. Except SDS, most metal ions and EDTA did

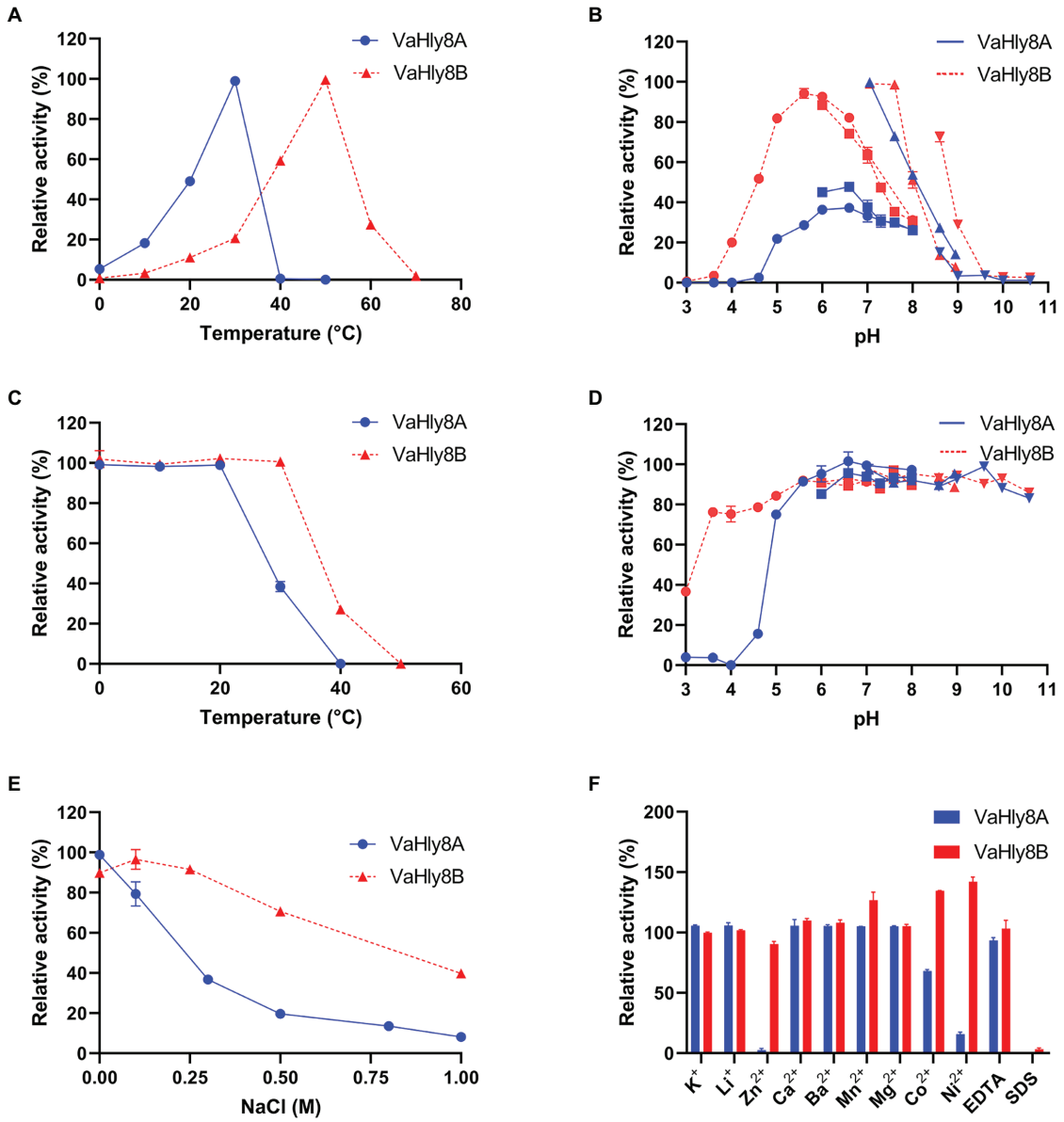

FIGURE 6 | Biochemical properties of the hyaluronate lyases VaHly8A and VaHly8B. **(A)** Effect of temperature. The enzyme activities of VaHly8A (1.69 μg/ml) and VaHly8B (9.76 μg/ml) were measured at 0–70°C. The highest specific activity of VaHly8A (106.70 U/mg) at 30°C and VaHly8B (17.57 U/mg) at 50°C were set as 100%. **(B)** Effect of pH. The enzyme activities of VaHly8A (1.13 μg/ml) and VaHly8B (6.62 μg/ml) were measured in 50 mM buffers, including Na_2HPO_4-Citrate buffer (pH 3.0–8.0; filled circles), NaH_2PO_4-Na_2HPO_4 buffer (pH 6.0–8.0; filled squares), Tris-HCl buffer (pH 7.05–8.95; positive triangles), and Glycine-NaOH buffer (pH 8.6–10.6; inverted triangles). The highest specific activity of VaHly8A (223.65 U/mg) and VaHly8B (23.70 U/mg) in Tris-HCl buffer (pH 7.05) was set as 100%. **(C)** Thermostability of VaHly8A and VaHly8B. The enzymes were incubated for 1 h at different temperatures (0–50°C), and the residual activities were measured at 30°C for VaHly8A (5.83 μg/ml) and 50°C for VaHly8B (55.50 μg/ml). The initial specific activity of VaHly8A (223.65 U/mg) and VaHly8B (23.70 U/mg) were set as 100%. **(D)** The pH stability of VaHly8A and VaHly8B. The enzymes were incubated in above buffers (pH 3.0–10.60) for 6 h at 0°C, and the residual activities were measured at 30°C for VaHly8A (10.73 μg/ml) and 50°C for VaHly8B (61.75 μg/ml). The initial specific activity of VaHly8A (223.65 U/mg) and VaHly8B (23.70 U/mg) were set as 100%. **(E)** Effect of NaCl. The enzyme activities were measured in Tris-HCl buffer (pH 7.05) containing different concentrations of NaCl ranging from 0 to 1.0 M at 30°C for VaHly8A (0.67 μg/ml) and 50°C for VaHly8B (4.39 μg/ml). The highest specific activity of VaHly8A (223.65 U/mg) without NaCl and VaHly8B (26.38 U/mg) in the presence of 0.1 M NaCl were set as 100%. **(F)** Effects of various compounds. The enzyme activities were measured in Tris-HCl buffer (pH 7.05) containing 1 mM various compounds at 30°C for VaHly8A (1.06 μg/ml) and 50°C for VaHly8B (3.60 μg/ml). The specific activity of VaHly8A (223.65 U/mg) and VaHly8B (26.38 U/mg) without tested compounds was set as 100%. Values represent the mean of three replicates ± SD.

not obviously inhibit the activity of VaHly8B. The result revealed that VaHly8B was resistant to many metal ions. VaHly8B can degrade HA in the complex environment, which is beneficial to its industrial application. The specific activity of hyaluronate lyases is generally tens to hundreds of units per milligram by A_{232} enzyme activity assay, such as HCLase

Er (13.8 U/mg) from *Vibrio* sp. FC509 (Peng et al., 2018), BniHL (136.7 U/mg) from *Bacillus niacin* (Kurata et al., 2015), and HAase (292.7 U/mg) from *Arthrobacter globiformis* A152 (Zhu et al., 2017a). In comparison, VaHly8A exhibited a higher specific activity. Our findings indicated that VaHly8A and VaHly8B are two hyaluronate lyases with novel enzymatic properties.

Hyaluronic acid exists extensively in diverse connective tissues and the nervous system of virtually all animals. *Vibrio alginolyticus*, a common pathogenic marine *Vibrio* species, is

TABLE 1 | Specific activity and kinetic parameters of VaHly8A and VaHly8B.

	Specific Activity (U·mg^{-1})	*Vmax* (μM·min^{-1})	*Km* (μM)	*Kcat* (s^{-1})	*kcat/Km* (s^{-1}·μM^{-1})
VaHly8A	223.65	10.61 ± 0.46	1.21 ± 0.14	477.93 ± 20.52	394.66 ± 62.61
VaHly8B	26.38	0.10 ± 0.00	0.78 ± 0.06	54.59 ± 1.18	69.98 ± 6.89

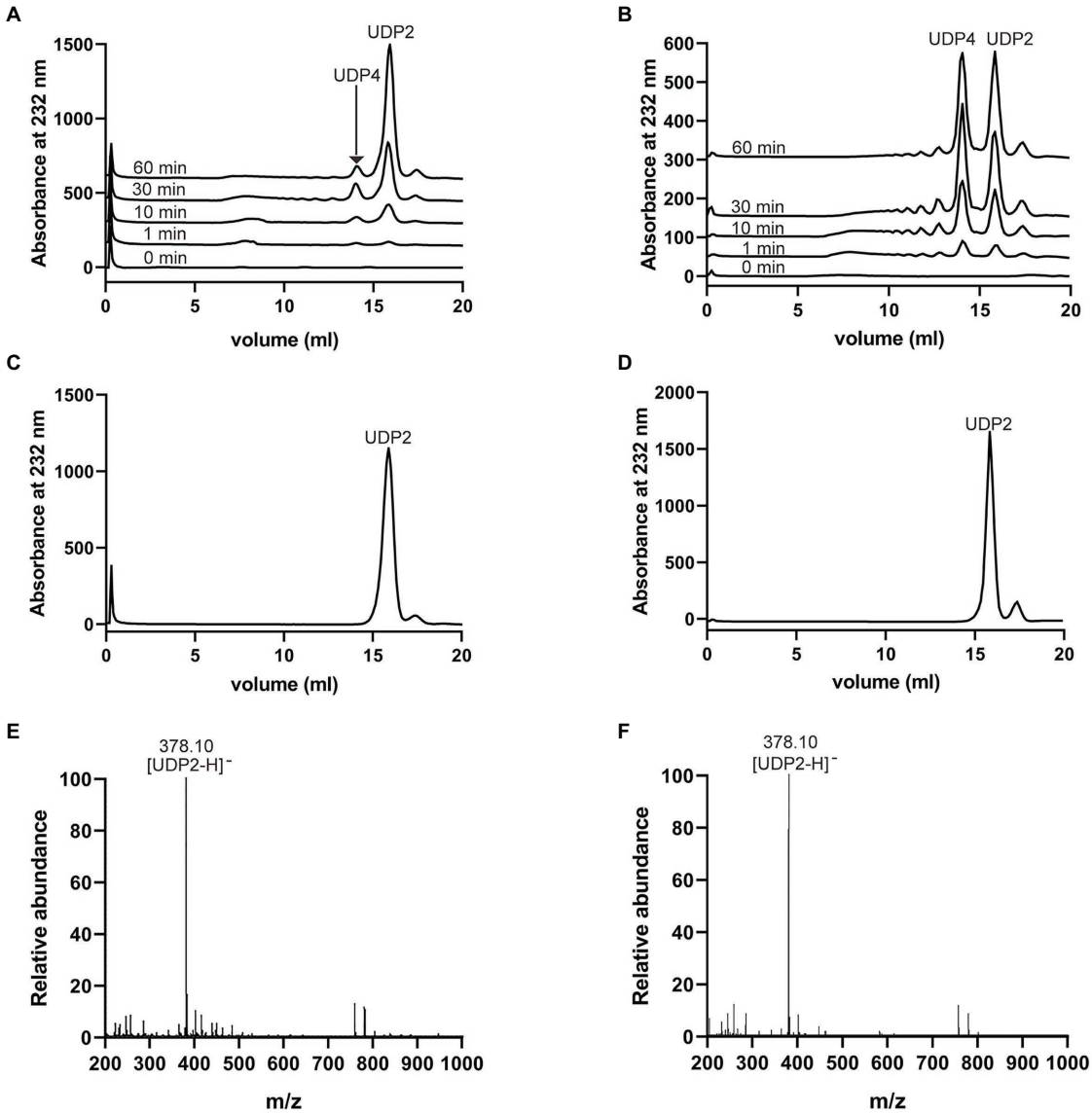

FIGURE 7 | Action modes and final products of VaHly8A and VaHly8B. **(A)** Time-course treatment of HA using VaHly8A at 30°C. **(B)** Time-course treatment of HA using VaHly8B at 50°C. Analysis of the final products of HA digested by VaHly8A **(C)** and VaHly8B **(D)** using gel filtration chromatography with a Superdex™ peptide 10/300 gel filtration column. Electrospray ionization-mass spectroscopy (ESI-MS) analysis of the final products of HA digested by VaHly8A **(E)** and VaHly8B **(F)**.

TABLE 2 | Comparison of the biochemical properties of VaHly8A and VaHly8B with other PL8 family enzymes.

Enzyme	Source	Optimal temperature (°C)	Optimal pH	pH stability	References
VaHly8A	*Vibrio alginolyticus* LWW-9	30	7.05	5.6–10.6	This study
VaHly8B	*Vibrio alginolyticus* LWW-9	50	7.05	3.6–10.6	This study
HylB	*Streptococcus zooepidemicus* ATCC39920	37	6	N/A	Sun et al., 2015
HAase	*Arthrobacter globiformis* A152	42	4	4–10	Zhu et al., 2017a
HAase-B	*Bacillus* sp. A50	44	6.5	5–7	Guo et al., 2014
BniHL	*Bacillus niacini*	45	6	6–10	Kurata et al., 2015
ScPL8H	*Streptomyces coelicolor* A3(2)	57	5.2	N/A	Elmabrouk et al., 2011
HCLase	*Vibrio* sp. FC509	30	8	N/A	Han et al., 2014
Vpa_0049	*Vibrio* sp. QY108	30	8	7–10.6	Zhang et al., 2020
HCLaseM	*Microbacterium* sp. H14	40	7	5–9	Sun et al., 2019
ChSase ABC	*Acinetobacter* sp. C26	42	6	5–10	Zhu et al., 2017b
ChonABC	Bacteroides thetaiotaomicron WAL2926	37	7.6	N/A	Shaya et al., 2008
ChSase ABC	*Sphingomonas paucimobilis*	40	6.5	N/A	Fu et al., 2018
cABC I	*Proteus vulgaris*	37	8	N/A	Hamai et al., 1997
AsChnAC	*Arthrobacter* sp.	37	7.2	N/A	Yin et al., 2016
ChSase AC	*Flavobacterium heparinum*	40	6.8	N/A	Gu et al., 1995
ChSase AC II	*Arthrobacter* sp. CS01	37	6.5	4.5–8.5	Fang et al., 2019
ChSase AC	*Bacteroides stercoris*	45–50	5.7–6.0	N/A	Hong et al., 2002

N/A, There are no clear data in the reference.

not only an emerging pathogen inducing human infection but also a common cause of economic loss in the aquaculture industry (Cao et al., 2018). *Vibrio alginolyticus* secrets extracellular and cell-surface hyaluronate lyases to degrade HA, leading to the breakdown of biophysical barrier of the host tissues and exposure of host cells to bacterial toxins. The degradation of HA promotes the invasion and spreading of *V. alginolyticus* in the host. Therefore, the PUL$_{HA}$ of *V. alginolyticus* reflects the bacterial ability to utilize the given glycan as a nutrient source for survival and to produce the "spreading factors" hyaluronate lyases for colonization.

Currently, antibiotics have been mainly used to resolve *V. alginolyticus*-related diseases (Grimes, 2020). However, the long-term use of antibiotics may result in harmful consequences, such as antibiotic residues and drug resistance (Langdon et al., 2016). Thus, finding an effective alternative method to regulate *V. alginolyticus* infection is highly significant. The functional characterization of PUL$_{HA}$ broadens our knowledge about the physiology and pathogenicity of *V. alginolyticus* and enables the development of novel preventive and therapeutic strategies against *V. alginolyticus*-associated infection.

In summary, we reported the discovery and characterization of a PUL that orchestrates the utilization of HA in a marine bacterium *V. alginolyticus* LWW-9. The PLs, GH, and enzymes related to monosaccharide metabolism encoded by PUL$_{HA}$ provide an example of how *V. alginolyticus* completely degrade HA. The presence of two novel hyaluronate lyases with distinct biochemical properties provides critical insights into how *V. alginolyticus* adapts to variable parameters of the aquatic habitats and hosts for survival and colonization. Our report strengthens the previous proposition (Blanvillain et al., 2007) that TBDTs related to glycan uptake evolved independently in *Proteobacteria* and *Bacteroidetes*. Furthermore, the functional characterization of PUL$_{HA}$ facilitates the illustration of physiology and pathogenicity of *V. alginolyticus* and promotes the development of alternative non-antibiotic-based means of controlling bacterial infections.

DATA AVAILABILITY STATEMENT

The datasets presented in this study can be found in online repositories. The names of the repository/repositories and accession number(s) can be found at: NCBI (accession: MW396717).

AUTHOR CONTRIBUTIONS

WY and FH: conceptualization. XW: methodology, investigation, and writing – original draft preparation. ZW and YL: investigation and data curation. HW: software and data curation. All authors contributed to the article and approved the submitted version.

FUNDING

This work was supported by the National Key R&D Program of China (2018YFC0311105), Shandong Provincial Natural Science Foundation (major basic research projects; ZR2019ZD18), and the Marine S&T Fund of Shandong Province for Pilot National Laboratory for Marine Science and Technology (Qingdao; 2018SDKJ0401-2).

SUPPLEMENTARY MATERIAL

The Supplementary Material for this article can be found online at: https://www.frontiersin.org/articles/10.3389/fmicb.2021.696096/full#supplementary-material

REFERENCES

Austin, B. (2010). Vibrios as causal agents of zoonoses. *Vet. Microbiol.* 140, 310–317. doi: 10.1016/j.vetmic.2009.03.015

Blanvillain, S., Meyer, D., Boulanger, A., Lautier, M., Guynet, C., Denance, N., et al. (2007). Plant carbohydrate scavenging through tonB-dependent receptors: a feature shared by phytopathogenic and aquatic bacteria. *PLoS One* 2:e224. doi: 10.1371/journal.pone.0000224

Cao, J., Zhang, J., Ma, L., Li, L., Zhang, W., and Li, J. (2018). Identification of fish source *Vibrio alginolyticus* and evaluation of its bacterial ghosts vaccine immune effects. *Microbiologyopen* 7:e00576. doi: 10.1002/mbo3.576

Dechet, A. M., Yu, P. A., Koram, N., and Painter, J. (2008). Nonfoodborne Vibrio infections: an important cause of morbidity and mortality in the United States, 1997-2006. *Clin. Infect. Dis.* 46, 970–976. doi: 10.1086/529148

Elmabrouk, Z. H., Vincent, F., Zhang, M., Smith, N. L., Turkenburg, J. P., Charnock, S. J., et al. (2011). Crystal structures of a family 8 polysaccharide lyase reveal open and highly occluded substrate-binding cleft conformations. *Proteins* 79, 965–974. doi: 10.1002/prot.22938

Fang, Y., Yang, S., Fu, X., Xie, W., Li, L., Liu, Z., et al. (2019). Expression, purification and characterization of chondroitinase AC II from marine bacterium Arthrobacter sp. CS01. *Mar. Drugs* 17:185. doi: 10.3390/md17030185

Finn, R. D., Bateman, A., Clements, J., Coggill, P., Eberhardt, R. Y., Eddy, S. R., et al. (2014). Pfam: the protein families database. *Nucleic Acids Res.* 42, D222–D230. doi: 10.1093/nar/gkt1223

Fu, J., Jiang, Z., Chang, J., Han, B., Liu, W., and Peng, Y. (2018). Purification, characterization of Chondroitinase ABC from Sphingomonas paucimobilis and in vitro cardiocytoprotection of the enzymatically degraded CS-A. *Int. J. Biol. Macromol.* 115, 737–745. doi: 10.1016/j.ijbiomac.2018.04.117

Grimes, D. J. (2020). The vibrios: scavengers, symbionts, and pathogens from the sea. *Microb. Ecol.* 80, 501–506. doi: 10.1007/s00248-020-01524-7

Grondin, J. M., Tamura, K., Déjean, G., Abbott, D. W., and Brumer, H. (2017). Polysaccharide utilization loci: fueling microbial communities. *J. Bacteriol.* 199, e00860–e00816. doi: 10.1128/jb.00860-16

Gu, K., Linhardt, R. J., Laliberté, M., Gu, K., and Zimmermann, J. (1995). Purification, characterization and specificity of chondroitin lyases and glycuronidase from Flavobacterium heparinum. *Biochem. J.* 312, 569–577. doi: 10.1042/bj3120569

Guo, X., Shi, Y., Sheng, J., and Wang, F. (2014). A novel hyaluronidase produced by *Bacillus* sp. A50. *PLoS One* 9:e94156. doi: 10.1371/journal.pone.0094156

Hamai, A., Hashimoto, N., Mochizuki, H., Kato, F., Makiguchi, Y., Horie, K., et al. (1997). Two distinct chondroitin sulfate ABC lyases. An endoeliminase yielding tetrasaccharides and an exoeliminase preferentially acting on oligosaccharides. *J. Biol. Chem.* 272, 9123–9130. doi: 10.1074/jbc.272.14.9123

Han, W., Wang, W., Zhao, M., Sugahara, K., and Li, F. (2014). A novel eliminase from a marine bacterium that degrades hyaluronan and chondroitin sulfate. *J. Biol. Chem.* 289, 27886–27898. doi: 10.1074/jbc.M114.590752

Hong, S. W., Kim, B. T., Shin, H. Y., Kim, W. S., Lee, K. S., Kim, Y. S., et al. (2002). Purification and characterization of novel chondroitin ABC and AC lyases from Bacteroides stercoris HJ-15, a human intestinal anaerobic bacterium. *Eur. J. Biochem.* 269, 2934–2940. doi: 10.1046/j.1432-1033.2002.02967.x

Ina-Salwany, M. Y., Al-Saari, N., Mohamad, A., Mursidi, F. A., Mohd-Aris, A., Amal, M. N. A., et al. (2019). Vibriosis in fish: a review on disease development and prevention. *J. Aquat. Anim. Health* 31, 3–22. doi: 10.1002/aah.10045

Kawai, K., Kamochi, R., Oiki, S., Murata, K., and Hashimoto, W. (2018). Probiotics in human gut microbiota can degrade host glycosaminoglycans. *Sci. Rep.* 8:10674. doi: 10.1038/s41598-018-28886-w

Kumar, S., Stecher, G., Li, M., Knyaz, C., and Tamura, K. (2018). MEGA X: molecular evolutionary genetics analysis across computing platforms. *Mol. Biol. Evol.* 35, 1547–1549. doi: 10.1093/molbev/msy096

Kurata, A., Matsumoto, M., Kobayashi, T., Deguchi, S., and Kishimoto, N. (2015). Hyaluronate lyase of a deep-sea *Bacillus niacini*. *Mar. Biotechnol.* 17, 277–284. doi: 10.1007/s10126-015-9618-z

Langdon, A., Crook, N., and Dantas, G. (2016). The effects of antibiotics on the microbiome throughout development and alternative approaches for therapeutic modulation. *Genome Med.* 8:39. doi: 10.1186/s13073-016-0294-z

Li, S., and Jedrzejas, M. J. (2001). Hyaluronan binding and degradation by *Streptococcus agalactiae* hyaluronate lyase. *J. Biol. Chem.* 276, 41407–41416. doi: 10.1074/jbc.M106634200

Lin, B., Hollingshead, S. K., Coligan, J. E., Egan, M. L., Baker, J. R., and Pritchard, D. G. (1994). Cloning and expression of the gene for group B streptococcal hyaluronate lyase. *J. Biol. Chem.* 269, 30113–30116. doi: 10.1016/S0021-9258(18)43783-0

Lombard, V., Golaconda Ramulu, H., Drula, E., Coutinho, P. M., and Henrissat, B. (2014). The carbohydrate-active enzymes database (CAZy) in 2013. *Nucleic Acids Res.* 42, D490–D495. doi: 10.1093/nar/gkt1178

Margulies, M., Egholm, M., Altman, W. E., Attiya, S., Bader, J. S., Bemben, L. A., et al. (2005). Genome sequencing in microfabricated high-density picolitre reactors. *Nature* 437, 376–380. doi: 10.1038/nature03959

Martens, E. C., Koropatkin, N. M., Smith, T. J., and Gordon, J. I. (2009). Complex glycan catabolism by the human gut microbiota: the Bacteroidetes sus-like paradigm. *J. Biol. Chem.* 284, 24673–24677. doi: 10.1074/jbc.R109.022848

Maruyama, Y., Oiki, S., Takase, R., Mikami, B., Murata, K., and Hashimoto, W. (2015). Metabolic fate of unsaturated glucuronic/iduronic acids from glycosaminoglycans: molecular identification and structure determination of streptococcal isomerase and dehydrogenase. *J. Biol. Chem.* 290, 6281–6292. doi: 10.1074/jbc.M114.604546

Neumann, A. M., Balmonte, J. P., Berger, M., Giebel, H. A., Arnosti, C., Voget, S., et al. (2015). Different utilization of alginate and other algal polysaccharides by marine Alteromonas macleodii ecotypes. *Environ. Microbiol.* 17, 3857–3868. doi: 10.1111/1462-2920.12862

Oiki, S., Mikami, B., Maruyama, Y., Murata, K., and Hashimoto, W. (2017). A bacterial ABC transporter enables import of mammalian host glycosaminoglycans. *Sci. Rep.* 7:1069. doi: 10.1038/s41598-017-00917-y

Oiki, S., Nakamichi, Y., Maruyama, Y., Mikami, B., Murata, K., and Hashimoto, W. (2019a). Streptococcal phosphotransferase system imports unsaturated hyaluronan disaccharide derived from host extracellular matrices. *PLoS One* 14:e0224753. doi: 10.1371/journal.pone.0224753

Oiki, S., Sato, M., Mikami, B., Murata, K., and Hashimoto, W. (2019b). Substrate recognition by bacterial solute-binding protein is responsible for import of extracellular hyaluronan and chondroitin sulfate from the animal host. *Biosci. Biotechnol. Biochem.* 83, 1946–1954. doi: 10.1080/09168451.2019.1630250

Patil, S., and Chaudhari, B. (2017). A simple, rapid and sensitive plate assay for detection of microbial hyaluronidase activity. *J. Basic Microbiol.* 57, 358–361. doi: 10.1002/jobm.201600579

Peng, C., Wang, Q., Wang, S., Wang, W., Jiao, R., Han, W., et al. (2018). A chondroitin sulfate and hyaluronic acid lyase with poor activity to glucuronyl 4,6-O-disulfated N-acetylgalactosamine (E-type)-containing structures. *J. Biol. Chem.* 293, 4230–4243. doi: 10.1074/jbc.RA117.001238

Reeves, A. R., Wang, G. R., and Salyers, A. A. (1997). Characterization of four outer membrane proteins that play a role in utilization of starch by Bacteroides thetaiotaomicron. *J. Bacteriol.* 179, 643–649. doi: 10.1128/JB.179.3.643-649.1997

Robert, X., and Gouet, P. (2014). Deciphering key features in protein structures with the new ENDscript server. *Nucleic Acids Res.* 42, W320–W324. doi: 10.1093/nar/gku316

Ruijssenaars, H. J., de Bont, J. A., and Hartmans, S. (1999). A pyruvated mannose-specific xanthan lyase involved in xanthan degradation by *Paenibacillus alginolyticus* XL-1. *Appl. Environ. Microbiol.* 65, 2446–2452. doi: 10.1128/AEM.65.6.2446-2452.1999

Shaya, D., Hahn, B. S., Park, N. Y., Sim, J. S., Kim, Y. S., and Cygler, M. (2008). Characterization of chondroitin sulfate lyase ABC from Bacteroides thetaiotaomicron WAL2926. *Biochemistry* 47, 6650–6661. doi: 10.1021/bi800353g

Sudha, P. N., and Rose, M. H. (2014). Beneficial effects of hyaluronic acid. *Adv. Food Nutr. Res.* 72, 137–176. doi: 10.1016/b978-0-12-800269-8.00009-9

Sun, J., Han, X., Song, G., Gong, Q., and Yu, W. (2019). Cloning, expression, and characterization of a new glycosaminoglycan lyase from microbacterium sp. H14. *Mar. Drugs* 17:681. doi: 10.3390/md17120681

Sun, X., Wang, Z., Bi, Y., Wang, Y., and Liu, H. (2015). Genetic and functional characterization of the hyaluronate lyase HylB and the beta-N-acetylglucosaminidase HylZ in Streptococcus zooepidemicus. *Curr. Microbiol.* 70, 35–42. doi: 10.1007/s00284-014-0679-4

Tancula, E., Feldhaus, M. J., Bedzyk, L. A., and Salyers, A. A. (1992). Location and characterization of genes involved in binding of starch to the surface of Bacteroides thetaiotaomicron. *J. Bacteriol.* 174, 5609–5616. doi: 10.1128/JB.174.17.5609-5616.1992

Theocharis, A. D., Skandalis, S. S., Gialeli, C., and Karamanos, N. K. (2016). Extracellular matrix structure. *Adv. Drug Deliv. Rev.* 97, 4–27. doi: 10.1016/j.addr.2015.11.001

Volpi, N., Schiller, J., Stern, R., and Soltés, L. (2009). Role, metabolism, chemical modifications and applications of hyaluronan. *Curr. Med. Chem.* 16, 1718–1745. doi: 10.2174/092986709788186138

Wang, W., Wang, J., and Li, F. (2017). Hyaluronidase and chondroitinase. *Adv. Exp. Med. Biol.* 925, 75–87. doi: 10.1007/5584_2016_54

Yin, F. X., Wang, F. S., and Sheng, J. Z. (2016). Uncovering the catalytic direction of chondroitin AC exolyase: from the reducing end towards the non-reducing end. *J. Biol. Chem.* 291, 4399–4406. doi: 10.1074/jbc.C115.708396

Zhang, Z., Su, H., Wang, X., Tang, L., Hu, J., Yu, W., et al. (2020). Cloning and characterization of a novel chondroitinase ABC categorized into a new subfamily of polysaccharide lyase family 8. *Int. J. Biol. Macromol.* 164, 3762–3770. doi: 10.1016/j.ijbiomac.2020.08.210

Zhang, H., Yohe, T., Huang, L., Entwistle, S., Wu, P., Yang, Z., et al. (2018). dbCAN2: a meta server for automated carbohydrate-active enzyme annotation. *Nucleic Acids Res.* 46, W95–w101. doi: 10.1093/nar/gky418

Zhu, C., Zhang, J., Li, L., Zhang, J., Jiang, Y., Shen, Z., et al. (2017a). Purification and characterization of hyaluronate lyase from Arthrobacter globiformis A152. *Appl. Biochem. Biotechnol.* 182, 216–228. doi: 10.1007/s12010-016-2321-3

Zhu, C., Zhang, J., Zhang, J., Jiang, Y., Shen, Z., Guan, H., et al. (2017b). Purification and characterization of chondroitinase ABC from Acinetobacter sp. C26. *Int. J. Biol. Macromol.* 95, 80–86. doi: 10.1016/j.ijbiomac.2016.10.044

Conflict of Interest: The authors declare that the research was conducted in the absence of any commercial or financial relationships that could be construed as a potential conflict of interest.

frontiers in Microbiology

ORIGINAL RESEARCH
published: 14 July 2021
doi: 10.3389/fmicb.2021.708480

Carbohydrate-Binding Module and Linker Allow Cold Adaptation and Salt Tolerance of Maltopentaose-Forming Amylase From Marine Bacterium *Saccharophagus degradans* 2-40^T

Ning Ding[1,2,3], Boyang Zhao[4], Xiaofeng Ban[1,2,3], Caiming Li[1,2,3], B. V. Venkataram Prasad[4,5], Zhengbiao Gu[1,2,3] and Zhaofeng Li[1,2,3]**

[1] State Key Laboratory of Food Science and Technology, Jiangnan University, Wuxi, China, [2] School of Food Science and Technology, Jiangnan University, Wuxi, China, [3] Collaborative Innovation Center for Food Safety and Quality Control, Jiangnan University, Wuxi, China, [4] Department of Molecular Virology and Microbiology, Baylor College of Medicine, Houston, TX, United States, [5] The Verna and Marrs McLean Department of Biochemistry and Molecular Biology, Baylor College of Medicine, Houston, TX, United States

OPEN ACCESS

Edited by:
Benwei Zhu,
Nanjing Tech University, China

Reviewed by:
Feng Han,
Ocean University of China, China
Hui Ni,
Jimei University, China

***Correspondence:**
Zhengbiao Gu
zhengbiaogu@jiangnan.edu.cn
Zhaofeng Li
zfli@jiangnan.edu.cn

Specialty section:
This article was submitted to Microbiotechnology, a section of the journal Frontiers in Microbiology

Received: 12 May 2021
Accepted: 21 June 2021
Published: 14 July 2021

Citation:
Ding N, Zhao B, Ban X, Li C, Venkataram Prasad BV, Gu Z and Li Z (2021) Carbohydrate-Binding Module and Linker Allow Cold Adaptation and Salt Tolerance of Maltopentaose-Forming Amylase From Marine Bacterium Saccharophagus degradans 2-40^T. Front. Microbiol. 12:708480. doi: 10.3389/fmicb.2021.708480

Marine extremophiles produce cold-adapted and/or salt-tolerant enzymes to survive in harsh conditions. These enzymes are naturally evolved with unique structural features that confer a high level of flexibility, solubility and substrate-binding ability compared to mesophilic and thermostable homologs. Here, we identified and characterized an amylase, SdG5A, from the marine bacterium *Saccharophagus degradans* 2-40^T. We expressed the protein in *Bacillus subtilis* and found that the purified SdG5A enabled highly specific production of maltopentaose, an important health-promoting food and nutrition component. Notably, SdG5A exhibited outstanding cold adaptation and salt tolerance, retaining approximately 30 and 70% of its maximum activity at 4°C and in 3 M NaCl, respectively. It converted 68 and 83% of starch into maltooligosaccharides at 4 and 25°C, respectively, within 24 h, with 79% of the yield being the maltopentaose. By analyzing the structure of SdG5A, we found that the C-terminal carbohydrate-binding module (CBM) coupled with an extended linker, displayed a relatively high negative charge density and superior conformational flexibility compared to the whole protein and the catalytic domain. Consistent with our bioinformatics analysis, truncation of the linker-CBM region resulted in a significant loss in activities at low temperature and high salt concentration. This highlights the linker-CBM acting as the critical component for the protein to carry out its activity in biologically unfavorable condition. Together, our study indicated that these unique properties of SdG5A have great potential for both basic research and industrial applications in food, biology, and medical and pharmaceutical fields.

Keywords: marine, cold adaptation, salt tolerance, maltopentaose, amylase, carbohydrate-binding module, linker

INTRODUCTION

Maltooligosaccharides are important carbohydrate sources due to their ability to control glycemic response, regulate the immune system, and improve the colonic condition or gut microbiota in humans (Zhu et al., 2011; Nguyen and Haltrich, 2013; Chegeni and Hamaker, 2015; Huang et al., 2019). Structurally, they consist of 3–10 α-D-glucopyranosyl units linked by α-1,4 glycosidic bonds. Given their high water solubility, mild sweetness, and suitable viscosity, maltooligosaccharides are considered palatable and superior nutrient foods for the aged and infants (Pan et al., 2017). In particular, maltopentaose (G5), which contains five glucosyl units, is essential in medical and pharmaceutical fields for its use as a dietary nutrient for patients having renal failure or calorie deprivation and as a diagnostic reagent for the detection of α-amylase in serum and urine (Kandra, 2003; Wang et al., 2015). Therefore, the discovery of natural or engineered enzymes that can efficiently produce G5 is of great interest for both industrial and clinical settings.

However, microbial amylases known to specifically produce G5 are rare and the optimum temperatures of most maltopentaose-forming amylases (G5As) were found to be in the range of 60–93°C (Morgan and Priest, 1981; Hatada et al., 2006; Jana et al., 2013). Although the high temperature could increase reaction rates and mass transfer, and reduce viscosity, the processes are energy- and power-intensive and contribute significantly to CO_2 emissions. Besides, high-temperature production might cause undesirable Maillard reaction, impair the physicochemical properties and nutritional value of maltooligosaccharides (Patel and Goyal, 2011). Hence, discovering G5As that enable efficiently producing G5 at low or room temperature is important. Interestingly, extremophiles, microorganisms that grow in extreme environmental conditions, were found to occasionally produce cold-adapted and/or salt-tolerant amylases evolved with unique structural features and physiological properties. These have provided economic and environmental advantages for their industrial applications (Sarmiento et al., 2015; Siddiqui, 2015; Santiago et al., 2016). For example, by using the cold-adapted amylases in the cleaning and detergent industry, a decrease of washing temperature from 40 to 30°C could reduce 30% electricity consumption and a further decrease of the temperature to 20°C has been expected to reduce CO_2 emissions by half (Siddiqui, 2015). Moreover, salt-tolerant amylases have been applied to starch saccharification that used renewable, sustainable and economical marine microalgae as the substrate (Matsumoto et al., 2003; Karan et al., 2012).

Marine extremophiles and their secreted extremozymes including amylases have been of increasing interest because of their outstanding cold adaptability and salt tolerance (Liu et al., 2011; Qin et al., 2014; Jin et al., 2019; Zhu et al., 2020). *Saccharophagus degradans* 2-40^T (Sde 2-40) is a marine bacterium considered to be one of the most versatile polysaccharide-degrading organisms (Weiner et al., 2008). The complete genome of Sde 2-40 has been recently sequenced with the putative function of 128 genes encoding glycoside hydrolases being annotated (Weiner et al., 2008; Hutcheson et al., 2011). A distinct and common feature found in these enzymes is the wide presence of carbohydrate-binding module (CBM), suggesting the possible role of CBM on adapting to the marine environment and capturing the polysaccharides substrates in this highly dilute aqueous system (Weiner et al., 2008). As the CBM-containing enzymes from Sde 2-40 such as agarose, alginate lyase, xylanase, and glucanase have been successively studied to show their relatively high activities at low temperature and/or high salt concentration, we expect Sde 2-40 might be a potential producer of extremozymes (Kim et al., 2010, 2012; Ko et al., 2016; Wang et al., 2016).

In this study, we cloned a gene (*sdg5a*) encoding maltopentaose-forming amylase from Sde 2-40 (SdG5A) and expressed the recombinant SdG5A in *Bacillus subtilis*. SdG5A displayed strong product specificity of G5 with characteristics of cold adaptability, alkali stability, and salt tolerance. Further, these unique properties were examined to be attributed to the presence of CBM in SdG5A. Together, our findings provide valuable information for both basic and applied research concerning the discovery and molecular mechanisms of marine extremozymes as well as energy-efficient and economically profitable production of G5.

MATERIALS AND METHODS

Bacterial Strains and Reagents

Escherichia coli JM109 and *B. subtilis* WB600 were used for recombinant DNA manipulations and protein production, respectively. Expression plasmid pST was obtained from laboratory stock. Maltooligosaccharides standards were purchased from Hayashibara Co., Ltd. (Okayama, Japan).

Gene Cloning of *sdg5a* and *sdg5a-cad*

SdG5A was encoded by gene *sdg5a* with GenBank accession of AIV43244.1. The plasmid *sdg5a*/pST was constructed by amplifying the synthesized *sdg5a* gene (GENEWIZ, Suzhou, China) followed by In-Fusion cloning (Takara, Tokyo, Japan) with pST vector. To truncate the C-terminal region (Ile^{428}-Phe^{542}) of SdG5A and construct *sdg5a-cad*/pST, we first amplified the insert encoding the N-terminal region of SdG5A (Gln^1-Ala^{427}) with 20-bp homologous overlaps and pST vector simultaneously, and then assembled the two fractions by In-Fusion cloning. The assembled constructs *sdg5a*/pST and *sdg5a-cad*/pST were transformed into *E. coli* JM109 competent cells.

Abbreviations: AHA, α-amylases from *Alteromonas haloplanctis*; BraG3A, maltotriose-forming amylase from *Brachybacterium* sp. LB25; CBM, carbohydrate-binding module; CorG6A, maltohexaose-forming amylase from *Corallococcus* sp. EGB; DNS, 3,5-dinitrosalicylic acid; G3A, maltotriose-forming amylase; G4A, maltotetraose-forming amylase; G5, maltopentaose; G5A, maltopentaose-forming amylase; G6A, maltohexaose-forming amylase; HPAEC, high-performance anion-exchange chromatographic; KitG3A, maltotriose-forming amylase from *Kitasatospora* sp. MK-1785; MFA, maltooligosaccharide-forming amylase; PAD, pulsed amperometry detector; PseG5A, maltopentaose-forming amylase from *Pseudomonas* sp. KO-8940; PstG4A, maltotetraose-forming amylase from *Pseudomonas stutzeri* MO-19; Sde 2-40, *Saccharophagus degradans* 2-40^T; SdG5A, maltopentaose-forming amylase from *Saccharophagus degradans* 2-40^T; SDS-PAGE, sodium dodecyl sulfate-polyacrylamide gel electrophoresis; ZPA, α-amylases from *Zunongwangia profunda*.

Plasmids were extracted using QIAprep Spin Miniprep Kit (Qiagen, Shanghai, China) and transformed into *B. subtilis* WB600 competent cells for producing SdG5A and SdG5A-CAD, respectively.

Expression and Purification of Recombinant SdG5A

Recombinant *B. subtilis* WB600 was inoculated into LB medium supplemented with kanamycin (50 μg mL^{-1}) and grown at 37°C overnight in an orbital shaker at 220 rpm. The overnight culture was then inoculated into expression medium (36 g L^{-1} yeast extract, 0.17 M KH_2PO_4, 0.72 M K_2HPO_4, 10 g L^{-1} NaCl, pH 6.5) supplemented with kanamycin (50 μg mL^{-1}) and incubated with shaking (220 rpm) at 25°C for 60 h. The extracellular crude enzymes were harvested by centrifugation at 10,000 × *g* for 30 min at 4°C.

Protein purification was performed using an ÄKTA purifier liquid chromatography system (Amersham Biosciences, Uppsala, Sweden). The supernatant containing crude protein was loaded onto a phenyl superose column (HR 10/10; Amersham Biosciences, Piscataway, NJ, United States) that had been pre-equilibrated with 20% $(NH_4)_2SO_4$ in buffer A (20 mM phosphate buffer, pH 7.0). The column was eluted using distilled, deionized H_2O at flow rate of 1 mL min^{-1}. The active fractions were collected and loaded onto a Superdex 75 10/300 GL gel filtration column (GE Healthcare Biosciences AB, Uppsala, Sweden) that had been pre-equilibrated with buffer A, and then eluted with distilled, deionized H_2O. Purified proteins were dialyzed against 10 mM phosphate buffer (pH 6.5) at 4°C for 24 h and determined on SDS-PAGE.

Enzyme Activity Assay

SdG5A activity was measured by determining the reducing sugars released from the hydrolysis of starch using the 3,5-dinitrosalicylic acid (DNS) method (Miller, 1959). The reaction mixture containing 0.2 mL of appropriately diluted enzyme and 1.8 mL of 1.0% (w/v) soluble starch (Sinapharm Chemical Reagent, Shanghai, China) in 50 mM $C_4H_2O_7$–Na_2HPO_4 buffer (pH 6.5), was incubated at 45°C for 15 min, quenched by adding 2.0 mL DNS reagent and boiled for 5 min. The absorbance was measured at 540 nm. One unit (U) of SdG5A activity was defined as the amount of enzyme that released reducing sugar equivalent to 1 μmol of glucose per minute under the assay conditions (45°C, pH 6.5).

Determination of Hydrolysis Products

The reaction mixtures containing 0.2 mL of purified enzymes (2.0 U g^{-1} dry weight of starch) and 5.8 mL of corn starch (2%, w/w) were incubated at 4, 25, and 45°C in water bath for 4, 12, 24, and 36 h and boiled for 10 min to terminate the reaction. Samples were then centrifuged at 10,000 × *g* for 10 min and the supernatant was filtered through 0.22-μm syringe filter for high-performance anion-exchange chromatographic (HPAEC) analysis. The retention time and peak area of maltooligosaccharides standards (glucose – maltoheptaose) were compared with those of hydrolysis samples for identification and quantification.

Separations were carried out using an HPAEC system equipped with a pulsed amperometry detector (PAD; Dionex ICS-5000, Sunnyvale, CA, United States). Ten microliters of the sample solution was injected onto a CarboPacTM PA200 column (Dionex), and eluted with eluents A (0.25 M NaOH), B (1.0 M sodium acetate), and C (distilled, deionized H_2O) at 30°C with a flow rate of 0.5 mL min^{-1} in a gradient elution program as follows: 0-6 min 8% A, 2% B, and 90% C; 6-6.5 min 8-12% A, 2-4% B, and 90-84% C; 6.5-18 min 12-24% A, 4-8% B, and 84-68% C; 18-25 min 24% A, 8-36% B, and 68-40% C; 25-40 min 24% A, 36% B, and 40% C; and 40-50 min 8% A, 2% B, and 90% C.

Biochemical Characterization

The optimal pH for hydrolysis activity of purified SdG5A was determined at 45°C in 50 mM $C_4H_2O_7$–Na_2HPO_4 buffer at a pH range of 2.5–8.0, and 50 mM glycine-NaOH buffer at a pH range of 8.0–12.0. The pH stability was determined by incubating the enzyme at varying pH values for 1 h at 4°C. The remaining activity was measured under the assay conditions (45°C, pH 6.5), and the activity before incubation was taken as 100%.

The optimal temperatures for hydrolysis activities of purified SdG5A and SdG5A-CAD were determined at temperatures ranging from 0 to 75°C in 50 mM $C_4H_2O_7$–Na_2HPO_4 buffer (pH 6.5). The thermostability was determined by measuring the residual activities after incubation of the enzyme in $C_4H_2O_7$–Na_2HPO_4 buffer (pH 6.5) at 25, 35, and 45°C for various periods. The remaining activity was measured under the assay conditions (45°C, pH 6.5), and the activity before incubation was taken as 100%.

To investigate the effects of different metal ions on the activity of SdG5A, activities were measured at 45°C and pH 6.5 with the addition of 50 mM of $BaCl_2$, $CaCl_2$, $CuSO_4$, $FeCl_3$, KCl, LiCl, $MgSO_4$, NaCl, and $ZnSO_4$. The salt tolerances of SdG5A and SdG5A-CAD were determined by measuring the residual activities after incubation of the enzyme in the presence of 0.1–4.0 M NaCl for 1 h at 4°C. The activity measured in the absence of any additive was taken as 100%.

Structural Identity

Three-dimensional structures of SdG5A were predicted using the RaptorX template-based and distance-based protein structure modeling servers[1] (Källberg et al., 2012; Xu, 2019). Quality of the predicted structure was evaluated using TM-score calculated by ResQ server[2] (Yang et al., 2016). Estimation of residue-specific distance to the equilibrium native state was implemented by ResQ server (Yang et al., 2016). Multiple sequence alignments were performed using Clustal Omega[3] (Sievers et al., 2011). Phylogenetic tree was constructed using the MEGA version 5.0 with the neighbor-joining algorithm (Tamura et al., 2014). Conserved domains were identified by the Conserved Domain

[1]http://raptorx.uchicago.edu

[2]https://zhanglab.ccmb.med.umich.edu/ResQ/

[3]https://www.ebi.ac.uk/Tools/msa/clustalo/

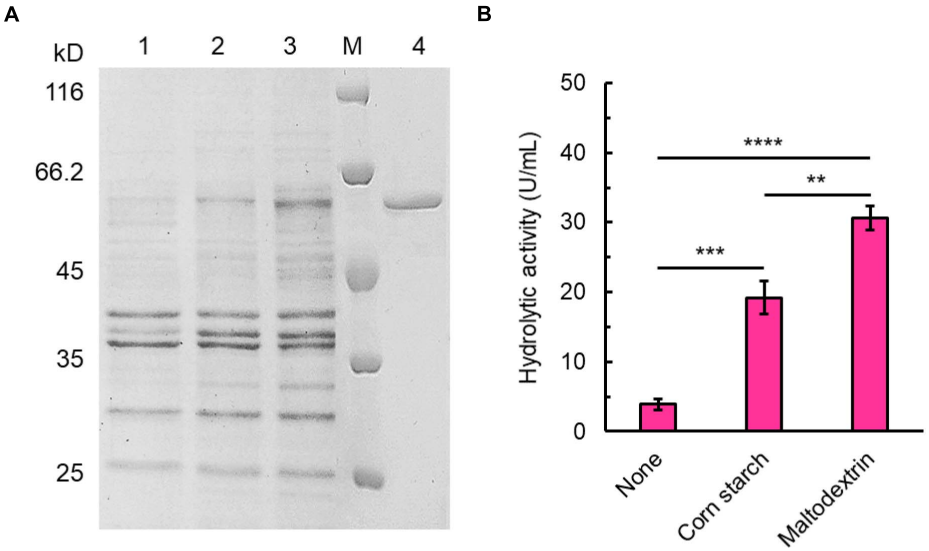

FIGURE 1 | Expression and purification of SdG5A. **(A)** SDS-PAGE analysis of SdG5A. Lane M, molecular-weight protein marker. Lane 1, culture supernatant collected from the basic expression medium; lane 2, culture supernatant collected from the expression medium containing 5 g L^{-1} corn starch; lane 3, culture supernatant collected from the expression medium containing 5 g L^{-1} maltodextrin; lane 4, purified SdG5A. **(B)** Hydrolytic activity of culture supernatant collected from the mediums with the indicated supplement. Each value represents the mean of three independent measurements (mean ± standard derivation).

Database[4] (Marchler-Bauer et al., 2017). Solvent accessibility was predicted by ResQ server (Yang et al., 2016). Structures were rendered using the PyMOL version 2.2.3 software.

Statistical Analysis

Three biologically independent replicates were used to calculate means and standard deviations. *P*-values were calculated using Prism 8 by performing two-tailed Student's *t*-test, with a statistical significance level represented as ns (not significant), $^{*}P \leq 0.05$, $^{**}P \leq 0.01$, $^{***}P \leq 0.001$, and $^{****}P \leq 0.0001$.

RESULTS

Expression and Purification of SdG5A

The open reading frame of SdG5A encodes a signal peptide of 21 amino acid residues at the N-terminus followed by mature protein of 542 amino acid residues, of which the calculated molecular mass was 60.06 kDa. Analysis of the open reading frame revealed the GC content of SdG5A to be 47.1%, which is similar to that of the Sde 2–40 whole genome (46.3%) and lower than maltooligosaccharide-forming amylases (MFAs) from other organisms (Weiner et al., 2008; Pan et al., 2017). We expressed SdG5A in the recombinant *B. subtilis* WB600 and purified SdG5A from the culture supernatant by the combination of phenyl superose and gel filtration column chromatography. The purity of SdG5A was confirmed by migration of the protein as a single band corresponding to a molecular mass of approximately 60 kDa on sodium dodecyl sulfate-polyacrylamide gel electrophoresis (SDS-PAGE) (**Figure 1A**). The specific activity of SdG5A was calculated to be 215 U mg^{-1}. Furthermore, supplementing corn starch or maltodextrin in the basal medium dramatically increased the expression level of SdG5A (**Figure 1A**). The highest extracellular hydrolytic activity of SdG5A reached 30.6 U mL^{-1} when 5 g L^{-1} maltodextrin was added (**Figure 1B**).

Production of Maltopentaose by SdG5A

To investigate the product profiles of SdG5A, hydrolysates of corn starch were assayed using HPAEC-PAD (**Figure 2A**). At 4°C, we observed SdG5A converted 77.7% of the starch substrate within 36 h. Surprisingly, 78.5% of the total products were G5 while all other components showed the proportion below 10%. The product profiles were also tested at 25°C and the result showed higher reaction rates with the substrate conversion rates being 82.5 and 88.3% at 24- and 36-h hydrolyzation, respectively. However, SdG5A exhibited 1.4–1.6-fold lower product ratio for G5, compared to those generated at 4°C (**Figure 2B**). An increase of temperature up to 45°C caused a significant decrease in both the conversion rate and G5 production (**Figure 2B**), indicating that SdG5A might be more conductive to react at low temperature. The temperature effect on the G5 production by SdG5A suggested its potential to adapt cold and overcome the challenges of low molecular thermal motion and limited substrate accessibility in the cold environment.

Cold Adaptation and Salt Tolerance of SdG5A

The temperature for the highest catalytic activity of SdG5A was observed at 45°C and approximately 30% of its maximum activity was kept at 0 and 4°C, indicating its strong adaptation to the cold temperature (**Figure 3A**). In the absence of substrate, the

[4]https://www.ncbi.nlm.nih.gov/cdd

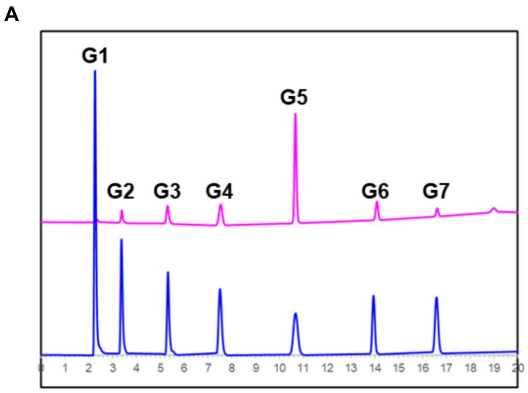

Products	Retention time (min)	Ratio (%)
Glucose (G1)	2.3	0.1
Maltose (G2)	3.4	1.4
Maltotriose (G3)	5.3	3.5
Maltotetraose (G4)	7.6	7.5
Maltopentaose (G5)	10.7	78.5
Maltohexaose (G6)	14.1	6.7
Maltoheptaose (G7)	16.6	2.3

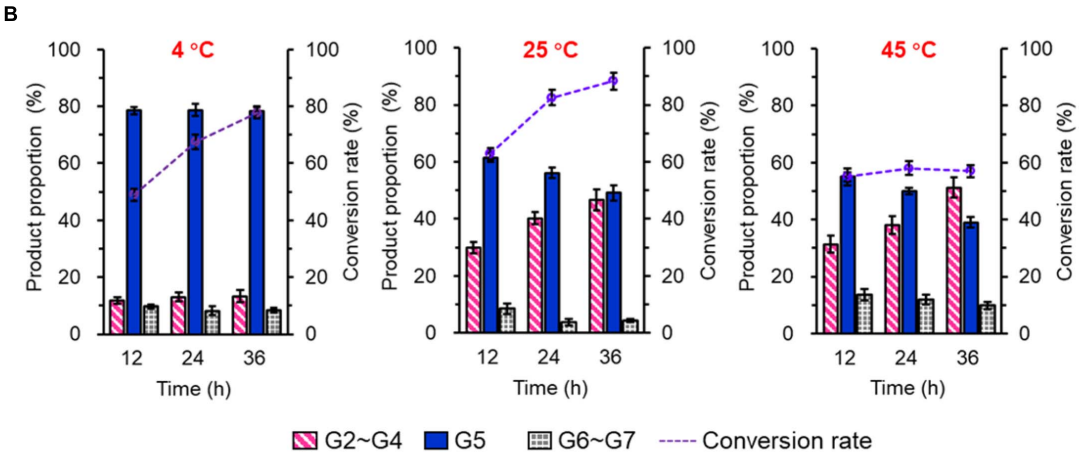

FIGURE 2 | Product profile of purified SdG5A. **(A)** HPAEC-PAD chromatograms of maltooligosaccharides standards (blue) and hydrolysis products of corn starch by SdG5A (pink). Product proportions calculated from the chromatogram are listed in the table. Substrates (2%, w/w) were hydrolyzed by the purified enzyme (2.0 U g^{-1} dry weight of starch) at 4°C for 4 h. **(B)** Product composition arising from the hydrolysis of corn starch by SdG5A at different temperatures. Substrates (10%) were hydrolyzed by the purified enzyme (2.0 U g^{-1} dry weight of starch). Each value represents the mean of three independent measurements (mean ± standard derivation).

purified SdG5A remained stable at 25 and 35°C for 30 min, retaining 95 and 80% of its maximal activity, respectively (**Figure 3B**). However, at 45°C the enzyme became heat-labile and the activity sharply decreased to 14% of the maximum within 5 min (**Figure 3A**). Although initially catalytically active at 45°C, SdG5A could also be deactivated within 20 min by incubating at the same temperature (**Figure 3B**). The purified SdG5A showed optimal activity within pH 6.5-7.0 (**Figure 3C**). Interestingly, no activity loss was observed even after the enzyme was incubated in the alkaline condition (pH 8.0-11.0) for 1 h without substrate added (**Figure 3D**). Additionally, the effects of various metal ions were studied under the optimal reaction condition (45°C, pH 6.5). We observed that several metal ions - Ba^{2+}, Ca^{2+},$Cu2^{+}$, Fe^{3+}, K^{+}, Li^{2+}, Mg^{2+}, Na^{+}, and Zn^{2+} - could enhance the activity by 1.4-1.8-fold (**Figure 3E**). Moreover, the enzyme showed strong tolerance to the high salt concentration, retaining greater than 70% of its maximal activity in presence of 3 M NaCl (**Figure 3F**).

In sum, although SdG5A exhibited its maximum activity at the mesothermal optimum temperature and neutral optimum pH, in case of the extremely harsh reaction condition it might manifest its naturally adapted molecular mechanisms to maintain the persistent activity.

Structure Analysis of SdG5A

To understand the potential mechanisms that might underlie the cold adaptation and salt tolerance of SdG5A, we conducted a comprehensive *in silico* structural analysis. The phylogenetic tree provides a visual representation of the evolutionary interrelations of proteins derived from a common ancestral (Saitou and Nei, 1987). Our phylogenetic analysis revealed that SdG5A is closely related to the putative amylase from the marine bacteria *Marinagarivorans algicola* (GenBank accession WP_053982064) with a 67% sequence identity (**Figure 4A**), but has low identities (15-44%) with other MFAs (data not shown). We then analyzed the conserved domains to find specific structural and functional units in SdG5A that may have given rise to its special properties during the molecular evolution. The conserved domain footprints of SdG5A were identified by searching in Conserved Domain Database, a collection of annotated multiple sequence alignment models (Marchler-Bauer et al., 2017). We found the modular structure of SdG5A comprises mainly three

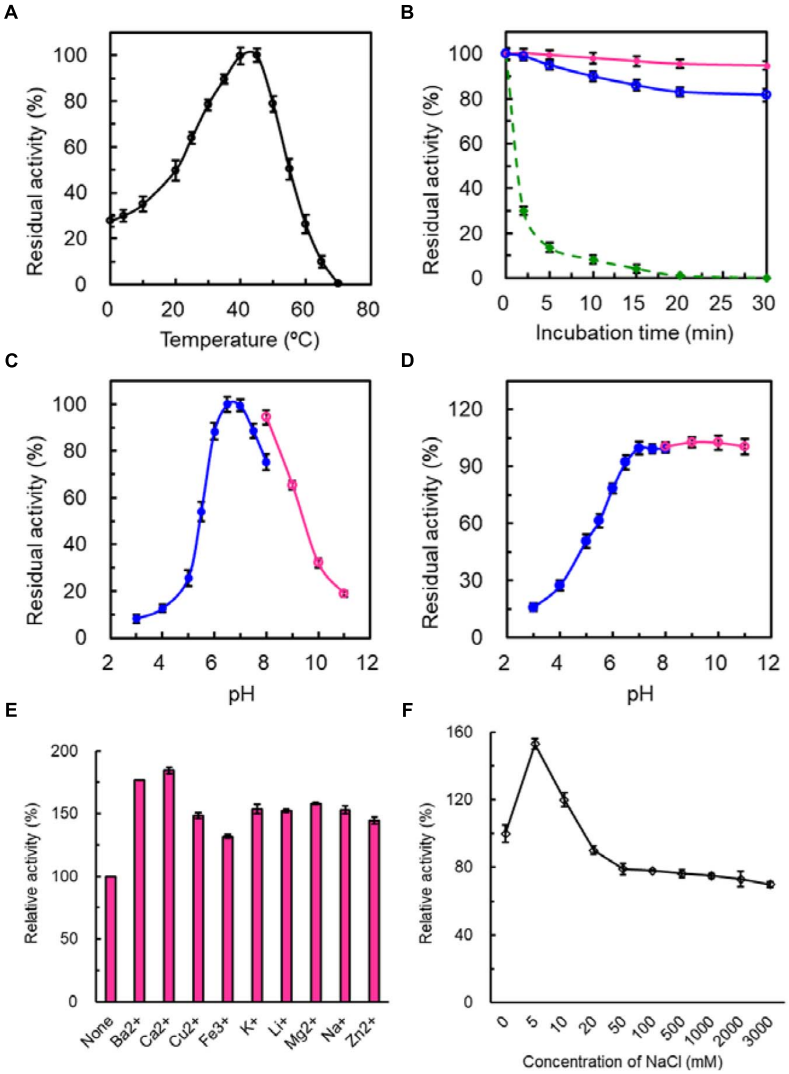

FIGURE 3 | Enzymatic properties of purified SdG5A. **(A)** Effect of temperature on the catalytic activity. The temperature profile was determined in $C_4H_2O_7$–Na_2HPO_4 buffer (pH 6.5) at different temperatures ranging from 0 to 70°C. The activity of the enzyme at 45°C was taken as 100%. **(B)** Effect of temperature on protein stability. To assess the thermostability, the enzyme was incubated at 25°C (pink), 35°C (blue), and 45°C (green). The residual activity was measured at pH 6.5 and 45°C. The activity before the incubation was taken as 100%. **(C)** Effect of pH on the catalytic activity. The pH profile was determined in 50 mM $C_4H_2O_7$–Na_2HPO_4 buffer at pH range of 2.5–8.0 (blue) and 50 mM glycine-NaOH buffer at a pH range of 8.0–11.0 (pink) at 45°C. The maximum activity obtained at pH 6.5 was considered as 100%. **(D)** Effect of pH on protein stability. The pH stability was determined by incubating the enzyme in 50 mM $C_4H_2O_7$–Na_2HPO_4 buffer at pH range of 2.5–8.0 (blue) and 50 mM glycine-NaOH buffer at pH range of 8.0–11.0 (pink) for 1 h at 4°C and the residual activity was measured at pH 6.5 and 45°C. The activity before the incubation was taken as 100%. **(E)** Effect of different metal ions on the catalytic activity. The activity of the enzyme with no addition was defined as 100%. **(F)** Effect of NaCl concentrations on the catalytic activity. The activity of the enzyme with no addition was defined as 100%. Each value represents the mean of three independent measurements (mean ± standard derivation).

domains - Domain of AmyAc_family superfamily (AmyAc, Arg^3 to Thr^{334}), Domain of Malt_amylase superfamily (Malt, Thr^{341} to Ala^{427}), and CBM20 (Val^{446} to Phe^{542}) (**Figure 4B**). Particularly, AmyAc and CBM20 located at the two terminals of SdG5A are accountable for catalysis and substrate binding, respectively. The two domains are separated by the accessory module Malt and an extended linker (Ile^{428} to Lys^{445}).

To characterize the extent of homology of SdG5A compared to other reported enzymes, we selected two other cold-adapted and salt-tolerant α-amylases from *Alteromonas haloplanctis* (AHA) and *Zunongwangia profunda* (ZPA) (Feller et al., 1992; Qin et al., 2014). At the same time, we selected five other non-extremophilic MFAs, including maltotriose-forming amylase from *Brachybacterium* sp. LB25 (BraG3A) and *Kitasatospora* sp. MK-1785 (KitG3A), maltotetraose-forming amylase from *Pseudomonas stutzeri* MO-19 (PstG4A), maltopentaose-forming amylase from *Pseudomonas* sp. KO-8940 (PseG5A) and maltohexaose-forming amylase from *Corallococcus* sp. EGB

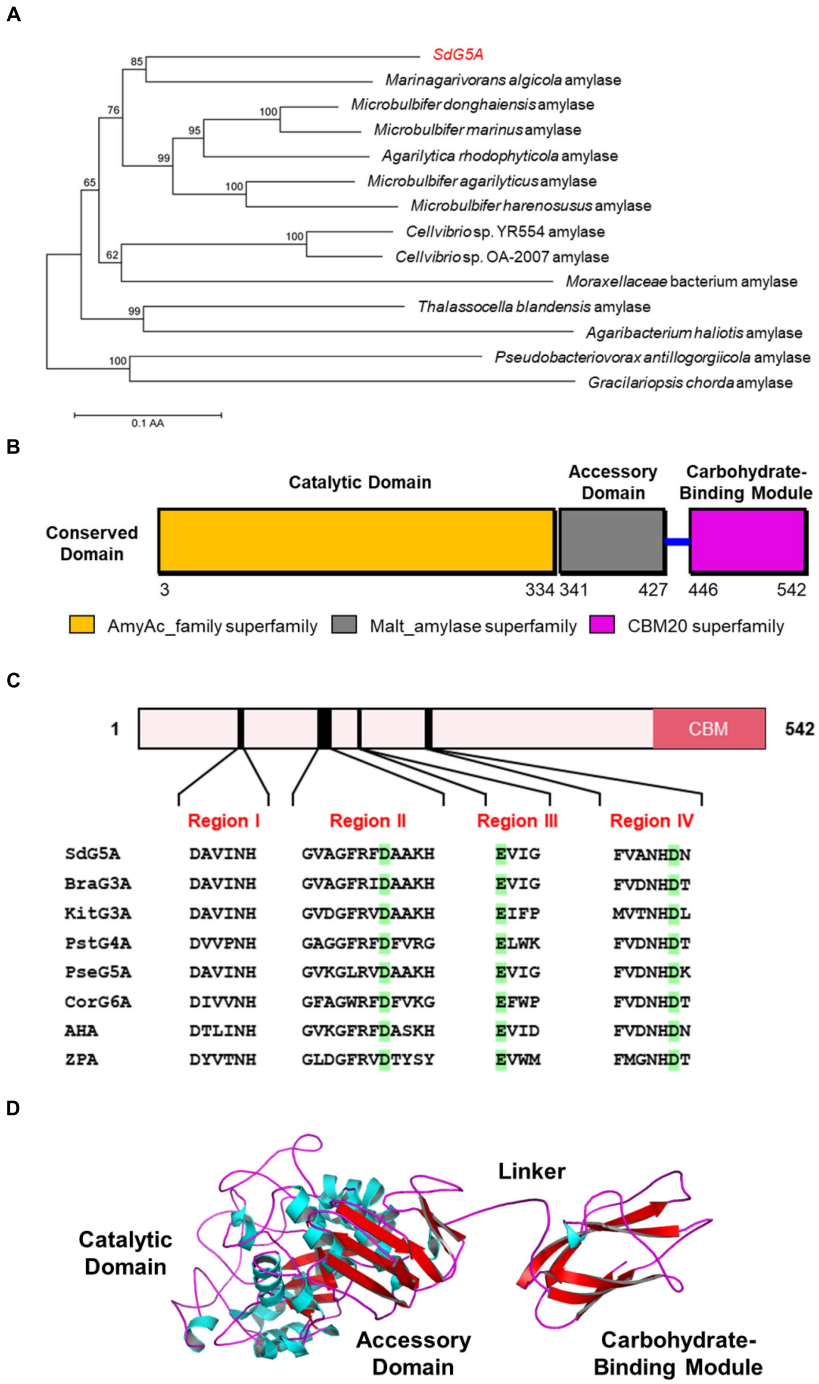

FIGURE 4 | Sequence and three-dimensional structure analysis of SdG5A. **(A)** Phylogenetic tree of the amino acid sequences of SdG5A. The tree was constructed using the neighbor-joining algorithm of the MEGA program (version 5.0). Bootstrap values (n = 1,000 replicates) are reported as percentages. The scale bar represents the number of changes per amino acid position. **(B)** Analysis of the conserved domains identified by Conserved Domain Database (Marchler-Bauer et al., 2017). **(C)** Conserved regions I–IV of α-amylases. Amino acid residues corresponding to catalysis are highlighted in green. **(D)** Template-based predicted structure model of SdG5A.

(CorG6A) for comparison (**Table 1**; Fujita et al., 1989; Shida et al., 1992; Doukyu et al., 2007; Kamon et al., 2015; Li et al., 2015). Four conserved sequence regions (Region I to IV) that had been discovered and used to define α-amylases in glycosyl hydrolase family 13 were found in all 8 amylase targets (**Figure 4C**; Janeček, 2002). Specifically, three conserved catalytic residues corresponding to Asp^{163}, Glu^{189}, and Asp^{254} in SdG5A were invariantly conserved throughout the MFAs, AHA, and

TABLE 1 | Information of the enzymes used for the comparison with SdG5A in this study.

Name	Enzyme	Source	GenBank accession[a]	References
AHA	α-Amylase	*Alteromonas haloplanctis*	P29957.3	Feller et al., 1992
ZPA	α-Amylase	*Zunongwangia profunda*	WP_013072233.1	Qin et al., 2014
Aga50D	β-Agarase	*Saccharophagus degradans* 2-40^T	4BQ4	Kim et al., 2010
Xyn10C	β-Glycosidase	*Saccharophagus degradans* 2-40^T	ABD82280.1	Ko et al., 2016
BraG3A	G3A	*Brachybacterium* sp. LB25	BAE94180.1	Doukyu et al., 2007
KitG3A	G3A	*Kitasatospora* sp. MK-1785	HW429890.1	Kamon et al., 2015
PstG4A	G4A	*Pseudomonas stutzeri* MO-19	AAA25707.1	Fujita et al., 1989
PseG5A	G5A	*Pseudomonas* sp. KO-8940	BAA01600.1	Shida et al., 1992
CorG6A	G6A	*Corallococcus* sp. EGB	AII00648.1	Li et al., 2015

[a]*Accession numbers deposited in the National Center for Biotechnology Information (NCBI) database (https://www.ncbi.nlm.nih.gov/). G3A, maltotriose-forming amylase; G4A, maltotetraose-forming amylase; G5A, maltopentaose-forming amylase; G6A, maltohexaose-forming amylase.*

TABLE 2 | Comparison of the frequencies of charged amino acid residues for different domains in SdG5A and other extremophilic amylases.

Parameter	SdG5A					AHA	ZPA
	Catalytic domain	Accessory domain	Linker	CBM	Entire protein		
Acidic residues (%)	9.9	7.5	27.8	9.3	10.0	10.2	15.0
Basic residues (%)	11.7	8.6	5.6	5.2	9.8	7.8	11.8
Net charge density (z, %)[a]	1.6	1.1	−22.2	−4.1	−0.2	−2.8	−3.7

[a]*Net charge density is estimated by* $z = (n_{basic} - n_{acidic})/length \times 100\%$, *where* n_{basic} *and* n_{acidic} *are the number of basic and acidic residues, respectively. Acidic residues include glutamic acid and aspartic acid. Basic residues include histidine, lysine, and arginine. All sequences are presented in the* ***Supplementary Material****. AHA, α-amylase from Alteromonas haloplanctis; ZPA, α-amylase from Zunongwangia profunda.*

ZPA (**Figure 4C**). It should be noted that all six MFAs contain multiple domains including a CBM20, which, however, is absent from AHA and ZPA.

We then implemented a template-based structural prediction of SdG5A using the RaptorX web server (**Figure 4D**; Källberg et al., 2012). The domains for AmyAc and Malt were simulated with the crystal structure of amylase from *Pseudoalteromonas haloplanktis* as template (PDB entry: 1AQH, 50.2% identity to SdG5A), while the domain for CBM20 was modeled based on the structure of cyclodextrin glucanotransferase from alkalophilic *Bacillus* sp. (PDB entry: 1I75, 35.5% identity to SdG5A). The overall structure showed high fitted score with the TM-score of 0.59 (TM-score ranging from 0.5 to 1.0 indicated the same fold with template). The catalytic domain adopted the structure of a $(\beta/\alpha)_8$-barrel formed by eight parallel β-strands surrounded by eight α-helices. At the opposite side of this catalytic domain, the CBM20 domain folded as an antiparallel β-barrel structure. As expected, the accessory module, which consisted only of β-sheets followed by a flexible linker, separated the N-terminal catalytic domain and C-terminal CBM20 to allow their independent movements toward and against each other (**Figure 4D**). Together, our general structural analysis established the enzymatic key players of SdG5A and provided possible indicators giving rise to its persistent function in the cold or high salt setting.

Structural Determinants of Cold Adaptation and Salt Tolerance

Distribution of Charged Amino Acid Residues

Bioinformatic studies have shown that a higher ratio of acidic (glutamic acid and aspartic acid) to basic (histidine, lysine, and arginine) residues is commonly observed from the cold-adapted and salt-tolerant enzymes. We analyzed the composition of amino acid residues for the different domains in SdG5A (**Supplementary Table 1**) and compared the frequencies of charged residues in SdG5A and each domain with those in single-domain AHA and ZPA (**Table 2**). Initially, the proportion of acidic residues and basic residues in SdG5A as a whole were similar, inconsistent with the postulation that acidic amino acid residues are dominant in the cold-adapted and salt-tolerant enzymes. However, different results were observed when we calculated the proportion for each domain separately. The proportion of acidic residues in the linker and CBM region was 22.2 and 4.1% higher than that of basic residues, respectively. The net charge densities were higher than that of AHA and ZPA, which possessed 2.8 and 3.7% excess acidic residues, respectively (**Table 2**). In contrast, for the catalytic domain and accessory domain, basic residues were found in excess in SdG5A (**Table 2**). This difference in the distribution of charged residues was visually represented in **Figure 5A**. In particular, numerous acidic amino acid residues being widespread along the trailing end of the linker was indicative to generate strong electrostatic repulsions between the neighboring residues and accommodate conditions for the CBM domain to have greater access to solvent and substrates in an unfavorable cold and hypersaline condition.

Protein Flexibility

One postulation of cold adaptation is that proteins require high conformational flexibility. To characterize the global flexibility of SdG5A, we used ResQ to estimate the distance to which each residue can travel from the same residue at its native state, at

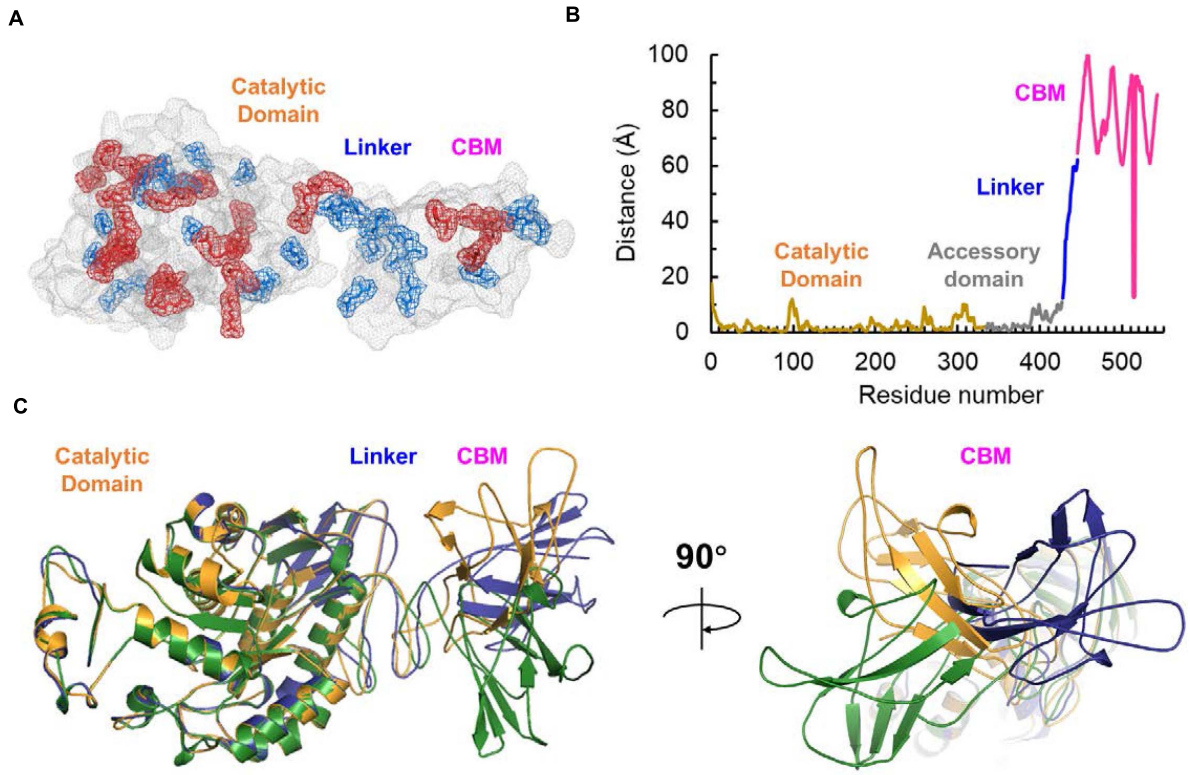

FIGURE 5 | Surface electrostatic potential and flexibility analysis of SdG5A. **(A)** Distribution of charged residues on the SdG5A surface. Acidic residues including glutamic acid and aspartic acid are indicated in blue; basic residues including histidine, lysine, and arginine are indicated in red. **(B)** Residue-specific distance to the equilibrium native state. The distance was estimated by ResQ server based on the support vector regressions. **(C)** Distance-based predicted structural model of SdG5A. All structures were predicted using the RaptorX web server and rendered using the PyMOL Version 2.2.3 software.

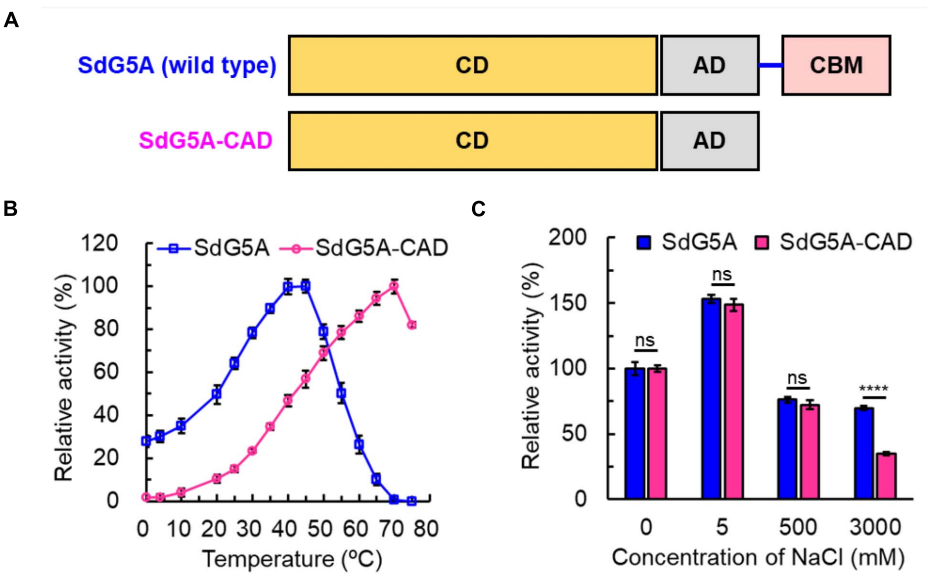

FIGURE 6 | Characterization of SdG5A-CAD. **(A)** Schematic of truncation of the linker-CBM region of SdG5A. **(B)** Effect of temperature on the activity. The temperature profile was determined in $C_4H_2O_7$–Na_2HPO_4 buffer (pH 6.5) at different temperatures ranging from 0 to 75°C. **(C)** Effect of NaCl concentrations on the activity. The activity of the enzyme with no addition was defined as 100%. Each value represents the mean of three independent measurements (mean ± standard derivation).

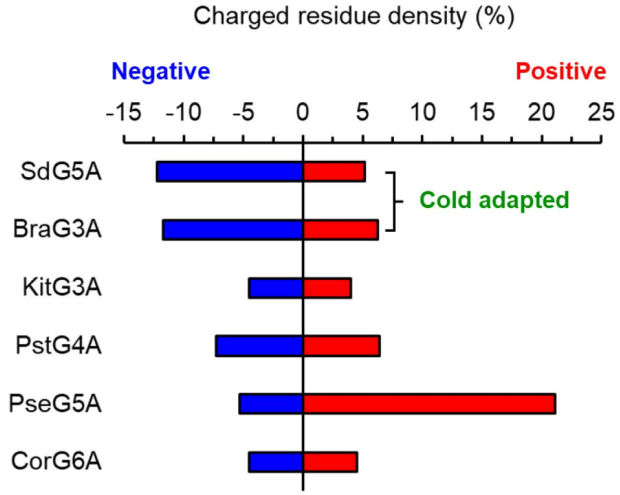

FIGURE 7 | Density of charged amino acid residues in the linker-CBM region of maltooligosaccharide-forming amylases.

which the protein atoms stay at the equilibrium position in the lowest free energy conformation (Yang et al., 2016). Across the residues of SdG5A, these distances stayed low and smooth for the catalytic domain but high and unsteady for the linker-CBM region, indicating a variety of conformational states the linker-CBM region of SdG5A could cover (**Figure 5B**). We further used a distance-based modeling based on the convolutional residual neural network to characterize the contact between the catalytic and linker-CBM region (Xu, 2019). Through the multiple models fitting of the prediction parameters, we observed that although the catalytic domain displayed similar folds and positions in different models, the linker could adopt a wide range of conformations, providing enough occurrences to stretch and bend and promoting contacts between the catalytic domain and CBM (**Figure 5C**).

Together, these findings indicated that the cold adaption and salt tolerance of SdG5A could largely be governed by the non-catalytic linker-CBM region having enhanced conformational mobility and flexibility compared to the catalytic domain.

Truncation of the Linker-CBM Region in SdG5A

To validate our bioinformatics analysis and further investigate the role of the linker-CBM region of SdG5A, we truncated the region of Ile^{428}-Phe^{542} and preserved the catalytic domain and accessory module to construct SdG5A-CAD (**Figure 6A**). SdG5A-CAD was expressed in *B. subtilis* WB600 and purified using phenyl superose and gel filtration column chromatography. Compared with the data of enzymatic properties observed from the full-length SdG5A, removal of the linker-CBM region resulted in approximately 30.2-fold reduction of the activity at 0°C (2.0 U mg^{-1}), and 2.0-fold reduction of the relative activity in 3 M NaCl (34.9%), suggesting that the linker-CBM region played a critical role for providing its cold adaptation and salt tolerance behavior (**Figures 6B,C**). These experimental results were consistent with our previous bioinformatics analysis and successfully demonstrated that SdG5A is a cold-adapted and salt-tolerant enzyme driven by its highly flexible, negatively charged and functionally distinct substrate-targeting linker-CBM region for the efficient G5 production.

DISCUSSION

Global energy consumption and warming are rapidly increasing due to industrial activities and advances. Food system was estimated to contribute 34% of all human-made CO_2 emissions (Crippa et al., 2021). Thus, the application of cold-adapted enzymes has great potential for large-scale industrial food biocatalytic processes due to the avoidance of heating reactors, which results in saving of energy consumption and CO_2 emissions. At the same time, the utilization of cold-adapted enzymes in food processing could improve the quality of food by minimizing undesirable chemical reactions, retaining volatile flavor compounds and preventing modification of heat-sensitive substrates and products occurring at high temperature during enzymatic reaction or inactivation (Sarmiento et al., 2015; Siddiqui, 2015; Santiago et al., 2016). It should be noted that G5, as one of the functional oligosaccharides, tends to suffer nutrition loss and changes in physicochemical properties at high temperature (Patel and Goyal, 2011). Therefore, compared to mesophilic or thermostable G5As, of which the optimum temperatures range between 60 and 93°C, SdG5A has greater prospects to be used in energy-efficient and environmentally friendly industrial production of G5. At room temperature, SdG5A could convert more than 80% of the corn starch into maltooligosaccharides with the yield of approximately 60% of G5 within 24 h. Among the previously reported G5As, the one secreted from *Bacillus megaterium* VUMB109 showed the highest efficacy for producing G5 at 90°C, with the conversion rate of corn starch and the product specificity being approximately 20 and 40%, respectively (**Supplementary Table 2**; Jana et al., 2013). In comparison, without intensive heating, SdG5A was able to increasing the G5 yield by approximately sixfold.

Another unique characteristic of SdG5A is the ability to tolerate high salt concentration. In recent years there has been an increasing interest in using microalgae to produce fermentable sugar (Matsumoto et al., 2003; Ma et al., 2020). Marine microalgae are superior to land crops as feedstocks for bioconversion because they are capable of converting solar energy and CO_2 to starch through photosynthesis (Khan et al., 2018). However, the utilization of marine microalgae as substrate for conventional amylases required desalinization, which led to additional cost (Matsumoto et al., 2003). Hence, the salt-tolerant SdG5A would be a promising candidate for the production of maltooligosaccharides with the abundant and renewable marine microalgae.

To date, there have been only two α-amylases found to be concurrently cold-adapted and salt-tolerant: amylase from Antarctic bacterium *Alteromonas haloplanctis* (AHA) and amylase from marine bacterium *Zunongwangia profunda* (ZPA) (Feller et al., 1992; Srimathi et al., 2007; Qin et al., 2014).

TABLE 3 | Properties of the cold-adapted enzymes from Sde 2-40 and the frequencies of charged amino acid residues for CBM.

Enzyme	SdG5A	Aga50D	Xyn10C
Properties	Retain ~30% of its maximum activity at 4°C	Retain ~78% of its maximum activity at 20°C	Retain ~80% of its maximum activity at 20°C
Acidic residues (%)	9.3	12.9	13.9
Basic residues (%)	5.2	9.3	4.9
Net charge density (*z*, %)[a]	−4.1	−3.6	−9.0

[a]*Net charge density is estimated by* $z = (n_{basic} - n_{acidic})/length \times 100\%$, *where* n_{basic} *and* n_{acidic} *are the number of basic and acidic residues, respectively. Acidic residues include glutamic acid and aspartic acid. Basic residues include histidine, lysine, and arginine. All sequences are presented in the* ***Supplementary Material****. Aga50D, β-agarase from Saccharophagus degradans 2-40*^{T}*; Xyn10C, β-glycosidase from Saccharophagus degradans 2-40*^{T}*.*

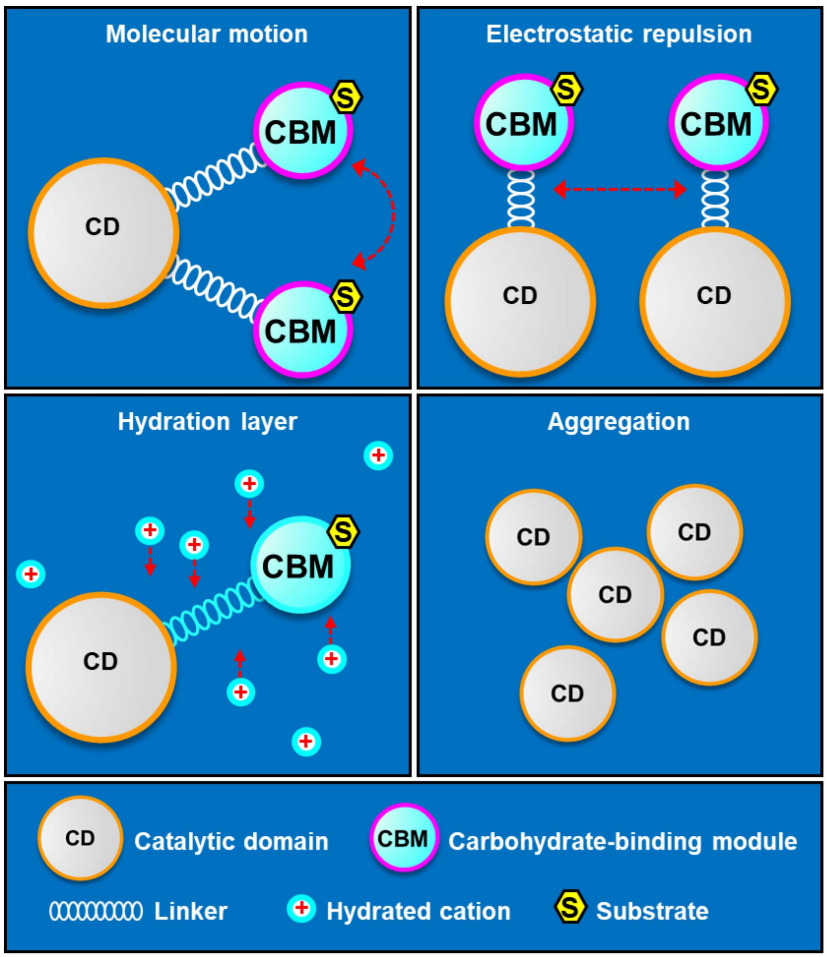

FIGURE 8 | Schematic diagram of structural determinants of cold adaptation and salt tolerance of SdG5A. The highly flexible linker-CBM structure allows an active molecular motion, which guarantees searching and capturing substrates for catalytic domain. The high density of identically charged residues in the linker-CBM region allows appreciable electrostatic repulsion, which prevents protein aggregation and inactivation. The acidic residue-rich linker-CBM structure allows the formation of hydration layer, which help protein maintain in soluble state.

Although the optimal temperatures of AHA and ZPA were lower than SdG5A by 10–20°C, the relative activities at 0°C for the three enzymes were comparable. In addition, compared to AHA and ZPA, which retained 80 and 74% of the initial activity at 4.5 and 4.0 M NaCl, respectively (the activity of the enzymes with no addition was defined as 100%), SdG5A showed relatively weaker salt tolerance, but significantly stronger salt tolerance compared to other reported G5As (**Supplementary Table 2**; Jana et al., 2013). With regard to the structural features that conferred cold adaptation and salt tolerance, all three amylases possessed high percentage of acidic residues and high conformational flexibility in entire or partial protein structure. In general, cold and high salinity affect properties and structures of enzymes by restricting the availability of free water

molecules for protein hydration (Karan et al., 2012). Therefore, improved characteristics are critical for extremozymes to prevent self-aggregation when water is scarce from their surfaces. The high density of identically charged residues promotes weak but appreciable repulsive protein–protein interactions, thus promoting molecular motion. Considering the contribution of charged residues on solubility, acidic residues are superior to basic residues due to their less hydrophobic solvent-accessible area of the side-chain components. Besides, the negatively charged residues bind to hydrated cations and form a hydration layer on the protein surface, thereby reducing their surface hydrophobicity (Karan et al., 2012). As a result of the improved solubility and flexibility, AHA, ZPA and SdG5A exhibited low aggregation and high activity at extremely temperatures and high salt concentrations. However, different from the single-domain amylases AHA and ZPA, SdG5A was composed of three domains and one extended linker. Instead of possessing an evolved overall structure, SdG5A only relied on the negative surface potential and high flexibility of the linker-CBM region to maintain the cold adaptation and salt tolerance. Consistent to our *in silico* analysis, truncation of the linker-CBM region resulted in a significant decline in the activities at low temperature and high salt concentration, indicating the linker-CBM acted as a critical component that endowed these unique properties to the protein to carry out its activity even in the biologically unfavorable condition. As for other multi-domain MFAs, mesophilic KitG3A, PstG4A, PseG5A, and CorG6A possessed equivalent acidic and basic amino acid residues or higher percentage of basic residues in the linker-CBM region, while only BraG3A followed the same trend as SdG5A (**Figure 7**). Although BraG3A has not been clearly defined as a cold-adapted enzyme, we note that a study has shown that it still had higher cold adaptivity than other MFAs, retaining approximately 25% of its maximal activity at 10°C (Doukyu et al., 2007). This reflects a close relationship between the linker-CBM region and cold adaptivity in MFAs. Furthermore, it is interesting to note that cysteine contributes to the highest ratio (22.2%) of the total amino acid residues in the linker region of SdG5A (**Supplementary Table 1**). This is contrary to the fact that cysteine residues are often buried and known to be the least abundant to get exposed on the protein surfaces during evolution due to its hydrophobicity (Marino and Gladyshev, 2010). The presence of exposed cysteines in the SdG5A linker highlights its unique functional behavior and adaptation which might be due to the intrinsic reactivity of cysteine residues affected by its large pK_a fluctuations to confer more protein flexibility (Marino, 2014).

Marine microbial enzymes have presented a promising outlook for both applied and basic research. Sde 2-40 was emerging as a vanguard of marine bacteria and functioning as a "super-degrader" of complex carbohydrates (Weiner et al., 2008). Like SdG5A, many of the enzymes from Sde 2-40 exhibited outstanding cold adaptation and architecture comprising the joint catalytic domain and CBM. However, the relationship between the unique properties and structure has not been adequately studied (Kim et al., 2010; Ko et al., 2016). Hence, we analyzed the frequencies of charged residues for CBM in the cold-adapted β-agarase (Aga50D) and β-glycosidase (Xyn10C) from Sde 2-40 (**Table 3**). Interestingly, both of the enzymes possess abundant excess acidic residues in their CBMs, which is similar to SdG5A. Therefore, it could be postulated that the role of CBM on protein adapting cold is also applicable to more carbohydrases in Sde 2-40 or other marine bacteria.

The mechanism of linker-CBM allowing cold adaptation and salt tolerance of SdG5A was summarized in **Figure 8**. First, the highly flexible linker-CBM structure in SdG5A has evolved to actively search and capture substrates to supply them to the catalytic core when water activity is perturbed by low temperature and/or high salinity. Second, the increased negative potential of the linker-CBM allows electrostatic repulsion between protein molecules, thus preventing them from aggregating. Third, the abundant acidic residues in the linker-CBM help improve the water-binding ability/solubility of SdG5A by binding hydrated cations and maintaining a stable hydration layer. In the case of the non-extremophilic counterpart of SdG5A (SdG5A-CAD), it may tend to aggregate and have lower activity due to the absence of sufficient hydration and mobility initially supported by the linker-CBM structure (**Figure 8**).

CONCLUSION

A cold-adapted and salt-tolerant G5A from marine bacterium Sde 2-40 was expressed in *B. subtilis* and demonstrated to be highly specific for producing G5. Bioinformatics analysis combined with experiments suggested the favorable cold adaptation and salt tolerance of SdG5A might be driven by the increased negative charges and flexible molecular motion of the linker-CBM region. Together, these properties indicated that SdG5A has great potential for both basic research and industrial applications.

DATA AVAILABILITY STATEMENT

The datasets presented in this study can be found in online repositories. The names of the repository/repositories and accession number(s) can be found in the article/**Supplementary Material**.

AUTHOR CONTRIBUTIONS

ND, ZG, and ZL designed the study. ND, BZ, and BV performed protein modeling and structure analysis. All authors wrote and edited the manuscript and have given approval to the final version of the manuscript.

FUNDING

This work was financially supported by the National Key R&D Program of China (2019YFD0901901), the National Natural Science Foundation of China (31722040), National First-class Discipline Program of Food Science

and Technology (JUFSTR20180204), the Jiangsu province "Collaborative Innovation Center of Food Safety and Quality Control" Industry development program, and the Qing Lan Project. We acknowledge support from the Robert Welch Foundation (Q1279) to BVVP.

SUPPLEMENTARY MATERIAL

The Supplementary Material for this article can be found online at: https://www.frontiersin.org/articles/10.3389/fmicb.2021.708480/full#supplementary-material

REFERENCES

Chegeni, M., and Hamaker, B. (2015). Induction of differentiation of small intestinal enterocyte cells by maltooligosaccharides. *FASEB J.* 29, 596–14. doi: 10.1007/BF03343586

Crippa, M., Solazzo, E., Guizzardi, D., Monforti-Ferrario, F., Tubiello, F. N., and Leip, A. (2021). Food systems are responsible for a third of global anthropogenic GHG emissions. *Nat. Food* 2, 198–209. doi: 10.1038/s43016-021-00225-9

Doukyu, N., Yamagishi, W., Kuwahara, H., Ogino, H., and Furuki, N. (2007). Purification and characterization of a maltooligosaccharide-forming amylase that improves product selectivity in water-miscible organic solvents, from dimethylsulfoxide-tolerant *Brachybacterium* sp. strain LB25. *Extremophiles* 11, 781–788. doi: 10.1007/s00792-007-0096-8

Feller, G., Lonhienne, T., Deroanne, C., Libioulle, C., Beeumen, J. V., and Gerday, C. (1992). Purification, characterization, and nucleotide sequence of the thermolabile alpha-amylase from the antarctic psychrotroph *Alteromonas haloplanctis* A23. *J. Biol. Chem.* 267, 5217–5221. doi: 10.1016/S0021-9258(18)42754-8

Fujita, M., Torigoe, K., Nakada, T., Tsusaki, K., Kubota, M., Sakai, S., et al. (1989). Cloning and nucleotide sequence of the gene (*amyP*) for maltotetraose-forming amylase from *Pseudomonas stutzeri* MO-19. *J. Bacteriol.* 171, 1333–1339. doi: 10.1128/jb.171.3.1333-1339.1989

Hatada, Y., Masuda, N., Akita, M., Miyazaki, M., Ohta, Y., and Horikoshi, K. (2006). Oxidatively stable maltopentaose-producing α-amylase from a deep-sea *Bacillus* isolate, and mechanism of its oxidative stability validated by site-directed mutagenesis. *Enzyme Microb. Technol.* 39, 1333–1340. doi: 10.1016/j.enzmictec.2006.03.022

Huang, Z., Peng, H., Sun, Y., Zhu, X., Zhang, H., Jiang, L., et al. (2019). Beneficial effects of novel hydrolysates produced by limited enzymatic broken rice on the gut microbiota and intestinal morphology in weaned piglets. *J. Funct. Foods* 62:103560. doi: 10.1016/j.jff.2019.103560

Hutcheson, S. W., Zhang, H., and Suvorov, M. (2011). Carbohydrase systems of *Saccharophagus degradans* degrading marine complex polysaccharides. *Mar. Drugs* 9, 645–665. doi: 10.3390/md9040645

Jana, M., Maity, C., Samanta, S., Pati, B. R., Islam, S. S., Mohapatra, P. K. D., et al. (2013). Salt-independent thermophilic α-amylase from *Bacillus megaterium* VUMB109: an efficacy testing for preparation of maltooligosaccharides. *Ind. Crops Prod.* 41, 386–391. doi: 10.1016/j.indcrop.2012.04.048

Janeček, Š (2002). How many conserved sequence regions are there in the α-amylase family?. *Biologia* 57, 29–41.

Jin, M., Gai, Y., Guo, X., Hou, Y., and Zeng, R. (2019). Properties and applications of extremozymes from deep-sea extremophilic microorganisms: a mini review. *Mar. Drugs* 17:656. doi: 10.3390/md17120656

Källberg, M., Wang, H., Wang, S., Peng, J., Wang, Z., Lu, H., et al. (2012). Template-based protein structure modeling using the RaptorX web server. *Nat. Protoc.* 7, 1511–1522. doi: 10.1038/nprot.2012.085

Kamon, M., Sumitani, J.-I., Tani, S., Kawaguchi, T., Kamon, M., Sumitani, J., et al. (2015). Characterization and gene cloning of a maltotriose-forming exo-amylase from *Kitasatospora* sp. MK-1785. *Appl. Microbiol. Biotechnol.* 99, 4743–4753. doi: 10.1007/s00253-015-6396-5

Kandra, L. (2003). α-Amylases of medical and industrial importance. *Comput. Theor. Chem.* 666, 487–498. doi: 10.1016/j.theochem.2003.08.073

Karan, R., Capes, M. D., and DasSarma, S. (2012). Function and biotechnology of extremophilic enzymes in low water activity. *Aquat. Biosyst.* 8:4. doi: 10.1186/2046-9063-8-4

Khan, M. I., Shin, J. H., and Kim, J. D. (2018). The promising future of microalgae: current status, challenges, and optimization of a sustainable and renewable industry for biofuels, feed, and other products. *Microb. Cell Fact.* 17:36. doi: 10.1186/s12934-018-0879-x

Kim, H. T., Ko, H.-J., Kim, N., Kim, D., Lee, D., Choi, I.-G., et al. (2012). Characterization of a recombinant endo-type alginate lyase (Alg7D) from *Saccharophagus degradans*. *Biotechnol. Lett.* 34, 1087–1092. doi: 10.1007/s10529-012-0876-9

Kim, H. T., Lee, S., Lee, D., Kim, H.-S., Bang, W.-G., Kim, K. H., et al. (2010). Overexpression and molecular characterization of Aga50D from *Saccharophagus degradans* 2-40: an exo-type β-agarase producing neoagarobiose. *Appl. Microbiol. Biotechnol.* 86, 227–234. doi: 10.1007/s00253-009-2256-5

Ko, J. K., Ko, H., Kim, K. H., and Choi, I.-G. (2016). Characterization of the biochemical properties of recombinant Xyn10C from a marine bacterium, *Saccharophagus degradans* 2-40. *Bioprocess Biosyst. Eng.* 39, 677–684. doi: 10.1007/s00449-016-1548-2

Li, Z., Wu, J., Zhang, B., Wang, F., Ye, X., Huang, Y., et al. (2015). AmyM, a novel maltohexaose-forming α-amylase from *Corallococcus* sp. strain EGB. *Appl. Environ. Microb.* 81, 1977–1987. doi: 10.1128/AEM.03934-14

Liu, J., Zhang, Z., Liu, Z., Zhu, H., Dang, H., Lu, J., et al. (2011). Production of cold-adapted amylase by marine bacterium *Wangia* sp. C52: optimization, modeling, and partial characterization. *Mar. Biotechnol.* 13, 837–844. doi: 10.1007/s10126-010-9360-5

Ma, Y., Wang, P., Wang, Y., Liu, S., and Wang, Y. (2020). Fermentable sugar production from wet microalgae residual after biodiesel production assisted by radio frequency heating. *Renew. Energy* 155, 827–836. doi: 10.1016/j.renene.2020.03.176

Marchler-Bauer, A., Bo, Y., Han, L., He, J., Lanczycki, C. J., Lu, S., et al. (2017). CDD/SPARCLE: functional classification of proteins via subfamily domain architectures. *Nucleic Acids Res.* 45, D200–D203. doi: 10.1093/nar/gkw1129

Marino, S. M. (2014). Protein flexibility and cysteine reactivity: influence of mobility on the H-Bond network and effects on pKa prediction. *Protein J.* 33, 323–336. doi: 10.1007/s10930-014-9564-z

Marino, S. M., and Gladyshev, V. N. (2010). Cysteine function governs its conservation and degeneration and restricts its utilization on protein surfaces. *J. Mol. Biol.* 404, 902–916. doi: 10.1016/j.jmb.2010.09.027

Matsumoto, M., Yokouchi, H., Suzuki, N., Ohata, H., and Matsunaga, T. (2003). Saccharification of marine microalgae using marine bacteria for ethanol production. *Appl. Biochem. Biotechnol.* 105-108, 247–254. doi: 10.1385/abab:105:1-3:247

Miller, G. L. (1959). Use of dinitrosalicylic acid reagent for determination of reducing sugar. *Anal. Chem.* 31, 426–428. doi: 10.1021/ac60147a030

Morgan, F. J., and Priest, F. G. (1981). Characterization of a thermostable α-amylase from *Bacillus licheniformis* NCIB 6346. *J. Appl. Microb.* 50, 107–114. doi: 10.1111/j.1365-2672.1981.tb00875.x

Nguyen, T.-H., and Haltrich, D. (2013). "Microbial production of prebiotic oligosaccharides," In *Microbial Production of Food Ingredients, Enzymes and Nutraceuticals*, eds B. McNeil, D. Archer, I Giavasis, L. Harvey (Cambridge: Woodhead Publishing), 494–530. doi: 10.1533/9780857093547.2.494

Pan, S., Ding, N., Ren, J., Gu, Z., Li, C., Hong, Y., et al. (2017). Maltooligosaccharide-forming amylase: characteristics, preparation, and application. *Biotechnol. Adv.* 35, 619–632. doi: 10.1016/j.biotechadv.2017.04.004

Patel, S., and Goyal, A. (2011). Functional oligosaccharides: production, properties and applications. *World J. Microbiol. Biotechnol.* 27, 1119–1128. doi: 10.1007/s11274-010-0558-5

Qin, Y., Huang, Z., and Liu, Z. (2014). A novel cold-active and salt-tolerant α-amylase from marine bacterium *Zunongwangia profunda*: molecular cloning, heterologous expression and biochemical characterization. *Extremophiles* 18, 271–281. doi: 10.1007/s00792-013-0614-9

Saitou, N., and Nei, M. (1987). The neighbor-joining method : a new method for reconstructing phylogenetic tree. *Mol. Biol. Evol.* 4, 406–425. doi: 10.1093/oxfordjournals.molbev.a040454

Santiago, M., Ramírez-Sarmiento, C. A., Zamora, R. A., and Parra, L. P. (2016). Discovery, molecular mechanisms, and industrial applications of cold-active enzymes. *Front. Microbiol.* 7:1408. doi: 10.3389/fmicb.2016.01408

Sarmiento, F., Peralta, R., and Blamey, J. M. (2015). Cold and hot extremozymes: industrial relevance and current trends. *Front. Bioeng. Biotech.* 3:148. doi: 10.3389/fbioe.2015.00148

Shida, O., Takano, T., Takagi, H., Kadowaki, K., and Kobayashi, S. (1992). Cloning and nucleotide sequence of the maltopentaose-forming amylase gene from *Pseudomonas* sp. KO-8940. *Biosci. Biotechnol. Biochem.* 56, 76–80. doi: 10.1271/bbb.56.76

Siddiqui, K. S. (2015). Some like it hot, some like it cold: temperature dependent biotechnological applications and improvements in extremophilic enzymes. *Biotechnol. Adv.* 33, 1912–1922. doi: 10.1016/j.biotechadv.2015.11.001

Sievers, F., Wilm, A., Dineen, D., Gibson, T. J., Karplus, K., Li, W., et al. (2011). Fast, scalable generation of high-quality protein multiple sequence alignments using Clustal Omega. *Mol. Syst. Biol.* 7:539. doi: 10.1038/msb.2011.75

Srimathi, S., Jayaraman, G., Feller, G., Danielsson, B., and Narayanan, P. R. (2007). Intrinsic halotolerance of the psychrophilic α-amylase from *Pseudoalteromonas haloplanktis*. *Extremophiles* 11, 505–515. doi: 10.1007/s00792-007-0062-5

Tamura, K., Peterson, D., Peterson, N., Stecher, G., Nei, M., and Kumar, S. (2014). MEGA5: molecular evolutionary genetics analysis using maximum likelihood, evolutionary distance, and maximum parsimony methods. *Mol. Biol. Evol.* 28, 2731–2739. doi: 10.1093/molbev/msr121

Wang, D., Kim, D. H., Seo, N., Yun, E. J., An, H. J., Kim, J.-H., et al. (2016). A novel glycoside hydrolase family 5 β-1,3-1,6-endoglucanase from *Saccharophagus degradans* 2-40^T and its transglycosylase activity. *Appl. Environ. Microb.* 82, 4340–4349. doi: 10.1128/AEM.00635-16

Wang, Q., Wang, H., Yang, X., Wang, K., Liu, R., Li, Q., et al. (2015). A sensitive one-step method for quantitative detection of α-amylase in serum and urine using a personal glucose meter. *Analyst* 140, 1161–1165. doi: 10.1039/c4an02033b

Weiner, R. M., Taylor, L. E., Henrissat, B., Hauser, L., Land, M., Coutinho, P. M., et al. (2008). Complete genome sequence of the complex carbohydrate-degrading marine bacterium, *Saccharophagus degradans* strain 2-40^T. *PLoS Genet.* 4:e1000087. doi: 10.1371/journal.pgen.1000087

Xu, J. (2019). Distance-based protein folding powered by deep learning. *Proc. Natl. Acad. Sci. U. S. A.* 116, 16856–16865. doi: 10.1073/pnas.1821309116

Yang, J., Wang, Y., and Zhang, Y. (2016). ResQ: an approach to unified estimation of *B*-factor and residue-specific error in protein structure prediction. *J. Mol. Biol.* 428, 693–701. doi: 10.1016/j.jmb.2015.09.024

Zhu, A., Romero, R., Huang, J. B., Clark, A., and Petty, H. R. (2011). Maltooligosaccharides from JEG-3 trophoblast-like cells exhibit immunoregulatory properties. *Am. J. Reprod. Immunol.* 65, 54–64. doi: 10.1111/j.1600-0897.2010.00851.x

Zhu, D., Adebisi, W. A., Ahmad, F., Sethupathy, S., Danso, B., and Sun, J. (2020). Recent development of extremophilic bacteria and their application in biorefinery. *Front. Bioeng. Biotech.* 8:483. doi: 10.3389/fbioe.2020.00483

Conflict of Interest: The authors declare that the research was conducted in the absence of any commercial or financial relationships that could be construed as a potential conflict of interest.

frontiers in Microbiology

ORIGINAL RESEARCH
published: 26 July 2021
doi: 10.3389/fmicb.2021.693985

Mle046 Is a Marine Mesophilic MHETase-Like Enzyme

*Ingrid E. Meyer-Cifuentes and Başak Öztürk**

Junior Research Group Microbial Biotechnology, Leibniz Institute DSMZ-German Collection of Microorganisms and Cell Cultures, Braunschweig, Germany

Accumulation of plastics in the oceans presents a major threat to diverse ecosystems. The introduction of biodegradable plastics into the market aims to alleviate the ecological burden caused by recalcitrant plastics. Poly (butylene adipate-co-terephthalate) (PBAT) is a biodegradable commercial plastic that can be biodegraded similarly to polyethylene terephthalate (PET) by PETase-like enzymes and MHETases. The role of MHETases is to hydrolyze the intermediate degradation product of PET, mono-2-hydroxyethyl terephthalate (MHET) to its monomers. We recently identified a homolog of the MHETase of the PET-degrading bacterium *Ideonella sakaiensis*, Mle046, from a marine microbial consortium. In this consortium, Mle046 was highly expressed when a PBAT-based blend film (PF) was supplied as the sole carbon source. In this study, we recombinantly expressed and biochemically characterized Mle046 under different conditions. Mle046 degrades MHET but also 4-(4-hydroxybutoxycarbonyl) benzoic acid (Bte), the intermediate of PF degradation. Mle046 is a mesophilic enzyme adapted to marine conditions, which rapidly degrades MHET to terephthalate and ethylene glycol at temperatures between 20 and 40°C. Mle046 degradation rates were similar for Bte and MHET. Despite its mesophilic tendency, Mle046 retains a considerable amount of activity at temperatures ranging from 10 to 60°C. In addition, Mle046 is active at a range of pH values from 6.5 to 9. These characteristics make Mle046 a promising candidate for biotechnological applications related to plastic recycling.

Keywords: biodegradable plastics, esterases, marine biotechnology, enzymology, marine bacteria

OPEN ACCESS

Edited by:
Benwei Zhu,
Nanjing Tech University, China

Reviewed by:
Shangyong Li,
Qingdao University, China
Tang Li,
Dalian Institute of Chemical Physics, Chinese Academy of Sciences, China

***Correspondence:**
Başak Öztürk
basak.oeztuerk@dsmz.de

Specialty section:
This article was submitted to Microbiotechnology, a section of the journal Frontiers in Microbiology

Received: *12 April 2021*
Accepted: *28 June 2021*
Published: *26 July 2021*

Citation:
Meyer-Cifuentes IE and Öztürk B (2021) Mle046 Is a Marine Mesophilic MHETase-Like Enzyme. Front. Microbiol. 12:693985. doi: 10.3389/fmicb.2021.693985

INTRODUCTION

Biodegradable plastics were introduced in the 1980s into the market as an ecologically friendlier substitute to non-biodegradable plastics (Chen, 2009). Most of these biodegradable plastics contain ester bonds that are prone to enzymatic hydrolysis. One of these biodegradable plastics is the copolymer poly (butylene adipate-co-terephthalate (PBAT), composed of the monomers terephthalic acid (Te), adipic acid, and 1, 4-butanediol (B). The combination of aliphatic and aromatic units in PBAT offers better physical properties than aliphatic–aliphatic biodegradable plastics (Jian et al., 2020). Their chemical structure gives them flexibility and strength similar to low-density polyethylene plastic (Jian et al., 2020). In contrast to polyethylene, however, PBAT is susceptible to microbial degradation in compost and soils (Witt et al., 1999; Zumstein et al., 2018). PBAT biodegradability and high performance make it suitable for packing films. This makes them more economically attractive than other biodegradable plastics (Ferreira et al., 2019). As

already mentioned, PBAT-based plastics can be biodegraded easily in compost by microorganisms (Witt et al., 1995, 1996, 2001). Their fate and biodegradability in aquatic natural environments, however, are still poorly understood. In a previous study, we revealed that a synergistic mechanism within a marine consortium was necessary to achieve complete mineralization of a PBAT-based polymer blend (PF) (Meyer-Cifuentes et al., 2020). In that study, several putative PETase-like (Ple) and MHETase-like (Mle) hydrolases as well as terephthalic acid degrading genes (TPD) were found in the metagenome. We proposed then the following mechanism for PF biodegradation: Ples hydrolyze the ester bonds of the polymeric PF, yielding the monoester 4-(4-hydroxybutoxycarbonyl) benzoic acid (Bte) and other oligomers. Bte can be further degraded by highly specific esterases, namely, Mles (**Figure 1**). In this respect, the suggested biodegradation mechanism for PF is similar to that of polyethylene terephthalate (PET) degradation by *Ideonella sakaiensis* (Yoshida et al., 2016). Degradation of PET by this bacterium is initiated by IsPETase to yield the monoester mono-2-hydroxyethyl terephthalate (MHET), the first intermediate of PET degradation. MHET is then further hydrolyzed by α/β-hydrolase, IsMHETase, to Te and ethylene glycol. *I. sakaiensis* can further degrade Te via a TPD cluster. Among the different Mles identified in our previous study (Meyer-Cifuentes et al., 2020), only Mle046, presumably produced by an Alphaproteobacterial strain, was consistently expressed and produced during PF degradation. This *mle046* is 100% identical to a homolog present in *Celeribacter manganoxidans* and its protein is 46.9% identical to IsMHETase. At the structural level, Mle046 contains a domain typical of feruloyl esterases compromising the canonical catalytic triad of these types of enzymes. The high expression in the presence of PF and its similarity to IsMHETase suggests that Mle046 is responsible for the PF degradation intermediate Bte and can also degrade the structurally similar PET degradation intermediate MHET.

In this study, we investigate the biochemical characteristics of a new MHETase-like enzyme, Mle046. Specifically, we demonstrate the ability of Mle046 to hydrolyze MHET, Bte under broad temperature and pH conditions. This novel MHETase-like enzyme could potentially be engineered in the near future to degrade plastics and produced plastic monomers in two-enzyme reactor systems as shown before (Barth et al., 2015; Knott et al., 2020).

MATERIALS AND METHODS

Gene Synthesis

Codon-optimized gene *mle046* was synthesized by BioCat GmbH (Heidelberg, Germany) and cloned into a pColdII vector. The codon-optimized sequence can be found in **Supplementary Table 1**. The signal peptide (first 27 amino acids) of the original protein was detected with the SignalP software v. 5.0 (Almagro Armenteros et al., 2019) and was excluded from the synthetic construct.

Expression of the Mle046 and Cell Lysis

The Mle046 was expressed following a protocol adapted from Palm et al. (2019). *Escherichia coli* Shuffle T7 cells (New England BioLabs, United States) were transformed with the pColdII plasmid containing the *mle046* insert. The transformants were plated on Lysogeny Broth (LB) agar plates with 50 mg/L of ampicillin and incubated at 37°C overnight. Pre-cultures were prepared by inoculating single colonies from the plates to liquid LB and incubated for 62 h at 20°C, 150 rpm. After this time, 1 mL of the pre-culture was inoculated to 200 mL of Terrific Broth containing 100 mg/L Carbenicillin (Sigma-Aldrich, United States) in 1 L baffled flasks. The cultures were incubated at 37°C at 150 rpm in a MaxQ™ 4000 orbital shaker (Fischer Scientific, Germany), until an $OD_{600\ nm}$ of 0.8–1.0 was reached. Then 0.5 mM of IPTG was added to cultures pre-cooled on ice for 15 min. Cultures were incubated overnight at 15°C, 150 rpm. After incubation, the pellets were collected by centrifuging at 4°C, 5,514 × *g* for 10 min in a Heraeus™ Multifuge™ X3 (Fischer Scientific, Germany), and resuspended in His-Tag binding buffer (20 mM sodium phosphate and 0.5 M NaCl, pH 7.4) at 1:10 of the original culture volume. Cells were disrupted by incubation with FastBreak™ Cell Lysis Reagent (Promega, United States) and 1 μL Pierce™ Universal Nuclease for Cell Lysis (Thermo Fischer Scientific, United States) at 20°C for 30 min with constant shaking in a MaxQ™ 4000 orbital shaker (Fischer Scientific, Germany). To separate and collect the soluble fraction, the lysates were centrifuged at 4°C, 15,000 × *g* for 30 min in a Heraeus™ Multifuge™ X3 (Fischer Scientific, Germany). The soluble fractions were filtered through a 0.2 μM filter.

Identification and Purification of the Mle046

Ten microliters of soluble fractions of induced and non-induced cells were mixed with 10 μL of 2× sodium dodecyl sulphate–polyacrylamide gel electrophoresis (SDS-PAGE) Protein loading buffer and boiled for 10 min at 95°C in an Eppendorf Thermomixer® C (Eppendorf, Germany). Insoluble fractions from the same experiments were resuspended in PBS and treated the same way as the soluble fractions as a control for denatured proteins or inclusion bodies. After cooling on ice, the samples were loaded into 12% SDS-PAGE gels and ran for 45 min at 25 V/cm in a Mini-PROTEAN® Tetra Cell (Bio-Rad Laboratories, United States). The presence of Mle046 was detected by comparing induced to non-induced samples and to a protein size standard (Precision Plus Protein™ Unstained Standards, Bio-Rad Laboratories, United States). As the protein was detected in the soluble fraction, insoluble fractions were not used for further experiments.

The soluble induced fractions were loaded into a 5 mL His-Trap™ HP affinity Ni-Sepharose column (Cytiva, Germany) connected to an ÄKTA™ Start Purification System (Cytiva, Germany). Proteins were bound and eluted from the column by using the predefined affinity purification protocol included in the UNICORN® start 1.1 software (Cytiva, Germany). The purity of the fractions presenting a peak was assessed as described

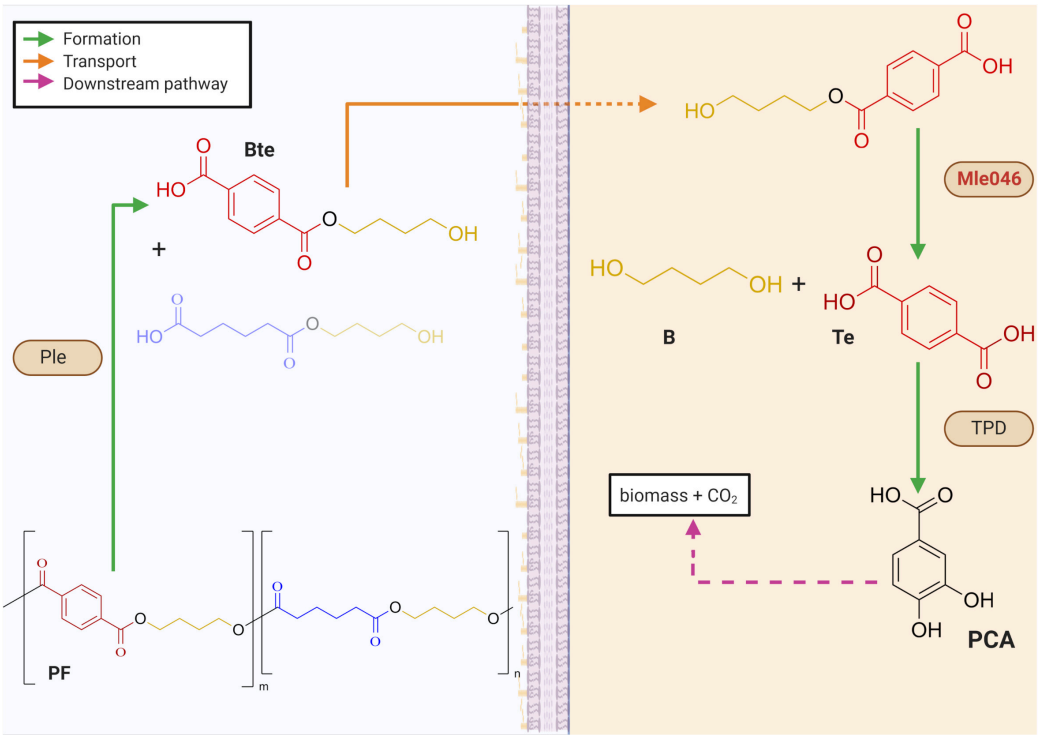

FIGURE 1 | Mechanisms for the biodegradation of a PBAT-based blend film (PF) within a biofilm. Periplasmatic α/β hydrolases (Ples) cleave the PF to produce oligomers of 1,4-butanediol (B) with either terephthalic acid (Te) or adipic acid. Mles (e.g., Mle046 shown in red) hydrolyzes inside the cell a mixture of terephthalate-butanediol monoester (Bte) that yields Te and B. Te is further degraded by a Te degradation cluster (TPD). Downstream degrading enzymes lead to the formation of protocatechuate (PCA) which can be further degraded to biomass and CO_2. Green arrows indicate the formation of intermediates after enzymatic catalysis; orange arrows show the transport of intermediates to the cell; pink-dashed arrows indicate downstream degradation pathways (created with Biorender.com).

before by SDS-PAGE. The fractions were further concentrated on a Pierce™ Protein Concentrator PES 10K MWCO (Thermo Fischer Scientific, United States). The affinity-purified fractions were further polished by size exclusion chromatography on a HiPrep™ 16/60 Sephacryl™ S-200 HR column (Cytiva, Germany) connected to an ÄKTA™ Start Purification System (Cytiva, Germany) in a buffer consisting of 25 mM Tris–HCl and 200 mM NaCl, pH 7.5. Fractions containing the Mle046 protein were pooled and concentrated on a Pierce™ Protein Concentrator PES 10K MWCO (Thermo Fischer Scientific, United States). The concentration of the purified protein was quantified by using the Qubit Protein Assay kit and measured on a Qubit 3.0 Fluorometer (Invitrogen, United States).

Hydrolysis of MHET by Mle046

To assay the hydrolysis of MHET by Mle046, the activity of the enzyme was measured in triplicate as described before (Palm et al., 2019) with a few modifications. Mle046 was used at a final concentration of 0.002 μg/μL and incubated in the presence of different concentrations of MHET (300–2,700 μM) dissolved in 40 mM sodium phosphate buffer, pH 7.5. Incubations were carried out for 21 min at 30°C and shaking at 300 rpm in an Eppendorf Thermomixer® C (Eppendorf, Germany). Every 3 min a sample was taken and immediately inactivated by adding an equal volume of methanol (Methanol Optigrade® for HPLC, Promochem, LGC Standards GmbH, Germany). The samples were then centrifuged at 17,000 × *g* for 10 min in a Microstar 17R centrifuge (VWR, United States) and the supernatants were transferred to standard HPLC vials. Negative controls containing only the substrate and buffer were also included. MHET degradation was detected with a 1260 Infinity II LC System (Agilent Technologies, United States). Samples were separated through a Agilent Poroshell 120 HPH-C18 column (Agilent Technologies, United States) with a gradient of acetonitrile 99.9% HPLC grade (Fischer Scientific, United States) and 0.1% (v/v) formic acid (98–100% Suprapur®, Sigma-Aldrich, United States) in Milli-Q water. The flow rate was set at 0.2 mL/min. One microliter of the sample was injected. Acetonitrile was increased from 5 to 44% until minute 12 and then to 70% at minute 15 remaining constant for other 3 min. MHET was detected at 240 nm.

Determination of Enzyme Kinetics

Mle046 rates were plotted against MHET concentrations, and the kinetic parameters were determined by using the GraphPad Prism v. 5. 01 software (GraphPad). Kinetics parameters such as maximum velocity (*Vmax*), Michaelis–Menten constant (*Km*), and the rate constant (*kcat*) were calculated with non-linear regression.

Hydrolysis of Bte by Mle046 and Substrate Affinity

To assess Mle046 activity on the PF degradation intermediate, Bte, 0.002 μg/μL of the enzyme was incubated in 40 mM sodium phosphate buffer, pH 7.5 in the presence of 1,000 μM of Bte (Bte was synthetized as indicated in the **Supplementary Material**). Negative controls containing only the substrate and buffer were also included. Reactions and controls were prepared in triplicates and incubated at 30°C, 21 min, and shaking at 300 rpm in an Eppendorf Thermomixer® C (Eppendorf, Germany). Every 3 min a sample was taken and immediately inactivated by adding an equal volume of methanol (Methanol Optigrade® for HPLC, Promochem, LGC Standards GmbH, Germany). The samples were then centrifuged at 17,000 × *g* for 10 min in a Microstar 17R centrifuge (VWR, United States), and the supernatants were transferred to standard HPLC vials. MHET degradation was detected with a 1260 Infinity II LC System (Agilent Technologies, United States). Samples were separated through an Agilent Poroshell 120 HPH-C18 column (Agilent Technologies, United States) with a gradient of acetonitrile 99.9% HPLC grade (Fischer Scientific, United States) and 0.1% (v/v) formic acid (98–100% Suprapur®, Sigma-Aldrich, United States) in Milli-Q water. The flow rate was set at 0.2 mL/min. One microliter of the sample was injected. Acetonitrile was increased from 5 to 44% until minute 12 and then to 70% at minute 15 remaining constant for other 3 min. Bte and Te formation was detected at 240 nm.

Additionally, we tested substrate range of Mle046 by incubating the enzyme in the presence of a mixture of Bte and BHET (bis 2-hydroxyethyl terephthalate, the precursor to MHET during PET degradation), only with Bte or only with BHET. For this, 1 μL Mle046 (0.005 μg/μL) was incubated in 40 mM sodium phosphate buffer, pH 7.5 with the following substrates: 800 μM of BHET, 800 μM of Bte, and a mixture of 800 μM of BHET and 800 μM Bte. Negative controls containing only the substrate and buffer were also included. Reactions and controls were prepared in triplicates and incubated at 20°C for 30 min in an Eppendorf ThermoMixer® C (Eppendorf, Germany). Three sampling points were taken at 0, 15, and 30 min. The samples were immediately inactivated after the addition of acidic (pH 2.5) 160 mM sodium phosphate buffer (Palm et al., 2019) and heating at 80°C for 10 min. Bte and BHET were further detected with a 1260 Infinity II LC System (Agilent Technologies, United States). Samples were separated through an Agilent Poroshell 120 HPH-C18 column (Agilent Technologies, United States). The mobile phase consisted of a gradient of acetonitrile 99.9% HPLC grade (Fischer Scientific, United States) and 0.1% (v/v) of formic acid (98–100% Suprapur®, Sigma-Aldrich, United States) in Milli-Q water. The flow rate was set at 0.2 mL/min. One microliter of the sample was injected. Acetonitrile was increased from 5 to 44% until minute 12 and then to 70% at minute 15 remaining constant for other 3 min. BHET and Bte were detected at 240 nm.

Determination of Optimum pH and Temperature

We tested Mle046 activity at different temperatures and pH values by measuring the formation of Te after degradation of MHET at different pH and temperatures. For the reaction, Mle046 (0.002 μg/μL) was incubated in 100 mM sodium phosphate buffer pH 7.5 with 800 μM MHET. Negative controls containing only the substrate and buffer were also included. Reactions and controls were prepared in triplicates. Incubations were performed in a Veriti™ 96-Well Thermal cycler (Applied Biosystems, United States) between 5 and 10–60°C with a 10°C increments. After 20 min, the reactions were immediately inactivated by adding an equal volume of methanol (Methanol Optigrade® for HPLC, Promochem, LGC Standards GmbH, Germany). The samples were then centrifuged at 17,000 × *g* for 10 min in a Microstar 17R centrifuge (VWR, United States), and the supernatants were transferred to standard HPLC vials. To test the effect of different pH values on Mle046 activity, we incubated the enzyme with 800 μM MHET as the substrate in 100 mM sodium phosphate buffer. The pH of the buffer was adjusted between 5 and 10 with 1 pH unit increments. Negative controls containing only the substrate and buffer were also included. Reactions and controls were prepared in triplicates and incubated at 20°C in a Veriti™ 96-Well Thermal cycler (Applied Biosystems, United States). After 20 min, the reactions were immediately inactivated by adding an equal volume of methanol (Methanol Optigrade® for HPLC, Promochem, LGC Standards GmbH, Germany). The samples were then centrifuged at 17,000 × *g* for 10 min in a Microstar 17R centrifuge (VWR, United States), and the supernatants were transferred to standard HPLC vials.

Temperature and pH optimum were assessed by measuring Te formation with a 1260 Infinity II LC System (Agilent Technologies, United States). Samples were separated through an Agilent Poroshell 120 HPH-C18 column (Agilent Technologies, United States) with a gradient of acetonitrile 99.9% HPLC grade (Fischer Scientific, United States) and 0.1% (v/v) formic acid (98–100% Suprapur®, Sigma-Aldrich, United States) in Milli-Q water. The flow rate was set at 0.2 mL/min. One microliter of the sample was injected. Acetonitrile was increased from 5 to 44% until minute 12 and then to 70% at minute 15 remaining constant for other 3 min. MHET and Te formation was detected at 240 nm.

Product Inhibition

The inhibition of Mle046 activity in the presence of the products Te (12,500, 10,000, 7,500, 5,000, and 2,500 μM) and 1,4-butanediol (B) (100,000, 200,000, and 450,000 μM) was tested. For this assay, the Te or B was diluted in 100 mM sodium phosphate buffer pH 7.5 in the presence of 1,000 μM of MpNPT (MpNPT was synthesized according to Palm et al., 2019) and 0.02 μg/μL of Mle046. Incubations were performed in triplicate at 20°C, in a Veriti™ 96-Well Thermal cycler (Applied Biosystems, United States). Negative controls consisting of only the substrate and buffer were included together with positive controls consisting of the substrate, the buffer, and Mle046 without an inhibitory product.

The absorbance of the samples was measured after 30 min of incubation at 450 nm in a TECAN Infinite® M200 plate reader (TECAN, Switzerland) and retrieved using the TECAN i-control v. 1.5.14.0 software (TECAN, Switzerland). The concentration of the produced 4-nitrophenol was obtained from a 4-nitrophenol standard curve prepared under the same assay conditions.

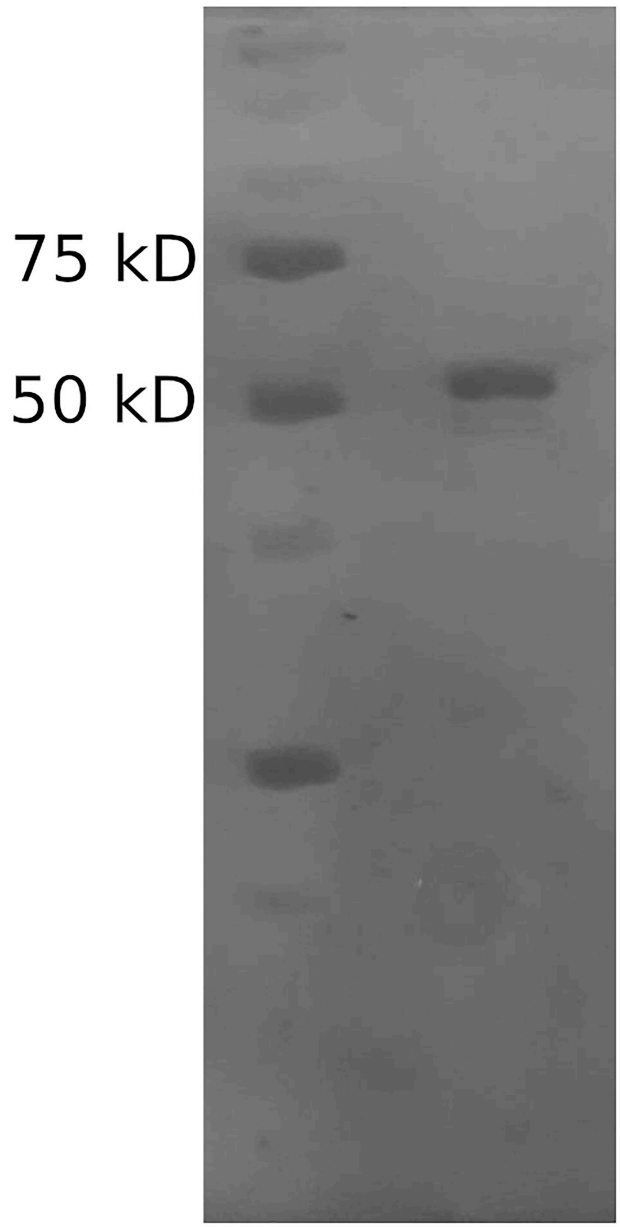

FIGURE 2 | Purified His-tagged Mle046 protein. The size of the purified protein agrees with the predicted size (62 kD).

RESULTS

Mle046 Purification and Identification

The Mle046 sequence obtained in a previous study (Meyer-Cifuentes et al., 2020) was used in this study and codon optimized for recombinant expression. The theoretical size of the His-tagged Mle046 is 62 kD. Structural analysis of the Mle046 sequence and its similarity to other MHETase-like enzymes were described in more detail previously (Meyer-Cifuentes et al., 2020).

The Mle046 protein was purified by affinity chromatography to determine degradation kinetics, substrate specificity, inhibition, and optimized conditions. The size of the purified Mle046 on an SDS-PAGE gel was similar to the expected size. The purest fraction was used in this study (**Figure 2**). The concentration and calculated yield of Mle046 after purification were 4 mg/mL and 60 mg of protein per 1 L of cell culture, respectively.

Mle046 Activity Toward MHET and Bte

Mle046 (0.002 μg/μL; 0.04 μM) can degrade MHET to concentrations up to 2,200 μM at 30°C. The highest rate was 1.4 μMs^{-1} with 1,570 μM of MHET. With 2,700 μM MHET, the rate of degradation declined to 0.47 μMs^{-1}. As shown in

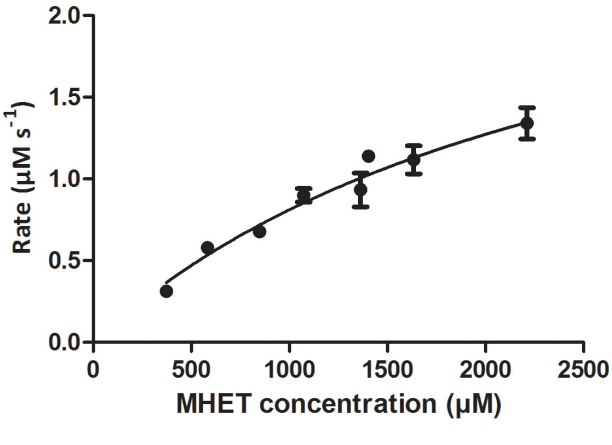

FIGURE 3 | Rate of MHET catalysis by Mle046 plotted against substrate concentration. Degradation rates are expressed in terms of μM MHET degraded per second. Error bars indicate standard deviation (n = 3).

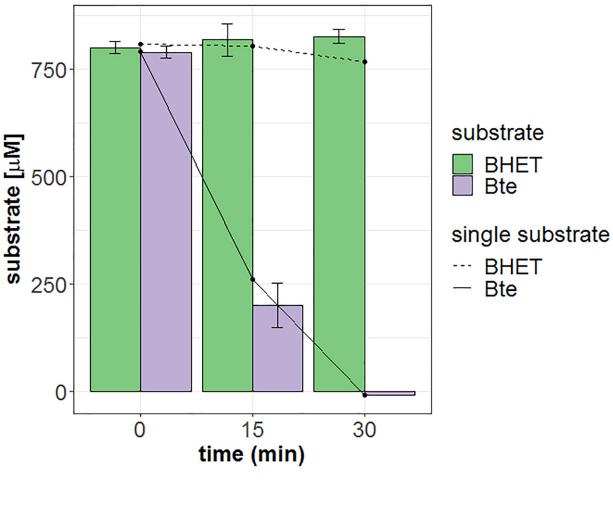

FIGURE 4 | Degradation of Bte, BHET, or a mixture of both by Mle046. Bte and BHET supplied as single substrates are shown as solid and dashed lines, respectively. The mixture of Bte and BHET is shown as purple and green filled bars, respectively. The sampling points are shown at 0, 15, and 30 min. Error bars indicate standard deviation (n = 3).

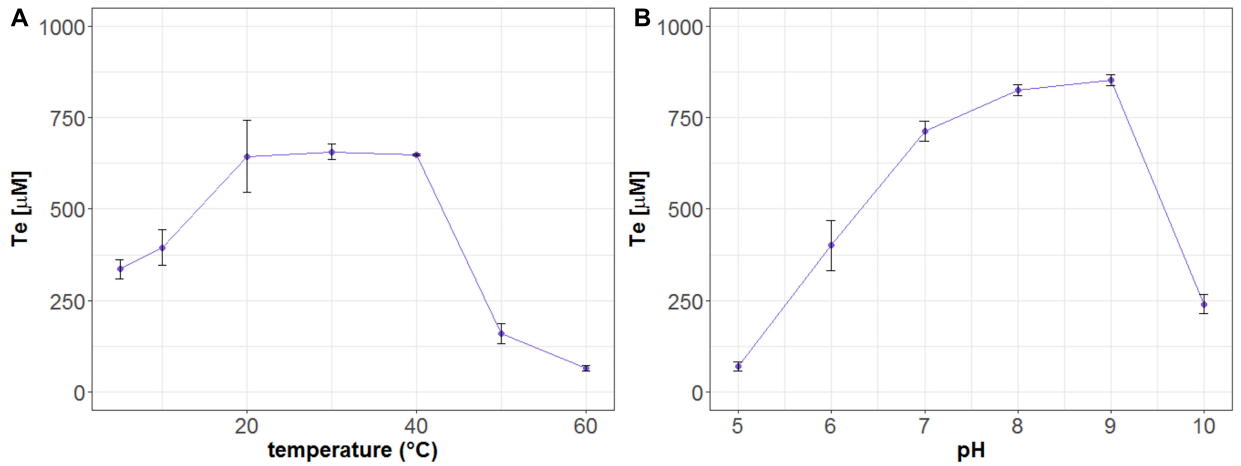

FIGURE 5 | Formation of Te (μM) after hydrolysis of MHET by Mle046. The release of Te by Mle046 was quantified after 20 min at **(A)** different temperatures and **(B)** different pH values. Error bars indicate standard deviation (n = 3).

Figure 3, Mle046 kinetics followed a Michaelis–Menten curve with concentrations up to 2,230 μM. Mle046 *Vmax*, *Km*, and the rate constant *kcat* were estimated as 2.9 μMs^{-1}, 2,638 μM (±797), and 80.9 s^{-1} (±15.8), respectively (**Supplementary Table 2**). The reaction efficiency of Mle046, *kcat*/*Km*, was 0.03. After 21 min of incubation, Mle046 degraded 92% of 800 μM of MHET relative to the first sampling point. On the contrary, when 2,700 μM of MHET was present, the Mle046 could be degraded only ∼10% of MHET. We also tested the activity of Mle046 on the first intermediate of PF degradation, Bte. The incubation of Mle046 (0.002 μg/μL) in the presence of 1,000 μM Bte led to 94% Bte degradation after 21 min (**Supplementary Figure 1**). The degradation rate with 1,000 μM of Bte, 0.82 μMs^{-1}, was almost the same as the degradation rate of Mle046 incubated with 1,140 μM MHET, 0.78 μMs^{-1}. After 21 min of incubation with 1,000 μM of Bte with Mle046, 861 μM of Te was formed. When Mle046 (0.005 μg/μL) was incubated with 800 μM Bte, 800 μM of BHET, or a mixture of both substrates, the degradation rate of Bte remained the same (0.62 ± 0.03 μMs^{-1}) with either of the substrates or in combination. Whether Bte was supplied alone or together with BHET, more than 70% of the initial amount of Bte was degraded after 15 min (**Figure 4**). This suggests that BHET has no inhibitory effect over Bte degradation. At the same time, Mle046 had no activity toward BHET.

Dependence of Mle046 Activity on Temperature and pH

Mle046 degraded MHET and produced Te at every temperature tested. At 20, 30, and 40°C, after 20 min of incubation, Mle046 released similar amounts of Te 644, 656, and 648 μM, respectively (**Figure 5A**). The released amount of Te decreased relative to the amount formed at 30°C; to 51% at 5°C, 60% at 10°C, 24% at 50°C, and 10% at 60°C. Mle046 formed the same amount of Te (98%) at 20 and 40°C.

We also analyzed the effect of pH on MHET degradation by the Mle046. Similar to the Mle046 activity at different temperatures, MHET was degraded in a broad range of pH conditions. As observed in this study, the activity of Mle046 was mostly affected by highly acidic (pH 5) or alkaline (pH 10) conditions (**Figure 5B**). The highest amount of Te was formed at pH 8 and 9 (839 ± 15 μM). Relative to the condition at pH 8, Te formation decreased to 8% at pH 5 and less than 30% at pH 10. Thus, the optimum pH of the enzyme activity is within a range of 7–9.

Mle046 Product Inhibition by Te and B

To test product inhibition, we incubated Mle046 at 20°C in the co-presence of MpNPT and Bte degradation products:

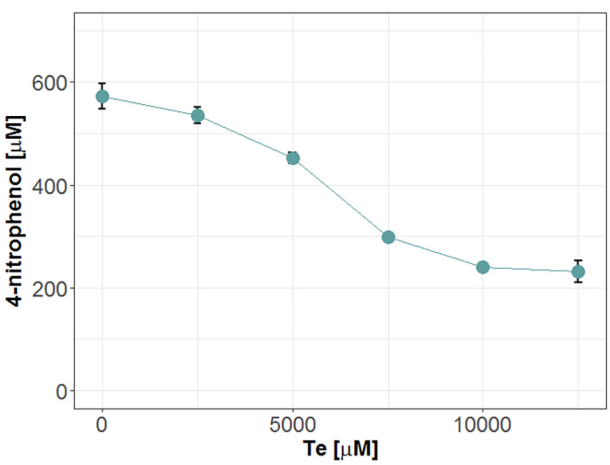

FIGURE 6 | Release of 4-nitrophenol after hydrolysis of MpNPT by Mle046 and in the presence of various concentrations of Te. Incubations were carried out for 30 min. Error bars indicate standard deviation (n = 3).

Te or B. The activity was then assessed by measuring the formation of 1,4-nitrophenol. Under these conditions, we observe that high concentrations of Te had a negative effect on the degradation of MpNPT by Mle046 (**Figure 6**). When we incubated Mle046 in the presence of Te concentrations of ≥7,500 μM, less than 50% of 4-nitrophenol was formed (relative to Mle046 without Te). With lower concentrations (<5,000 μM), Mle046 produced the same amount of 4-nitrophenol as when Mle046 was incubated in the absence of Te or B. In the presence of 2,500 μM of Te, Mle046 formed 530 μM of 4-nitrophenol similarly to the 570 μM 4-nitrophenol formed in the absence of Te. This means that with 2,500 μM of Te, the degradation rate was reduced only by 7%. Contrary to Te, none of the B concentrations tested in this study had a negative effect on the formation of 4-nitrophenol by Mle046 (data not shown).

DISCUSSION

In this study, we expressed, purified, and biochemically characterized an MHETase-like enzyme, Mle046, identified previously in a marine microbial consortium (Meyer-Cifuentes et al., 2020). To the best of our knowledge, this is the first identified and characterized marine MHETase-like enzyme.

We show that Mle046 degrades not only the first intermediate of PF degradation, Bte, but also the first intermediate of PET degradation, MHET. Mle046 can degrade MHET over a wide range of concentrations at 30°C. Its *Km* is, however, high (2,638 μM ± 797) when compared to those of IsMHETase (7.3 ± 0.6 μM) (Palm et al., 2019) and IsMHETase homologs of *Comamonas thiooxydans* and *Hydrogenophaga* sp. PML113 (174.70 ± 4.75 and 41.09 ± 3.38 μM, respectively) (Knott et al., 2020). This implies that Mle046 has a lower affinity to MHET and that the enzyme does not accept MHET as efficiently as the previously described homologs. However, enzymes which catalyze the same reaction but are from different organisms can have widely differing *Km* values (Robinson, 2015). As already suggested by Palm et al. (2019), low substrate affinity can be a disadvantage for bacteria in natural environments where low substrate concentrations are expected. The turnover rate (*kcat*) of MHET by Mle046 was, however, much higher than those that were reported for other MHETases. The turnover of the IsMHETase calculated in different studies ranges between 11.1 and 31 s^{-1} (Yoshida et al., 2016; Palm et al., 2019; Knott et al., 2020), while the turnover of *Hydrogenophaga* sp. PML113 and *C. thiooxydans* MHETases is 3.8 ± 2.5 and 9.5 ± 0.8 s^{-1}, respectively (Knott et al., 2020). Due to the higher km value, the catalytic efficiency of Mle046 (0.03) is ∼40 times lower than that of IsMHETase but in the same order of magnitude as the *Hydrogenophaga* sp. PML113 and *C. thiooxydans* MHETases (Knott et al., 2020). Knott et al. (2020) demonstrated that an S131G mutant of the IsMHETase had a lower affinity to MHET and a much higher *Km* than the wild type. The position 131 is a glycine in the Mle046 (Gly117), as it is in the two homologs in *Hydrogenophaga* sp. PML113 and *C. thiooxydans* (**Supplementary Figure 2**). We therefore suggest that this residue is a determining factor for the substrate affinity of Mle046.

We also investigated if Mle046 is subjected to product inhibition, similar to IsMHETase, its homologs and other feruloic acid esterases (Crepin et al., 2003; Knott et al., 2020). We did not observe a strong inhibition of Mle046 by Te, one of the products of MHET and Bte degradation. Palm et al. (2019) proposed that substrate recognition by IsMHETase strongly relies on the aromatic ring of the substrate and that, therefore, Te might bind and inhibit the IsMHETase. Knott et al. (2020) suggested that the aforementioned S131G mutation reduces inhibition due to the reduced affinity of the enzyme to the substrate, which may explain the lack of Te inhibition for Mle046 as well. In the context of plastic degradation in the natural environment, Te inhibition would be less limiting, since this product is rapidly metabolized (Meyer-Cifuentes et al., 2020).

IsMHETase and some homologs such at TfCa from *Thermobifida fusca* present activity toward BHET (Belisário-Ferrari et al., 2019; Sagong et al., 2020). Yet, when Mle046 was incubated with Bte and BHET, Mle046 could not degrade BHET. In addition, the presence of this substrate did not inhibit Mle046 activity toward Bte. High specificity of Mle046 toward MHET might be beneficial in dual-enzyme systems designed to degrade plastics with a mixture of PETases and MHETases enzymes (Knott et al., 2020).

We also found that Mle046 is active at low temperatures, retaining ∼50% of its activity at 5°C compared to 30°C. We conclude that Mle046 is a mesophilic but cold-active enzyme, rather than a psychrophilic enzyme. At higher temperatures (>40°C), however, we observed a decline in Mle046 activity which indicates that Mle046 is heat-labile to a certain degree but not completely inactivated, retaining some of its activity at temperatures up to 60°C. The mesophilic and cold-active tendency of Mle046 is likely associated with the marine nature of the Mle046-producing bacteria were collected from. Mle046 originates from a mixed culture that was enriched using inocula collected from the North, Aegean, and Tyrrehenian seas. Overall, the surface temperatures of these areas range between 15 and 25°C yearly. Previously, we have shown that Mle046 was acquired via a transposable element from an Alphaproteobacterial conjugative plasmid, pDY25-B. Within this group, *C. manganoxidans* and *Sulfitobacter* sp. HI0023 contain the pDY25-B plasmid with the incorporated *mle046* sequence. *Celeribacter* species have been commonly isolated either from coastal surface seawater or deep-sea sediments (Lee et al., 2012; Baek et al., 2014; Lai et al., 2014; Wang et al., 2015). Like *Celeribacter* species, *Sulfitobacter* sp. HI0023 was isolated from the Pacific Ocean (Sosa et al., 2015). These findings strongly indicate that Mle046 contained in the pDY25-B plasmid evolved and adapted together with its hosts to mild-to-cold temperatures in the oceans.

Mle046 remains active at temperatures above 30°C and up to 60°C albeit at lower degradation rates. The activity of IsMHETase on the other hand rapidly falls at temperatures above 45°C and

at 60°C the enzyme is virtually inactivate (Palm et al., 2019). Thus, Mle046 is an enzyme that can be used in two-enzyme degradation systems where high temperatures, typically around 60°C, are needed for more efficient PET degradation (Barth et al., 2015; De Castro et al., 2017; Wei and Zimmermann, 2017; Samak et al., 2020). In these systems, the PETases and MHETase-like enzymes can be additionally engineered to improve their hydrolytic properties (Austin et al., 2018; Ma et al., 2018; Son et al., 2019, 2020; Knott et al., 2020).

We conclude that Mle046 is a marine MHETase which can degrade the degradation intermediates of both PET and PBAT. With its activity at a broad range of temperatures and pH values, it is a contender as an enzyme to complement PETase activity in dual-enzyme systems for biotechnological applications. Engineering of the active site can improve the catalytic efficiency and substrate affinity.

DATA AVAILABILITY STATEMENT

The data presented in the study are deposited in the Genbank repository, accession number MZ408123.

AUTHOR CONTRIBUTIONS

IM-C designed and performed the experiments, analyzed the data, and wrote the manuscript. BÖ designed the experiments, analyzed the data, wrote the manuscript, and supervised the project. Both authors contributed to the editing of the manuscript and agreed on the final version.

ACKNOWLEDGMENTS

The authors thank Anja Heuer, Justyna Barys, Dominik Werner, and Marcel Schleuning (Microbial Biotechnology group, DSMZ) for technical assistance and support. Meina Neumann-Schaal (Department of Analytics, group Metabolomics, DSMZ) is acknowledged for the generation of LC-MS data. The authors also thank BASF SE for financial support.

SUPPLEMENTARY MATERIAL

The Supplementary Material for this article can be found online at: https://www.frontiersin.org/articles/10.3389/fmicb.2021.693985/full#supplementary-material

REFERENCES

Almagro Armenteros, J. J., Tsirigos, K. D., Sønderby, C. K., Petersen, T. N., Winther, O., Brunak, S., et al. (2019). SignalP 5.0 improves signal peptide predictions using deep neural networks. *Nat. Biotechnol.* 37, 420–423. doi: 10.1038/s41587-019-0036-z

Austin, H. P., Allen, M. D., Donohoe, B. S., Rorrer, N. A., Kearns, F. L., Silveira, R. L., et al. (2018). Characterization and engineering of a plastic-degrading aromatic polyesterase. *Proc. Natl. Acad. Sci. U.S.A.* 115:E4350. doi: 10.1073/pnas.1718804115

Baek, K., Choi, A., Kang, I., and Cho, J.-C. (2014). Celeribacter marinus sp. nov., isolated from coastal seawater. *Int. J. Sys. Evol. Microbiol.* 64, 1323–1327. doi: 10.1099/ijs.0.060673-0

Barth, M., Oeser, T., Wei, R., Then, J., Schmidt, J., and Zimmermann, W. (2015). Effect of hydrolysis products on the enzymatic degradation of polyethylene terephthalate nanoparticles by a polyester hydrolase from Thermobifida fusca. *Biochem. Eng. J.* 93, 222–228. doi: 10.1016/j.bej.2014.10.012

Belisário-Ferrari, M. R., Wei, R., Schneider, T., Honak, A., and Zimmermann, W. (2019). Fast turbidimetric assay for analyzing the enzymatic hydrolysis of polyethylene terephthalate model substrates. *Biotechnol. J.* 14:1800272. doi: 10.1002/biot.201800272

Chen, G. Q. (2009). A microbial polyhydroxyalkanoates (PHA) based bio- and materials industry. *Chem. Soc. Rev.* 38, 2434–2446. doi: 10.1039/b812677c

Crepin, V. F., Faulds, C. B., and Connerton, I. F. (2003). A non-modular type B feruloyl esterase from Neurospora crassa exhibits concentration-dependent substrate inhibition. *Biochem. J.* 370, 417–427. doi: 10.1042/BJ20020917

De Castro, A. M., Carniel, A., Nicomedes Junior, J., Da Conceição Gomes, A., and Valoni, É (2017). Screening of commercial enzymes for poly(ethylene terephthalate) (PET) hydrolysis and synergy studies on different substrate sources. *J. Ind. Microbiol. Biotechnol.* 44, 835–844. doi: 10.1007/s10295-017-1942-z

Ferreira, F. V., Cividanes, L. S., Gouveia, R. F., and Lona, L. M. F. (2019). An overview on properties and applications of poly(butylene adipate-co-terephthalate)–PBAT based composites. *Polym. Eng. Sci.* 59, E7–E15. doi: 10.1002/pen.24770

Jian, J., Xiangbin, Z., and Xianbo, H. (2020). An overview on synthesis, properties and applications of poly(butylene-adipate-co-terephthalate)–PBAT. *Adv. Ind. Eng. Polym. Res.* 3, 19–26. doi: 10.1016/j.aiepr.2020.01.001

Knott, B. C., Erickson, E., Allen, M. D., Gado, J. E., Graham, R., Kearns, F. L., et al. (2020). Characterization and engineering of a two-enzyme system for plastics depolymerization. *Proc. Natl. Acad. Sci. U.S.A.* 117:25476. doi: 10.1073/pnas.2006753117

Lai, Q., Cao, J., Yuan, J., Li, F., and Shao, Z. (2014). Celeribacter indicus sp. nov., a polycyclic aromatic hydrocarbon-degrading bacterium from deep-sea sediment and reclassification of Huaishuia halophila as Celeribacter halophilus comb. nov. *Int. J. Sys. Evol. Microbiol.* 64, 4160–4167. doi: 10.1099/ijs.0.069039-0

Lee, S.-Y., Park, S., Oh, T.-K., and Yoon, J.-H. (2012). Celeribacter baekdonensis sp. nov., isolated from seawater, and emended description of the genus Celeribacter Ivanova et al. 2010. *Int. J. Syst. Evol. Microbiol.* 62, 1359–1364. doi: 10.1099/ijs.0.032227-0

Ma, Y., Yao, M., Li, B., Ding, M., He, B., Chen, S., et al. (2018). Enhanced poly(ethylene terephthalate) hydrolase activity by protein engineering. *Engineering* 4, 888–893. doi: 10.1016/j.eng.2018.09.007

Meyer-Cifuentes, I. E., Werner, J., Jehmlich, N., Will, S. E., Neumann-Schaal, M., and Öztürk, B. (2020). Synergistic biodegradation of aromatic-aliphatic copolyester plastic by a marine microbial consortium. *Nat. Commun.* 11:5790. doi: 10.1038/s41467-020-19583-2

Palm, G. J., Reisky, L., Bottcher, D., Muller, H., Michels, E.a.P, Walczak, M. C., et al. (2019). Structure of the plastic-degrading Ideonella sakaiensis MHETase bound to a substrate. *Nat. Commun* 10:1717. doi: 10.1038/s41467-019-09326-3

Robinson, P. K. (2015). Enzymes: principles and biotechnological applications. *Essays Biochem.* 59, 1–41. doi: 10.1042/bse0590001

Sagong, H.-Y., Seo, H., Kim, T., Son, H. F., Joo, S., Lee, S. H., et al. (2020). Decomposition of the PET film by MHETase using Exo-PETase function. *ACS Catal.* 10, 4805–4812. doi: 10.1021/acscatal.9b05604

Samak, N. A., Jia, Y., Sharshar, M. M., Mu, T., Yang, M., Peh, S., et al. (2020). Recent advances in biocatalysts engineering for polyethylene terephthalate plastic waste green recycling. *Environ. Int.* 145:106144. doi: 10.1016/j.envint.2020.106144

Son, H. F., Cho, I. J., Joo, S., Seo, H., Sagong, H.-Y., Choi, S. Y., et al. (2019). Rational protein engineering of thermo-stable PETase from Ideonella sakaiensis

for highly efficient PET degradation. *ACS Catal.* 9, 3519–3526. doi: 10.1021/acscatal.9b00568

Son, H. F., Joo, S., Seo, H., Sagong, H.-Y., Lee, S. H., Hong, H., et al. (2020). Structural bioinformatics-based protein engineering of thermo-stable PETase from Ideonella sakaiensis. *Enzyme Microb.Technol.* 141:109656. doi: 10.1016/j.enzmictec.2020.109656

Sosa, O. A., Gifford, S. M., Repeta, D. J., and Delong, E. F. (2015). High molecular weight dissolved organic matter enrichment selects for methylotrophs in dilution to extinction cultures. *ISME J.* 9, 2725–2739. doi: 10.1038/ismej.2015.68

Wang, L., Liu, Y., Wang, Y., Dai, X., and Zhang, X.-H. (2015). Celeribacter manganoxidans sp. nov., a manganese-oxidizing bacterium isolated from deep-sea sediment of a polymetallic nodule province. *Int. J. Sys. Evol. Microbiol.* 65, 4180–4185. doi: 10.1099/ijsem.0.000558

Wei, R., and Zimmermann, W. (2017). Microbial enzymes for the recycling of recalcitrant petroleum-based plastics: how far are we? *Microb. Biotechnol.* 10, 1308–1322. doi: 10.1111/1751-7915.12710

Witt, U., Einig, T., Yamamoto, M., Kleeberg, I., Deckwer, W. D., and Müller, R. J. (2001). Biodegradation of aliphatic–aromatic copolyesters: evaluation of the final biodegradability and ecotoxicological impact of degradation intermediates. *Chemosphere* 44, 289–299. doi: 10.1016/S0045-6535(00)00162-4

Witt, U., Müller, R.-J., and Deckwer, W.-D. (1995). New biodegradable polyester-copolymers from commodity chemicals with favorable use properties. *J. Environ. Polym. Degrad.* 3, 215–223. doi: 10.1007/bf02068676

Witt, U., Müller, R. J., and Deckwer, W. D. (1996). Evaluation of the biodegradability of copolyesters containing aromatic compounds by investigations of model oligomers. *J. Environ. Polym. Degrad.* 4, 9–20. doi: 10.1007/bf02083878

Witt, U., Yamamoto, M., Seeliger, U., Müller, R. J., and Warzelhan, V. (1999). Biodegradable polymeric materials-Not the origin but the chemical structure determines biodegradability. *Angew. Chem. Int. Ed. Engl.* 38, 1438–1442.

Yoshida, S., Hiraga, K., Takehana, T., Taniguchi, I., Yamaji, H., Maeda, Y., et al. (2016). A bacterium that degrades and assimilates poly(ethylene terephthalate). *Science* 351:1196. doi: 10.1126/science.aad6359

Zumstein, M. T., Schintlmeister, A., Nelson, T. F., Baumgartner, R., Woebken, D., Wagner, M., et al. (2018). Biodegradation of synthetic polymers in soils: tracking carbon into CO2 and microbial biomass. *Sci. Adv.* 4:eaas9024. doi: 10.1126/sciadv.aas9024

Conflict of Interest: The authors declare that the research was conducted in the absence of any commercial or financial relationships that could be construed as a potential conflict of interest.

Publisher's Note: All claims expressed in this article are solely those of the authors and do not necessarily represent those of their affiliated organizations, or those of the publisher, the editors and the reviewers. Any product that may be evaluated in this article, or claim that may be made by its manufacturer, is not guaranteed or endorsed by the publisher.

frontiers in Microbiology

ORIGINAL RESEARCH
published: 04 August 2021
doi: 10.3389/fmicb.2021.697218

Cloning, Heterologous Expression, and Characterization of a βκ-Carrageenase From Marine Bacterium *Wenyingzhuangia funcanilytica*: A Specific Enzyme for the Hybrid Carrageenan–Furcellaran

Siqi Cao[1], Yuying Zhang[1], Guangning Chen[1], Jingjing Shen[1], Jin Han[1], Yaoguang Chang[1,2], Hang Xiao[3] and Changhu Xue[1,2]*

[1] College of Food Science and Engineering, Ocean University of China, Qingdao, China, [2] Laboratory for Marine Drugs and Bioproducts, Pilot National Laboratory for Marine Science and Technology, Qingdao, China, [3] Department of Food Science, University of Massachusetts, Amherst, MA, United States

OPEN ACCESS

Edited by:
Francesco Secundo, National Research Council (CNR), Italy

Reviewed by:
Digvijay Verma, Babasaheb Bhimrao Ambedkar University, India
Hongjie Li, Ningbo University, China

***Correspondence:**
Yaoguang Chang
changyg@ouc.edu.cn

Specialty section:
This article was submitted to Microbiotechnology, a section of the journal Frontiers in Microbiology

Received: *19 April 2021*
Accepted: *09 July 2021*
Published: *04 August 2021*

Citation:
Cao S, Zhang Y, Chen G, Shen J, Han J, Chang Y, Xiao H and Xue C (2021) Cloning, Heterologous Expression, and Characterization of a βκ-Carrageenase From Marine Bacterium Wenyingzhuangia funcanilytica: A Specific Enzyme for the Hybrid Carrageenan–Furcellaran. Front. Microbiol. 12:697218. doi: 10.3389/fmicb.2021.697218

Carrageenan is a group of important food polysaccharides with high structural heterogeneity. Furcellaran is a typical hybrid carrageenan, which contains the structure consisted of alternative β-carrageenan and κ-carrageenan motifs. Although several furcellaran-hydrolyzing enzymes have been characterized, their specificity for the glycosidic linkage was still unclear. In this study, we cloned, expressed, and characterized a novel GH16_13 furcellaran-hydrolyzing enzyme Cgbk16A_Wf from the marine bacterium *Wenyingzhuangia fucanilytica* CZ1127. Cgbk16A_Wf exhibited its maximum activity at 50°C and pH 6.0 and showed high thermal stability. The oligosaccharides in enzymatic products were identified by liquid chromatography coupled with high-resolution mass spectrometry (LC-HRMS) and nuclear magnetic resonance (NMR) spectroscopy. It was confirmed that Cgbk16A_Wf specifically cleaves the β-1,4 linkages between β-carrageenan and κ-carrageenan motifs from non-reducing end to reducing end. Considering the structural heterogeneity of carrageenan and for the unambiguous indication of the specificity, we recommended to name the furcellaran-hydrolyzing activity represented by Cgbk16A as "βκ-carrageenase" instead of "furcellaranase".

Keywords: carrageenan, furcellaran, βκ-carrageenase, GH16_13, specificity

INTRODUCTION

Carrageenan is a group of important polysaccharides extracted from the cell wall of red algae, which is widely applied in the food industry because of its desirable rheological properties (Chopin et al., 1999). The structures of carrageenan are complex. Depending on the occurrence of 4-linked-3,6-anhydro-α-D-galactopyranose and the sulfation pattern, carrageenan can be classified

into several different types (Campo et al., 2009). Besides, carrageenan has strong intramolecular structural heterogeneity (van de Velde, 2008). Furcellaran, extracted from *Furcellaria lumbricalis*, is a kind of typical hybrid carrageenan which contained the structure consisting of an alternative β-carrageenan motif [comprising repeating 4-linked-α-D-3,6-anhydrogalactose (DA) and 3-linked-β-D-galactopyranose (G) residues] and κ-carrageenan motif [comprising 4-linked-α-D-3,6-anhydrogalactose (DA) and 3-linked-4-*O*-sulfated-β-D-galactopyranose (G4S) residues] (Knutsen et al., 1990; **Supplementary Figure 1**). As an important material for studying the structure–function relationship of carrageenan, furcellaran has received increasing research interest in the recent decade (Jamróz et al., 2020; Saluri et al., 2021).

Carrageenase is a group of glycoside hydrolases (GHs) that could specifically hydrolyze carrageenans (Chauhan and Saxena, 2016). They could serve as favorable tools in the structural and functional studies of carrageenans. Up to date, all reported carrageenases were found hydrolyzing β-1,4 glycosidic linkages in carrageenan. Moreover, according to their substrates, carrageenases could be divided into different types, including κ-carrageenase, ι-carrageenase, λ-carrageenase, β-carrageenase, and furcellaran-hydrolyzing carrageenases, which respectively, belonging to families GH16_17 (Shen et al., 2018; Zhu et al., 2018), GH82 (Li et al., 2017; Shen et al., 2017), GH150 (Ohta and Hatada, 2006; Guibet et al., 2007), GH167 (Hettle et al., 2019), and GH16_13 (Schultz-Johansen et al., 2018; Christiansen et al., 2020). The enzymatic activity for hydrolyzing furcellaran was discovered by Schultz-Johansen et al. (2018), based on the characterization of several novel enzymes, i.e., ph1656, ph1663, and ph1675, from the marine bacterium *Paraglaciecola hydrolytica* S66; the activity was named as "furcellaranase" in the report (Schultz-Johansen et al., 2018). Lately, two enzymes from *Colwellia echini* A3, Ce358 and Ce387, were also confirmed to degrade furcellaran (Christiansen et al., 2020). Moreover, the roles of those enzymes in the carrageenan-utilizing cascade of their originated organism were revealed. Nevertheless, the glycosidic linkage specificity of the furcellaran-hydrolyzing enzyme remained unclear. Due to the structural heterogeneity of furcellaran, two types of β-1,4 linkage present in its molecular chain, i.e., the β-1,4 linkage between β-carrageenan and κ-carrageenan from non-reducing end to reducing end (DA-Gβ1→4DA-G4S) and the β-1,4 linkage between κ-carrageenan and β-carrageenan (DA-G4Sβ1→ 4DA-G). The specificity of characterized furcellaranases on which β-1,4 linkage has not been reported.

A marine bacterium *Wenyingzhuangia fucanilytica* CZ1127^{T} (=CCTCC AB 2015089^{T} = KCTC 42864^{T}) was previously isolated, identified, and sequenced (GenBank accession No. CP014224) by our lab. The bioinformatics analysis of the *W. fucanilytica* CZ1127^{T} genome showed the existence of an ORF (GenBank accession number WP_083194645.1; *cgbk16A*) coding a putative GH16_13 sequence. This study was aimed to clone, express, and characterize the GH16_13 protein from *W. fucanilytica*, hereinto named as Cgbk16A_Wf. Particularly, by employing Cgbk16A_Wf as a representative, the specificity of the GH16_13 furcellaran-hydrolyzing enzyme was investigated.

MATERIALS AND METHODS

Materials

The furcellaran employed as substrate was purchased from Carbosynth (Berkshire, England). Its molecular weight (Mw) was analyzed by using high-performance size exclusion chromatography coupled with multi-angle laser light scattering and a refractive index detector (HPSEC-MALLS-RI) (Xu et al., 2016) and consequently determined as 621.3 kDa.

Bioinformatics Analysis

The online tool dbCAN (Yin et al., 2012) and SignalP 4.1 (Petersen et al., 2011) were applied to predict possible domain structures in the protein sequence. The theoretical molecular weight and isoelectric point were calculated by ExPASy (Gasteiger, 2003). The sequence similarity of Cgbk16A_Wf and other GH16_13 family enzymes was evaluated by the BLASTP program (Altschul et al., 1997). Multiple-sequence alignments were performed by the ClustalX2 program (Thompson et al., 1997). The phylogenetic tree including Cgbk16A_Wf and all reported GH16_13 carrageenases was constructed based on the neighbor-joining method by MEGA6 (Tamura et al., 2013).

Gene Cloning and Protein Expression

The genomic DNA of *W. fucanilytica* CZ1127 was extracted by TIANamp Bacteria DNA Kit (Tiangen, Beijing, China). The gene sequence was amplified by PCR, and the forward and reverse primers were 5′-GACACGAATTCGATAATATCACGTCTGATGATCACGTGGTT-3′ and 5′-GACACCTCGAGTTATTGAATTTTATTTTTTTGCCAAACCCT-3′. The purified product was subsequently digested by restriction enzymes *Eco*RI/*Xho*I and inserted into the pET 28a(+) vector (Novagen, San Diego, CA, United States) which contains a 6× His-tag at the N terminus. The recombinant plasmid was transformed into *Escherichia coli* BL21 (DE3) cells (Biomed, Beijing, China), and the cells were cultured in the Luria–Bertani (LB) medium (Hope Bio-Technology, Qingdao, China) containing 30 μg/ml kanamycin at 37°C until OD_{600} reached 0.4. Subsequently, the expression of the protein was induced with 0.1 mM isopropyl β-D-1-thiogalactopyranoside at 17°C for 12 h, and cells were harvested and disrupted by sonication in citrate-phosphate buffer (20 mM, pH 6.0).

The purification was conducted at 4°C, and all chromatographic steps were performed applying the ÄKTA^{TM} Prime Plus system (GE Healthcare, Uppsala, Sweden). The supernatant of the cell lysate was applied onto the HisTrap^{TM} HP columns (GE Healthcare, Uppsala, Sweden) and was eluted by 0–0.5 M imidazole in 20 mM Tris–HCl buffer (pH 8.0) with 0.3 M NaCl. The active fractions were desalted by utilizing the HiTrap^{TM} Desalting columns (GE Healthcare, Uppsala, Sweden) with 20 mM citrate-phosphate buffer (pH 6.0). The purity and Mw of purified protein were evaluated by SDS-PAGE with 5% stacking gel and 12% running gel. Protein bands were visualized by Coomassie brilliant blue. The Mw of the enzyme was calculated with markers (Page Ruler^{TM} prestained protein ladder, Fermentas, Waltham, MA, United States). The

purified recombinant enzyme was employed in the following characterizations.

The Activity Assay and Analysis of Hydrolytic Pattern

Unless otherwise stated, the furcellaran-hydrolyzing activity was assayed by incubating Cgbk16A_Wf with 2 mg/ml furcellaran in 20 mM citrate-phosphate buffer (pH 6.0) at 45°C for 10 min. The released reducing sugar in the incubation was quantified by utilizing the para-hydroxybenzoic acid hydrazide (pHBAH) method (Lever, 1972) (pHBAH was purchased from Sigma-Aldrich, St. Louis, MO, United States). One unit of the activity was defined as the amount of enzyme required to produce 1.0 μmol reducing sugar (measured as D-galactose) per minute. The protein concentration was determined by a BCA Protein Assay Kit (Beyotime Biotechnology, Shanghai, China) with bovine serum albumin as the standard.

The 0.1 U Cgbk16A_Wf was incubated with 10 mg furcellaran at 45°C for 30 min. Aliquots were taken out at time intervals and heated at 100°C for 5 min to inactivate the enzyme. The high-performance size exclusion chromatography coupled with refractive index detector (HPSEC-RID) (Agilent 1260, Agilent Technologies, Santa Cruz, CA, United States) and a TSKgel SuperAW4000 column (Tosoh Corporation, Kanagawa, Japan) were employed to analyze the products. The eluent was 0.2 M NaCl, and the flow rate was set as 0.5 ml/min.

Biochemical Characterization

The effect of temperature on the activity was evaluated by incubating furcellaran and Cgbk16A_Wf at 20–60°C. The activity of Cgbk16A_Wf without any treatment was set as 100%, and the thermal stability was assayed by measuring the residual activity of the enzyme after being pretreated at 4, 25, 30, 45, and 50°C for 24 h.

The optimal pH was determined by incubating Cgbk16A_Wf in 20 mM various buffers with pH 3.0–11.0 (citrate-phosphate buffer for pH 3.0–6.5, NaH_2PO_4–Na_2HPO_4 buffer for pH 6.5–9.0, and Na_2CO_3–$NaHCO_3$ buffer for pH 9.0–11.0). The pH stability was determined by pretreating Cgbk16A_Wf in buffers, respectively, at 4°C for 1 h, and the residual activity was measured after adjusting the pH back to 6.0.

The impacts of metal ions and reagents on activity were determined by adding them to the reaction mixture, respectively, with the final concentrations of 1 and 5 mM and measuring the activity ratio (%). Particularly, the effects of NaCl were assessed at different concentrations (0–0.5 M).

Kinetic constants including *Vmax*, *Km*, *Kcat* were determined by incubating Cgbk16A_Wf and furcellaran with concentrations from 0.05 to 1.60 mg/ml. The data were plotted according to the Michaelis-Menten equation by using GraphPad Prism (GraphPad Software, San Diego, CA, United States).

LC-HRMS Analysis of Reaction Products

Different dosages of the enzyme (1–50 U) were, respectively, incubated with 50 ml furcellaran solution (2 mg/ml) at 45°C for 24 h and heated at 100°C for 5 min to inactivate the enzyme. Thereafter, the solution was centrifuged at 8,000 × *g* for 30 min after being placed at 4°C overnight and identified by the LC-HRMS technique. The LC-HRMS system was equipped with an ultra-performance liquid chromatography unit (Dionex Ultimate 3000, Thermo Fisher Scientific, San Jose, CA, United States) and the Thermo Fisher Scientific Q Exactive Orbitrap mass spectrometer (Thermo Fisher Scientific, San Jose, CA, United States) with an ACQUITY UPSEC BEH 125 SEC column (4.6 mm × 150 mm, Waters, Milford, MA, United States) for the online separation. The eluent was 20% (v/v) methanol containing 10 mM ammonium acetate, and the flow rate was set as 0.2 ml/min. The inject volume was 10 μl. The parameters for the mass spectrometer were as follows: negative ionization mode; capillary temperature, 300°C; spray voltage, 2,000 V; sheath gas pressure, 40 psi; S-lens RF level, 50 V; m/z range, 200–2,000. For assigning the detected ions, the theoretical molecular weights of carrageenan oligosaccharides were calculated with the GlycReSoft software (version 1.0) (listed in **Supplementary Table 1**). Besides, the "mass tolerance" was set as 5 ppm and the decimal of mass precision was set as 4.

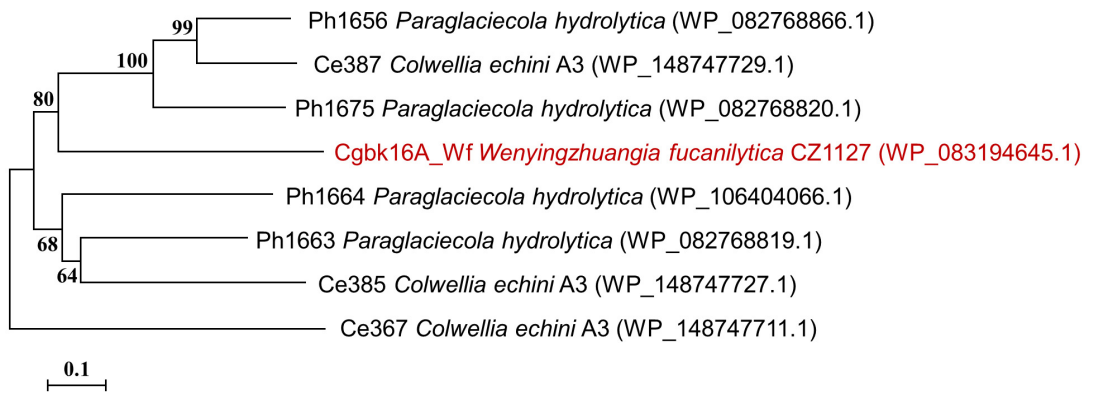

FIGURE 1 | Phylogenetic tree of Cgbk16A_Wf (highlighted in red) and previously characterized GH16_13 family enzymes. The protein name, organism name, and GenBank accession number (in bracket) are successively listed in labels.

The structural information of interested oligosaccharides was further analyzed by using LC-MS/MS. The enzymatic products were reduced by deuteration according to the previous report (Zhang et al., 2006). For MS/MS product-ion scanning, the collision energy was adjusted at 30 eV, and the other conditions were the same as above.

NMR Analysis of Reaction Products

The final product of Cgbk16A_Wf was prepared by conducting an exhaustive enzymatic hydrolysis (incubating 100 mg furcellaran with 50 U Cgbk16A_Wf for 24 h). The product was separated on a HiLoad 26/600 Superdex 30 pg column (GE Healthcare, Uppsala, Sweden) by using the ÄKTA^{TM} Prime Plus system (GE Healthcare, Uppsala, Sweden). The eluent was 5 mM ammonium formate, and the flow rate was set as 2.6 ml/min. The purified oligosaccharides were co-evaporated with D_2O twice by lyophilization and consequently dissolved in 500 μl D_2O. The external standard was calibrated according to the eternal 4,4-dimethyl-4-silapentane-1-sulfonic acid (DSS) (0.00 ppm). The spectra of one-dimensional ^1H NMR and two-dimensional correlation spectroscopy (COSY) and total correlation spectroscopy (TOCSY) were recorded by Bruker AVANCE III 600 (Bruker, Berlin, Germany) at 600 MHz under 25°C with sufficient acquisition time.

Homology Modeling

The tertiary structure of Cgbk16A_Wf was predicted by the homology modeling server SWISS-MODEL (Guex and Peitsch, 1997). The crystal structure of κ-carrageenase PcCgkA from *Pseudoalteromonas carrageenovora* ATCC 43555 (PDB: 5OCQ) (Matard-Mann et al., 2017) was utilized as a model. The predicted structure was superimposed onto the structure of PcCgkA employing the Match Maker function of UCSF Chimera (version 1.13.1) (Pettersen et al., 2004).

Statistical Analysis

All experiments were performed at least three times. All the data were expressed as average ± standard deviation. SPSS Statistics 19.0 (SPSS Inc., Chicago, IL, United States) was utilized to perform the Tukey's *post hoc* test (ANOVA). The *p*-value under 0.05 was considered statistically significant.

RESULTS AND DISCUSSION

Bioinformatics Analysis

Cgbk16A_Wf was composed of 321 amino acid residues, and it contained a GH16_13 family domain (residues 60–315) without a signal peptide. The phylogenetic tree constructed by characterized furcellaranases from the GH16_13 family (**Figure 1**) manifested that Cgbk16A_Wf is deeply located in the branch of the GH16_13 family. The multiple-sequence alignment showed that Cgbk16A_Wf is highly conserved at ExDxxE (E179, D181, and E184 correspondingly, **Supplementary Figure 2**) which is the commonality of the GH16 family (Cui et al., 2017). Moreover, Cgbk16A_Wf shared the highest sequence similarity with ph1663 from *P. hydrolytica* S66 (Schultz-Johansen et al., 2018) of 40% among all reported enzymes. The above bioinformatics analysis suggested that Cgbk16A_Wf was a putative GH16_13 carrageenase.

Cloning and Expression

The supernatant of the cell lysate was purified by nickel affinity chromatography, and the active fraction was eluted at an approximate imidazole concentration of 0.25 mol/l. The purified enzyme showed a single band on SDS-PAGE (**Figure 2**). The specific activity of the purified enzyme on furcellaran was determined as 53.75 U/mg.

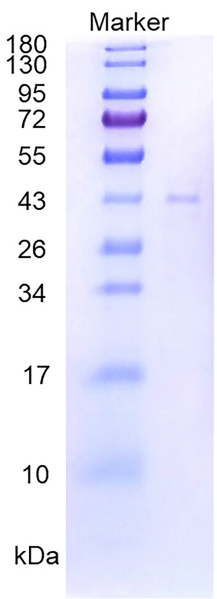

FIGURE 2 | SDS-PAGE of the purified recombinant Cgbk16A_Wf.

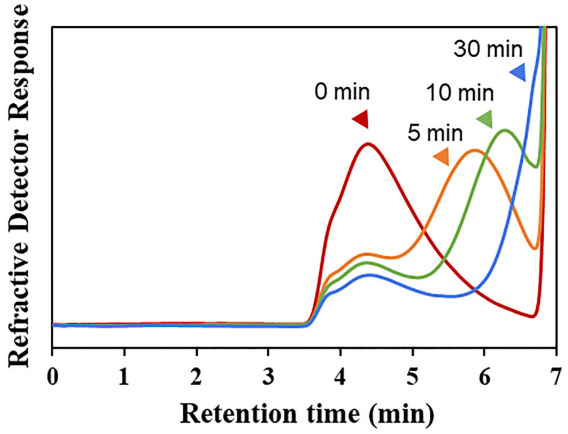

FIGURE 3 | HPSEC-RID chromatograms of degradation products of Cgbk16A_Wf were examined by using the TSKgel SuperAW4000 column.

The hydrolytic pattern of Cgbk16A_Wf was analyzed by HPSEC-RID, and a significant delay of elution peak of the substrate could be observed in 5 min (**Figure 3**), which indicated that furcellaran was degraded rapidly by the enzyme. It suggested that Cgbk16A_Wf was an endo-acting carrageenase.

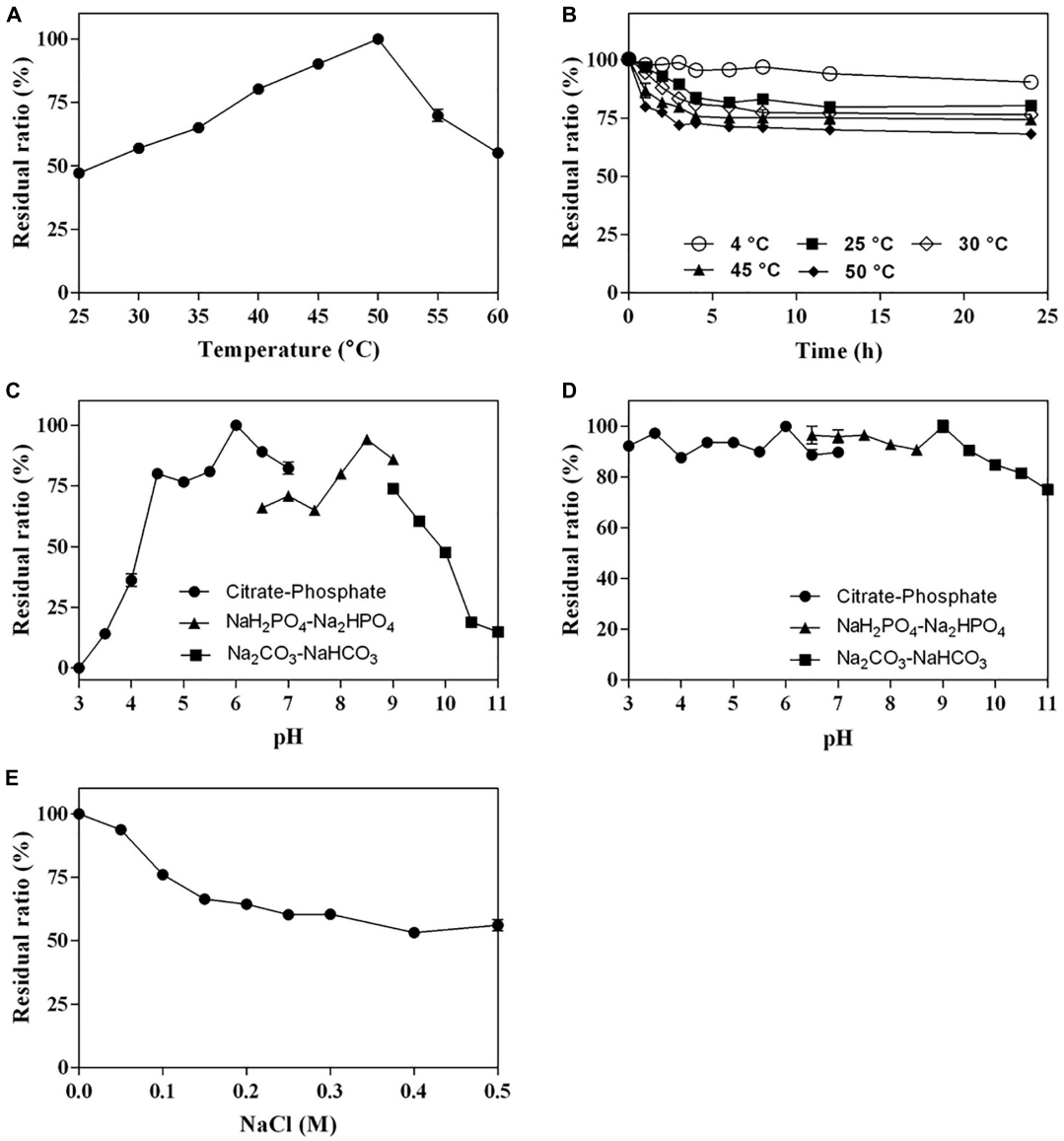

FIGURE 4 | Biochemical characteristics of Cgbk16A_Wf: **(A)** effect of temperatures on enzyme activity; **(B)** thermal stability; **(C)** effect of pH on enzyme activity; **(D)** pH stability; and **(E)** impact of NaCl concentration.

TABLE 1 | Effect of metal ions and reagents (1 and 5 mmol/l) on the activity of Cgbk16A_Wf.

Compound	Relative activity (%)		Compound	Relative activity (%)	
	1 mM	5 mM		1 mM	5 mM
$CaCl_2$	90.10 ± 2.47	95.23 ± 3.38	$CuSO_4$	46.18 ± 4.45	110.45 ± 3.19
MgSO4	80.93 ± 3.35	97.98 ± 1.46	$MnSO_4$	70.84 ± 4.06	64.88 ± 4.74
SDS	99.36 ± 4.77	99.54 ± 0.57	$CrCl_3$	115.13 ± 4.42	102.29 ± 0.57
EDTA	122.10 ± 3.97	89.27 ± 2.21	β-mercaptoethanol	86.70 ± 3.17	71.94 ± 1.93
$HgCl_2$	7.02 ± 3.91	−0.31 ± 1.15	KCl	100.73 ± 2.44	96.06 ± 1.65

Biochemical Characteristics of Cgbk16A_Wf

The optimum temperature of Cgbk16A_Wf was 50°C (**Figure 4A**). The enzyme presented favorable thermal stability, and 68% of the activity could be maintained after being incubated at 50°C for 24 h (**Figure 4B**). Cgbk16A_Wf exhibited its maximum activity in pH 6.0 citrate–phosphate buffer (**Figure 4C**), and it showed more than 80% of the maximum enzymatic activity at a wide pH range from 3.0 to 10.0 (**Figure 4D**). Cgbk16A_Wf exhibited a high activity without NaCl (**Figure 4E**), suggesting that the action of Cgbk16A_Wf did not depend on NaCl, which was beneficial to the preparation of oligosaccharides. The influences of metal ions and chemicals on the activity are shown in **Table 1**. Cgbk16A_Wf lost most of its activity in the presence of Hg^{2+} or β-mercaptoethanol, which implied that those chemicals are able to alter the enzyme conformation and thiol-containing amino acid residues might be critical for the function of the enzyme (Sharon et al., 1998; Shen et al., 2018). The kinetics parameters K_m, V_{max}, and K_{cat} of Cgbk16A_Wf were determined as 4.81 mg/ml, 370.37 U/mg, and 270.75 s^{-1}, respectively.

The Glycosidic Linkage Specificity of Cgbk16A_Wf

The final product prepared by incubating 50 U Cgbk16A_Wf with 100 mg furcellaran for 24 h was identified by LC-HRMS (**Figure 5**). Without considering the isomers, two disaccharides (DA-G4S, DA-G), three tetrasaccharides [$(DA\text{-}G4S)_2$, $(DA\text{-}G)_2$, $(DA\text{-}G4S)_1(DA\text{-}G)_1$], and four hexasaccharides [$(DA\text{-}G4S)_3$, $(DA\text{-}G)_3$, $(DA\text{-}G4S)_2(DA\text{-}G)_1$, $(DA\text{-}G4S)_1(DA\text{-}G)_2$] were observed. Among them, the hexasaccharide $(DA\text{-}G4S)_2(DA\text{-}G)_1$ showed the highest response which accounted for 54.4% of total oligosaccharides according to peak areas of their extracted ion chromatograms. $(DA\text{-}G4S)_2(DA\text{-}G)_1$ was thus selected and analyzed by LC-HRMS/MS. The MS/MS fragment B5 with high intensity (**Figure 6**) demonstrated that the G residue was situated at the reducing end, and it further indicated that the sequence of $(DA\text{-}G4S)_2(DA\text{-}G)_1$ was DA-G4S-DA-G4S-DA-G.

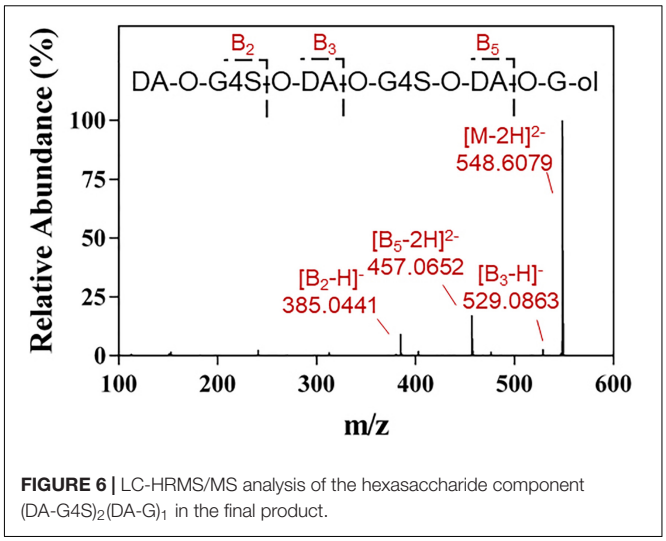

FIGURE 6 | LC-HRMS/MS analysis of the hexasaccharide component $(DA\text{-}G4S)_2(DA\text{-}G)_1$ in the final product.

Furthermore, the hexasaccharide $(DA\text{-}G4S)_2(DA\text{-}G)_1$ was prepared, purified, and identified by NMR. Several spin systems were found in its ^{1}H-NMR, COSY, and TOCSY spectra. Referring to the reported data of carrageenan (Knutsen and Grasdalen, 1992; Kolender and Matulewicz, 2004), the chemical shifts of H1 to H4 of α-Gr (α-G residue

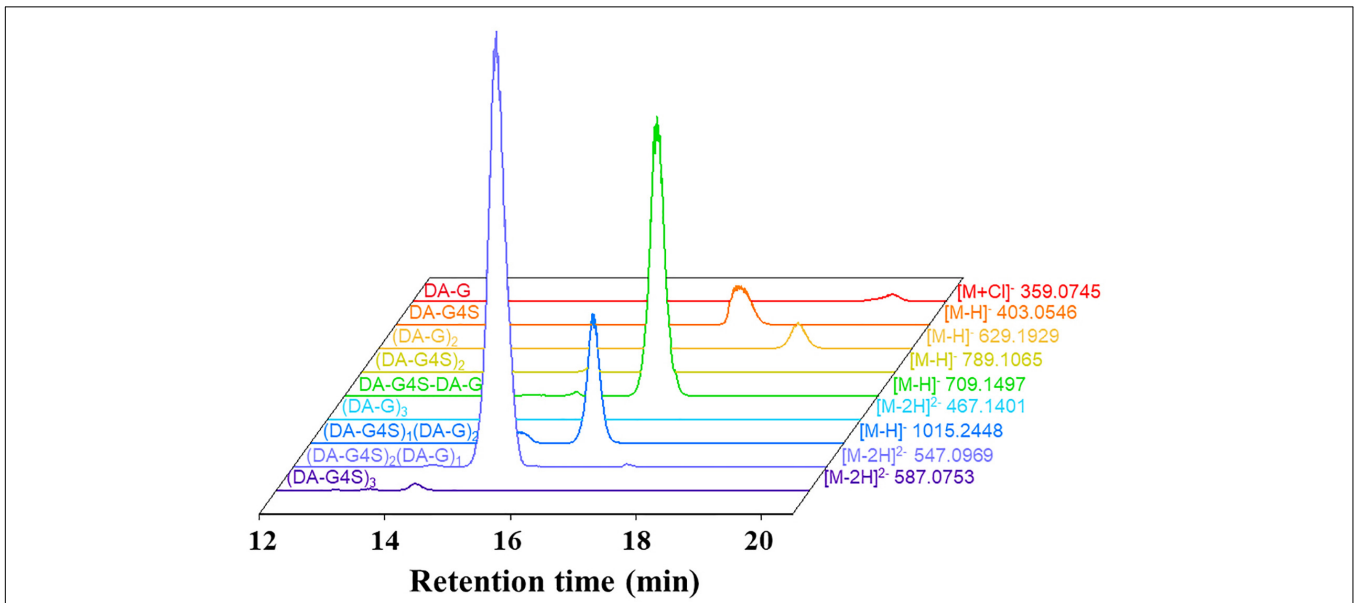

FIGURE 5 | Extracted ion chromatograms of oligosaccharides in the final product.

located at the reducing end) were confirmed and assigned as δ 5.29, δ 3.90, δ 4.03, and δ 4.18 ppm (**Figure 7**). The result was consistent with that of the above LC-MS/MS analysis. Besides, the hexasaccharide $(DA\text{-}G4S)_1(DA\text{-}G)_2$ was also purified and identified by NMR (**Supplementary Figure 3**). The spectra confirmed that the reducing end of $(DA\text{-}G4S)_1(DA\text{-}G)_2$ was also a G residue. The corresponding assignments of chemical shift (ppm) are listed in **Supplementary Table 2**. It was concluded that Cgbk16A_Wf displayed a strict requirement for the G residue at its −1 subsite, i.e., the Cgbk16A_Wf specifically recognized and cleaved the β-1,4 linkages between β-carrageenan motifs and

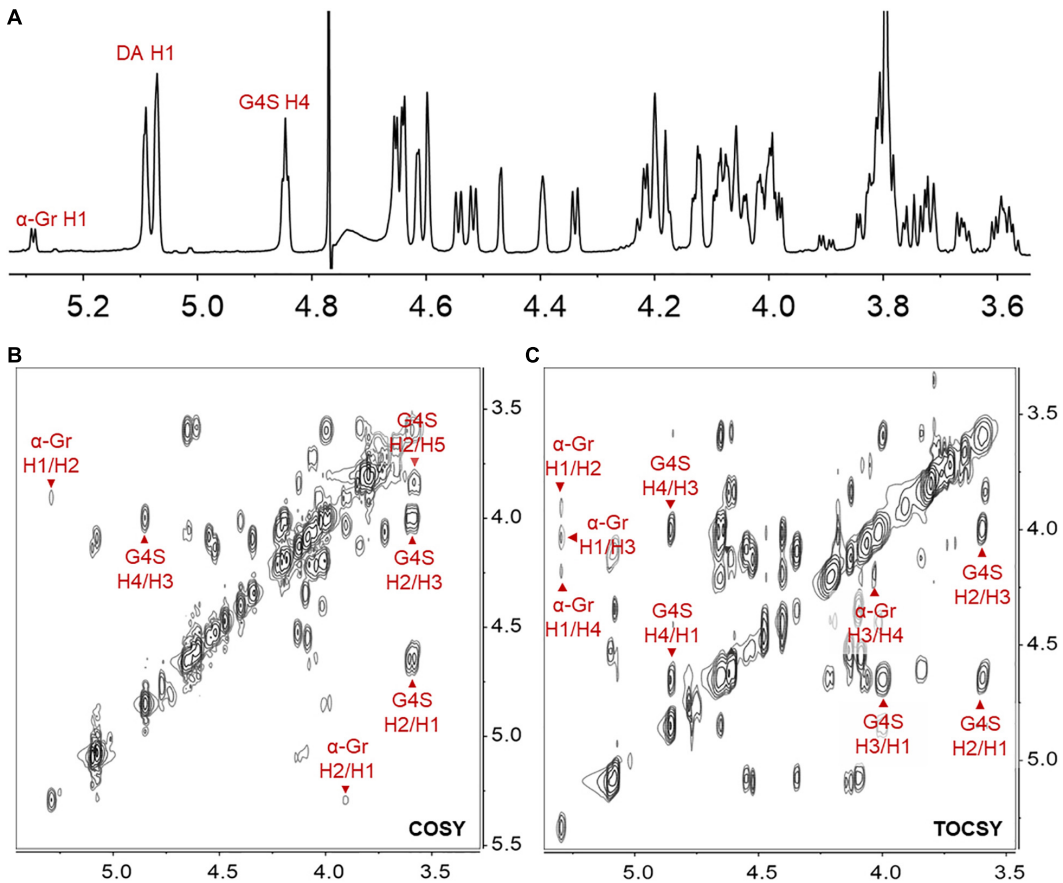

FIGURE 7 | The ^{1}H NMR **(A)**, COSY **(B)**, and TOCSY **(C)** spectra of the hexasaccharide $(DA\text{-}G4S)_2(DA\text{-}G)_1$ purified from the final product. The axes are ^{1}H chemical shifts (ppm). The α-Gr indicated the α-G residue located at the reducing end; H1/H2 indicated the cross-peak between H-1 and H-2, etc. The ^{1}H NMR, COSY, and TOCSY spectra of another hexasaccharide component $(DA\text{-}G4S)_1(DA\text{-}G)_2$ are found in **Supplementary Figure 3**.

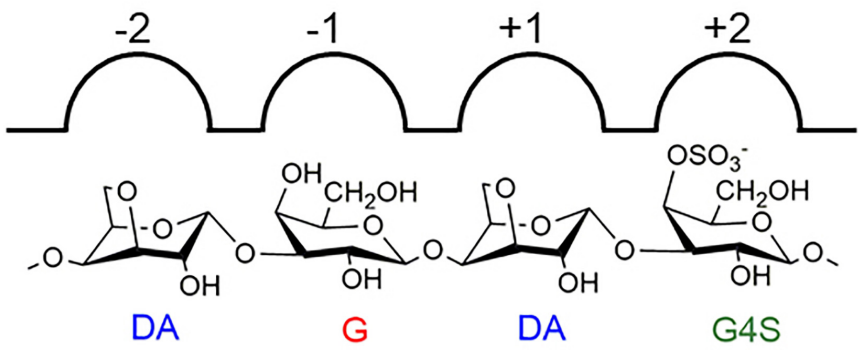

FIGURE 8 | An illustration of the specificity of Cgbk16A_Wf.

κ-carrageenan motifs from non-reducing end to reducing end (DA-Gβ1→4DA-G4S) (**Figure 8**).

To further investigate the action of Cgbk16A_Wf, products prepared by different dosages of the enzyme were identified by using LC-HRMS (**Figure 9** and **Supplementary Figure 4**). Various oligosaccharides observed in low enzyme dosage (1 U) further verified that the enzyme was an endo-acting carrageenase. The hexasaccharide $(DA\text{-}G4S)_2(DA\text{-}G)_1$ consistently showed the majority in all products (**Figure 9**). As the enzyme dosage increased, the disaccharides and the tetrasaccharides continuously accumulated. Meanwhile, the hexasaccharides $(DA\text{-}G4S)_2(DA\text{-}G)_1$ and $(DA\text{-}G4S)_1(DA\text{-}G)_2$ increased initially and thereafter decreased. Due to the heterogeneity of the substrate, the identical composition (m/z) could be shared by several isomers with different structures. As exampled by $(DA\text{-}G4S)_2(DA\text{-}G)_1$ (molar mass as 1096.2094), an oligosaccharide with this composition might be DA-G4S-DA-G4S-DA-G, DA-G4S-DA-G-DA-G4S, or DA-G-DA-G4S-DA-G4S. Among them, DA-G4S-DA-G-DA-G4S and DA-G-DA-G4S-DA-G4S which contained the β-1,4 linkage in DA-Gβ1→4DA-G4S would be further degraded when the enzyme dosage increased, while DA-G4S-DA-G4S-DA-G was resistant to the degradation. Therefore, the observed change of hexasaccharides could be explained. Besides, it was noticed that trace oligosaccharides of $(DA\text{-}G)_n$ and $(DA\text{-}G4S)_n$ were produced (**Figure 9**); according to the specificity of Cgbk16A_Wf, we supposed that the oligosaccharides were, respectively, hydrolyzed from the non-reducing ends and reducing ends of polysaccharide chains of furcellaran rather than from its inside.

The tertiary structure of Cgbk16A_Wf was constructed (the Qmean was −6.32) by using the well-characterized κ-carrageenase PcCgkA (PDB: 5OCQ) (Matard-Mann et al., 2017) with a ligand (DA-G4S-DA-G4S) as a model, and further aligned to it. Cgbk16A_Wf shared the highest sequence identity with PcCgkA of 23.9% among all reported carrageenases with a crystal structure. It is acknowledged that κ-carrageenase could accommodate G4S at its −1 subsite. A relatively wide pocket at the −1 subsite in PcCgkA which could comfortably accommodate the sulfate group of G4S was found (**Supplementary Figure 5**), while in the structure of Cgbk16A_Wf, the side chain of K276 (correspondingly G258 in PcCgkA) penetrated into this pocket and spatially conflicted with the sulfate group, which implied that K276 would prevent G4S from fitting into subsite −1. It was speculated that unsulfated G residues in β-carrageenan motifs could suit the narrow −1 subsite of Cgbk16A_Wf. Nevertheless, the lysine residue was not conserved in all GH16_13 enzymes, and the molecular mechanisms behind the specificities of carrageenases in GH16 family deserve further investigation.

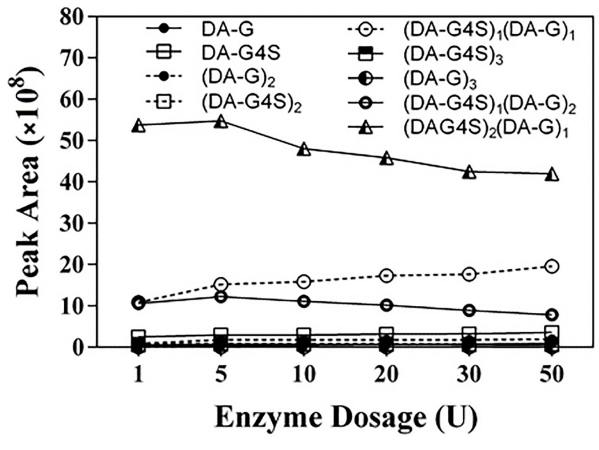

FIGURE 9 | LC-HRMS analysis of products prepared by incubating 100 mg substrate with different enzyme dosages (1–50 U) of Cgbk16A_Wf for 24 h. Respective plots for disaccharides, tetrasaccharides, and hexasaccharide are found in **Supplementary Figure 4**.

To the best of our knowledge, the currently reported carrageenases all specifically hydrolyzed the β-1,4 linkages rather than α-1,3 linkages in their corresponding substrates. There is only one type of β-1,4 linkage in κ-, ι-, λ-, and β-carrageenans. Therefore, the terms "κ-carrageenase," "ι-carrageenase," "λ-carrageenase," and "β-carrageenase" could well reflect the substrate specificity and the glycosidic linkage specificity of these enzymes. However, as the typical hybrid carrageenan, furcellaran contains at least two kinds of β-1,4 linkages, e.g., DA-Gβ1→4DA-G4S and DA-G4Sβ1→4DA-G. Therefore, the term "furcellaranase" could only indicate its activity on furcellaran, while the glycosidic linkage specificity could not be suggested. Based on this background, we proposed that the enzymes represented by Cgbk16A_Wf with the activity of hydrolyzing the β-1,4 linkage in DA-Gβ1→4DA-G4S could be named as "βκ-carrageenase" instead of "furcellaranase." The potential benefits of this nomenclature included the following: (1) the glycosidic linkage specificity could be precisely indicated; (2) similar to "κ-carrageenase," "ι-carrageenase," "λ-carrageenase," and "β-carrageenase," the carrageenase nature of the "βκ-carrageenase" could be intuitively conveyed; (3) considering the high heterogeneity of carrageenan, there would be more enzymes that are specifically active on hybrid carrageenans being discovered, and the nomenclature of "βκ-carrageenase" would provide a reference for the naming of these enzymes. Intriguingly, the carrageenases that could specifically hydrolyze the β-1,4 linkage in DA-G4Sβ1→4DA-G, which might be called as "κβ-carrageenase," have not been reported yet, and we are conducting the gene exploration to discover this enzyme.

To the best of our knowledge, there are no commercial standard hybrid carrageenan oligosaccharides. In this experiment, several κ/β-hybrid oligosaccharides with high purity were obtained by using Cgbk16A_Wf, which indicated that the enzyme could serve as a powerful tool for preparing κ/β-hybrid oligosaccharides. The functional investigation on those oligosaccharides was ongoing in our lab.

CONCLUSION

In conclusion, a novel GH16_13 family furcellaran-hydrolyzing enzyme Cgbk16A_Wf was cloned, expressed, and characterized.

The enzyme exhibited its highest activity at 50°C and pH 6.0. It presented favorable thermal stability and maintained 68% activity after being incubated at 50°C for 24 h. Cgbk16A_Wf was an endo-acting enzyme. It displayed a strict requirement for G residue at the −1 subsite and could specifically cleave the β-1,4 linkages between β-carrageenan and κ-carrageenan from non-reducing end to reducing end. We proposed to name the activity represented by Cgbk16A_Wf as "βκ-carrageenase" instead of "furcellaranase," which would better indicate its substrate specificity and glycosidic linkage specificity. The novel specificity, the favorable thermal stability, and the endo-acting hydrolysis mechanism indicated that Cgbk16A_Wf could serve as a powerful tool for preparing κ/β-hybrid oligosaccharides. Furthermore, it could also be utilized as a promising biotechnological tool in the structural investigation of carrageenan to reveal its heterogeneity.

DATA AVAILABILITY STATEMENT

The datasets presented in this study can be found in online repositories. The names of the repository/repositories and accession number(s) can be found below: https://www.ncbi.nlm.nih.gov/genbank/, WP_083194645.1.

AUTHOR CONTRIBUTIONS

SC and YC conceptualized and designed the studies and wrote the manuscript. YZ and GC designed the methodology. SC and JH performed the experimental operations. JS conducted the research and investigation. SC performed the data analyses. YC, HX, and CX revised the manuscript. All authors read and approved the final manuscript.

FUNDING

This work was supported by the National Key R&D Program of China (Grant No. 2018YFC0311203) and the Fundamental Research Funds for the Central Universities (Grant No. 202012020).

SUPPLEMENTARY MATERIAL

The Supplementary Material for this article can be found online at: https://www.frontiersin.org/articles/10.3389/fmicb.2021.697218/full#supplementary-material

Supplementary Figure 1 | The major structure of furcellaran.

Supplementary Figure 2 | Amino acid sequence alignment of Cgbk16A_Wf with characterized GH16_13 family enzymes. Critical catalytic residues were marked by stars.

Supplementary Figure 3 | The ^{1}H NMR **(A)**, COSY **(B)**, and TOCSY **(C)** spectra of the hexasaccharide (DA-G4S)$_1$(DA-G)$_2$. The α-Gr indicated α-G residue located at the reducing end; H1/H2 indicated the cross-peak between H-1 and H-2, etc. The assignment of ^{1}H chemical shifts of α-Gr and G4S were listed in **Supplementary Table 2**.

Supplementary Figure 4 | LC-HRMS analysis of products prepared by incubating 100 mg substrate with different enzyme dosages (1–50 U) of Cgbk16A_Wf for 24 h. **(A)** Disaccharide. **(B)** Tetrasaccharide. **(C)** Hexasaccharide.

Supplementary Figure 5 | The superimposition of Cgbk16A_Wf (in cyan) onto PcCgkA (in tan), focusing on the scene of −1 subsites. The ligand and the surface of PcCgkA were shown.

Supplementary Table 1 | The theoretical m/z of carrageenan oligosaccharides.

Supplementary Table 2 | The ^{1}H chemical shift (ppm) of α-Gr and G4S residues in hexasaccharide (DA-G4S)$_2$(DA-G)$_1$ and (DA-G4S)$_1$(DA-G)$_2$.

REFERENCES

Altschul, S. F., Madden, T. L., Schaffer, A. A., Zhang, J., Zhang, Z., Miller, W., et al. (1997). Gapped BLAST and PSI-BLAST: a new generation of protein database search programs. *Nucleic Acids Res.* 25, 3389–3402. doi: 10.1093/nar/25.17.3389

Campo, V. L., Kawano, D. F. Jr., Da Silva, D. B., and Carvalho, I. (2009). Carrageenans: biological properties, chemical modifications and structural analysis - a review. *Carbohyd. Polym.* 77, 167–180. doi: 10.1016/j.carbpol.2009.01.020

Chauhan, P. S., and Saxena, A. (2016). Bacterial carrageenases: an overview of production and biotechnological applications. *3 Biotech.* 6:146. doi: 10.1007/s13205-016-0461-3

Chopin, T., Kerin, B. F., and Mazerolle, R. (1999). Phycocolloid chemistry as a taxonomic indicator of phylogeny in the *Gigartinales*, *Rhodophyceae*: a review and current developments using Fourier transform infrared diffuse reflectance spectroscopy. *Phycol. Res.* 47, 167–188. doi: 10.1046/j.1440-1835.1999.00170.x

Christiansen, L., Pathiraja, D., Bech, P. K., Schultz-Johansen, M., Hennessy, R., Teze, D., et al. (2020). A multifunctional polysaccharide utilization gene cluster in *Colwellia echini* encodes enzymes for the complete degradation of κ - carrageenan, ι-carrageenan, and hybrid β/κ-carrageenan. *mSphere* 5:e00719-92. doi: 10.1128/mSphere.00792-19

Cui, H., Peng, Y., Zhao, B., Liu, Y., Chen, F., Wu, H., et al. (2017). Cloning, identification and characterization of a novel κ-carrageenase from marine bacterium *Cellulophaga lytica* strain N5-2. *Int. J. Biol. Macromol.* 105, 509–515. doi: 10.1016/j.ijbiomac.2017.07.071

Gasteiger, E. (2003). ExPASy: the proteomics server for in-depth protein knowledge and analysis. *Nucleic Acids Res.* 31, 3784–3788. doi: 10.1093/nar/gkg563

Guex, N., and Peitsch, M. C. (1997). SWISS-MODEL and the swiss-Pdb viewer: an environment for comparative protein modeling. *Electrophoresis* 18, 2714–2723. doi: 10.1002/elps.1150181505

Guibet, M., Colin, S., Barbeyron, T., Genicot, S., Kloareg, B., Michel, G., et al. (2007). Degradation of lambda-carrageenan by *Pseudoalteromonas carrageenovora* lambda-carrageenase: a new family of glycoside hydrolases unrelated to kappa- and iota-carrageenases. *Biochem. J.* 404, 105–114. doi: 10.1042/BJ20061359

Hettle, A. G., Hobbs, J. K., Pluvinage, B., Vickers, C., Abe, K. T., Salama-Alber, O., et al. (2019). Insights into the κ/ι-carrageenan metabolism pathway of some marine *Pseudoalteromonas* species. *Commun. Biol.* 2:474. doi: 10.1038/s42003-019-0721-y

Jamróz, E., Khachatryan, G., Kopel, P., Juszczak, L., Kawecka, A., Krzyściak, P., et al. (2020). Furcellaran nanocomposite films: the effect of nanofillers on the structural, thermal, mechanical and antimicrobial properties of biopolymer films. *Carbohyd. Polym.* 240:116244. doi: 10.1016/j.carbpol.2020.116244

Knutsen, S. H., and Grasdalen, H. (1992). The use of neocarrabiose oligosaccharides with different length and sulphate substitution as model compounds for 1H-NMR spectroscopy. *Carbohydr. Res.* 229, 233–244. doi: 10.1016/s0008-6215(00)90573-1

Knutsen, S. H., Myslabodski, D. E., and Grasdalen, H. (1990). Characterization of carrageenan fractions from *Norwegian Furcellaria lumbricalis* (Huds.) Lamour. by 1H-n.m.r. spectroscopy. *Carbohydr. Res.* 206, 367–372.

Kolender, A. A., and Matulewicz, M. C. (2004). Desulfation of sulfated galactans with chlorotrimethylsilane. Characterization of β-carrageenan by 1H NMR spectroscopy. *Carbohyd. Res.* 339, 1619–1629. doi: 10.1016/j.carres.2004.03.029

Lever, M. (1972). A new reaction for colorimetric determination of carbohydrates. *Anal. Biochem.* 47, 273–279. doi: 10.1016/0003-2697(72)90301-6

Li, S., Hao, J., and Sun, M. (2017). Cloning and characterization of a new cold-adapted and thermo-tolerant iota-carrageenase from marine bacterium *Flavobacterium* sp. YS-80-122. *Int. J. Biol. Macromol.* 102, 1059–1065. doi: 10.1016/j.ijbiomac.2017.04.070

Matard-Mann, M., Bernard, T., Leroux, C., Barbeyron, T., Larocque, R., Préchoux, A., et al. (2017). Structural insights into marine carbohydrate degradation by family GH16 κ-carrageenases. *J. Biol. Chem.* 292, 19919–19934. doi: 10.1074/jbc.M117.808279

Ohta, Y., and Hatada, Y. (2006). A novel enzyme, λ-carrageenase, isolated from a deep-sea bacterium. *J. Biochem.* 140, 475–481. doi: 10.1093/jb/mvj180

Petersen, T. N., Brunak, S., von Heijne, G., and Nielsen, H. (2011). SignalP 4.0: discriminating signal peptides from transmembrane regions. *Nat. Methods* 8, 785–786. doi: 10.1038/nmeth.1701

Pettersen, E. F., Goddard, T. D., Huang, C. C., Couch, G. S., Greenblatt, D. M., Meng, E. C., et al. (2004). UCSF Chimera: a visualization system for exploratory research and analysis. *J. Comput. Chem.* 25, 1605–1612. doi: 10.1002/jcc.20084

Saluri, M., Kaljuvee, K., Paalme, T., Reile, I., and Tuvikene, R. (2021). Structural variability and rheological properties of furcellaran. *Food Hydrocolloid.* 111:106227. doi: 10.1016/j.foodhyd.2020.106227

Schultz-Johansen, M., Bech, P. K., Hennessy, R. C., Glaring, M. A., Barbeyron, T., Czjzek, M., et al. (2018). A novel enzyme portfolio for red algal polysaccharide degradation in the marine bacterium *Paraglaciecola hydrolytica* S66(T) encoded in a sizeable polysaccharide utilization locus. *Front. Microbiol.* 9:839. doi: 10.3389/fmicb.2018.00839

Sharon, C., Furugoh, S., Yamakido, T., Ogawa, H. I., and Kato, Y. (1998). Purification and characterization of a lipase from *Pseudomonas aeruginosa* KKA-5 and its role in castor oil hydrolysis. *J. Ind. Microbiol. Biot.* 20, 304–307. doi: 10.1038/sj.jim.2900528

Shen, J., Chang, Y., Chen, F., and Dong, S. (2018). Expression and characterization of a κ-carrageenase from marine bacterium *Wenyingzhuangia aestuarii* OF219: a biotechnological tool for the depolymerization of κ-carrageenan. *Int. J. Biol. Macromol.* 112, 93–100. doi: 10.1016/j.ijbiomac.2018.01.075

Shen, J., Chang, Y., Dong, S., and Chen, F. (2017). Cloning, expression and characterization of a ι-carrageenase from marine bacterium *Wenyingzhuangia fucanilytica*: a biocatalyst for producing ι-carrageenan oligosaccharides. *J. Biotechnol.* 259, 103–109. doi: 10.1016/j.jbiotec.2017.07.034

Tamura, K., Stecher, G., Peterson, D., Filipski, A., and Kumar, S. (2013). MEGA6: molecular evolutionary genetics analysis version 6.0. *Mol. Biol. Evol.* 30, 2725–2729. doi: 10.1093/molbev/mst197

Thompson, J. D., Gibson, T. J., Plewniak, F., Jeanmougin, F., and Higgins, D. G. (1997). The CLUSTAL_X windows interface: flexible strategies for multiple sequence alignment aided by quality analysis tools. *Nucleic Acids Res.* 25, 4876–4882. doi: 10.1093/nar/25.24.4876

van de Velde, F. (2008). Structure and function of hybrid carrageenans. *Food Hydrocolloid* 22, 727–734. doi: 10.1016/j.foodhyd.2007.05.013

Xu, X., Xue, C., Chang, Y., Chen, F., and Wang, J. (2016). Conformational and physicochemical properties of fucosylated chondroitin sulfate from sea cucumber *Apostichopus japonicus*. *Carbohyd. Polym.* 152, 26–32. doi: 10.1016/j.carbpol.2016.06.061

Yin, Y., Mao, X., Yang, J., Chen, X., Mao, F., and Xu, Y. (2012). dbCAN: a web resource for automated carbohydrate-active enzyme annotation. *Nucleic Acids Res.* 40, W445–W451. doi: 10.1093/nar/gks479

Zhang, Z., Yu, G., Zhao, X., Liu, H., Guan, H., Lawson, A. M., et al. (2006). Sequence analysis of alginate-derived oligosaccharides by negative-ion electrospray tandem mass spectrometry. *J. Am. Soc. Mass Spectr.* 17, 621–630. doi: 10.1016/j.jasms.2006.01.002

Zhu, B., Ni, F., Ning, L., Yao, Z., and Du, Y. (2018). Cloning and biochemical characterization of a novel κ-carrageenase from newly isolated marine bacterium *Pedobacter hainanensis* NJ-02. *Int. J. Biol. Macromol.* 108, 1331–1338. doi: 10.1016/j.ijbiomac.2017.11.040

Conflict of Interest: The authors declare that the research was conducted in the absence of any commercial or financial relationships that could be construed as a potential conflict of interest.

Publisher's Note: All claims expressed in this article are solely those of the authors and do not necessarily represent those of their affiliated organizations, or those of the publisher, the editors and the reviewers. Any product that may be evaluated in this article, or claim that may be made by its manufacturer, is not guaranteed or endorsed by the publisher.

frontiers in Microbiology

ORIGINAL RESEARCH
published: 09 August 2021
doi: 10.3389/fmicb.2021.710533

Secretory Expression of an Alkaline Alginate Lyase With Heat Recovery Property in *Yarrowia lipolytica*

Lu Liu[1,2†], Zhipeng Wang[3†], Zhihong Zheng[4], Ze Li[5], Xiaofeng Ji[1], Haihua Cong[4*] and Haiying Wang[1*]*

[1] Key Laboratory of Sustainable Development of Polar Fishery, Ministry of Agriculture and Rural Affairs, Yellow Sea Fisheries Research Institute, Chinese Academy of Fishery Sciences, Qingdao, China, [2] School of Medicine and Pharmacy, Ocean University of China, Qingdao, China, [3] School of Marine Science and Engineering, Qingdao Agricultural University, Qingdao, China, [4] College of Food Science and Engineering, Dalian Ocean University, Dalian, China, [5] College of Advanced Agricultural Sciences, Linyi Vocational University of Science and Technology, Linyi, China

OPEN ACCESS

Edited by:
Haijin Mou,
Ocean University of China, China

Reviewed by:
Satya P. Singh,
Saurashtra University, India
Fu-Li Li,
Qingdao Institute of Bioenergy and Bioprocess Technology, Chinese Academy of Sciences (CAS), China

***Correspondence:**
Xiaofeng Ji
jixf@ysfri.ac.cn
Haihua Cong
haihuacong@dlou.edu.cn
Haiying Wang
wanghy@ysfri.ac.cn

[†] These authors have contributed equally to this work and share first authorship

Specialty section:
This article was submitted to Microbiotechnology, a section of the journal Frontiers in Microbiology

Received: 16 May 2021
Accepted: 30 June 2021
Published: 09 August 2021

Citation:
Liu L, Wang Z, Zheng Z, Li Z, Ji X, Cong H and Wang H (2021) Secretory Expression of an Alkaline Alginate Lyase With Heat Recovery Property in Yarrowia lipolytica. Front. Microbiol. 12:710533. doi: 10.3389/fmicb.2021.710533

Alginate lyase possesses wide application prospects for the degradation of brown algae and preparation of alginate oligosaccharides, and its degradation products display a variety of biological activities. Although many enzymes of this type have been reported, alginate lyases with unique properties are still relatively rare. In the present work, an alginate lyase abbreviated as Alyw203 has been cloned from *Vibrio* sp. W2 and expressed in food-grade *Yarrowia lipolytica*. The Alyw203 gene consists of an open reading frame (ORF) of 1,566 bp containing 521 amino acids, of which the first 17 amino acids are considered signal peptides, corresponding to secretory features. The peak activity of the current enzyme appears at 45°C with a molecular weight of approximately 57.0 kDa. Interestingly, Alyw203 exhibits unique heat recovery performance, returning above 90% of its initial activity in the subsequent incubation for 20 min at 10°C, which is conducive to the recovery of current enzymes at low-temperature conditions. Meanwhile, the highest activity is obtained under alkaline conditions of pH 10.0, showing outstanding pH stability. Additionally, as an alginate lyase independent of NaCl and resistant to metal ions, Alyw203 is highly active in various ionic environments. Moreover, the hydrolyzates of present enzymes are mainly concentrated in the oligosaccharides of DP1–DP2, displaying perfect product specificity. The alkali suitability, heat recovery performance, and high oligosaccharide yield of Alyw203 make it a potential candidate for industrial production of the monosaccharide and disaccharide.

Keywords: alginate lyase, heat recovery, *Yarrowia lipolytica*, NaCl-independent, oligosaccharides

INTRODUCTION

Alginate was a linear heteropoly glucuronic polymer extracted from brown algae, consisting of two sugar monomers linked through 1,4-glycoside, occupying approximately 22–44% of its parts dry weight (Gacesa, 1992). Owing to the favorable gel properties, alginate was comprehensively used in food processing. For instance, it could be applied as a thickener and stabilizer to enhance the viscosity and stability of ice cream (Turquois and Gloria, 2000). However, in view of the serious defect of low bioavailability, the wide application of alginate with high molecular weight (Mw) was greatly restricted (Qian et al., 2020). Interestingly, alginate could be dissociated into smaller-molecular-weight alginate oligosaccharides by enzymatic hydrolysis, displaying a

variety of biological functions, such as anti-oxidation, antibacterial activity, antitumor, and immunomodulatory effects (Powell et al., 2013; Pritchard et al., 2017). Therefore, the development of alginate lyase with excellent performance for application in marine drug research possessed considerable theoretical and practical value.

As one variety of polysaccharide lyase (PL), alginate lyase could degrade alginate and generate trehalose oligosaccharides through cutting the 1,4-glycosidic bond between C4 and C5 (Ertesvag, 2015). In consideration of the enzyme's substrate specificity, high efficiency, and mild reaction conditions, the application of alginate lyase in industrial production, particularly during the manufacture of alginate oligosaccharides, has raised more and more concerns. Moreover, the amino acid sequence analysis results showed that they pertained to PL families of 5, 6, 7, 14, 15, 17, 18, 31, 32, 34, 36, and 39 on the basis of the carbohydrate-active enzyme (CAZy) database (Helbert et al., 2019; Ji et al., 2019), of which majority of the alginate lyases were polyM lyases. So far, although many alginate lyases have been recorded, there were relatively few enzymes with special functions such as high activity, heat resistance, or cold adaptability (Jagtap et al., 2014; Bonugli-Santos et al., 2015; Chen et al., 2016). Li et al. cloned a new type of alginate lyase, AlyPL6, with high enzymatic activity from *Pedobacter hainanensis* NJ-02 and immobilized it on mesoporous titanium dioxide granules to enhance thermal stability (Qian et al., 2020). Yang et al. (2020) acquired the alginate lyase cAlyM and corresponding mutant 102C300C with thermostable as well as high enzymatic activity, which were further successfully expressed in *Pichia pastoris*. We have previously reported that Alyw201, an alginate lyase from *Vibrio* sp. W2, possessed strong pH stability and cold adaptation and exhibited superior salt tolerance performance (Wang et al., 2020). However, alginate lyases with thermal stability and heat recovery performance are still rare in the meantime. In fact, the screening of alginate lyase with stable property in industrial production had significant application prospects. For example, heat resistance was conducive to saving energy, reducing production cost, and lowering pollution risk. The heat-resistant alginate lyase could continuously degrade the substrate at high temperatures, thereby reducing the viscosity of the substrate, which was of great significance to the production of alginate oligosaccharides.

In the present work, a novel alginate lyase Alyw203 was characterized and successfully expressed in *Yarrowia lipolytica*. The prepared enzyme exhibited excellent thermal stability and unique heat recovery performance at 10°C. This article not only provided new insights for exploring enzymes with special functions but also laid a solid foundation for the application of Alyw203 alginate lyase in alginate oligosaccharide manufacturing.

MATERIALS AND METHODS

Materials and Strains

Sodium alginate and alginate stochastically consisting of M block and G block were acquired from BZ Oligo Co., Ltd., Prof. Chi Zhenming from the Ocean University of China provided the expression vector pINA1312 and uracil mutant *Y. lipolytica* URA- strain. A YNB medium composed of 5.0 g/L $(NH_4)_2SO_4$, 1.8 g/L yeast nitrogen base containing no amino acids, 25.0 g/L agar, and 10.0 g/L glucose was used for *Y. lipolytica* URA-transformant screening (Madzak, 2015). Recombinant alginate lyase production was performed on GPPB media containing 3.0 g/L K_2HPO_4, 2.5 g/L yeast extract, 1.5 g/L $(NH_4)_2SO_4$, 0.2 g/L $MgSO_4$, 30.0 g/L glucose, and 2.0 g/L KH_2PO_4 (Wang et al., 2020).

Sequence Analysis

With the sake of appraising the gene encoding Alyw203, the genomic DNA was annotated and sequenced using Novogene. Annotated information about sugar-active enzymes could be obtained by comparing the gene protein sequence with the CAZy database. The sequencing result showed that there was a gene encoding Alyw203 with an open reading frame (ORF) of 1,556 bp (Cantarel et al., 2009). The SignalP 4.0 server was applied for signal peptide analysis[1]. The domain analysis of Alyw203 alginate lyase was conducted with the CDD[2]. Both theoretical isoelectric point (pI) and Mw of the present enzyme were forecasted online[3]. DNAMAN 6.0 was used for multiple sequence alignment among the alginate lyases of the PL7 family.

Expression and Purification of Alyw203

The gene of Alyw203 bearing the XPR2 signal peptide at its 5′ end was synthesized in the subsequent codon optimization and further transformed into the URA- strain. After incubation in the GPPB fluid nutrient medium for 84 h at 30°C, we detected a positive transformant of alginate lyase activity, of which the strain A32 displayed the optimal activity. The biomass and the activity of alginate lyase were measured at fixed time intervals during the subsequent fermentation of the A32 strain. The measurements above were carried out three times.

After adjusting the pH of the obtained supernatant to 7.5, the protein was purified using the Ni-NTA Sepharose column (GE Healthcare, Stanford, United States). A Hi-Trap desalting column (Amersham Biosciences) was applied to further purify the alginate lyase. The Mw and purity of Alyw203 were detected *via* SDS-PAGE on 12% (w/v) gel. In order to study substrate preference of the current Alyw203 alginate lyase, polyG, polyM, and alginate were used as substrates to research the enzyme activity. As previously reported, Alyw203 activity assay was determined by applying 0.5% (w/v) alginate solution as a substrate (Qin et al., 2018). Alyw203 activity confirmation is achieved by measuring the UV absorption at 235 nm (obs235). During the whole experiment, the usage amount of enzyme to increase obs235 by 0.1 per min was considered as one unit (U) of enzyme activity (Wang et al., 2019).

[1]http://www.cbs.dtu.dk/services/SignalP/

[2]https://www.ncbi.nlm.nih.gov/cdd

[3]http://web.expasy.org/compute_pi/

Effects of Temperature and pH on Alyw203

With sake of determining the optimal temperature, the Alyw203 alginate lyase-catalyzed hydrolysis reaction was carried out in 8 mM citric acid–NaOH media (pH 10.0) within a temperature scope of 20–60°C. Furthermore, the residual enzyme activity was determined at 45°C to detect the thermostability of the present alginate lyase after culturing for 8 h at 20 to 60°C. For the purpose of confirming the optimum temperature for restoring activity, the enzyme treated in a water bath (100°C, 5 min) is incubated at a gradient temperature (4–50°C) for 30 min, and the corresponding activity is measured. In addition, the enzyme (preboiled for 5 min) was cultured at 10°C for different periods (5–50 min) to assess the influence of cold treatment time on the recovery of activity. The measurements above were carried out three times.

To confirm the Alyw203's optimal reaction pH, alginates within the pH scope of 3.0 to 10.0 buffers were applied as substrates. Additionally, following the culturing of current alginate lyase in media within different pHs for 8 h at 45°C, the remaining activity was measured to detect Alyw203's pH stability. The measurements above were carried out three times.

Effects of Ions and NaCl on Activity of Alyw203

Purified Alyw203 enzyme was incubated with the relevant ions dissolved in alginate at 45°C for 25 min; then the activity was measured to evaluate the influence of these matters on the enzyme activity. During the experiment, metal ion and SDS and EDTA solutions with a concentration of 1 and 10 mM, respectively, were used. Moreover, catalyzing reactions of Alyw203 were carried out in alginate liquor with concentrations of NaCl from 0 to 3.0 M at 45°C. The control group was the original alginate without extra substance. The measurements above were carried out three times.

End Product Analysis of Alyw203

For the purpose of affirming the degradation products of Alyw203, 10 ml of 0.5% sodium alginate solution with purified alginate lyase (40 U) was incubated for 40 min at 45°C. During the whole experiment, the ultraviolet absorption at 235 nm was measured every 5 min. When the absorbance was stable, the samples were desalted, and the degradation products were identified using TLC and ESI-MS methods as reported (Wang et al., 2019).

RESULTS

Sequence Analysis of Alyw203

Firstly, genome DNA of the present alginate lyase from *Vibrio* sp. W2 strain has been sequenced, and the results reveal the existence of a putative alginate lyase encoding gene, Alyw203, which is composed of an ORF of 1,566 bp containing 521 amino acids. Further bioinformatics analysis shows that the

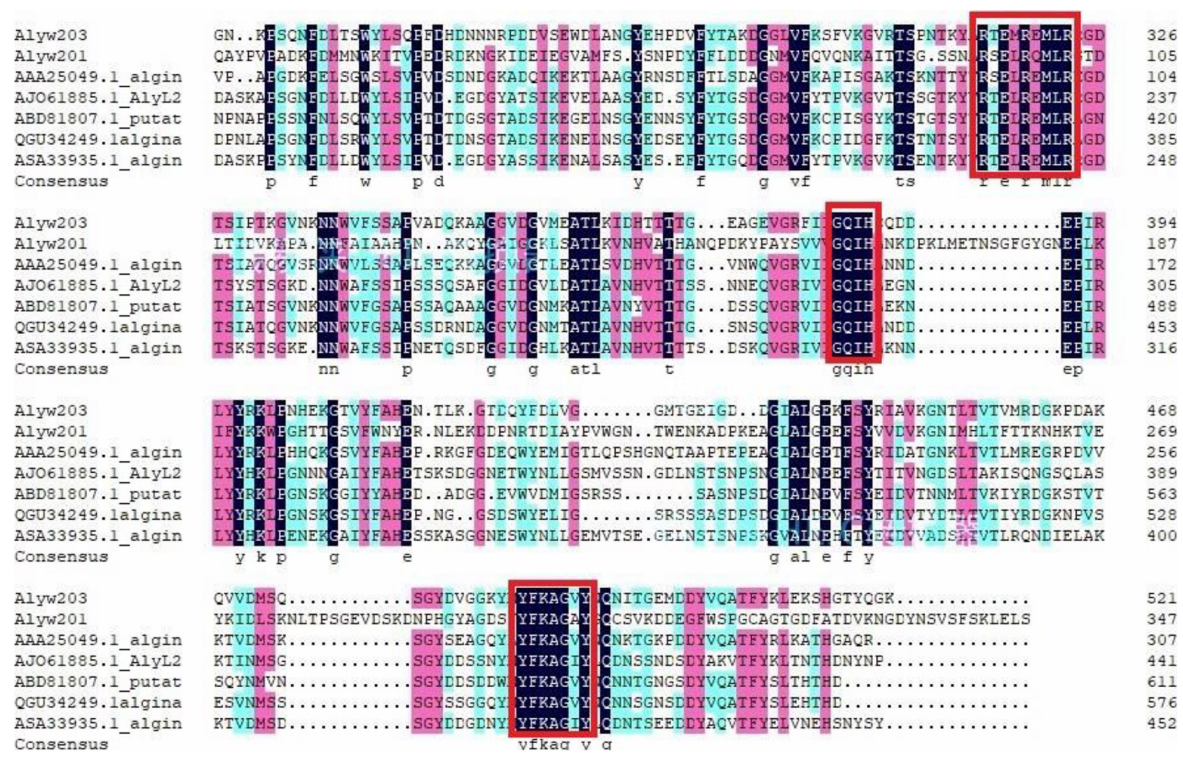

FIGURE 1 | Sequence comparative analysis of Alyw203 with six relevant alginate lyases. The conserved amino acid regions are listed in the red block.

theoretical Mw and pI of current mature Alyw203 are 57.0 kDa and 6.09, respectively. The first 17 amino acids are regarded as signal peptides, which correspond to secretion characteristics. A detailed retrieval of the Conserved Domain Database from NCBI reveals Alyw203 is a novel type of alginate lyase belonging to superfamily 2.

Alyw203 was blasted in NCBI and found to be evolutionarily close with alginate lyases in the PL7 family. According to Alyw203 and other reported sequences of superfamily 7 alginate lyase, a phylogenetic tree has been constructed to further determine the attribution of the current enzyme. Additionally, in the phylogenetic tree, the cluster of deep branches has been constituted among the enzyme from *Klebsiella pneumoniae* (GenBank number: AAA25049.1), the enzyme from *Agarivorans* sp. L11 (GenBank number: AJO61885.1), the enzyme from *Saccharophagus degradans* 2-40 (GenBank number: ABD81807.1) (Kim et al., 2015; Li et al., 2015), the enzyme from *Marinimicrobium* sp. (GenBank number: QGU34249.1), and the enzyme from *Vibrio* sp. (GenBank number: ASA33935.1) (Zhu et al., 2018b; Yan et al., 2019). According to sequence comparison, the Alyw203 includes typical conserved regions of the PL7 family, namely, "QIH," "RTELREMLR," and "MYFKAG" (**Figure 1**).

Secretory Expression of Alyw203 Alginate Lyase in *Y. lipolytica*

Majority of the reported alginate lyase expression is achieved in *Escherichia coli*. However, the extensive application of *E. coli* in industrial production is limited owing to the serious defects of poor secretion capability, presence of pyrogen, and endotoxin production (Miyamoto et al., 2009). In the current work, Alyw203 has been successfully expressed in *Y. lipolytica*, a heterologous host with excellent extracellular secretion ability (Madzak, 2015). Additionally, this system possesses the advantages of being safe, having high activity, and having no need to add antibiotics. As shown in **Figure 2**, after 72 h of culture in GPPB medium, the recombinant alginate lyase activity reached a peak of 25.9 U/ml, with a biomass of 12.5 g/L. Further SDS-PAGE analysis of purified Alyw203 protein shows that a clear band arises on the lane, meaning the Mw of Alyw203 is approximately 57.0 kDa (**Figure 3**), which is roughly in line with the theoretical Mw. Correspondingly, Zhuge et al. (2008) reported for the first time the cloning and functional expression of the *Bacillus subtilis* gene encoding alkaline pectate lyase in *Pichia pastoris*. The Mw calculated from the deduced amino acid sequence was similar to that of the protein secreted by yeast, approximately 43.6 kDa (Zhuge et al., 2008). Similarly, we previously reported that the alginate lyase gene Alyw201 from *Vibrio* was successfully expressed in the food-grade host *Y. lipolytica*. Studies have shown that the theoretical Mw of the enzyme and the measured actual Mw were 36.4 and 38.0 kDa, respectively, showing that there is little significant difference between them (Wang et al., 2020).

pH Properties of Alyw203

As displayed in **Figure 4A**, Alyw203 alginate lyase exhibits the highest catalytic activity at pH 10.0. As for the pH stability study of the present enzyme, it can be seen from **Figure 4B** that exceeding 40% of the activity is reserved after incubation in the pH range of 3.0–12.0.

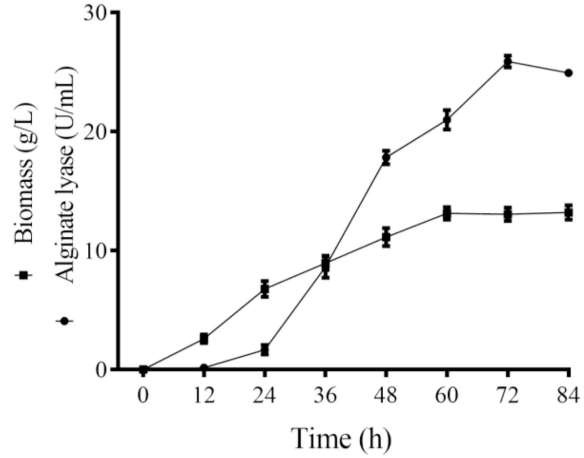

FIGURE 2 | Time course of the Alyw203 activity secreted into the medium. Values are expressed as mean ± standard deviation (SD), $n = 3$.

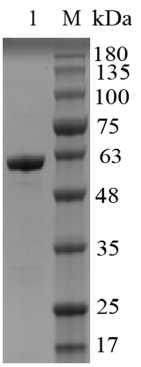

FIGURE 3 | Analysis of Alyw203 by SDS-PAGE. Lane 1, purified Alyw203; Lane M, prestained protein ladder.

Temperature Properties and Heat Recovery of Alyw203

It can be intuitively seen from **Figure 5** that the highest activity of Alyw203 alginate lyase has been detected at 45°C, while it shows over 80% of the activity at 40–55°C. When the temperature exceeds 55°C, the corresponding enzyme activity drops sharply; meanwhile, the catalytic activity is lower than 60% of the highest activity at a temperature below 35°C. As for thermal stability, Alyw203 exhibits superior stability at temperatures below 45°C, retaining more than 80% of its highest activity in the subsequent incubation at 45°C for 3 h.

Interestingly, in the process of determining the thermal stability of Alyw203, we find that the residual activity of the heat-treated enzyme after cold incubation can be significantly restored to a certain extent; that is to say, alginate lyase Alyw203 possesses a unique heat recovery performance. As

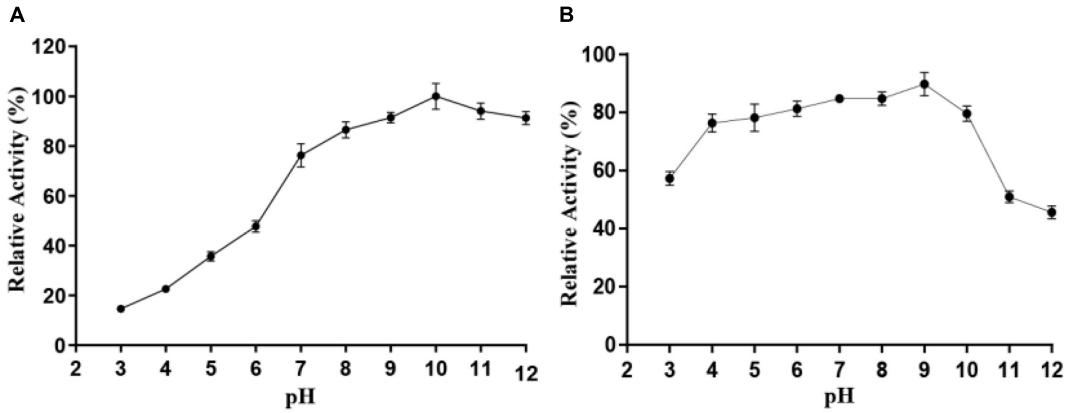

FIGURE 4 | Effect of pH on the activity **(A)** and stability **(B)** of Alyw203. Values are expressed as mean ± standard deviation (SD), *n* = 3.

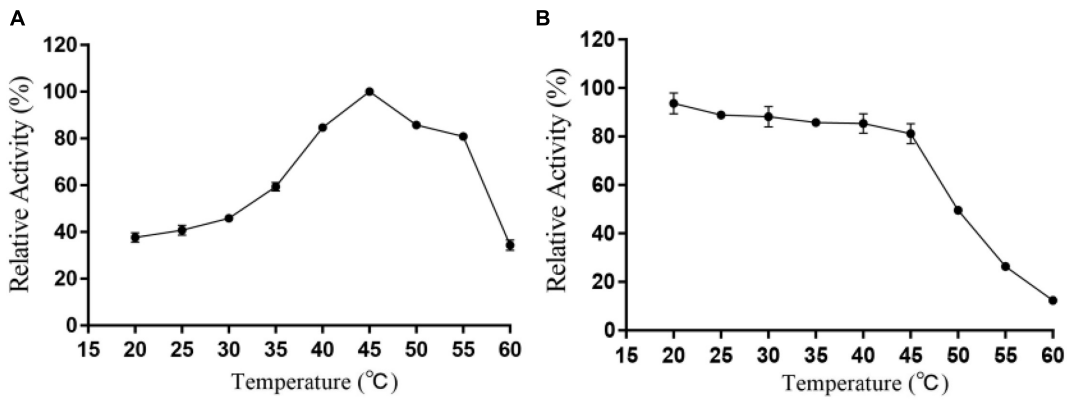

FIGURE 5 | Effects of temperature on the activity **(A)** and stability **(B)** of Alyw203. Values are expressed as mean ± SD, *n* = 3.

shown in **Figure 6A**, the enzyme activity recovers to 96.3, 93.9, and 78.1% in the subsequent cultivation at 4, 10, and 20°C; while the incubation temperature exceeds 30°C, the activity recovery rate is less than 40%. For the purpose of further confirming the optimum incubation time for activity recovery, the current enzyme has been incubated at 10°C for different periods of time with the results illustrated in **Figure 6B**. As displayed in the figure, the activity of Alyw203 increases with the extension of the incubation time, which reaches the highest activity at 20 min and then basically remains unchanged. Interestingly, even after 5 and 10 min of incubation at 10°C, the activity of the current enzyme can be rapidly restored to the relative activity of 45.2 and 78.3%. These observations indicate that the current enzyme exhibits a thermal recovery character, which is conducive to the recovery of Alyw203 at low-temperature conditions.

Effects of Ions and NaCl on Alyw203 Activity

No significant activation effect of 1 mM metal ion on Alyw203 alginate lyase has been observed as displayed in **Figure 7A**, in which the relative activity increases to 138.0% merely under the condition of adding Mn^{2+}. Nevertheless, 1 mM EDTA and SDS perform an obvious inhibitory effect on the present enzyme, wherein the relative activity is decreased to 14.7 and 62.8%, respectively. Under the condition of 10 mM, many ions including Fe^{3+}, Cu^{2+}, Zn^{2+}, Al^{3+}, SDS, and EDTA possess a powerful inactivation effect on the present enzyme, while no ions show an activation effect. Therefore, Alyw203 alginate lyase illustrates favorable ion tolerance. Additionally, as displayed in **Figure 7B**, the addition of NaCl (in the concentration range 0–3 M) slightly enhances the degradation activity of Alyw203 throughout the experiment, of which the highest activity achieved is 148.2% in the presence of 2 M NaCl.

Product Analysis of Alyw203

During the degradation process, the alginate polysaccharide is continuously degraded accompanied by the generation of oligosaccharides with various degrees of polymerization (DP). The degraded sample has been analyzed by TLC to determine the end product. It can be observed intuitively from **Figure 8A** that the two obvious spots of the final product on the TLC board are consistent with the alginate monosaccharide (DP1) and disaccharide (DP2) labels. ESI-MS (negative ion

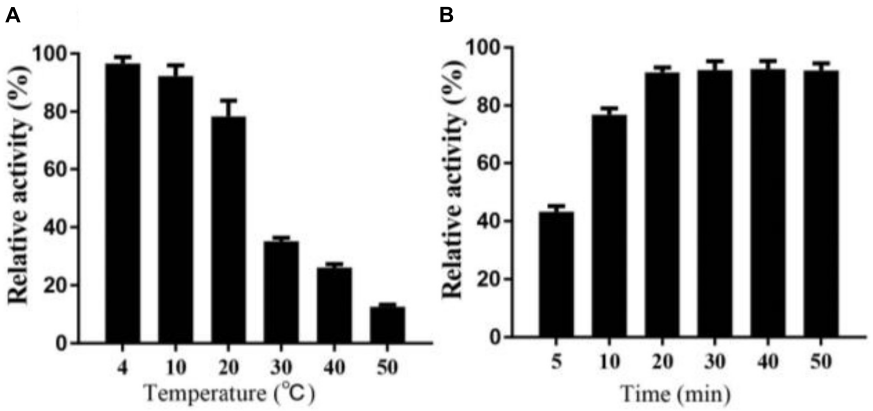

FIGURE 6 | Heat recovery analysis of Alyw203. **(A)** Determination of the optimum incubation temperature for restoring activity of Alyw203 after 5 min of heat treatment. **(B)** Influence of incubation time on activity recovery of heat-treated Alyw203 at 10°C. Values are expressed as mean ± SD, $n = 3$.

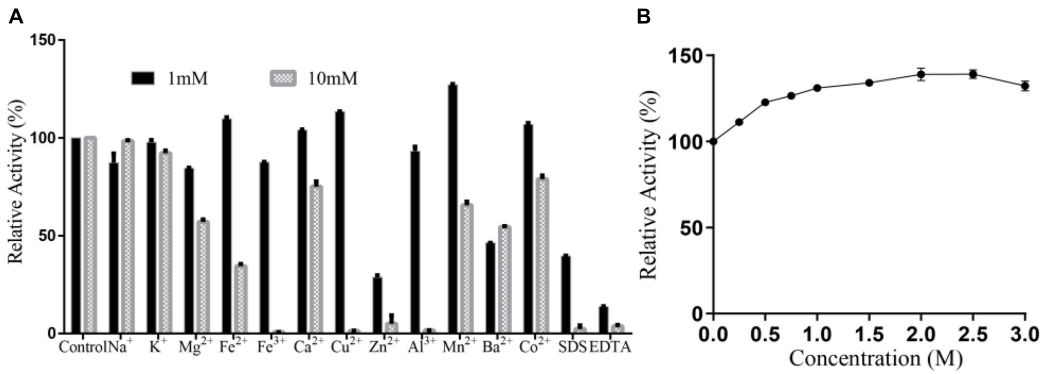

FIGURE 7 | (A) Effects of ions on Alyw203. **(B)** Effects of NaCl on Alyw203. Values are expressed as mean ± SD, $n = 3$.

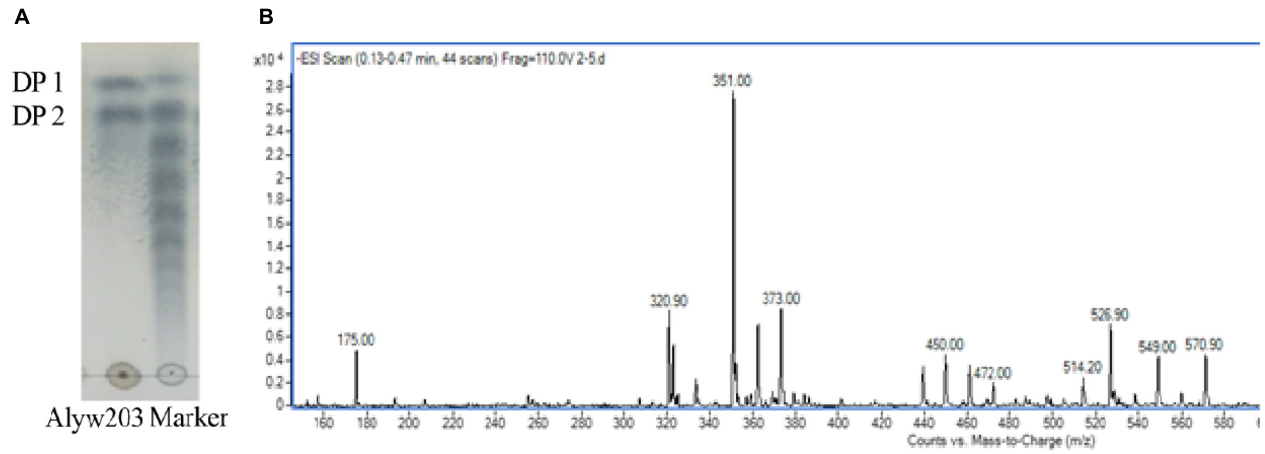

FIGURE 8 | Degradation product analysis of Alyw203 by **(A)** TLC: Lane Alyw203, hydrolytic products of Alyw203; Lane Marker, standard alginate oligosaccharides; and **(B)** ESI-MS.

electrospray ionization mass spectrometry, **Figure 8B**) analysis further proves that these two spectra correspond to the Mws of unsaturated alginate monosaccharides (175.00 *m/z*) and disaccharides (351.00 *m/z*), indicating that the current Alyw203 enzyme effectively degrades alginate polymers into monosaccharides and disaccharides in an endo-type manner.

DISCUSSION

In the detailed work of the present study, a novel alginate lyase, abbreviated as Alyw203, was successfully purified, cloned, and identified from *Vibrio* sp. W2. Sequence analysis displayed that the current enzyme was a novel alginate lyase pertaining to the PL2 family. As illustrated in **Figure 9**, Alyw203 was located on the same branch as the other two enzymes from *S. degradans* 2-40 (ABD81807.1) and *Agarivorans* sp. L11 (AJO61885.1). The results of multiple sequence comparison showed that Alyw203 contained three typical conserved regions: "QIH," "RTELREMLR," and "MYFKAG." Moreover, since the "QVH" or "QIH" motifs played a pivotal part in the substrate selection of alginate lyase and the enzymes containing "QIH" motifs displayed a polyG preference (Huang et al., 2013; Swift et al., 2018), the current Alyw203 enzyme including the "QIH" conserved region revealed a predilection for polyG blocks. After comprehending the various characteristics of the alginate lyase shown in **Figure 1**, majority of the enzymes did display a predilection for polyG blocks (Wang et al., 2020). Interestingly, further sequence analysis indicated that the "QVH" motif may be an important indicator of polyM block preference, indicating that Alyw203 could be applied for the degradation of brown seaweed (Uchimura et al., 2010).

The current alginate lyase exhibited excellent pH stability. In general, majority of alginate lyases were inclined to catalyze degradation reaction within the small pH scope and neutral conditions as previously reported (Wang et al., 2019). Compared

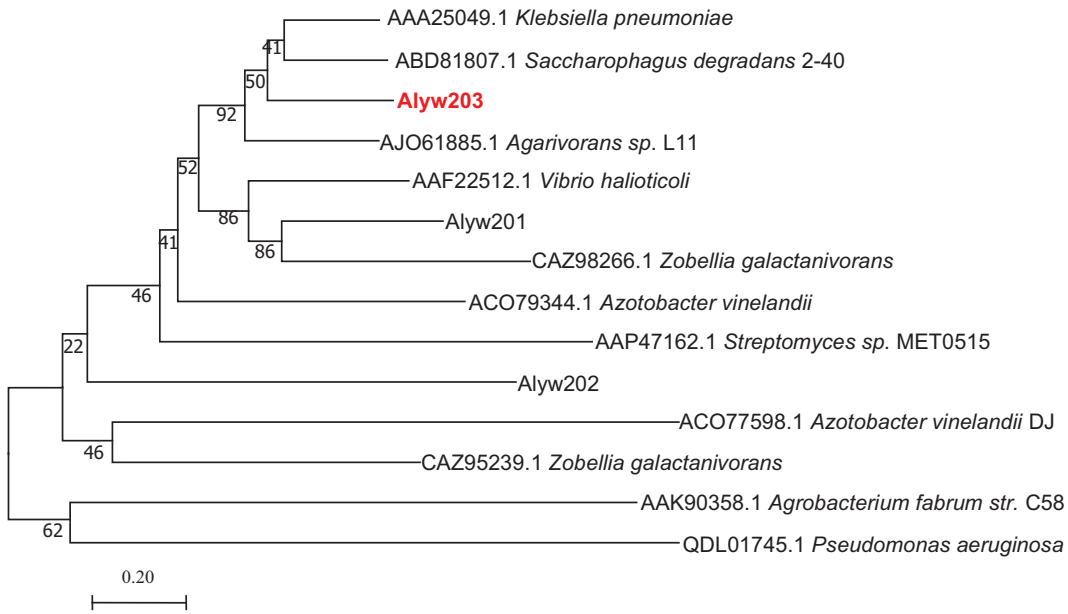

FIGURE 9 | Phylogenetic relationship of the Alyw203 with other reported alginate lyases. Phylogenetic tree generated according to the ITS rDNA gene sequences with the neighbor-joining method. The number listed first represents the serial login number. The branching correlation numbers are bootstrapped values (confidence limits) that represent the replacement frequency of each amino acid residue.

TABLE 1 | Comparison of Alyw203 performances with other alginate lyases.

Name	Source	Optimal pH/temperature (°C)	Temperature stable range (°C)	pH stable range	Product (DP)	References
NitAly	*Nitratiruptor* sp. SB155-2	6.0/70	40–80	4–7	3–5	Inoue et al., 2016
Alyw201	*Vibrio* sp.	8.0/35	4–10	4–10	2–6	Wang et al., 2020
TsAly6A	*Thalassomonas* sp.	8.0/35	0–30	6.6–8.95	2–3	Gao et al., 2018
TsAly7B	*Thalassomonas* sp.	8.0/20	0–25	7.3–8.6	2–3	Zhang et al., 2019
AlyPM	*Pseudoalteromonas* sp.	8.0/35	–	–	1	Chen et al., 2016
ZH0-IV	*Sphingomonas* sp.	7.5/35	25–42	6.0–9.0	1	He et al., 2018
AlyGC	*Glaciecola chathamensis*	7.0/30	–	–	1	Xu et al., 2017
Algb	*Vibrio* sp. W13	8.0/30	10–40	4.0–10.0	2–5	Zhu et al., 2015
A9m	*Vibrio* sp. A9mT	7.5/30	2–40	7.0–10.0	–	Uchimura et al., 2010
AlgNJU-03	*Vibrio* sp. NJU-03	7.0/30	10–40	6.0–9.0	2–5	Zhu et al., 2018b
Alyw203	*Vibrio* sp. W2	10.0/45	20–45	3.0–12.0	1–2	This study

with the alginate lyase listed in **Table 1**, Alyw203 possessed catalytic activity within a wider pH range; that is, the current enzyme showed superior pH stability. For instance, ZH0-IV alginate lyase from *Sphingomonas* sp. (He et al., 2018) displayed the highest activity at pH 7.5, with a pH stability range of 6.0–9.0. A9m from *Vibrio* sp. A9m (Uchimura et al., 2010) possessed a neutral pH of 7.5 for optimum activity as well as a narrow pH stability range of 7.0–10.0. These enzymes had preferably neutral-pH conditions but had poor stability in alkaline environments. In addition, the Alyw203 and the reported pH-stable as well as highly active AlgNJ04 alginate lyase exhibited similar pH stability, which reserved over 80% of highest activity at an extensive pH from 4.0 to 10.0, indicating that the present enzyme could be applied for the extraction of active substances in brown algae (Zhu et al., 2018a).

The current enzyme possessed the highest activity detected at 45°C and showed a relative activity of more than 80% at 40–55°C. It is worth noting that Alyw203 alginate lyase displayed a unique heat recovery performance; that is, after cultivation for 20 min at 10°C, the activity of the enzyme boiled for 5 min could recover to over 90%. Considering that the inactivated enzyme could recover its activity after a short incubation period at 10°C, the thermal recovery properties of Alyw203 may effectively facilitate transportation and storage.

The study of the effect of ions on the present enzyme activity has shown that 1 mM metal ions could not effectively promote the activation of Alyw203, while Fe^{3+}, Cu^{2+}, Zn^{2+}, and Al^{3+} exhibited obvious inactivation effects under the condition of 10 mM. Additionally, SDS and EDTA had remarkable inhibitory effects on the present enzyme. Alyw203 was not a strong NaCl-dependent enzyme. For many reported alginate lyases, a certain concentration of NaCl was a superior improver of enzyme activity. Like the activity of Aly08 from *Vibrio* sp., that of SY01 has been greatly increased by approximately eight times under the condition of 0.3 M NaCl. Similarly, activity of AlgM4 from *Vibrio weizhoudaoensis* has also been raised approximately seven times under the condition of 1 M NaCl. In comparison, the Alyw203 was not strongly dependent on NaCl. More interestingly, the activity of the current enzyme was still improved even in high concentrations of NaCl. In view of its superior salt tolerance, the Alyw203 alginate lyase was competent for specific production demands.

The main product of Alyw203 alginate lyase was DP1–DP2 oligosaccharide. Since alginate oligosaccharides are extensively used in the food, paper, and cosmetic industries (Falkeborg et al., 2014; Zhang et al., 2014; Qu et al., 2017), they have especially found important applications in the field of biomedical engineering in recent years; enzymatic production of single homogeneous oligosaccharides possessed a broad application prospect. However, majority of alginase degradation products found were a blend of DP2–DP6. For instance, the main products of Algb alginate lyase from *Vibrio* sp. W13 were DP2–DP5 (Zhu et al., 2015). Moreover, TsAly6A from *Thalassomonas* sp. (Gao et al., 2018) has DP2 and DP3 as its final degradation products. In comparison, the degradation products of the current alginate-degrading enzyme Alyw203 were concentrated in monosaccharide and disaccharide, which was conducive to further extraction as well as efficient production, showing potential drug application prospects.

DATA AVAILABILITY STATEMENT

The datasets presented in this study can be found in online repositories. The names of the repository/repositories and accession number(s) can be found in the article/supplementary material.

AUTHOR CONTRIBUTIONS

LL and HW: conceptualization, methodology, writing–original draft, and writing–review and editing. ZW: manuscript review and revision. ZZ and ZL: formal analysis and writing–original draft. LL: data curation and methodology. XJ and HC: funding acquisition and writing–review and editing. All authors have read and agreed to the published version of the manuscript.

FUNDING

This project was funded by the National Key R&D Program of China (2019YFD0901902).

REFERENCES

Bonugli-Santos, R. C., Vasconcelos, M. R., Passarini, M. R., Vieira, G. A., Lopes, V. C., Mainardi, P. H., et al. (2015). Marine-derived fungi: diversity of enzymes and biotechnological applications. *Front. Microbiol.* 6:269. doi: 10.3389/fmicb.2015.00269

Cantarel, B. L., Coutinho, P. M., Rancurel, C., Bernard, T., Lombard, V., and Henrissat, B. (2009). The carbohydrate-active enzymes database (CAZy): an expert resource for glycogenomics. *Nucleic Acids Res.* 37, 233–238. doi: 10.1093/nar/gkn663

Chen, X. L., Dong, S., Xu, F., Dong, F., Li, P. Y., Zhang, X. Y., et al. (2016). Characterizationof a new cold-adapted and salt-activated polysaccharide lyase family 7 alginate lyase from *Pseudoalteromonas* sp. SM0524. *Front. Microbiol.* 7:1120. doi: 10.3389/fmicb.2016.01120

Ertesvag, H. (2015). Alginate-modifying enzymes: biological roles and biotechnological uses. *Front. Microbiol.* 6:523. doi: 10.3389/fmicb.2015.00523

Falkeborg, M., Cheong, L. Z., Gianfico, C., Sztukiel, K. M., Kristensen, K., Glasius, M., et al. (2014). Alginate oligosaccharides: enzymatic preparation and antioxidant property evaluation. *Food Chem.* 164, 185–194. doi: 10.1016/j.foodchem.2014.05.053

Gacesa, P. (1992). Enzymic degradation of alginates. *Int. J. BioChemiPhysics.* 24, 545–552. doi: 10.1016/0020-711X(92)90325-U

Gao, S., Zhang, Z., Li, S., Su, H., Tang, L., Tan, Y., et al. (2018). Characterization of a new endo-type polysaccharide lyase (PL) family 6 alginate lyase with cold-adapted and metal ions-resisted property. *Int. J. Biol. Macromol.* 120, 729–735. doi: 10.1016/j.ijbiomac.2018.08.164

He, M., Guo, M., Zhang, X., Chen, K., Yan, J., and Irbis, C. (2018). Purification and characterization of alginate lyase from *Sphingomonas*

sp. ZH0. *J. Biosci. Bioeng.* 126, 310–316. doi: 10.1016/j.jbiosc.2018.01.017

Helbert, W. L., Poulet, S., Drouillard, S., Mathieu, M., Loiodice, M., Couturier, V., et al. (2019). Discovery of novel carbohydrate-active enzymes through the rational exploration of the protein sequences space. *Proc. Natl. Acad. Sci. U.S.A.* 116, 6063–6068. doi: 10.1073/pnas.1815791116

Huang, L. S., Zhou, J. G., Li, X., Peng, Q., Lu, H., and Du, Y. G. (2013). Characterization of a new alginate lyase from newly isolated *Flavobacterium* sp. S20. *J. Ind. Microbiol. Biotechnol.* 40, 113–122. doi: 10.1007/s10295-012-1210-1

Inoue, A., Anraku, M., Nakagawa, S., and Ojima, T. (2016). Discovery of a novel alginate lyase from *Nitratiruptor* sp. SB155-2 thriving at deep-sea hydrothermal vents and identification of the residues responsible for its heat stability. *J. Biol. Chem.* 291, 15551–15563. doi: 10.1074/jbc.m115.713230

Jagtap, S. S., Hehemann, J. H., Polz, M. F., Lee, J. K., and Zhao, H. (2014). Comparative biochemical characterization of three exolytic oligoalginate lyases from *Vibrio splendidus* reveals complementary substrate scope, temperature, and pH adaptations. *Appl. Environ. Microbiol.* 80, 4207–4214. doi: 10.1128/AEM.01285-14

Ji, S. Q., Dix, S. R., Aziz, A. A., Sedelnikova, S. E., Baker, P. J., Rafferty, J. B., et al. (2019). The molecular basis of endolytic activity of a multidomain alginate lyase from defluviitalea phaphyphila, a representative of a new lyase family, PL39. *J. Biol. Chem.* 294, 18077–18091.

Kim, H. T., Ko, H. J., Kim, N., Kim, D., Lee, D., Choi, I. G., et al. (2015). Characterization of a recombinant endo-type alginate lyase (Alg7D) from Saccharophagus degradans. *Biotechnol. Lett.* 34, 1087–1092. doi: 10.1007/s10529-012-0876-9

Li, S., Yang, X., Bao, M., Wu, Y., Yu, W., and Han, F. (2015). Family 13 carbohydrate-binding module of alginate lyase from *Agarivorans* sp. L11 enhances its catalytic efficiency and thermostability, and alters its substrate preference and product distribution. *FEMS Microbiol. Lett.* 362, fnv054. doi: 10.1093/femsle/fnv054

Madzak, C. (2015). *Yarrowia lipolytica*: recent achievements in heterologous protein expression and pathway engineering. *Appl. Microbiol. Biotechnol.* 99, 4559–4577. doi: 10.1007/s00253-015-6624-z

Miyamoto, T., Okano, S., and Kasai, N. (2009). Inactivation of *Escherichia coli* endotoxin by soft hydrothermal processing. *Appl. Environ. Microbiol.* 75, 5058–5063. doi: 10.1128/AEM;00122-09

Powell, L. A., Sowedan, S., Khan, C., Wright, K., Hawkins, E., Onsøyen, R., et al. (2013). The effect of alginate oligosaccharides on the mechanical properties of gram-negative biofilms. *Biofouling* 29, 413–421. doi: 10.1080/08927014.2013.777954

Pritchard, M., Powell, L., Jack, A., Powell, K., Beck, K., Florance, H., et al. (2017). A low-molecular-weight alginate oligosaccharide disrupts pseudomonal microcolony formation and enhances antibiotic effectiveness. *Antimicrob. Agents Chemother.* 61, 792–807. doi: 10.1128/AAC.00762-17

Qian, L. A., Fu, H. A., Mw, B., Bz, A., Fang, N. A., and Zhong, Y. A. (2020). Elucidation of degradation pattern and immobilization of a novel alginate lyase for preparation of alginate oligosaccharides. *Int. J. Biol. Macromol.* 146, 579–587. doi: 10.1016/j.ijbiomac.2019.12.238

Qin, H. M., Miyakawa, T., Inoue, A., Nishiyama, R., Nakamura, A., Asano, A., et al. (2018). Structural basis for controlling the enzymatic properties of polymannuronate preferred alginate lyase FlAlyA from the PL-7 family. *Chem. Commun.* 54, 555–558. doi: 10.1039/c7cc06523j

Qu, Y., Wang, Z. M., Zhou, H. H., Kang, M. Y., Dong, R. P., and Zhao, J. W. (2017). Oligosaccharide nanomedicine of alginate sodium improves therapeutic results of posterior lumbar interbody fusion with cages for degenerative lumbar disease in osteoporosis patients by downregulating serum miR-155. *Int. J. Nanomed.* 12, 8459–8469. doi: 10.2147/IJN.S143824

Swift, S. M., Hudgens, J. W., Heselpoth, R. D., Bales, P. M., and Nelson, D. C. (2018). Characterization of AlgMsp, an alginate lyase from *Microbulbifer* sp. 6532A. *PLoS One* 9:e112939. doi: 10.1371/journal.pone.0112939

Turquois, T., and Gloria, H. (2000). Determination of the absolute molecular weight averages and molecular weight distributions of alginates used as ice cream stabilizers by using multiangle laser light scattering measurements. *J. Agric. Food Chem.* 48, 5455–5458. doi: 10.1021/jf000003v

Uchimura, K., Miyazaki, M., Nogi, Y., Kobayashi, T., and Horikoshi, K. (2010). Cloning and sequencing of alginate lyase genes from deep-sea strains of *Vibrio* and *Agarivorans* and characterization of a new *Vibrio* enzyme. *Mar. Biotechnol.* 12, 526–533. doi: 10.1007/s10126-009-9237-7

Wang, Y., Chen, X., Bi, X., Ren, Y., and Li, S. (2019). Characterization of an alkaline alginate lyase with pH-stable and thermo-tolerance property. *Mar. Drugs* 17:308. doi: 10.3390/md17050308

Wang, Z. P., Cao, M., Li, B., Ji, X. F., and Wang, H. Y. (2020). Cloning, secretory expression and characterization of a unique pH-stable and cold-adapted alginate lyase. *Mar. Drugs* 18:189. doi: 10.3390/md18040189

Xu, F., Dong, F., Wang, P., Cao, H. Y., Li, C. Y., Li, P. Y., et al. (2017). Novel molecular insights into the catalytic mechanism of marine bacterial alginate lyase AlyGC from polysaccharide lyase family 6. *J. Biol. Chem.* 29, 4457–4468. doi: 10.1016/j.jbiosc.2018.01.017

Yan, J., Chen, P., Zeng, Y., Men, Y., Mu, S., Zhu, Y., et al. (2019). The characterization and modification of a novel bifunctional and robust alginate lyase derived from *Marinimicrobium* sp. H1. *Mar. Drugs* 17:10. doi: 10.3390/md17100545

Yang, S., Liu, Z., Fu, X., Zhu, C., and Mou, H. (2020). Expression and characterization of an alginate lyase and its thermostable mutant in *Pichia Pastoris*. *Mar. Drugs* 18:305. doi: 10.3390/md18060305

Zhang, Y. H., Yin, H., Zhao, X. M., Wang, W. X., Du, Y. G., He, A., et al. (2014). The promoting effects of alginate oligosaccharides on root development in Oryza sativa L. mediated by auxin signaling. *Carbohydr. Polym.* 113, 446–454. doi: 10.1016/j.carbpol.2014.06.079

Zhang, Z., Tang, L., Bao, M., Liu, Z., Yu, W., and Han, F. (2019). Functional characterization of carbohydrate-binding modules in a new alginate lyase, TsAly7B, from *Thalassomonas* Sp. LD5. *Mar. Drugs* 18:25. doi: 10.3390/md18010025

Zhu, B., Ni, F., Ning, L., Sun, Y., and Yao, Z. (2018a). Cloning and characterization of a new pH-stable alginate lyase with high salt tolerance from marine *Vibrio* sp. NJ-04. *Int. J. Biol. Macromol.* 115, 1063–1070.

Zhu, B., Sun, Y., Ni, F., Ning, L., and Yao, Z. (2018b). Characterization of a new endo-type alginate lyase from *Vibrio* sp. NJU-03. *Int. J. Biol. Macromol.* 108, 1140–1147. doi: 10.1016/j.ijbiomac.2017.10.164

Zhu, B., Tan, H., Qin, Y., Xu, Q., Du, Y., and Yin, H. (2015). Characterization of a new endo-type alginate lyase from *Vibrio* sp. W13. *Int. J. Biol. Macromol.* 75, 330–337. doi: 10.1016/j.ijbiomac.2015.01.053

Zhuge, B., Du, G. C., and Wei, S. (2008). Expression of a *Bacillus subtilis* pectate lyase gene in *Pichia pastoris*. *Biochem. Eng. J.* 40, 92–98. doi: 10.1016/j.bej.2007.11.018

Conflict of Interest: The authors declare that the research was conducted in the absence of any commercial or financial relationships that could be construed as a potential conflict of interest.

The handling editor declared a shared affiliation with one of the authors LL at the time of review.

Publisher's Note: All claims expressed in this article are solely those of the authors and do not necessarily represent those of their affiliated organizations, or those of the publisher, the editors and the reviewers. Any product that may be evaluated in this article, or claim that may be made by its manufacturer, is not guaranteed or endorsed by the publisher.

frontiers in Microbiology

ORIGINAL RESEARCH
published: 01 September 2021
doi: 10.3389/fmicb.2021.722347

Improvement of the Catalytic Ability of a Thermostable and Acidophilic β-Mannanase Using a Consensus Sequence Design Strategy

Qingping Liang[1], Yuming Zhan[2], Mingxue Yuan[1], Linyuan Cao[1], Changliang Zhu[1], Haijin Mou[1] and Zhemin Liu[1]**

[1]College of Food Science and Engineering, Ocean University of China, Qingdao, China, [2]Shandong Provincial Key Laboratory of Quality Safety Monitoring and Risk Assessment for Animal Products, Jinan, China*

In order to improve the catalytic efficiency of a thermostable and acidophilic β-mannanase (ManAK; derived from marine *Aspergillus kawachii* IFO 4308), three mutants were designed by amino acid sequence consensus analysis with a second β-mannanase (ManCbs), which also belongs to the glycoside hydrolase family 5 (GH5) and has excellent catalytic efficiency. Three mutants were constructed and their biochemical characteristics were measured after heterologous expression in *Pichia pastoris*. The results revealed that the k_{cat}/K_m values of the three recombinant mannanases ManAK^{C292V}, ManAK^{L293V}, and ManAK^{L294H} were enhanced by 303.0, 280.4, and 210.1%, respectively. Furthermore, ManAK^{L293V} showed greater thermostability than ManAK, retaining 36.5% of the initial enzyme activity after incubation at 80°C for 5 min. This study therefore provides a rational design strategy based on consensus sequence analysis to develop industrially valuable β-mannanase for future applications in marine aquafeed.

Keywords: β-mannanase, consensus sequence design, catalytic ability, thermostability, rational design

OPEN ACCESS

Edited by:
Lei Chen,
Tianjin University, China

Reviewed by:
Abdul Munir Abdul Murad,
Universiti Kebangsaan Malaysia, Malaysia
Michael Benedik,
Texas A&M University, United States

****Correspondence:***
Haijin Mou
mousun@ouc.edu.cn
Zhemin Liu
ocean2013@126.com

Specialty section:
This article was submitted to Microbiotechnology, a section of the journal Frontiers in Microbiology

Received: *08 June 2021*
Accepted: *05 August 2021*
Published: *01 September 2021*

Citation:
Liang Q, Zhan Y, Yuan M, Cao L, Zhu C, Mou H and Liu Z (2021) Improvement of the Catalytic Ability of a Thermostable and Acidophilic β-Mannanase Using a Consensus Sequence Design Strategy. Front. Microbiol. 12:722347. doi: 10.3389/fmicb.2021.722347

INTRODUCTION

β-Mannanases are endo-hydrolases, which can hydrolyze mannan to small molecular degradation products (Chauhan et al., 2012; Finn et al., 2014; Srivastava and Kapoor, 2017). They have been used as food stabilizers, bleaching agents in papermaking, and washing and cleaning agents (Kaira et al., 2016). They are also added into fish feedstuffs (such as soybean meal) to improve the nutritional value (Cai et al., 2011), and can significantly reduce the viscosity of coffee extract to reduce the energy consumption of large-scale coffee production (Chauhan et al., 2014a). Furthermore, manno-oligosaccharides (MOS), which are regarded as potential novel prebiotics, and are added into aquafeed, can be prepared by hydrolysis with β-mannanases (Jana et al., 2020). Therefore, improved enzymatic properties of β-mannanases, such as thermal stability, acid tolerance, and high catalytic ability would be desirable.

In our previous work, a β-mannanase (ManAK) derived from marine *Aspergillus kawachii* IFO 4308 was heterologously expressed in *Pichia pastoris* (Liu et al., 2020b). ManAK is a thermostable and acidophilic enzyme, with an optimal catalytic temperature of 80°C and pH optimum of 2.0. This characteristic makes ManAK a valuable enzyme in MOS preparation

from plant gums [e.g., konjac gum, locust bean gum (LBG), and guar gum], because both high temperature and acidic conditions could decrease the stickiness of the substances and accelerate enzymatic hydrolysis (Zheng et al., 2018; La Rosa et al., 2019). However, the low catalytic efficiency of ManAK has restricted the economic production of MOS. Therefore, improvement of the catalytic efficiency of ManAK without impairing its innate thermostability and acid tolerance is meaningful.

Consensus sequence design (CSD) strategy offers a promising solution for designing enzymes of evaluated catalytic efficiency, while retaining other original properties (Sternke et al., 2019). Since the amino acid sequence of the catalytic region is generally recognized as one of the most important factors affecting the catalytic efficiency of enzymes, amino acids in the catalytic region are normally selected as the mutation targets to improve the catalytic efficiency of enzymes. Ratananikom et al. (2013), for example, reported that two β-glucosidases (Dalcochinase and Abg) had different levels of catalytic efficiency toward glycone substrates, and believed that it might be caused by the difference in amino acid residues around the glycobase-binding region. Based on this, three mutants of dalcochinase were constructed (F196H, S251V, and M369E), and the catalytic efficiency was shown to have been significantly improved. However, this CSD strategy has rarely been used to improve the catalytic efficiency of β-mannanases.

According to the classification of the carbohydrate activity database,[1] ManAK is in the GH5 family (Larsson et al., 2006; van Zyl et al., 2010; Liu et al., 2020b). β-mannanases of this family share a similar $(\beta/\alpha)_8$-folded barrel structure and catalyze the reaction by complying with the double substitution reaction mechanism (Hilge et al., 1998; Zhang et al., 2008). ManCbs, derived from the fibrolytic bacterium *Cellulosimicrobium* sp. strain HY-13, is a neutral-type mannanase in the same family, but has much higher catalytic activity than ManAK. The specific activity of ManCbs can be as high as 14,711 IU mg^{-1} (Kim et al., 2011), which is greater than that of ManAK. Considering that ManAK and ManCbs share high sequence similarity (86.4%) in the catalytic region, it is theoretically feasible to enhance the catalytic efficiency of ManAK according to CSD strategy.

In this study, the CSD strategy was adopted to rationally design potential enzyme mutants with elevated catalytic efficiency. Three recombinant ManAK mutants were heterologously expressed by *P. pastoris*. The recombinant enzymes were purified, and their enzymatic properties were fully assayed. Changes in enzymatic properties were illustrated in terms of the structure-function relationship by analyzing the alterations in non-covalent bond interactions between ManAK and its mutants.

MATERIALS AND METHODS

Materials

Thermostable and acidophilic β-mannanase was purified from *A. kawachii* IFO 4308 (BioProject accession: PRJDA66971), and the coding sequence was derived from the gene sequence published by NCBI with the GenBank accession No.: GAA89125.1 as previously reported (Liu et al., 2020b). The *Escherichia coli* DH5α and the *P. pastoris* X33 (Invitrogen, United States) were purchased from Sigma-Aldrich (St. Louis, MO, United States). These strains were used to prepare expression plasmids and as expression hosts, respectively. All chemicals and reagents used were purchased from Sigma-Aldrich (St. Louis, MO, United States) and of analytical grade.

Alignment Analysis of Gene Sequences of ManAK and ManCbs

Thermostable and acidophilic β-mannanase and ManCbs belong to the GH5 family, and the two gene sequences are highly conserved and homologous. The tertiary structure of ManAK was automatically modeled by the Phyre2 program[2] based on the reported crystal structure of ManBK (PDB code: 3WH9; 95% identity), and the tertiary structures of ManCbs were modeled by the same way. Sequence alignment and structure analysis were performed by Discovery Studio 2.5 software (Accelrys, San Diego, CA, United States). Figure rendering was performed by PyMOL software (version 1.7.2; Delano Scientific, United States).

Construction of Recombinant Expression Plasmids of ManAK

Three mutants ($ManAK^{C292V}$, $ManAK^{L293V}$, and $ManAK^{L294H}$) were created based on the amino acid sequence consensus analysis between ManAK and ManCbs. Vector NTI 13.5 was used to design and analyze the PCR mutation primers according to the rational design sequence of ManAK. To insert the mutated gene into the expression vector pPICZα A, all primers had homology arm sequences at both ends of the vector insertion site (**Table 1**). The T_m values of all primers were approximately 60°C, and GC% was kept below 60%. Both primers were synthesized by the Ruibo Xingke Company, Beijing.

pPICZα A-AK was constructed by ligating the original ManAK gene (GenBank accession No.: GAA89125.1) into the pPICZα A expression plasmid, and the integrated vector was transformed into *E. coli* DH5α, which was considered as the template for the preparation of the other three recombinant expression plasmids. Synthetic primers were used to amplify the three mutant enzyme genes by PCR reaction according to the Mut Express® II kit instructions. The three recombinant expression plasmids were constructed by homologous recombination of the genes prepared with the pPICZα A expression plasmid; named pPICZα A-$ManAK^{C292V}$, pPICZα A-$ManAK^{L293V}$, and pPICZα A-$ManAK^{L294H}$.

Heterologous Expression of Recombinant Mutants in *P. pastoris* and Purification

The recombinant expression plasmids pPICzα A-$ManAK^{C292V}$, pPICzα A-$ManAK^{L293V}$, and pPICzα A-$ManAK^{L294H}$ were

[1]http://www.cazy.org

[2]http://www.sbg.bio.ic.ac.uk/phyre2/html/page.cgi?id=index

TABLE 1 | Primers used for site-directed mutagenesis.

Mutants	Primers
ManAK^{C292V}	Reverse: 5'-TGGTAAGCCAGTTTTGTTGGAAGAATACGGTGTTACTTCTAACCAT-3' Forward: 5'-CTTCCAACAAAACTGGCTTACCAGCAGCCTTACAAGC-3'
ManAK^{L294H}	Reverse: 5'-TAAGCCATGTGTTTTGGAAGAATACGGTGTTACTTCTAACCATTG-3' Forward: 5'-ATTCTTCCAAAACACATGGCTTACCAGCAGCCTTACAAG-3'
ManAK^{L294H}	Reverse: 5'-GCCATGTTTGGATGAAGAATACGGTGTTACTTCTAACCATTGTTCT-3' Forward: 5'-CGTATTCTTCATCCAAACATGGCTTACCAGCAGCCTTAC-3'

linearized and digested with Sal I enzyme, and transformed into *P. pastoris* X33 by electroporation. The transformed colonies were grown on YPD solid plates containing 100 μg/ml Zeocin (Thermo Scientific) and incubated at 30°C for 5 days. Colonies were then transferred to Buffered Minimal Glycerol-complex Medium, and 1.0% (v/v) methanol was added to induce protein expression. The cultures were incubated in a shaker at 30°C for 3 days to allow secretion of the expression product. Supernatant was collected and concentrated by ultrafiltration with a 50 kDa membrane. The sample was then loaded onto a Ni-Sepharose 6FF column (GE Healthcare, United States), and the sample eluted according to the method described by Zhang et al. (2019). The sample was dialyzed against 50 mM potassium phosphate buffer (pH 5.5) and analyzed by SDS-PAGE gel chromatography. The concentration of the purified enzyme solution was determined by the Bradford method (Bradford, 1976).

Biochemical Characterization of Recombinant ManAK^{C292V} and ManAK^{L293V} and ManAK^{L294H}

To assess the effects of the site directed mutagenesis, the biochemical characteristics of the recombinant enzymes were measured. The enzymatic activity of mannanases was determined using the 3,5-dinitrosalicylic acid (DNS) method: the expressed enzyme solution was diluted with 50 mM sodium acetate buffer, and reacted with an equal volume of 0.5% (w/v) D-mannan (Sigma, St. Louis, MO, United States) at 37°C for 30 min. The D-mannan used here was LBG (Sigma), which was dissolved in boiling sodium acetate buffer, and then diluted to 100 ml to prepare the substrate. Subsequently, DNS reagent was added and the reaction incubated in a boiling water bath for 5 min, and then the optical density measured at 540 nm (Miller, 1959). One unit (U) of mannanase activity is defined as the amount of enzyme needed to generate 1 μmol of reducing sugar/minute at pH 5.5 and 37°C from a solution of 3 mg/ml mannan.

The optimal temperature for activity of the mannanases was determined by comparing the relative enzyme activity of the sample at a range of temperatures between 35 and 85°C (in 50 mM sodium acetate buffer, pH 5.5). The mixture samples of enzymes and substrate were reacted at various temperatures for 5 min to access the recombinant mannanase activity. In addition, the thermal stability of the enzymes was determined after preincubation of enzymes without substrate in 50 mM sodium acetate buffer (pH 5.5) at different temperatures (60, 70, and 80°C) for different times (5, 10, 15, 20, and 25 min). After this thermal treatment, the enzymes were mixed with substrate and reacted under standard conditions (pH 5.5, 37°C, and 30 min) to obtain the residual rate of enzyme activity after heat treatment.

Dilute mannanase enzyme solution was tested with the different pH buffers (i) Glycine-HCl (pH 1.0–4.0), (ii) sodium acetate buffer (pH 4.0–6.0), and (iii) Tris-HCl buffer (pH 6.0–8.0). Using the 0.5% (w/v) LBG under different pH conditions (1.0–8.0) as substrates, the optimal pH of recombinant mannanases was determined under standard conditions (37°C, 30 min). After the sample was treated with a buffer of the same pH value range (1.0–8.0) at 37°C for 2 h, the residual rate of enzyme activity was measured according to the same method to obtain the pH stability.

To obtain the kinetic characteristics of the mannanase samples, the enzyme activity was measured under standard conditions using 1–10 mg/ml LBG as a substrate. The data were analyzed by Origin 8.5 software and the dynamic parameters K_m and k_{cat} were obtained. Dynamic curves were drawn according to the nonlinear regression method.

The three-dimensional structures of ManAK and recombinant mutants were modeled by the Phyre2 website (see Footnote 2; Kelley et al., 2016). Using Auto Dock Tools 1.5.6, the three recombinant samples were docked by molecular simulation and compared. The differences between the structure of the native ManAK and the modified versions around the mutated sites were then obtained. The software used in the molecular visualization and graphics drawing process was PyMOL (v1.7.2; Delano Scientific, United States), and Discovery Studio 2.5 software was used to make a simulated two-dimensional diagram of the interaction force between molecules.

Analysis of Hydrolysis Products

In order to understand and compare the degradation efficiency and mode of action of ManAK and its mutant forms, the hydrolysis products of the mannobiose (M2), mannotriose (M3), mannotetraose (M4), and mannopentaose (M5) standard of MOS were analyzed using the ManAK^{L293V} mutant. The reaction was carried out at 37°C for 10 min for all MOS, and the reactants were 5 U purified enzyme and 20 mM MOS standard solution. The reaction was terminated by boiling the sample in water for 10 min, then the macromolecules were removed using a 3-kDa Millipore membrane (Millipore, United States) for ultrafiltration. After centrifugation at 13,000 *g* for 10 min,

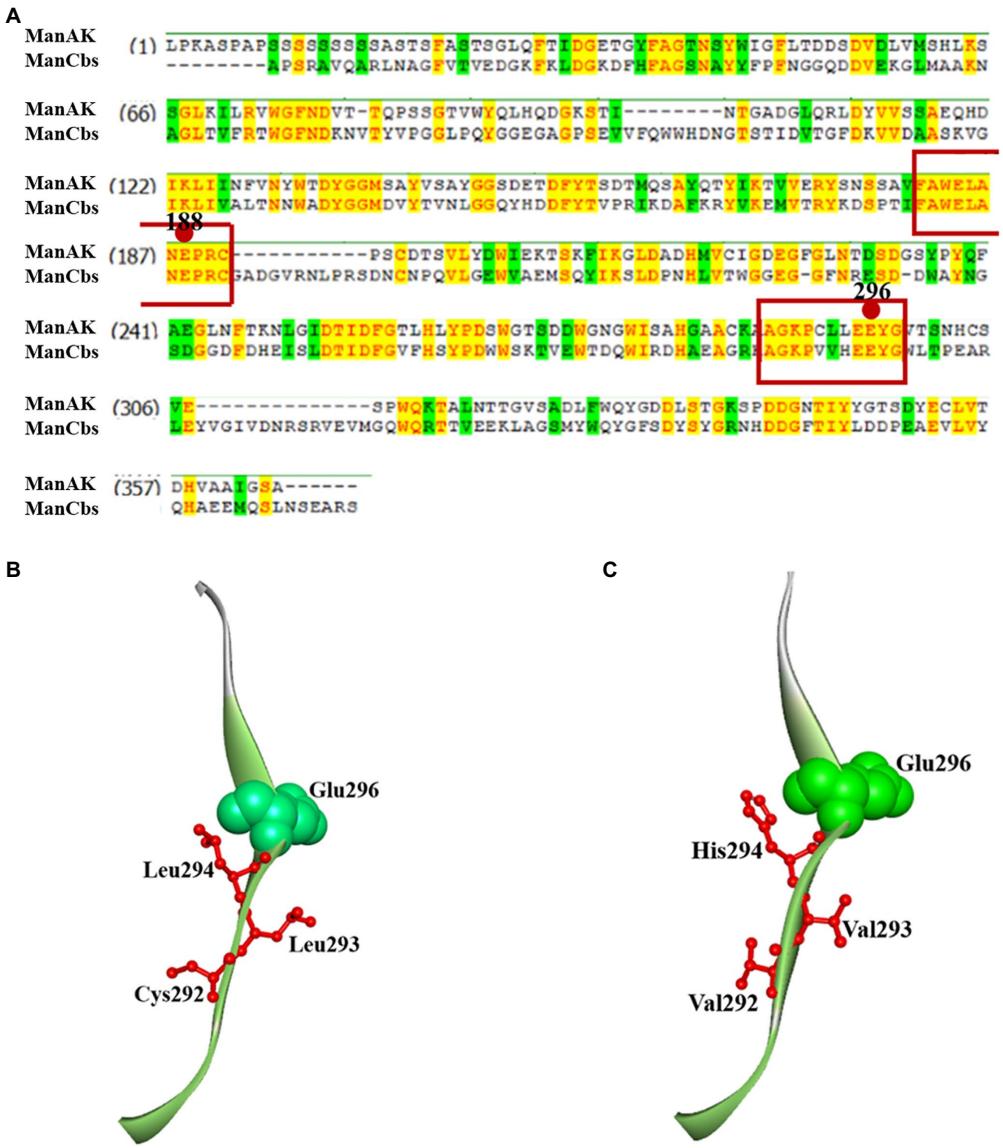

FIGURE 1 | Amino acid consensus sequence analysis and secondary structure around E296 of thermostable and acidophilic β-mannanase (ManAK) and ManCbs. **(A)** Amino acid consensus sequence analysis of ManAK and ManCbs. Strictly conserved residues are shaded yellow. The active site residues in catalytic regions are boxed and circles indicate the catalytic sites in catalytic region. **(B)** Secondary structure around E296 of ManAK. **(C)** Secondary structure around E296 of ManCbs. The amino acids in position 292, 293, and 294 are indicated in red, and E296 is indicated in green balls.

supernatants were collected and analyzed according to the procedure as previously described (Katrolia et al., 2013), using TLC plate (Silica gel 60F254, Merck, Darmstadt, Germany) to analyze the samples.

The hydrolysis products of recombinant ManAK and the mutant ManAK^{L293V} were further analyzed using high-performance liquid chromatography [HPLC; Agilent 1260 Infinity system TSKgel G-oligo-PW column (7.5 mm × 300 mm), Tosoh Corporation Co. Japan]. Purified ManAK and ManAK^{L293V} were diluted with 50 mM sodium acetate buffer (pH 5.5) to give a final enzyme activity of 5 U, and reacted with 20 mM MOS standard solution (M4 and M5) at 37°C for 20 min. The products were detected with ultra-pure water as the mobile phase at a flow rate of 0.6 ml/min. All samples were injected after filtering through a 0.22 μm filter membrane, and the hydrolysis products were analyzed sequentially.

The release of reducing sugar was determined as follows: 5 U purified enzyme and 0.5% (w/v) D-mannan (Sigma, United States) in 50 mM sodium acetate buffer (pH 5.5) were incubated at 37°C for varying lengths of time, and the concentration of released reducing sugars measured by the DNS method as above.

To explore the application of this β-mannanase, the recombinant ManAK and the ManAK^{L293V} mutant were assessed for their hydrolytic performance, using LBG as a substrate.

LBG was dissolved in 50 mM sodium acetate buffer (pH 5.5) to give a final concentration of 1.0%, and purified ManAK and ManAK^{L293V} were diluted with 50 mM sodium acetate buffer (pH 5.5) to 5 enzyme activity units. The reaction was carried out at 37°C for 12 h. Molecular weight distribution of the hydrolysis products was detected by the HPLC [Agilent 1260 Infinity system TSKgel G4000PWXL column (7.8 mm × 300 mm), Tosoh Corporation Co. Japan]. The mobile phase of the detection system was 0.2 M $NaNO_3$ and 0.01 M NaH_2PO_4, and the flow rate was 0.2 ml/min.

TABLE 2 | Kinetic parameters of ManAK, ManAK^{C292V}, ManAK^{L293V}, and ManAK^{L294H}.

	V_{max} (U/mg·min)	K_m (mg/ml)	K_{cat} (S^{-1})	K_{cat}/K_m (ml/s·mg)
ManAK^{C292V}	126.80 ± 8.29	0.10 ± 0.09	83.67	803.22
ManAK^{L293V}	154.22 ± 12.32	0.14 ± 0.12	101.72	758.07
ManAK^{L294H}	64.29 ± 20.52	0.07 ± 0.18	42.41	618.01
ManAK	329.30 ± 25.50	1.09 ± 0.28	217.21	199.30

Statistical Analysis

All experimental results were repeated three times, and they were statistically analyzed using ANOVA (*t*-test) with IBM SPSS Statistics 26 software. Differences with a threshold of $p < 0.05$ were considered statistically significantly.

RESULTS

Sequence Alignment Analysis of ManAK and ManCbs Based on CSD Strategy

Analysis of the conserved domains of the gene sequences of ManAK and ManCbs showed that they both belonged to the GH5 family, and that the proportion of amino acid sequence homology in the catalytic region was as high as 86.4%. Two key amino acids (Glu188 and Glu296) in the catalytic sites of ManAK exist as proton donors and nucleophiles, respectively, which play an important role in hydrolysis (Zhang et al., 2019). When ManAK binds to the substrates, a catalytic cleft is formed between the two catalytic

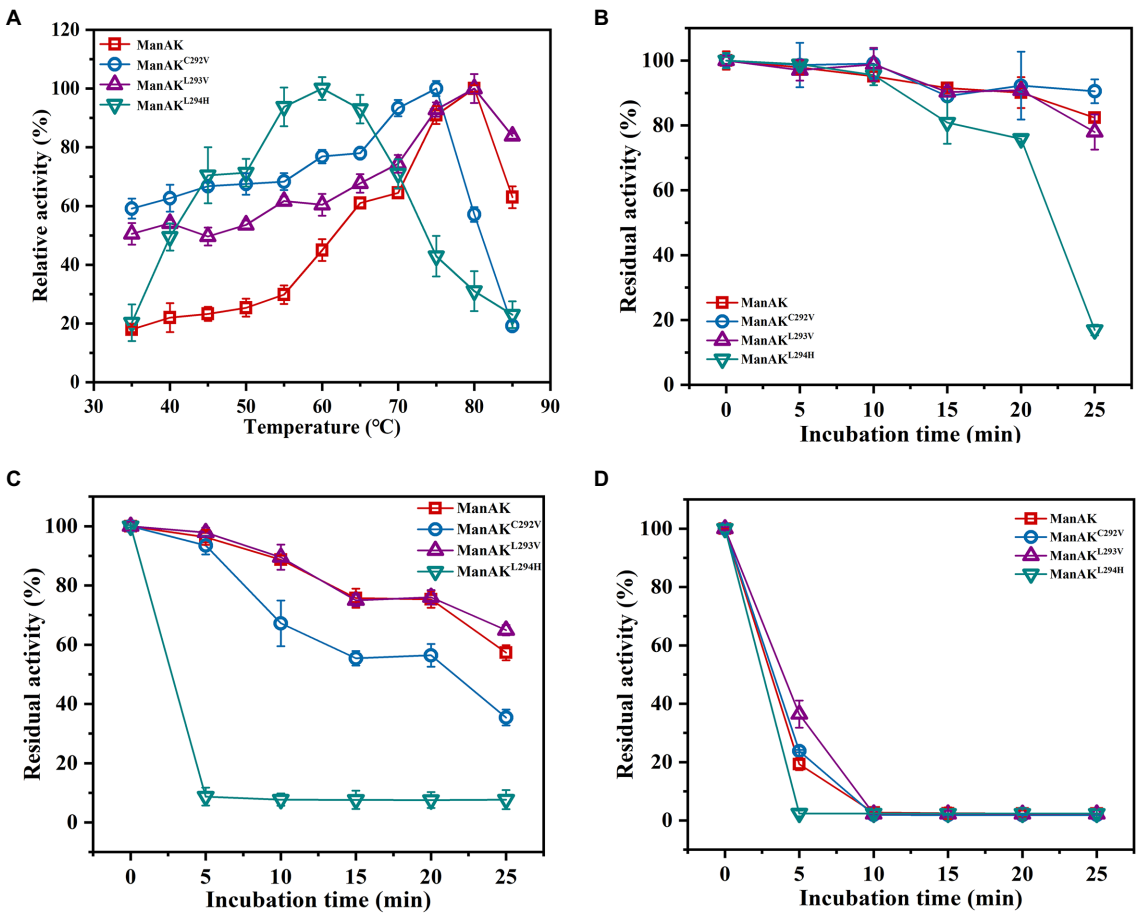

FIGURE 2 | Effects of temperature on activity and stability of recombinant β-mannanases. **(A)** The optimum temperature was determined in 50 mM sodium acetate buffer (pH 5.5) with a range of 35–85°C for 5 min; the thermal stability was evaluated under standard conditions (pH 5.5, 37°C, and 30 min) after the enzymes without substrate were treated at 60 **(B)**, 70 **(C)**, and 80°C **(D)** for 5–25 min.

domains (Glu188 and Glu296), and the amino acid residues around them assist with hydrolysis (Hilge et al., 1998).

The sequence comparison also showed that the amino acid sequence of the catalytic region around Glu188 was highly consistent (**Figure 1**). However, the amino acids around Glu296 in ManAK (Cys292, Cys293, and Leu294) were different from those in ManCbs (Val292, Val293, and His294). Combined with the structural analysis of ManAK and ManCbs in the catalytic region of Glu296, it was shown that the three different amino acids in positions 292, 293, and 294 were in the same β-sheet structure, and were adjacent to Glu298 (**Figures 1B,C**). The amino acid sequence of the three sites is likely to have a significant impact on the catalytic efficiency of the enzyme. Thus, through consensus sequence analysis, and structure analysis on the different amino acids in catalytic region, three mutants (ManAK^{C292V}, ManAK^{L293V}, and ManAK^{L294H}) were constructed to assess the underlying influences of the three amino acids on the catalytic efficiency of ManAK.

Kinetic Parameters and Catalytic Efficiency of Recombinant Mannanases

The recombinant plasmids pPICZα A-ManAK^{C292V}, pPICZα A-ManAK^{L293V}, pPICZα A-ManAK^{L294H} were transformed into the expression host *P. pastoris* X33. SDS-PAGE showed that the detected molecular weights of recombinant enzymes were approximately 50 kDa.

Locust bean gum was used as a substrate to determine the kinetic parameters of ManAK and its mutants. According to the Michaelis-Menten equation, the results demonstrated that the V_{max} and K_m values of ManAK were 329.3 U/mg·min and 1.09 mg/ml, and the catalytic efficiency k_{cat}/K_m value was 199.3 ml/s·mg (**Table 2**). Although, the V_{max} of the three recombinant mannanases was not obviously improved, the K_m values were changed from 1.09 mg/ml (ManAK) to 0.10 mg/ml (ManAK^{C292V}), 0.14 mg/ml (ManAK^{L293V}), and 0.07 mg/ml (ManAK^{L294H}), which indicated that the substrate affinity of the three mutants was improved.

The mutated amino acids, Val292, Val293, and His294, were shown to greatly affect the catalytic efficiency of ManAK. The results revealed that the k_{cat}/K_m values of the three recombinant mannanases ManAK^{C292V}, ManAK^{L293V}, and ManAK^{L294H} were enhanced by 303.0, 280.4, and 210.1%, respectively (**Table 2**). This proved that the CSD strategy was effective in improving the catalytic efficiency of mannanase. Further study is needed to show whether other properties of the enzyme could be similarly improved using this modification strategy.

Other Biochemical Characteristics of ManAK and Mutants

Thermostable and acidophilic β-mannanase showed excellent temperature characteristics with an optimal temperature for activity of 80°C (**Figure 2A**); and even retained approximately 19.3% of enzyme activity after incubation at 80°C for 5 min (**Figure 2D**). Three mutants of ManAK were constructed and their biochemical characteristics were accessed. While the catalytic efficiency was improved, the thermal stability of ManAK^{L293V} was further enhanced. Compared with the original enzyme ManAK, the optimum temperature of ManAK^{L293V} was unchanged, remaining at 80°C, but that of ManAK^{C292V} and ManAK^{L294H} dropped to 75 and 60°C, respectively (**Figure 2A**). Interestingly, after heating at 80°C for 5 min, ManAK^{L293V} retained 36.5% of the initial enzymatic activity, while ManAK retained only 19.3% (**Figure 2D**).

The ManAK is an extremely acidophilic mannanase with an optimal pH of 2.0 (**Figure 3A**), and after treatment in a buffer solution at pH 2.0, 84.3% relative enzymatic activity of ManAK was retained. Similarly, the pH profiles of the three mutants revealed that they retained strong activity under acidic conditions, and the optimal pH was acidic (**Figure 3A**). However, ManAK^{L294H} only retained 3.68% activity after

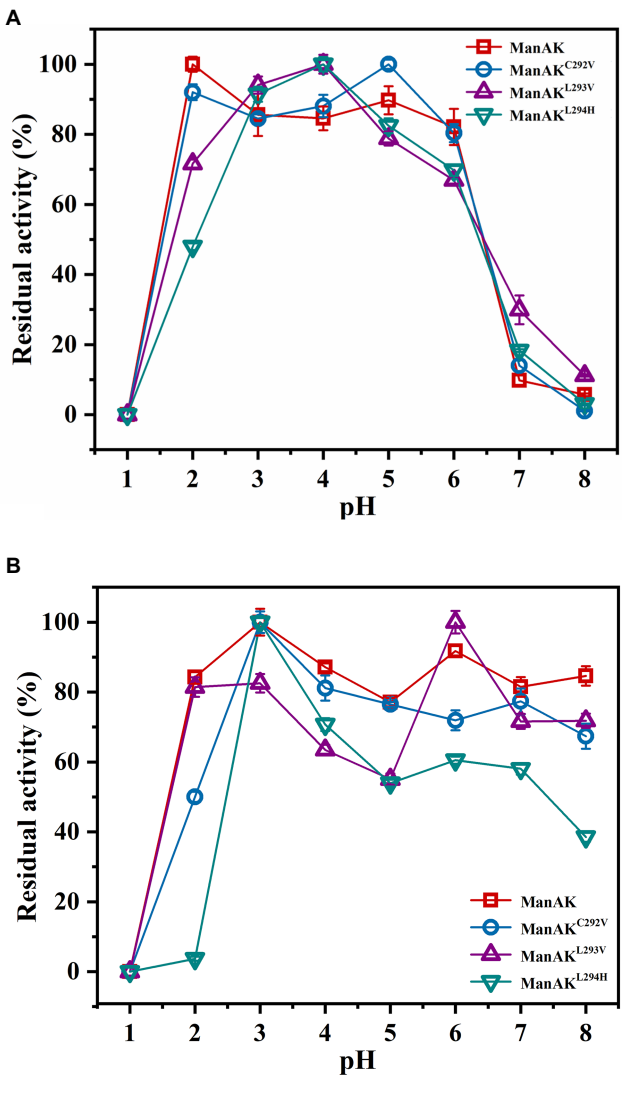

FIGURE 3 | Effects of pH on activity and stability of recombinant β-mannanases. **(A)** The pH optimum was determined in glycine–HCl buffer (pH 1.0–4.0), sodium acetate buffer (pH 4.0–6.0), and Tris-HCl buffer (pH 6.0–8.0), respectively. **(B)** The pH stability was determined after the enzymes were incubated at 37°C for 2 h in different buffers as described above.

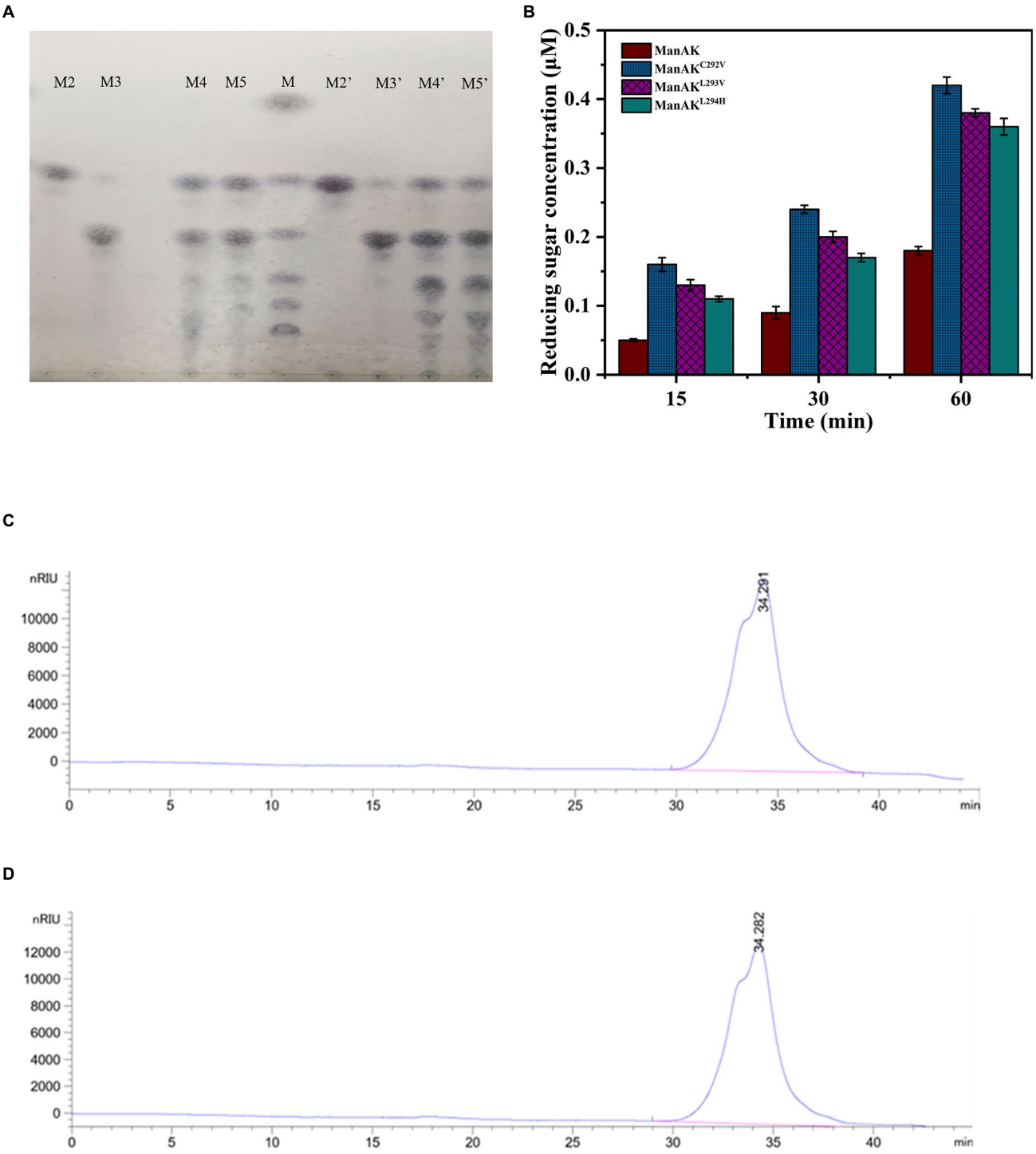

FIGURE 4 | Analysis of hydrolysis products. **(A)** The hydrolysis of substrates by ManAK and ManAK^{L293V}, and thin-layer chromatography (TLC) analysis of hydrolysis products from manno-oligosaccharides (MOS) standards (M2–M5). The reaction was carried out at 37°C for 10 min, and the reactants were 5 U purified enzyme and 20 mM MOS standard solution. Lanes: (M) the MOS standards consist of mannose, mannobiose, manninotriose, mannotetrose, mannopentose, and mannohexose (from top to bottom; M2–M5) the hydrolysis products of mannobiose, manninotriose, mannotetrose, and mannopentose, respectively, (M2'–M5') the same indication as above, analysis of hydrolysis products of ManAK^{L293V}. **(B)** The release of reducing sugar concentration of recombinant mannanases incubated with D-mannan in 50 mM sodium acetate buffer (pH 5.5) at 37°C. **(C)** High-performance liquid chromatography (HPLC) analysis of the molecular weight distribution of hydrolysis products from locust bean gum (LBG) by ManAK (reaction carried out at 37°C for 12 h). **(D)** HPLC analysis of the molecular weight distribution of hydrolysis products from LBG by ManAK^{L293V} (reaction carried out at 37°C for 12 h).

TABLE 3 | High-performance liquid chromatography analysis of the hydrolysis products of mannan polymers by ManAK and ManAK^{L293V}.

Substrate	Composition (%) of products formed by hydrolysis reaction					
	M1	M2	M3	M4	M5	M6
ManAK						
M4	6.3	20.9	42.9	23.6	4.9	1.2
M5	16.4	21.1	36.4	17.5	8.1	0.4
ManAK^{L293V}						
M4	7.2	22.4	43.5	20.1	6.2	0.6
M5	15.4	25.6	38.2	13.1	6.9	0.8

treatment in a buffer solution at pH 2.0, possibly because H294 is a basic amino acid (**Figure 3B**).

Analysis of Hydrolysis Products

In order to verify whether the hydrolytic performance of the recombinant mannanase was affected, the hydrolysis products from the mutant ManAK^{L293V} and ManAK were compared. The results showed that there was no significant difference between the hydrolysis products (**Figures 4A,C,D**), indicating that the site-mutation of L293V had no negative influence on hydrolysis.

The enzymes were unable to cleave M2 and showed very limited cleavage of M3, which indicated that ManAK was an endo-mannanase (**Figure 4A**). The enzymes were able to efficiently hydrolyze M4 and M5, proving that the enzyme was useful for the preparation of prebiotic oligosaccharides. In addition, M5 sugars were detected during the hydrolysis of M4 (**Figure 4A**), showing that ManAK and ManAK^{L293V} shared similar transglycosylation activity. Therefore, the modification strategy used in this work did not affect the hydrolysis mode.

According to the results of the TLC analysis, M4 and M5 were selected as substrates to further analyze the hydrolysis products by the HPLC. The results were consistent with the results of TLC analysis. As show in **Table 3**, both ManAK and ManAK^{L293V} can effectively degrade M4 and M5 to generate small molecule oligosaccharides, and M5 can be detected during the degradation of M4, and M6 can be detected during the degradation of M5. Furthermore, when degrading M4 and M5, the main products generated by ManAK were M3, with a composition of 42.9 and 36.4%, respectively.

To better understand the improvement in catalytic efficiency of the three recombinant mannanases, the reducing sugars released were measured under the same conditions. The results demonstrated that the yields of reducing sugars of the different mutants were all higher than that of ManAK, which corresponded with the results of the kinetic analysis (**Figure 4B**).

Locust bean gum was used as a substrate to illustrate the application potential of ManAK and the mutant ManAK^{L293V}. The results showed that they can effectively degrade LBG (**Figures 4C,D**), and the products hydrolyzed were oligosaccharides with a molecular weight below 3,000 Da, which indicated that ManAK had application potential in the preparation of MOS.

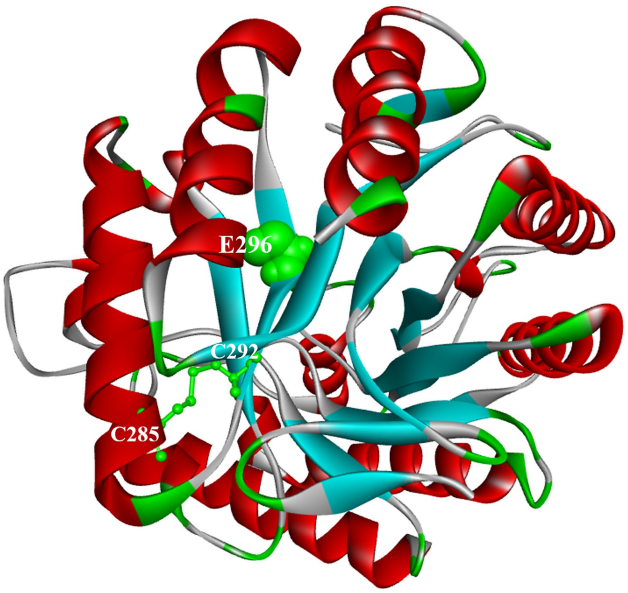

FIGURE 5 | Docking analysis and overall structure of ManAK. The catalytic region around E296 is illustrated in ball forms and colored in green. The disulfide bond formed between C292 and C285 is shown as stick models and colored in green.

Analysis of Structures and Interaction Forces in Mutated Sites of ManAK and Mutants

The three-dimensional structures of ManAK and recombinant mutants were modeled. The results showed that the structures and interaction forces of the three mutants at the mutated sites were changed compared with those of ManAK (**Figures 5–7**). The modeled three-dimensional structure of ManAK indicated that a disulfide bond was formed between C292 and C285 (**Figure 5**). The ManAK^{C292V} mutation destroyed the disulfide bond seen in the original enzyme. As shown in **Figure 6**, ManAK and ManAK^{L293V} both had a parallel folded β-sheet, while ManAK^{L293V} had a newly force (Alkyl) compared with the original interaction forces (van der Waals, Pi-Alkyl, Conventional Hydrogen Bond, and Covalent bond) seen in ManAK. The modeled structures of ManAK^{L294H} and ManAK in position 294 showed that they all involved in the secondary structure of α-helix and β-sheet (**Figures 7A,B**).

However, the results of analysis of interaction forces at the 294 position demonstrated that the mutant ManAK^{L294H} had a newly introduced Pi-Pi stacked interaction and one less conventional hydrogen bond than ManAK (**Figures 7C,D**).

DISCUSSION

Since β-mannanase has excellent potential in the production of industrial feedstuff, its catalytic efficiency has garnered attention. In this study, CSD strategy, a method previously used to improve the catalytic efficiency of β-glucosidases (Ratananikom et al., 2013), was applied to ManAK. The K_m values of the three mutants were reduced compared with ManAK, which demonstrated that mutations (C292V, L293V, and L294H) could improve the substrate affinity of ManAK. The K_m values of the mutants were also lower than those of most reported mannanases, such as those from *Bacillus* sp. HJ14 (2.20 mg/ml; Zhang et al., 2016), *Phialophora* sp. P13 (2.50 mg/ml; Zhao et al., 2010), *Bacillus* sp. JAMB-602 (3.10 mg/ml; Takeda et al., 2004), *Bacillus halodurans* PPKS-2 (3.85 mg/ml; Vijayalaxmi et al., 2013), *Phialophora pinophilum* C1 (5.60 mg/ml; Cai et al., 2011), *Bacillus subtilis* BE-91 (7.14 mg/ml; Cheng et al., 2016), *Bacillus nealsonii* PN-11 (7.22 mg/ml; Chauhan et al., 2014b), *B. subtilis* WY34 (7.60 mg/ml; Jiang et al., 2006), *B. subtilis* MAFIC-S11 (8.00 mg/ml; Lv et al., 2013), *Bacillus* sp. MSJ-5 (11.67 mg/ml; Zhang et al., 2009), and *B. subtilis* YH12 (30.00 mg/ml; Liu et al., 2015).

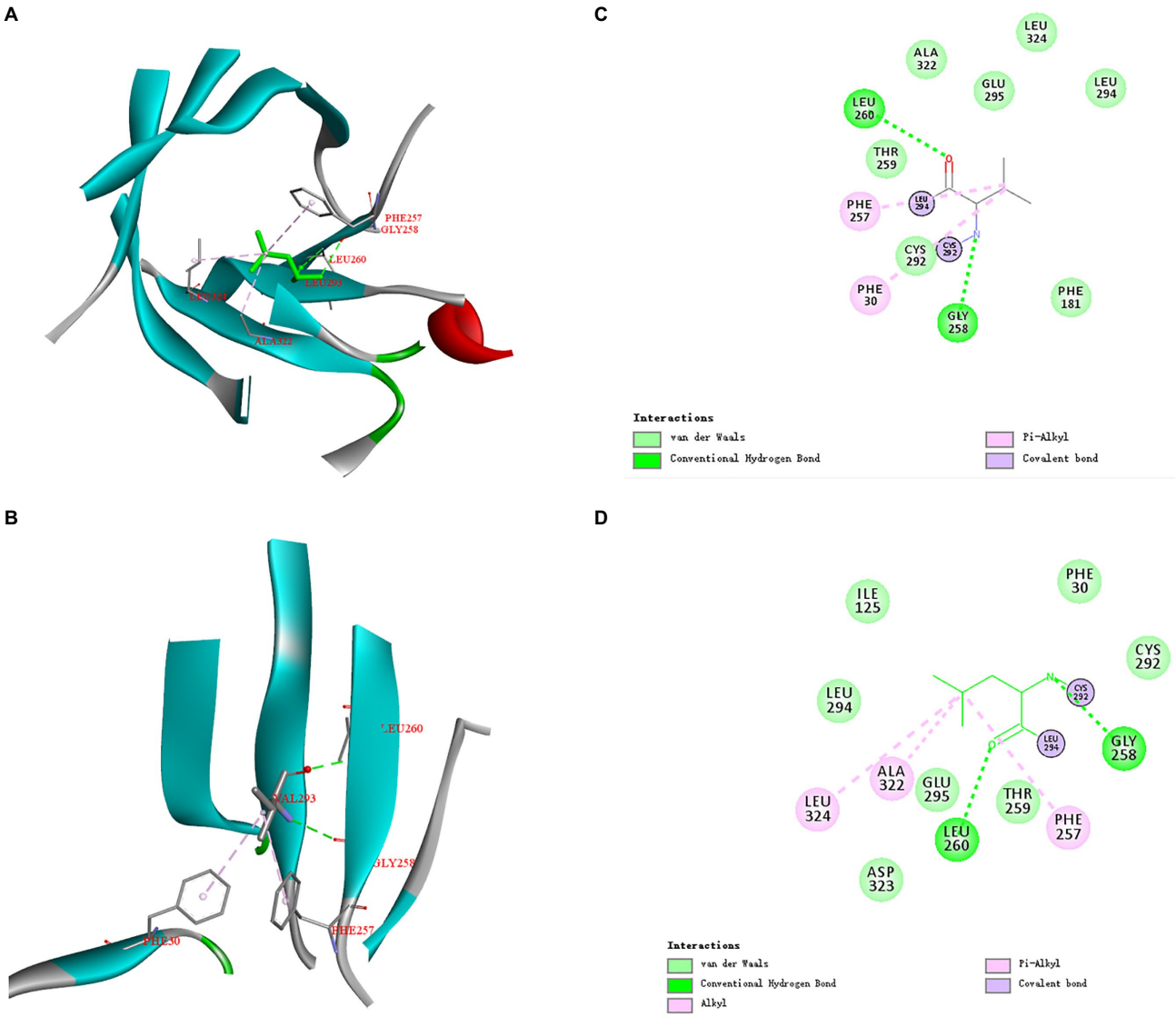

FIGURE 6 | Overall structure and modeled complex structures of ManAK **(A)** and ManAK^{L293V} **(B)** in position 293. The amino acid residues around position 293 are indicated in red. The interactions between them are represented by a dashed line. Interaction analysis of amino acid site ManAK **(C)** and ManAK^{L293V} **(D)**. The green dashed line indicates Conventional Hydrogen Bond interaction; the pink dashed line indicates Alkyl and Pi-Alkyl interaction. Amino acid residues that form van der Waals interactions with amino acid in position 293 are indicated in light green balls and Covalent bond are indicated in purple.

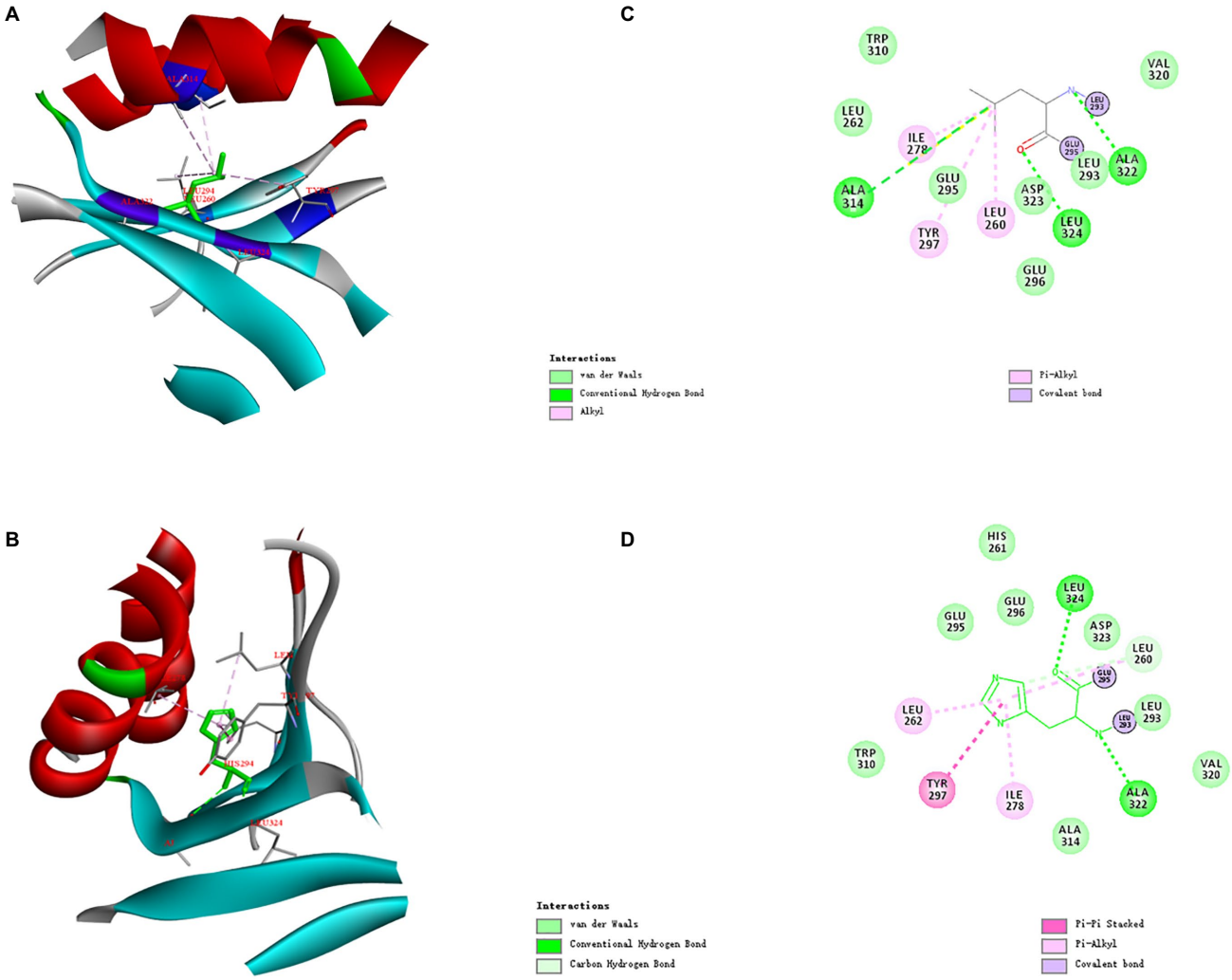

FIGURE 7 | Overall structure and modeled complex structures of ManAK **(A)** and ManAK^{L294H} **(B)** in position 294. The amino acid residues around position 294 are indicated in red. The interactions between them are represented by a dashed line. Interaction analysis of amino acid site ManAK **(C)** and ManAK^{L294H} **(D)**. The green dashed line indicates Conventional Hydrogen Bond interaction; the pink dashed line indicates Alkyl and Pi-Alkyl interaction; the deep pink dashed line indicates Pi-Pi stacked interaction. Amino acid residues that form van der Waals interactions with amino acid in position 294 are indicated in light green balls and Covalent bond are indicated in purple.

The k_{cat}/K_m of the three mutants was significantly improved compared to ManAK. This was superior to the previously reported catalytic efficiency of mannanases, such as those from *Penicillium canescens* (Sinitsyna et al., 2008) and *Rhizomucor miehei* (Katrolia et al., 2012). The substrate affinity of the three mutants was greatly enhanced due to the significant decrease in K_m values, which might increase the k_{cat}/K_m values. However, the improvement in catalytic efficiency may be limited. With the constant increase in substrate concentration, the advantage of high catalytic efficiency may be reduced. In fact, within a certain range of substrate concentrations, these three recombinant mannanases can show superior catalytic efficiency. Moreover, interestingly, even though these three mutants all displayed elevated catalytic efficiencies, changes in their thermostability were either improved (ManAK^{L293V}), remained the same (ManAK^{C292V}), or decreased (ManAK^{L294H}).

Nowadays, molecular simulation is widely used to infer the changes of non-covalent forces in the mutation site region before and after the alteration, which is helpful to explain the reasons for the changes in the thermostability and the catalytic efficiency of mutants. Molecular simulation can be used for most enzymes, including mannanases (Chauhan et al., 2015; Chauhan and Jaiswar, 2017; Liu et al., 2020a), xylanase (Cheng et al., 2015), and β-glucosidases (Dadheech et al., 2019). Therefore, in this study, the structure-function relationships of the three mutants were analyzed by docking analysis and a molecular simulation method.

ManAK^{C292V} showed elevated catalytic efficiency, which was increased by 303.0% compared with the starting enzyme ManAK, and a reduced K_m value. The modeled three-dimensional structure of ManAK indicated that a disulfide bond was formed between C292 and C285 (**Figure 5**). After the mutation, amino acid V292 destroyed the original disulfide bond, which in turn affected

the original spatial structure. ManAK^{C292V} eliminated the disulfide bond to provide more flexibility at the active site, and the flexibility of the β-sheet in the catalytic region E296 was also increased, possibly increasing the affinity between enzyme and substrate. However, the thermal stability of ManAK^{C292V} was reduced (**Figures 2A,C**), possibly because the disulfide bond contributes to the maintenance of the stability of the enzyme.

The mutant ManAK^{L293V} showed increased catalytic activity, suggesting the importance of residue V293. The alkyl side chain of V293 was smaller than that of L293, which meant that the steric hindrance of this amino site was smaller, indicating that it provided a larger space for substrate entry and product release. Interestingly, mutant ManAK^{L293V} also showed improved thermal stability. No significant difference was detected in the spatial structure at this position between ManAK and ManAK^{L293V}, with both having a parallel folded β-sheet (**Figures 6A,B**). However, a newly formed interaction force between alkyl groups (**Figures 6C,D**) might have a positive influence on the thermal stability of enzyme, which meant that V293 was thought to be the critical site for the improvement of stability.

Similar results for ManAK^{L294H} were observed in both the kinetic study and catalytic ability; it displayed a lower K_m value and higher catalytic efficiency, which meant the substrate-binding affinity was greatly increased. Residue Y297 of ManAK is located adjacent to the key catalytic amino site E296, and although, it might not directly interact with the substrate it generated a π-π stacking interaction with the new corresponding residue of H294 (**Figure 7D**). The substitution of H294 has a heteroaryl structure, which tends to form the π-π stacking interaction with the substrates, thus promoting the substrate-binding affinity and catalytic efficiency. Similar cases have been reported in previous studies in which a new stacking force is formed by the aryl of the mutant amino acid, and is conducive to substrate entry (Huang et al., 2014; Cheng et al., 2015). In contrast to the positive results, ManAK^{L294H} showed a drastically reduced optimum temperature and thermal stability (**Figures 2A–D**). From the complex structure model in 294 position, ManAK had a conventional hydrogen bond between L294 and A314 (**Figure 7C**), and involved in α-helix and β-sheet (**Figure 7A**). In ManAK^{L294H}, the conventional hydrogen bond was destroyed and the secondary structure of α-helix was excluded (**Figure 7B**), indicating that the conventional hydrogen bond between L294 and A314 is indispensable for the stability of ManAK. The destruction and disappearance of this original force may have a negative impact on the stability of the protein itself.

CONCLUSION

A thermostable and acidophilic β-mannanase, ManAK, derived from marine *Aspergillus kawachii* IFO 4308 would be especially suitable for MOS preparation, except for its low catalytic efficiency. To compensate for this defect, a CSD method was adopted to engineer the catalytic efficiency of ManAK. Three positive mutants (ManAK^{C292V}, ManAK^{L293V}, and ManAK^{L294H}) showing increased k_{cat}/K_m values were generated. Minor changes were detected in their optimal pH values and acid tolerance, while their thermostabilities varied. The mechanisms underlying the stability and catalytic efficiency were investigated, which provided an intuitive understanding of structure-function relationships. Most importantly, a superior mutant (ManAK^{L293V}) with both enhanced catalytic efficiency and thermostability was acquired, which can further advance the application of ManAK in MOS preparation.

DATA AVAILABILITY STATEMENT

The original contributions presented in the study are included in the article/Supplementary Material, further inquiries can be directed to the corresponding authors.

AUTHOR CONTRIBUTIONS

QL contributed to the experiment planning and conduct, writing – original draft preparation, and methodology. YZ and MY also contributed to experiment conduct and revision of the writing – original draft. LC contributed to data collation and analysis, graphics drawing, and statistical analysis. CZ contributed to write and revise the manuscript. ZL contributed to software application, conceptualization, and data curation. HM contributed to writing-review, supervision, funding acquisition, and project administration. All authors contributed to the article and approved the submitted version.

FUNDING

This work was supported by National Key Research and Development (R&D) Program of China 2019YFD0901805 and National Nature Science Fund of China 31872893.

REFERENCES

Bradford, M. M. (1976). A rapid and sensitive method for the quantitation of microgram quantities of protein utilizing the principle of protein-dye binding. *Anal. Biochem.* 72, 248–254. doi: 10.1016/0003-2697(76)90527-3

Cai, H., Shi, P., Luo, H., Bai, Y., Huang, H., Yang, P., et al. (2011). Acidic β-mannanase from *Penicillium pinophilum* C1: cloning, characterization and assessment of its potential for animal feed application. *J. Biosci. Bioeng.* 112, 551–557. doi: 10.1016/j.jbiosc.2011.08.018

Chauhan, P. S., and Jaiswar, S. (2017). Molecular dynamic simulation studies of bacterial thermostable mannanase unwinding the enzymatic catalysis. *Biocatal. Agric. Biotechnol.* 9, 41–47. doi: 10.1016/j.bcab.2016.11.003

Chauhan, P. S., Puri, N., Sharma, P., and Gupta, N. (2012). Mannanases: microbial sources, production, properties and potential biotechnological applications. *Appl. Microbiol. Biotechnol.* 93, 1817–1830. doi: 10.1007/s00253-012-3887-5

Chauhan, P. S., Sharma, P., Puri, N., and Gupta, N. (2014a). Purification and characterization of an alkali-thermostable β-mannanase from *Bacillus nealsonii* PN-11 and its application in mannooligosaccharides preparation having prebiotic potential. *Eur. Food Res. Technol.* 238, 927–936. doi: 10.1007/s00217-014-2170-7

Chauhan, P. S., Sharma, P., Puri, N., and Gupta, N. (2014b). A process for reduction in viscosity of coffee extract by enzymatic hydrolysis of mannan. *Bioprocess Biosyst. Eng.* 37, 1459–1467. doi: 10.1007/s00449-013-1118-9

Chauhan, P. S., Tripathi, S. P., Sangamwar, A. T., Puri, N., Sharma, P., and Gupta, N. (2015). Cloning, molecular modeling, and docking analysis of alkali-thermostable β-mannanase from *Bacillus nealsonii* PN-11. *Appl. Microbiol. Biotechnol.* 99, 8917–8925. doi: 10.1007/s00253-015-6613-2

Cheng, Y. S., Chen, C. C., Huang, J. W., Ko, T. P., Huang, Z., and Guo, R. T. (2015). Improving the catalytic performance of a GH11 xylanase by rational protein engineering. *Appl. Microbiol. Biotechnol.* 99, 9503–9510. doi: 10.1007/s00253-015-6712-0

Cheng, L., Duan, S., Feng, X., Zheng, K., Yang, Q., and Liu, Z. (2016). Purification and characterization of a thermostable β-mannanase from *Bacillus subtilis* BE-91: potential application in inflammatory diseases. *Biomed. Res. Int.* 2016, 1–7. doi: 10.1155/2016/6380147

Dadheech, T., Jakhesara, S., Chauhan, P. S., Pandit, R., Hinsu, A., Kunjadiya, A., et al. (2019). Draft genome analysis of lignocellulolytic enzymes producing *Aspergillus terreus* with structural insight of β-glucosidases through molecular docking approach. *Int. J. Biol. Macromol.* 125, 181–190. doi: 10.1016/j.ijbiomac.2018.12.020

Finn, R. D., Bateman, A., Clements, J., Coggill, P., Eberhardt, R. Y., Eddy, S. R., et al. (2014). Pfam: The protein families database. *Nucleic Acids Res.* 42, 1–9. doi: 10.1093/nar/gkt1223

Hilge, M., Gloor, S. M., Rypniewski, W., Sauer, O., Heightman, T. D., Zimmermann, W., et al. (1998). High-resolution native and complex structures of thermostable β-mannanase from *Thermomonospora fusca* - substrate specificity in glycosyl hydrolase family 5. *Structure* 6, 1433–1444. doi: 10.1016/S0969-2126(98)00142-7

Huang, J. W., Chen, C. C., Huang, C. H., Huang, T. Y., Wu, T. H., Cheng, Y. S., et al. (2014). Improving the specific activity of β-mannanase from *Aspergillus niger* BK01 by structure-based rational design. *Biochim. Biophys. Acta, Proteins Proteomics* 1844, 663–669. doi: 10.1016/j.bbapap.2014.01.011

Jana, U. K., Suryawanshi, R. K., Prajapati, B. P., and Kango, N. (2020). Prebiotic mannooligosaccharides: synthesis, characterization and bioactive properties. *Food Chem.* 342:128328. doi: 10.1016/j.foodchem.2020.128328

Jiang, Z., Wei, Y., Li, D., Li, L., Chai, P., and Kusakabe, I. (2006). High-level production, purification and characterization of a thermostable β-mannanase from the newly isolated *Bacillus subtilis* WY34. *Carbohydr. Polym.* 66, 88–96. doi: 10.1016/j.carbpol.2006.02.030

Kaira, G. S., Panwar, D., and Kapoor, M. (2016). Recombinant endo-mannanase (ManB-1601) production using agro-industrial residues: development of economical medium and application in oil extraction from copra. *Bioresour. Technol.* 209, 220–227. doi: 10.1016/j.biortech.2016.02.133

Katrolia, P., Yan, Q., Zhang, P., Zhou, P., Yang, S., and Jiang, Z. (2013). Gene cloning and enzymatic characterization of an alkali-tolerant endo-1,4-β-mannanase from *Rhizomucor miehei*. *J. Agric. Food Chem.* 61, 394–401. doi: 10.1021/jf303319h

Katrolia, P., Zhou, P., Zhang, P., Yan, Q., Li, Y., Jiang, Z., et al. (2012). High level expression of a novel β-mannanase from *Chaetomium* sp. exhibiting efficient mannan hydrolysis. *Carbohydr. Polym.* 87, 480–490. doi: 10.1016/j.carbpol.2011.08.008

Kelley, L. A., Mezulis, S., Yates, C. M., Wass, M. N., and Sternberg, M. J. (2016). The Phyre2 web portal for protein modeling, prediction and analysis. *Nat. Protoc.* 10, 845–858. doi: 10.1038/nprot.2015.053

Kim, D. Y., Ham, S. J., Lee, H. J., Cho, H. Y., Kim, J. H., Kim, Y. J., et al. (2011). Cloning and characterization of a modular GH5 β-1,4-mannanase with high specific activity from the fibrolytic bacterium *Cellulosimicrobium* sp. strain HY-13. *Bioresour. Technol.* 102, 9185–9192. doi: 10.1016/j.biortech.2011.06.073

La Rosa, S. L., Leth, M. L., Michalak, L., Hansen, M. E., Pudlo, N. A., Glowacki, R., et al. (2019). The human gut Firmicute *Roseburia intestinalis* is a primary degrader of dietary β-mannans. *Nat. Commun.* 10, 1–14. doi: 10.1038/s41467-019-08812-y

Larsson, A. M., Anderson, L., Xu, B., Muñoz, I. G., Usón, I., Janson, J. C., et al. (2006). Three-dimensional crystal structure and enzymic characterization of β-mannanase Man5A from blue mussel *Mytilus edulis*. *J. Mol. Biol.* 357, 1500–1510. doi: 10.1016/j.jmb.2006.01.044

Liu, S., Cui, T., and Song, Y. (2020a). Expression, homology modeling and enzymatic characterization of a new β-mannanase belonging to glycoside hydrolase family 1 from *Enterobacter aerogenes* B19. *Microb. Cell Factories* 19, 1–19. doi: 10.1186/s12934-020-01399-w

Liu, H. X., Gong, J. S., Li, H., Lu, Z. M., Li, H., Qian, J. Y., et al. (2015). Biochemical characterization and cloning of an endo-1,4-β-mannanase from *Bacillus subtilis* YH12 with unusually broad substrate profile. *Process Biochem.* 50, 712–721. doi: 10.1016/j.procbio.2015.02.011

Liu, Z., Ning, C., Yuan, M., Yang, S., Wei, X., Xiao, M., et al. (2020b). High-level expression of a thermophilic and acidophilic β-mannanase from *Aspergillus kawachii* IFO 4308 with significant potential in mannooligosaccharide preparation. *Bioresour. Technol.* 295:122257. doi: 10.1016/j.biortech.2019.122257

Lv, J., Chen, Y., Pei, H., Yang, W., Li, Z., Dong, B., et al. (2013). Cloning, expression, and characterization of β-mannanase from *Bacillus subtilis* MAFIC-S11 in *Pichia pastoris*. *Appl. Biochem. Biotechnol.* 169, 2326–2340. doi: 10.1007/s12010-013-0156-8

Miller, G. L. (1959). Use of dinitrosalicylic acid reagent for determination of reducing sugar. *Anal. Chem.* 31, 426–428. doi: 10.1021/ac60147a030

Ratananikom, K., Choengpanya, K., Tongtubtim, N., Charoenrat, T., Withers, S. G., and Kongsaeree, P. T. (2013). Mutational analysis in the glycone binding pocket of *Dalbergia cochinchinensis* β-glucosidase to increase catalytic efficiency toward mannosides. *Carbohydr. Res.* 373, 35–41. doi: 10.1016/j.carres.2012.10.018

Sinitsyna, O. A., Fedorova, E. A., Vakar, I. M., Kondratieva, E. G., Rozhkova, A. M., Sokolova, L. M., et al. (2008). Isolation and characterization of extracellular α-galactosidases from *Penicillium canescens*. *Biochemist* 73, 97–106. doi: 10.1007/s10541-008-1015-z

Srivastava, P. K., and Kapoor, M. (2017). Production, properties, and applications of endo-β-mannanases. *Biotechnol. Adv.* 35, 1–19. doi: 10.1016/j.biotechadv.2016.11.001

Sternke, M., Tripp, K. W., and Barrick, D. (2019). Consensus sequence design as a general strategy to create hyperstable, biologically active proteins. *Proc. Natl. Acad. Sci. U. S. A.* 166, 11275–11284. doi: 10.1073/pnas.1816707116

Takeda, N., Hirasawa, K., Uchimura, K., Nogi, Y., Hatada, Y., Akita, M., et al. (2004). Alkaline mannanase from a novel species of *Alkaliphilic bacillus*. *J. Appl. Glycosci.* 51, 229–236. doi: 10.5458/jag.51.229

van Zyl, W. H., Rose, S. H., Trollope, K., and Görgens, J. F. (2010). Fungal β-mannanases: Mannan hydrolysis, heterologous production and biotechnological applications. *Process Biochem.* 45, 1203–1213. doi: 10.1016/j.procbio.2010.05.011

Vijayalaxmi, S., Prakash, P., Jayalakshmi, S. K., Mulimani, V. H., and Sreeramulu, K. (2013). Production of extremely alkaliphilic, halotolerent, detergent, and thermostable mannanase by the free and immobilized cells of *Bacillus halodurans* PPKS-2. Purification and characterization. *Appl. Biochem. Biotechnol.* 171, 382–395. doi: 10.1007/s12010-013-0333-9

Zhang, M., Chen, X. L., Zhang, Z. H., Sun, C. Y., Chen, L. L., He, H. L., et al. (2009). Purification and functional characterization of endo-β-mannanase MAN5 and its application in oligosaccharide production from konjac flour. *Appl. Microbiol. Biotechnol.* 83, 865–873. doi: 10.1007/s00253-009-1920-0

Zhang, Y., Ju, J., Peng, H., Gao, F., Zhou, C., Zeng, Y., et al. (2008). Biochemical and structural characterization of the intracellular mannanase AaManA of *Alicyclobacillus acidocaldarius* reveals a novel glycoside hydrolase family belonging to clan GH-A. *J. Biol. Chem.* 283, 31551–31558. doi: 10.1074/jbc.M803409200

Zhang, W., Liu, Z., Zhou, S., Mou, H., and Zhang, R. (2019). Cloning and expression of a β-mannanase gene from *Bacillus* sp. MK-2 and its directed evolution by random mutagenesis. *Enzym. Microb. Technol.* 124, 70–78. doi: 10.1016/j.enzmictec.2019.02.003

Zhang, R., Song, Z., Wu, Q., Zhou, J., Li, J., Mu, Y., et al. (2016). A novel surfactant-, NaCl-, and protease-tolerant β-mannanase from *Bacillus* sp. HJ14. *Folia Microbiol.* 61, 233–242. doi: 10.1007/s12223-015-0430-y

Zhao, J., Shi, P., Luo, H., Yang, P., Zhao, H., Bai, Y., et al. (2010). An acidophilic and acid-stable β-mannanase from *Phialophora* sp. P13 with high mannan hydrolysis activity under simulated gastric conditions. *J. Agric. Food Chem.* 58, 3184–3190. doi: 10.1021/jf904367r

Zheng, C., Li, F., Hao, Z., and Liu, T. (2018). Effects of adding mannan oligosaccharides on digestibility and metabolism of nutrients, ruminal fermentation parameters, immunity, and antioxidant capacity of sheep. *J. Anim. Sci.* 96, 284–292. doi: 10.1093/jas/skx040

Conflict of Interest: The authors declare that the research was conducted in the absence of any commercial or financial relationships that could be construed as a potential conflict of interest.

Publisher's Note: All claims expressed in this article are solely those of the authors and do not necessarily represent those of their affiliated organizations, or those of the publisher, the editors and the reviewers. Any product that may

be evaluated in this article, or claim that may be made by its manufacturer, is not guaranteed or endorsed by the publisher.

frontiers in Microbiology

ORIGINAL RESEARCH
published: 14 September 2021
doi: 10.3389/fmicb.2021.677126

Extraction of Chitin From Shrimp Shell by Successive Two-Step Fermentation of *Exiguobacterium profundum* and *Lactobacillus acidophilus*

Jingwen Xie[1], Wancui Xie[1,2], Jing Yu[1], Rongyu Xin[1], Zhenping Shi[1,2], Lin Song[1,2] and Xihong Yang[1,2,3]**

[1] College of Marine Science and Biological Engineering, Qingdao University of Science and Technology, Qingdao, China, [2] Shandong Provincial Key Laboratory of Biochemical Engineering, Qingdao, China, [3] Qingdao Keda Future Biotechnology Co., Ltd, Qingdao, China

As an environmentally friendly and efficient method, successive two-step fermentation has been applied for extracting chitin from shrimp shells. To screen out the microorganisms for fermentation, a protease-producing strain, *Exiguobacterium profundum*, and a lactic acid-producing strain, *Lactobacillus acidophilus*, were isolated from the traditional fermented shrimp paste. Chitin was extracted by successive two-step fermentation with these two strains, and 85.9 ± 1.2% of protein and 95 ± 3% of minerals were removed. The recovery and yield of chitin were 47.82 and 16.32%, respectively. Fourier transform infrared spectroscopy, X-ray diffraction, and scanning electron microscopy (SEM) were used to characterize the chitin. The crystallinity index was 54.37%, and the degree of deacetylation was 3.67%, which was lower than that of chitin extracted by the chemical method. These results indicated that successive two-step fermentation using these two bacterial strains could be applied to extract chitin. This work provides a suitable strategy for developing an effective method to extract chitin by microbial fermentation.

Keywords: successive two-step fermentation, *Lactobacillus acidophilus*, *Exiguobacterium profundum*, chitin, demineralization, deproteinization, shrimp shell

OPEN ACCESS

Edited by:
Francesco Secundo, National Research Council (CNR), Italy

Reviewed by:
Carmen Wacher, National Autonomous University of Mexico, Mexico
Joo Shun Tan, Universiti Sains Malaysia (USM), Malaysia

****Correspondence:***
Lin Song
03231@qust.edu.cn
Xihong Yang
yangxihong63@163.com

Specialty section:
This article was submitted to Microbiotechnology, a section of the journal Frontiers in Microbiology

Received: *07 March 2021*
Accepted: *09 August 2021*
Published: *14 September 2021*

Citation:
Xie J, Xie W, Yu J, Xin R, Shi Z, Song L and Yang X (2021) Extraction of Chitin From Shrimp Shell by Successive Two-Step Fermentation of Exiguobacterium profundum and Lactobacillus acidophilus. Front. Microbiol. 12:677126. doi: 10.3389/fmicb.2021.677126

INTRODUCTION

Chitin, an insoluble linear homopolymer of β-(1→4)-linked-*N*-acetyl-D-glucosamine (**Figure 1**; Duan et al., 2012; Sharp, 2013), is the second-largest carbohydrate polymer in nature (Younes et al., 2014). It exhibits good biocompatibility (Sedaghat et al., 2017), antibacterial activity, and biodegradability (Mao et al., 2013), which enables its wide application in medicine, biotechnology, nutrition, and food processing (Oh et al., 2007). In recent decades, chitin from shrimp shells attracted extensive attention. Chemical treatment and enzymatic reactions have been extensively studied to prepare chitin (Xin et al., 2020). The process of extracting and preparing chitin from shrimp shells involves demineralization (DM), deproteinization (DP), deacetylation, and depolymerization (Fu et al., 2019). However, the use of harmful chemicals can affect the environment (Kim and Park, 2015). Due to the increasing use of commercial enzymes, high costs make it difficult to produce them on a large scale on an industrial scale (Bougatef, 2013). Therefore,

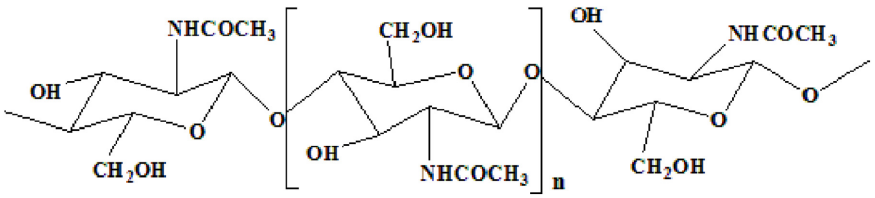

FIGURE 1 | Fully acetylated chitin polymer chain.

an effective and environmentally friendly technology can easily recover chitin without affecting the environment (Duan et al., 2012).

As an eco-friendly, technically flexible, and economically viable method, microbial fermentation has become a promising approach for extracting chitin. Protease from microorganisms has been successfully adopted for DP and DM during the process of chitin-rich marine crustacean shells. Previous studies reported about microorganisms, including *Lactobacillus plantarum* (Rao and Stevens, 2005), *Lactobacillus helveticus* (Arbia et al., 2013), *Pediococcus acidolactici* (Bhaskar et al., 2007), *Bacillus subtilis* (Sun and Mao, 2016), *Bacillus cereus* (Manni et al., 2010), *Bacillus licheniformis* (Hajji et al., 2015), *Pseudomonas aeruginosa* (Oh et al., 2007), and *Streptococcus thermophilus* (Mao et al., 2013). For example, *Lactobacillus* sp. B2 could remove 56% of protein and 88% of minerals from the crab wastes (Flores-Albino et al., 2012). *Bacillus* spp. could remove more than 80% of protein and less than 67% of mineral from the shrimp waste (Ghorbel-Bellaaj et al., 2012). *L. plantarum* 541 was used by Rao and Stevens (2005) to remove 66% of protein and 63% of minerals. However, pure chitin cannot be obtained by single-strain fermentation. Therefore, it is necessary to improve the removal efficiency of proteins and minerals in shrimp shell fermentation.

In order to improve the removal efficiency of proteins and minerals in chitin from shrimp shells, a successive two-step fermentation was employed in this study. A strain with high protease activity, *Exiguobacterium profundum*, and a stain capable of producing lactic acid, *L. acidophilus*, were isolated from a traditional fermented shrimp paste. The DP and DM efficiency were significantly improved, which indicates the applicable potential in chitin extraction.

MATERIALS AND METHODS

Materials

Shrimp shells were purchased from Kaiping Road farmer's market, Qingdao, China. The obtained shells were washed with running water for removing the shrimp residue and other impurities. Then the shells were washed with distilled water and dried. Finally, the dried samples were disintegrated with a grinder (Yongkang Platinum Metal Products Co., Ltd., China), and broken carefully into 2–3-mm sizes. *E. profundum* and *L. acidophilus* were screened out from fermented shrimp paste in previous experiments.

Isolation and Identification of Microorganisms

Sample treatment and bacterial isolation were conducted according to Sun and Mao (2016) with minor modifications as follows: after diluting and dispersing, the solution was spread onto marine agar containing 2% (w/v) skim milk and MRS agar containing 2% (w/v) $CaCO_3$ and incubated for 3 days. The colonies were identified as genera *Exiguobacterium* and *Lactobacillus* using traditional morphological methods. 16S rDNA sequence analysis was done to identify *E. profundum* and *L. acidophilus*. A phylogenetic tree was constructed using MEGA software (version 7.0) by the neighbor-joining method using the 16S rDNA sequences of selected and type strains (Sun and Mao, 2016).

Culture Conditions

The bacterial strains were isolated from traditional fermented shrimp paste and stored in a 25% glycerol preservation tube at −80°C. For *E. profundum* fermentation, the culture medium used by Anbu et al. (2013) contained shrimp shells as the sole nitrogen source. For *L. acidophilus* fermentation, the medium (per 1000 ml distilled water) contained 10 g peptone, 5 g CH_3COONa, 2 g ammonium citrate, 0.58 g $MgSO_4$, 0.25 g $MnSO_4$, 50 g glucose, 2.0 g K_2HPO_4, and 50 g/L shrimp shell (pH 6.2 ± 0.2). For successive two-step fermentation, the initial fermentation medium contained 10 g peptone, 5 g CH_3COONa, 2 g ammonium citrate, 0.58 g $MgSO_4$, 0.25 g $MnSO_4$, 50 g glucose, 2.0 g K_2HPO_4, and 50 g/L shrimp shell (pH 6.2 ± 0.2), and the medium for replacement contained shrimp shells fermented by the first step containing 2.5 g glucose, 5.0 g NaCl, 2.5 g/L K_2HPO_4 (pH 7.3 ± 0.2).

Fermentation

The experimental flowsheet was shown in **Figure 2**. For *L. acidophilus* fermentation, each 100-ml fermentation medium was seeded with *L. acidophilus* (10^8–10^9 CFU/ml) in a shaking incubator (140 rpm) at room temperature for 120 h with a fermented supernatant collected at 12-h intervals for growth curve statistics. The pH was determined using a pH meter (Leici, PHS-2F, Shanghai, China), and the total titratable acidity (TTA) of the supernatant was diluted with 0.1 mol/L NaOH (pH = 8.4) (Prameela et al., 2010). The glucose consumption was determined by the dinitrosalicylic acid (DNS) method. The biomass was determined by the plate counting method; in brief, biofilm solutions were serially diluted prior to plating, and three

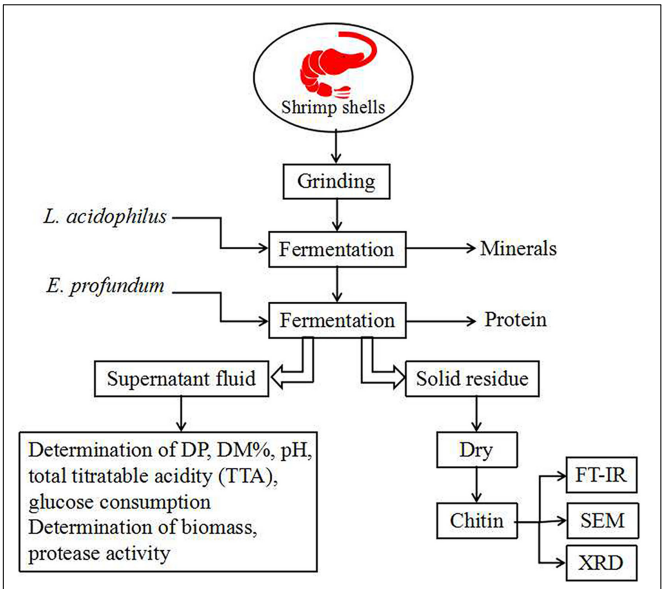

FIGURE 2 | Flowsheet of the process for this study. DP, deproteination; DM, demineralization.

different dilutions were plated out in order to obtain at least one plate containing 20–200 CFUs. The total number of original colonies was obtained according to the multiple of dilution.

For *E. profundum* fermentation, fermentation conditions were similar to *L. acidophilus* but the fermented supernatant was collected at 24-h intervals. The protease activity was measured according to the method described by Kembhavi (1993). The soluble peptide in the supernatant fraction was measured using tyrosine as a reference (Todd, 1949). One unit of protease activity is defined as the amount of enzyme required to liberate 1 μmol of tyrosine per minute (Zhang et al., 2012).

For successive two-step fermentation, fermentation was carried out using *L. acidophilus* in the same manner. After 96 h, the fermentation medium was replaced (see section "Culture Conditions"), and *E. profundum* was used for fermentation. The fermented sample was filtered and washed with deionized water and then dried at 60°C for 48 h.

Chemical Extraction of Chitin

Shrimp shells were treated with 1.5 mol/L HCl at a ratio of 1:10 (w/v) for 6 h at 25°C (No et al., 2003). After removing minerals, samples were washed in pure water until neutral. After the excess water was removed, they were put into the reflux device, and 20 ml of 10% NaOH was added to reflux (90°C) for 2–3 h. After the treatment, the samples were washed in pure water and then dried at 60°C for 48 h.

Measurement of Parameters

The ash content was determined at 550°C (Healy et al., 2003). The total nitrogen content of the shrimp shells was determined using the Kjeldahl method (Sjaifullah and Santoso, 2016). The corrected protein content was calculated by subtracting the chitin nitrogen from the total nitrogen content and multiplying it by 6.25.

DP% was calculated by Eq. 1, as follows (Nasri et al., 2011):

$$DP\% = \frac{[(P_O \times O) - (P_R \times R)]}{P_O \times O} \times 100 \quad (1)$$

Where P_O and P_R are the protein concentrations (%) before and after fermentation; while O and R represent the mass (g) of the original sample and fermented residues on a dry weight basis, respectively.

DM% was evaluated by Eq. 2, as follows:

$$DM\% = \frac{[(M_O \times O) - (M_R \times R)]}{M_O \times O} \times 100 \quad (2)$$

Where M_O and M_R are ash content (%) before and after fermentation; O and R represent the mass (g) of the original sample and fermented residue on a dry weight basis, respectively (Hamdi et al., 2017a,b).

After fermentation, the samples were treated with 1.5 mol/L HCl for 5 h at 25°C and 10% NaOH under reflux conditions (90°C) for 2 h to remove protein and mineral completely. The solid residues were dried at 60°C for 48 h. Residual protein and mineral content were determined by the method of section "Measurement of parameters." Chitin recovery and yield from the samples were determined by Eqs 3 (Doan et al., 2019) and 4 (Zhang et al., 2017), respectively, as follows:

$$\text{Chitin recovery\%} = \frac{\text{Dry weight of chitin in residue}}{\text{Dry weight of sample}} \times 100 \quad (3)$$

$$\text{Chitin yield\%} = \frac{\text{Chitin weight in fermented products} \times \text{weight of fermented products}}{\text{weight of shrimp shell}} \times 100 \quad (4)$$

Scanning Electron Microscopy Analysis

The electron microscopic images of shrimp shells were taken by JEOL JSM-6700F scanning electron microscopy (SEM), and *L. acidophilus* fermentation was compared to display the effects of successive two-step fermentation on chitin in shrimp shell (Liu et al., 2014).

Fourier Transform Infrared Analysis

The samples were measured using a Bruker VERTEX70 Fourier transform infrared spectrophotometer (FT-IR). Spectral scanning was performed in the wavelength region between 4000 and 400 cm^{-1} at a resolution of 4 cm^{-1} with a scan speed of 2 mm/s.

The absorption bands at 1655 and 3450 cm^{-1} were used to calculate the degree of deacetylation (DD%) according to Eq. 5 (Ben Seghir and Benhamza, 2017), as follows:

$$DD\% = 100 - [(A_{1655}/A_{3450}) \times 115] \quad (5)$$

where A_{1655} and A_{3450} are the absorbances of samples at wavenumbers of 1655 and 3450 cm^{-1}, respectively.

X-Ray Diffraction Analysis

X-ray diffractograms on powder samples were obtained using a Rigaku D/max 2500/PC full-automatic X-ray diffractometer (XRD) where working conditions were 40 kV and 40 mA with Cu $K_{\alpha 1}$ radiation at $\lambda = 1.54$ Å between 2θ angles of 5° and 70°. The scanning rate was 4.8° min^{-1} (Nasri et al., 2011).

The crystallinity index (I_{CR}) was calculated by Eq. 6, as follows:

$$I_{CR} = [(I_{110} - I_{am})/I_{110}] \times 100 \quad (6)$$

where I_{am} is the intensity of amorphous diffraction at 16°, and I_{110} is the maximum intensity at 20°.

Statistical Analysis

The results are expressed as mean ± SD. Correlation and regression analysis were performed using the Origin 9.0 program. Correlation analysis by the phylogenetic tree was carried out using the SeqMan program.

RESULTS AND DISCUSSION

Isolation and Identification of Bacterial Strains

Thirteen strains of lactic acid-producing bacteria were isolated from traditional fermented shrimp paste, and one of the strains with high lactic acid yield was identified as *L. acidophilus* by 16S rDNA sequence analysis (**Figure 3A**). Ten strains with high protease activity were isolated from the traditional fermented shrimp paste, and one of these was identified as *E. profundum* using 16S rDNA sequence analysis (**Figure 3B**). The strain was found to belong to *Exiguobacterium* sp. by constructing a neighbor-joining phylogenetic tree. *E. profundum*

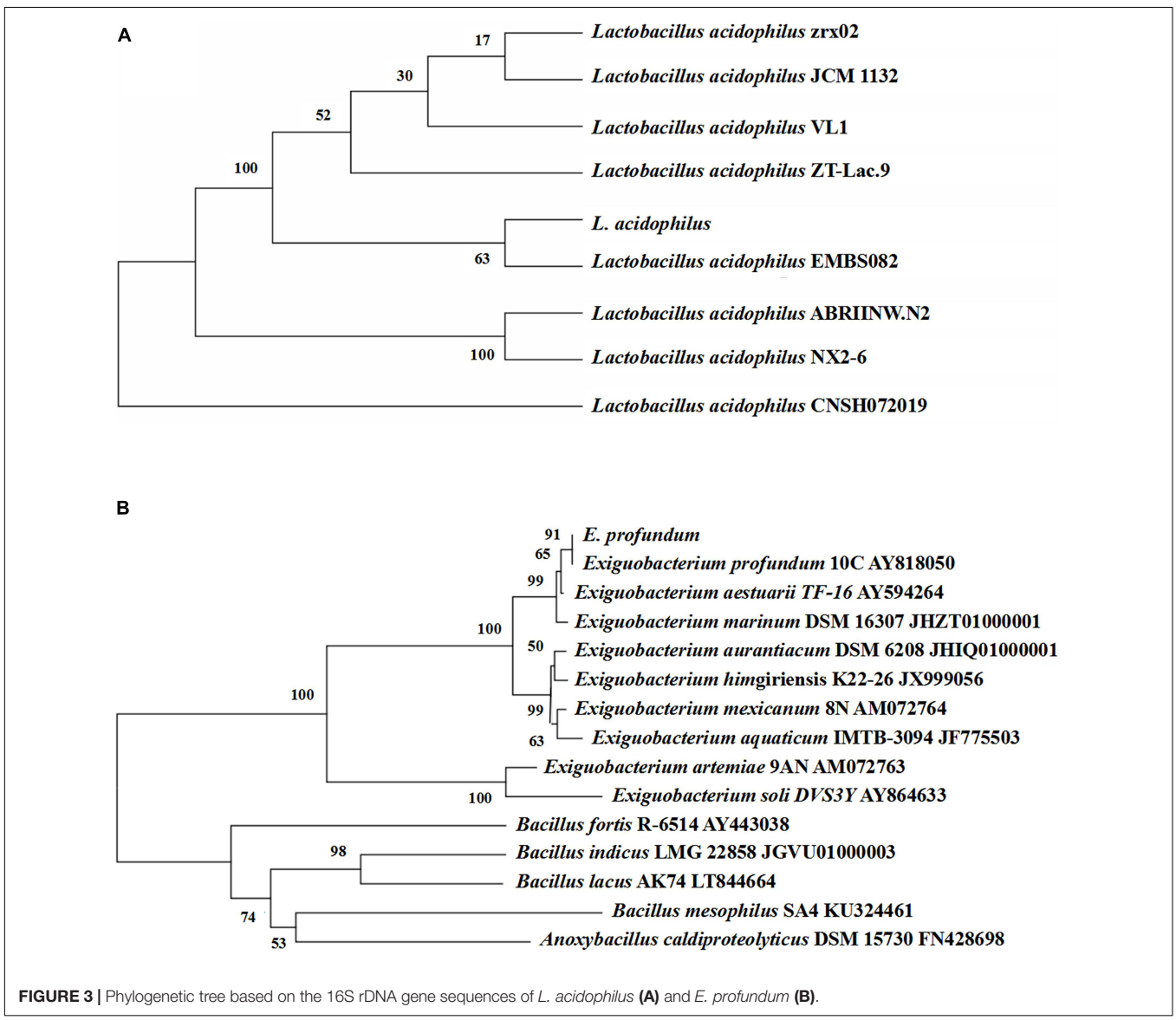

FIGURE 3 | Phylogenetic tree based on the 16S rDNA gene sequences of *L. acidophilus* **(A)** and *E. profundum* **(B)**.

can produce a high level of protease that hydrolyzes proteins in food. The present study showed that *E. profundum* could be cultivated in a medium containing shrimp shells as a sole nitrogen source.

Analysis of *L. acidophilus* Fermentation Process

At the early stage of fermentation, pH = 8 was observed (**Figure 4A**). The pH = 8 was attributed to two reasons (Duan et al., 2012). Many amino acids and peptides produced buffering capacity by the hydrolysis of protease from shrimp shells and *L. acidophilus*. Carbonate in shrimp shells consume some lactic acids. The pH was decreased drastically within 48 h, and the amounts of total TTA and glucose consumption were gradually increased (**Figures 4B,C**). TTA may be closely related to lactic acid (Castro et al., 2018). Therefore, it could be reasonably assumed that TTA was directly derived from the lactic acid. After 108 h of fermentation, the TTA reached its highest point, and the increase in TTA reduced the pH of fermented liquor from 8.0 to less than 4.6. After 60 h of fermentation, the number of *Lactobacillus acidophilus* increased rapidly (**Figure 4C**) due to the logarithmic growth phase. It indicated that *L. acidophilus* was well adapted to growth in shrimp shell medium. After 108 h, the number of *L. acidophilus* was stable, and TTA and glucose consumption reached the highest level at this time (**Figures 4B,D**), indicating that *L. acidophilus* was inhibited in the acidic environment and gradually entered the autolysis stage. When microorganisms grew using available carbohydrate sources, lactic acid was released. The abundant lactic acid, which was responsible for DM, could dissolve $CaCO_3$ to obtain water-soluble calcium lactate. Changes in glucose concentration were consistent with changes in *L. acidophilus* population, TTA, and lactic acid (Duan et al., 2012).

Analysis of *E. profundum* Fermentation Process

Maximum cell growth reached after 96 h of fermentation (2.29×10^9 CFU/mL) (**Figure 5A**). Maximum proteolytic activity

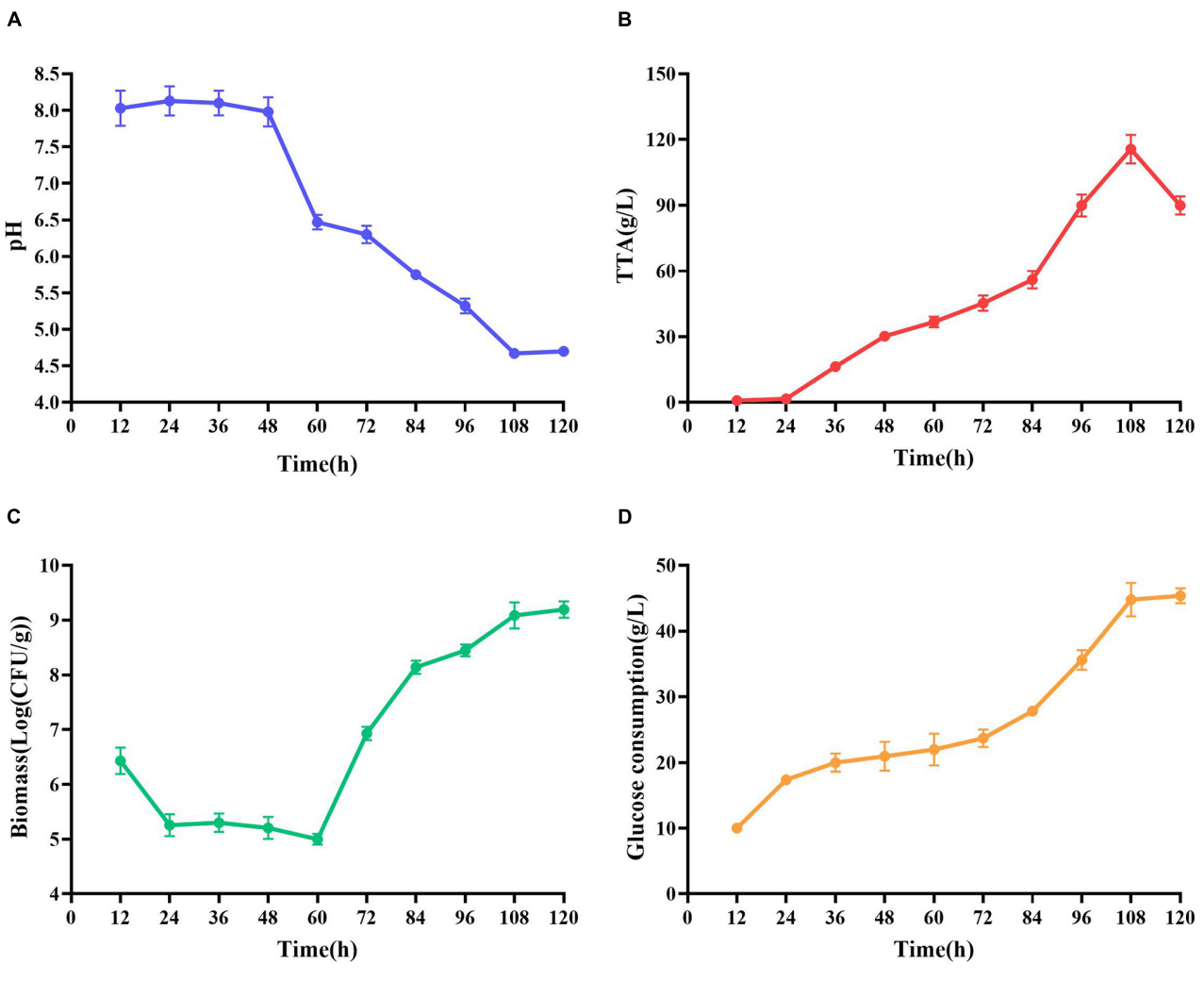

FIGURE 4 | Changes in related parameters during fermentation of *L. acidophilus*. **(A)** pH; **(B)** total titratable acidity (TTA); **(C)** biomass; and **(D)** glucose consumption.

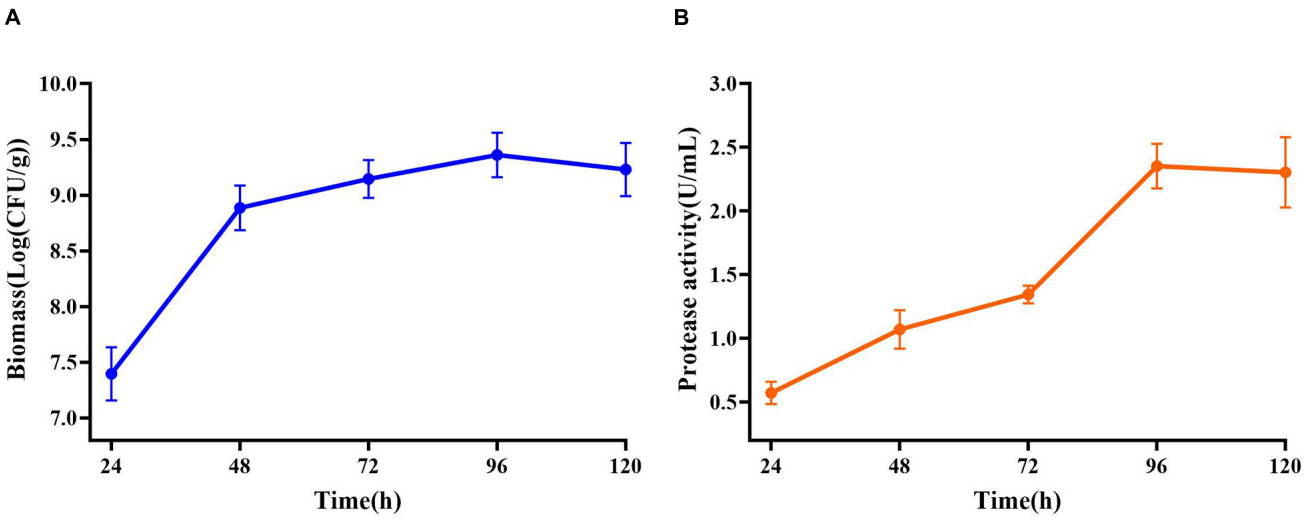

FIGURE 5 | Changes in related parameters during fermentation of *E. profundum*. **(A)** Biomass; **(B)** protease activity.

was 4.65 U/ml, after 96 h, and then the activity decreased to 4.30 U/ml (**Figure 5B**) at the end of the process indicating that protease produced by *E. profundum* could hydrolyze proteins in shrimp shells and obtain carbon and nitrogen sources from the hydrolyzate. Therefore, shrimp shells can replace nutrients, which significantly reduces the cost of culture (Sedaghat et al., 2017).

Successive Two-Step Fermentation With *L. acidophilus* and *E. profundum*

In raw shrimp shells, protein (26.0 ± 0.53%) and ash (47.4 ± 2.2%) content were preferably high (**Table 1**), which are consistent with the previous studies (Ghorbel-Bellaaj et al., 2011; Hamdi et al., 2017a,b). The existence of proteins and ash with main components of minerals make shrimp shell hard, which blocks the release of chitin from shrimp shells. Decomposition or removal of proteins and minerals becomes a key procedure in the process of chitin extraction. Our results showed that the removing rate of minerals by *L. acidophilus* fermentation was 88.7 ± 2.2%. The degree of DM was higher than that reported by Rao and Stevens (2005) and was close to that reported by Flores-Albino et al. (2012) The degree of DP (66.8 ± 2.8%) was not satisfactory. *E. profundum* removed 76.4 ± 0.92% of protein, but the DM capacity (57.9 ± 2.0%) was weak. Successive two-step fermentation could remove 85.9 ± 1.2% of protein and 95 ± 3% of minerals (**Figure 6**). Chitin recovery and yield from samples were 47.82 and 16.32%, respectively (**Table 2**). The ash and protein content were reduced to 2.52 ± 0.25 and 4.65 ± 0.58%, respectively (**Table 1**). Low protein and mineral content strongly indicated the good quality of extracted chitins (Castro et al., 2018).

Jung et al. (2006) extracted chitin from red crab (*Gecarcoidea natalis*) shell wastes by co-fermentation with *Lactobacillus paracasei* KCTC-3074 and *Serratia marcescens* FS-3. After 168 h of fermentation, the yields of DM and DP were 94.3 and 68.9%, respectively. Zhang et al. (2012) extracted chitin by successive two-step fermentation using *S. marcescens* B742 and *L. plantarum* ATCC 8014. After 6 days of fermentation,

TABLE 1 | Protein and ash content of the fermented residue.

Sample	Protein (%)	Ash (%)
Raw material	26.0 ± 0.53	47.4 ± 2.2
Residue of successive two-step fermentation	4.65 ± 0.58	2.52 ± 0.25

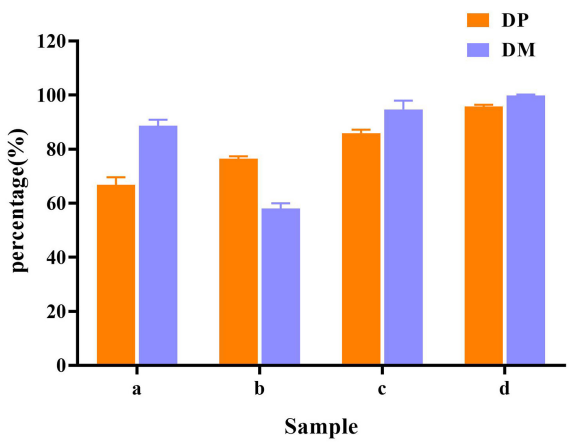

FIGURE 6 | Demineralization (DM) and deproteination (DP) efficiency in different fermentation methods. (a) *L. acidophilus* fermentation; (b) *E. profundum* fermentation; (c) successive two-step fermentation; and (d) chemical extraction method.

TABLE 2 | Chitin recovery and yield of the fermented residue.

Sample	Chitin recovery	Chitin yield
Residue of successive two-step fermentation	47.82%	16.32%

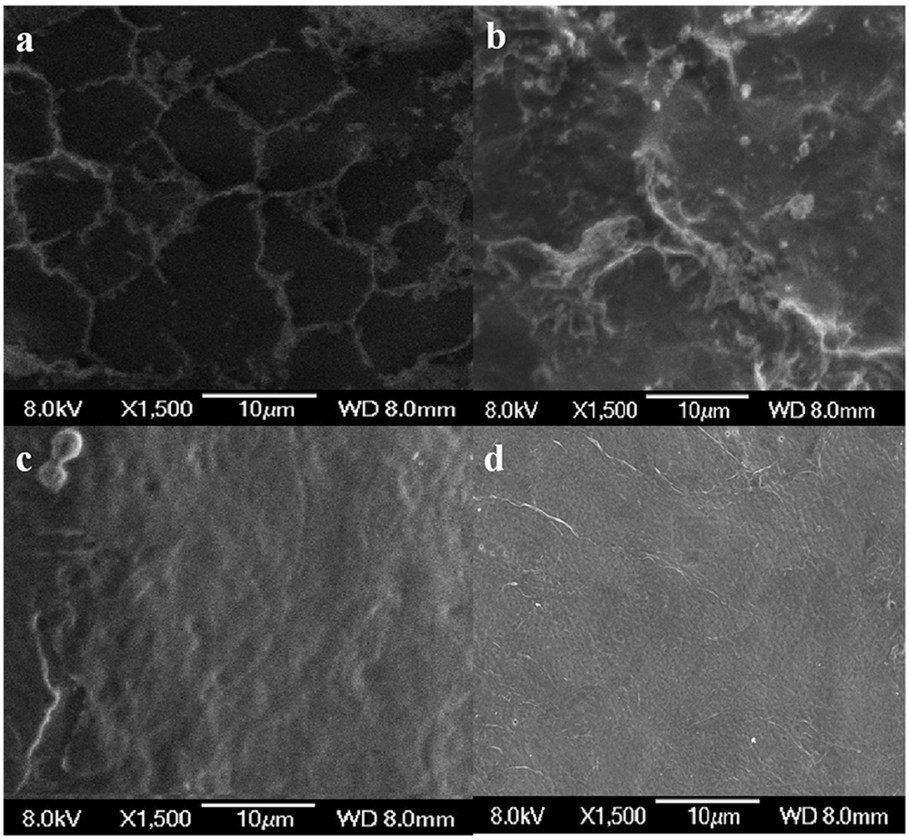

FIGURE 7 | Scanning electron microscopy (SEM) micrographs of chitin obtained from shrimp shells **(a)**, *L. acidophilus* **(b)**, successive two-step fermented sample **(c)**, and chemical extraction method **(d)**.

DP and DM reached 94.5 and 93.0%, respectively. Although the DP efficiency was slightly lower than the values reported in the same study, both *L. acidophilus* and *E. profundum* are safe organisms. *S. marcescens* acts as a conditional pathogen, but does not meet the requirements of the food industry. However, harmful acid caused depolymerization of the product. The inherent properties of chitin were changed, resulting in a decrease in its molecular weight and degree of acetylation. The intrinsic properties of purified chitin were also affected (Shamshina et al., 2016). The successive two-step fermentation helps to avoid many drawbacks of chemical treatment, which is a simple and environment-friendly alternative to chemical methods employed in the chitin extraction (Hajji et al., 2015).

SEM Analysis

The results of SEM showed that the surface of the shrimp shell was rough (**Figure 7a**). Many inorganic components were present and strongly embedded in chitin gaps and flexible protein macromolecules. *L. acidophilus* fermented sample (**Figure 7b**) surface was rough because of the presence of residual protein. The successive two-step fermented sample (**Figure 7c**) had a smooth surface, which has become uniform and porous with a lamellar organized structure (Flores-Albino et al., 2012). It was consistent with the description of Knidri et al. (2016), who found that the chitin structure showed several fine united leaves, with a highly porous, a lamellar organized and dense structure. It was similar to the chitin extracted by the chemical extraction (**Figure 7d**).

FT-IR Analysis

As shown in **Figure 8**, the bands at 1656 cm^{-1} and 1380 cm^{-1} were C=O and C–H deformation bands, which are related to the acetamide group of chitin (Sedaghat et al., 2017). The band at 1320 cm^{-1} was an aliphatic C–H flexural vibration. The bands between 1250 and 800 cm^{-1} were related to the pyranoside ring (Rao and Stevens, 2005; Hajji et al., 2015). The DDs of samples after chemical extraction, *L. acidophilus* fermentation and successive two-step fermentation were 43.36, 8.11, and 3.67%, respectively. The density of peak area is positively correlated with the degree of acetylation (Zhang et al., 2017). These results were consistent with the calculated DD results. The high degree of deacetylation of chitin reflects the severity of its degradation (Younes et al., 2016). The low deacetylation degree of successive two-step fermented samples indicated that the deacetylation process of the chemical

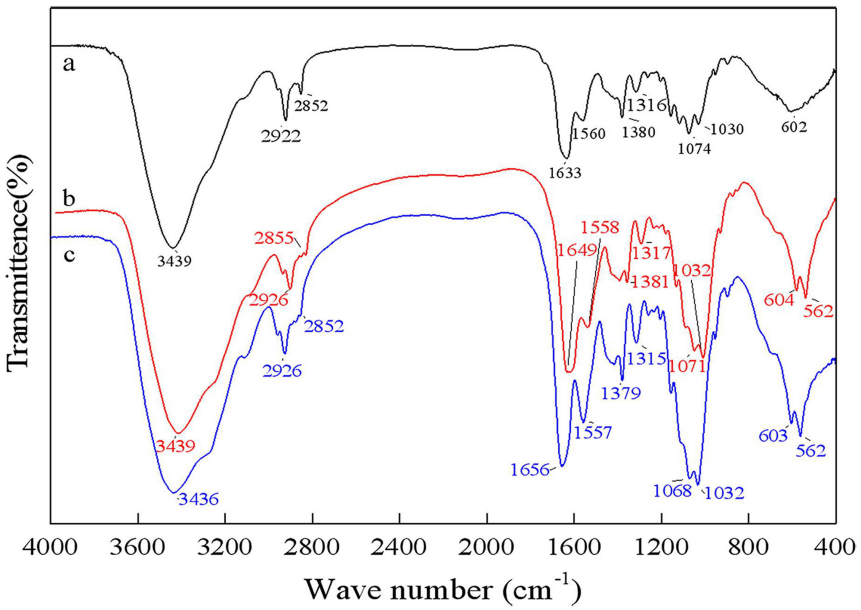

FIGURE 8 | Fourier transform infrared spectrophotometer (FT-IR) spectrum for chitin obtained by chemical extraction method (a), *L. acidophilus* fermentation (b), and successive two-step fermentation (c).

extraction of chitin was declined. Although pure chitin can be produced by chemical methods, the product obtained from this process can be a suitable product (Beaney et al., 2005). Biotechnological processes might be a viable option to overcome environmental and safety issues associated with chemical processes.

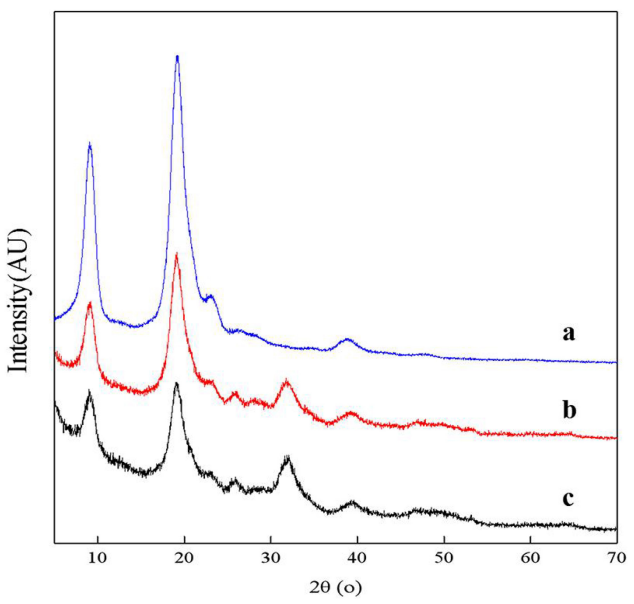

FIGURE 9 | X-ray diffractometer (XRD) spectrum for chitin obtained by chemical extraction method (a), successive two-step fermentation (b), and *L. acidophilus* fermentation (c).

XRD Analysis

The XRD spectra of samples showed two main diffraction peaks at 9.3° and 19.2° and 3 weaks diffraction peaks at 12.9°, 23.4°, and 26.4° which are the characteristic peaks of the crystal lattice type of α-chitin as shown in **Figure 9** (Jung et al., 2006). The diffraction peaks of $CaCO_3$ at approximately 2θ = 29.55° were not shown, indicating that chitin extracted by fermentation contained no minerals. The I_{CR} values of chitin extracted by successive two-step fermentation, chemical method, and *L. acidophilus* fermentation were 54.37, 75.12, and 38.85%, respectively. The relatively low I_{CR} could be attributed to the breaking of intramolecular and intermolecular hydrogen bonds and the formation of amorphous chitin (Zhao et al., 2019), providing more possibilities for the subsequent chemical modification of chitin. In addition, fermentation broths rich in protein hydrolyzates (amino acids and polypeptides) should also be considered for further recycling (Todd, 1949).

CONCLUSION

After successive two-step fermentation, 85.94 ± 1.22% of protein and 94.68 ± 3.25% of minerals were removed, with a chitin recovery of 47.82%. The low levels of residual minerals (2.52 ± 0.25%) and protein (4.65 ± 0.58%) indicated the superior quality of the extracted chitin. The chitin from successive two-step fermentation contained a low deacetylation degree, avoiding the chitin deacetylation process during the chemical extraction. Its low crystallinity value would provide the possibility for more efficient chemical modification in the subsequent processing steps. The method significantly reduced the use of required chemicals and produced a large amount of protein-rich

fermentation broth with high nutritional value, which has great potential to produce high-value proteins for consumption. This study provides a relatively simple and environmentally friendly alternative method for preparing chitin from shrimp shells.

DATA AVAILABILITY STATEMENT

The original contributions presented in the study are included in the article/supplementary material, further inquiries can be directed to the corresponding author/s.

AUTHOR CONTRIBUTIONS

RX: conceptualization. WX: data curation. JY: writing—original draft preparation. JX: writing—review and editing. ZS and LS: supervision. XY: project administration. All authors have read and agreed to the published version of the manuscript.

FUNDING

This work was financially supported by the National Key R&D Program of China (2019YFD0901703) and Chinese National Natural Science Foundation (No. 32072348).

REFERENCES

Anbu, P., Annadurai, G., and Hur, B. K. (2013). Production of alkaline protease from a newly isolated *Exiguobacterium profundum* BK-P23 evaluated using the response surface methodology. *Biologia* 68, 186–193. doi: 10.2478/s11756-013-0159-5

Arbia, W., Adour, L., Amrane, A., and Lounici, H. (2013). Optimization of medium composition for enhanced chitin extraction from *Parapenaeus longirostris* by *Lactobacillus helveticus* using response surface methodology. *Food Hydrocoll.* 31, 392–403. doi: 10.1016/j.foodhyd.2012.10.025

Beaney, P., Lizardi-Mendoza, J., and Healy, M. (2005). Comparison of chitins produced by chemical and bioprocessing methods. *J. Chem. Technol. Biotechnol.* 80, 145–150. doi: 10.1002/jctb.1164

Ben Seghir, B., and Benhamza, M. H. (2017). Preparation, optimization and characterization of chitosan polymer from shrimp shells. *J. Food Meas. Charact.* 11, 1137–1147. doi: 10.1007/s11694-017-9490-9

Bhaskar, N., Suresh, P. V., Sakhare, P. Z., and Sachindra, N. M. (2007). Shrimp biowaste fermentation with *Pediococcus acidolactici* cfr2182: optimization of fermentation conditions by response surface methodology and effect of optimized conditions on deproteination/demineralization and carotenoid recovery. *Enzyme Microb. Tech.* 40, 1427–1434. doi: 10.1016/j.enzmictec.2006.10.019

Bougatef, A. (2013). Trypsins from fish processing waste: characteristics and biotechnological applications-comprehensive review. *J. Clean. Prod.* 57, 257–265. doi: 10.1016/j.jclepro.2013.06.005

Castro, R., Guerrero-Legarreta, I., and Bórquez, R. (2018). Chitin extraction from *Allopetrolisthes punctatus* crab using lactic fermentation. *Biotechnol. Rep.* 20:e00287. doi: 10.1016/j.btre.2018.e00287

Doan, C. T., Tran, T. N., Nguyen, V. B., Vo, T. P., Nguyen, A. D., and Wang, S. (2019). Chitin extraction from shrimp waste by liquid fermentation using an alkaline protease-producing strain, *Brevibacillus parabrevis*. *Int. J. Biol. Macromol.* 131, 706–715. doi: 10.1016/j.ijbiomac.2019.03.117

Duan, S., Li, L., Zhuang, Z., Wu, W., Hong, S., and Zhou, J. (2012). Improved production of chitin from shrimp waste by fermentation with epiphytic lactic acid bacteria. *Carbohyd. Polym.* 89, 1283–1288. doi: 10.1016/j.carbpol.2012.04.051

Flores-Albino, B., Arias, L., Gomez, J., Castillo, A., Gimeno, M., and Shirai, K. (2012). Chitin and L(+)-lactic acid production from crab (*Callinectes bellicosus*) wastes by fermentation of *Lactobacillus* sp. B2 using sugar cane molasses as carbon source. *Bioproc. Biosyst. Eng.* 35, 1193–1200. doi: 10.1007/s00449-012-0706-4

Fu, X., Zhu, L., Li, L., Zhang, T., Li, M., and Mou, H. (2019). Eco-friendly preparation of chitooligosaccharides with different degrees of deacetylation from shrimp shell waste and their effects on the germination of wheat seeds. *Mar. Life Sci. Technol.* 1, 95–103. doi: 10.1007/s42995-019-00012-3

Ghorbel-Bellaaj, O., Hmidet, N., Jellouli, K., Younes, I., Maâlej, H., Hachicha, R., et al. (2011). Shrimp waste fermentation with *Pseudomonas aeruginosa* A2: optimization of chitin extraction conditions through Plackett-Burman and response surface methodology approaches. *Int. J. Biol. Macromol.* 48, 596–602. doi: 10.1016/j.ijbiomac.2011.01.024

Ghorbel-Bellaaj, O., Younes, I., Maâlej, H., Hajji, S., and Nasri, M. (2012). Chitin extraction from shrimp shell waste using *Bacillus* bacteria. *Int. J. Biol. Macromol.* 51, 1196–1201. doi: 10.1016/j.ijbiomac.2012.08.034

Hajji, S., Ghorbelbellaaj, O., Younes, I., Jellouli, K., and Nasri, M. (2015). Chitin extraction from crab shells by *Bacillus* bacteria. Biological activities of fermented crab supernatants. *Int. J. Biol. Macromol.* 79, 167–173. doi: 10.1016/j.ijbiomac.2015.04.027

Hamdi, M., Hajji, S., Affes, S., Taktak, W., Maâlej, H., Nasri, M., et al. (2017a). Development of a controlled bioconversion process for the recovery of chitosan from blue crab (*Portunus segnis*) exoskeleton. *Food Hydrocoll.* 77, 534–548. doi: 10.1016/j.foodhyd.2017.10.031

Hamdi, M., Hammami, A., Hajji, S., Jridi, M., Nasri, M., and Nasri, R. (2017b). Chitin extraction from blue crab (*Portunus segnis*) and shrimp (*Penaeus kerathurus*) shells using digestive alkaline proteases from *P. segnis* viscera. *Int. J. Biol. Macromol.* 101, 455–463. doi: 10.1016/j.ijbiomac.2017.02.103

Healy, M., Green, A., and Healy, A. (2003). Bioprocessing of marine crustacean shell waste. *Acta Biotechnol.* 23, 151–160. doi: 10.1002/abio.200390023

Jung, W. J., Jo, G. H., Kuk, J. H., Kim, K. Y., and Park, R. D. (2006). Extraction of chitin from red crab shell waste by cofermentation with *Lactobacillus paracaseisub* sp. *Tolerans* KCTC-3074 and *Serratia marcescens* FS-3. *Appl. Microbiol. Biotechnol.* 71, 234–237. doi: 10.1007/s00253-005-0126-3

Kembhavi, A. A. (1993). Salt-tolerant and thermostable alkaline protease from *Bacillus subtilis* NCIM no. 64. *Appl. Biochem. Biotechnol.* 38, 83–92. doi: 10.1007/bf02916414

Kim, Y., and Park, R. D. (2015). Progress in bioextraction processes of chitin from crustacean biowastes. *J. Korean Soc. Appl. Biol. Chem.* 58, 545–554. doi: 10.1007/s13765-015-0080-4

Knidri, H. E., Khalfaouy, R. E., Laajeb, A., Addaou, A., and Lahsini, A. (2016). Eco-friendly extraction and characterization of chitin and chitosan from the shrimp shell waste via microwave irradiation. *Process. Saf. Environ.* 104, 395–405. doi: 10.1016/j.psep.2016.09.020

Liu, P., Liu, S., Guo, N., Mao, X., Lin, H., Xue, C., et al. (2014). Cofermentation of *Bacillus licheniformis* and *Gluconobacter oxydans* for chitin extraction from shrimp waste. *Biochem. Eng. J.* 91, 10–15. doi: 10.1016/j.bej.2014.07.004

Manni, L., Ghorbelbellaaj, O., Jellouli, K., Younes, I., and Nasri, M. (2010). Extraction and characterization of chitin, chitosan, and protein hydrolysates prepared from shrimp waste by treatment with crude protease from bacillus cereussv1. *Appl. Biochem. Biotech.* 162, 345–357. doi: 10.1007/s12010-009-8846-y

Mao, X., Zhang, J., Kan, F., Gao, Y., Lan, J., Zhang, X., et al. (2013). Antioxidant production and chitin recovery from shrimp head fermentation with *Streptococcus thermophilus*. *Food Sci. Biotechnol.* 22, 1023–1032. doi: 10.1007/s10068-013-0179-5

Nasri, R., Younes, I., Lassoued, I., Ghorbel, S., Ghorbelbellaaj, O., and Nasri, M. (2011). Digestive alkaline proteases from *Zosterisessor ophiocephalus*, *Raja clavata*, and *Scorpaena scrofa*: characteristics and application in chitin extraction. *J. Amino Acids* 2011:913616. doi: 10.4061/2011/913616

No, H. K., Lee, S. H., Park, N. Y., and Meyers, S. P. (2003). Comparison of physicochemical, binding, and antibacterial properties of chitosans prepared without and with deproteinization process. *J. Agr. Food Chem.* 51, 7659–7663. doi: 10.1021/jf030226w

Oh, K., Kim, Y., Nguyen, V. N., Jung, W., and Park, R. (2007). Demineralization of crab shell waste by *Pseudomonas aeruginosa* F722. *Process Biochem.* 42, 1069–1074. doi: 10.1016/j.procbio.2007.04.007

Prameela, K., Mohan, C. M., Smitha, P. V., and Hemalatha, K. P. (2010). Bioremediation of shrimp biowaste by using natural probiotic for chitin and carotenoid production an alternative method to hazardous chemical method. *Int. J. Appl. Biol. Pharm. Technol.* 1, 903–910.

Rao, M. S., and Stevens, W. F. (2005). Chitin production by *Lactobacillus* fermentation of shrimp biowaste in a drum reactor and its chemical conversion to chitosan. *J. Chem. Technol. Biotechnol.* 80, 1080–1087. doi: 10.1002/jctb.1286

Sedaghat, F., Yousefzadi, M., Toiserkani, H., and Najafipour, S. (2017). Bioconversion of shrimp waste *Penaeus merguiensis* using lactic acid fermentation: An alternative procedure for chemical extraction of chitin and chitosan. *Int. J. Biol. Macromol.* 104, 883–888. doi: 10.1016/j.ijbiomac.2017.06.099

Shamshina, J. L., Barber, P. S., Gurau, G., Griggs, C. S., and Rogers, R. D. (2016). Pulping of crustacean waste using ionic liquids: to extract or not to extract. *ACS Sustain Chem. Eng.* 4, 6072–6081. doi: 10.1021/acssuschemeng.6b01434

Sharp, R. G. (2013). A review of the applications of chitin and its derivatives in agriculture to modify plant-microbial interactions and improve crop yields. *Agronomy* 3, 757–793. doi: 10.3390/agronomy3040757

Sjaifullah, A., and Santoso, A. B. (2016). Autolytic isolation of chitin from white shrimp (*Penaues vannamei*) waste. *Procedia Chem.* 18, 49–52. doi: 10.1016/j.proche.2016.01.009

Sun, J., and Mao, X. (2016). An environmental friendly process for antarctic krill (*Euphausia superba*) utilization using fermentation technology. *J. Clean. Prod.* 127, 618–623. doi: 10.1016/j.jclepro.2016.04.020

Todd, E. W. (1949). Quantitative studies on the total plasmin and the trypsin inhibitor of human blood serum: i. methods for the titration of total plasmin and of trypsin inhibitor. *J. Exp. Med.* 89, 295–308. doi: 10.1084/jem.89.3.295

Xin, R., Wancui, X., Zhiying, X., Hongxia, C., Zuoxing, Z., and Xihong, Y. (2020). Efficient extraction of chitin from shrimp waste by mutagenized strain fermentation using atmospheric and room-temperature plasma. *Int. J. Biol. Macromol.* 155, 1561–1568.

Younes, I., Hajji, S., Frachet, V., Rinaudo, M., Jellouli, K., and Nasri, M. (2014). Chitin extraction from shrimp shell using enzymatic treatment. Antitumor, antioxidant and antimicrobial activities of chitosan. *Int. J. Biol. Macromol.* 69, 489–498. doi: 10.1016/j.ijbiomac.2014.06.013

Younes, I., Hajji, S., Rinaudo, M., Chaabouni, M., Jellouli, K., and Nasri, M. (2016). Optimization of proteins and minerals removal from shrimp shells to produce highly acetylated chitin. *Int. J. Biol. Macromol.* 84, 246–253. doi: 10.1016/j.ijbiomac.2015.08.034

Zhang, H., Jin, Y., Deng, Y., Wang, D., and Zhao, Y. (2012). Production of chitin from shrimp shell powders using *Serratia marcescens* B742 and *Lactobacillus plantarum* ATCC 8014 successive two-step fermentation. *Carbohyd. Res.* 362, 13–20. doi: 10.1016/j.carres.2012.09.011

Zhang, H., Yun, S., Song, L., Zhang, Y., and Zhao, Y. (2017). The preparation and characterization of chitin and chitosan under large-scale submerged fermentation level using shrimp by-products as substrate. *Int. J. Biol. Macromol.* 96, 334–339. doi: 10.1016/j.ijbiomac.2016.12.017

Zhao, D., Huang, W., Guo, N., Zhang, S., Xue, C., and Mao, X. (2019). Two-step separation of chitin from shrimp shells using citric acid and deep eutectic solvents with the assistance of microwave. *Polymers* 11:409. doi: 10.3390/polym11030409

Conflict of Interest: XY was employed by company Qingdao Keda Future Biotechnology Co., Ltd.

The remaining authors declare that the research was conducted in the absence of any commercial or financial relationships that could be construed as a potential conflict of interest.

Publisher's Note: All claims expressed in this article are solely those of the authors and do not necessarily represent those of their affiliated organizations, or those of the publisher, the editors and the reviewers. Any product that may be evaluated in this article, or claim that may be made by its manufacturer, is not guaranteed or endorsed by the publisher.

frontiers in Microbiology

REVIEW
published: 15 October 2021
doi: 10.3389/fmicb.2021.758886

Mini Review: Advances in 2-Haloacid Dehalogenases

Yayue Wang[1], *Qiao Xiang*[1,2], *Qingfeng Zhou*[1], *Jingliang Xu*[3,4]* *and Dongli Pei*[1]*

[1] College of Biology and Food, Shangqiu Normal University, Shangqiu, China, [2] College of Life Sciences, Henan Normal University, Xinxiang, China, [3] School of Chemical Engineering, Zhengzhou University, Zhengzhou, China, [4] Zhengzhou Tuoyang Industrial Co., Ltd., Zhengzhou, China

The 2-haloacid dehalogenases (EC 3.8.1.X) are industrially important enzymes that catalyze the cleavage of carbon–halogen bonds in 2-haloalkanoic acids, releasing halogen ions and producing corresponding 2-hydroxyl acids. These enzymes are of particular interest in environmental remediation and environmentally friendly synthesis of optically pure chiral compounds due to their ability to degrade a wide range of halogenated compounds with astonishing efficiency for enantiomer resolution. The 2-haloacid dehalogenases have been extensively studied with regard to their biochemical characterization, protein crystal structures, and catalytic mechanisms. This paper comprehensively reviews the source of isolation, classification, protein structures, reaction mechanisms, biochemical properties, and application of 2-haloacid dehalogenases; current trends and avenues for further development have also been included.

Keywords: 2-haloacid dehalogenases, protein structure, catalytic mechanism, biochemical properties, application

OPEN ACCESS

Edited by:
Benwei Zhu,
Nanjing Tech University, China

Reviewed by:
Fahrul Huyop,
Universiti Teknologi Malaysia, Malaysia
Dirk Tischler,
Ruhr University Bochum, Germany

***Correspondence:**
Jingliang Xu
xujl@zzu.edu.cn
Dongli Pei
peidongli@126.com

Specialty section:
This article was submitted to Microbiotechnology, a section of the journal Frontiers in Microbiology

Received: *15 August 2021*
Accepted: *13 September 2021*
Published: *15 October 2021*

Citation:
Wang Y, Xiang Q, Zhou Q, Xu J and Pei D (2021) Mini Review: Advances in 2-Haloacid Dehalogenases. Front. Microbiol. 12:758886. doi: 10.3389/fmicb.2021.758886

INTRODUCTION

Halogenated organic compounds show excellent thermal conductivity, insulation, heat resistance, lipophilicity, and biological activity (Kim et al., 2020; Zakary et al., 2021). They are widely used in industrial, agricultural, medical, and military fields as cleaning agents, biocides, gasoline additives, solvents, degreasers, pesticides, and intermediates for chemical synthesis, yielding enormous economic and social benefits (Kurumbang et al., 2014; Zhang et al., 2019; Gul et al., 2020b; Ameen et al., 2021). However, increasing amounts of halogenated compounds are discharged into the environment due to overproduction and extensive use, which results in environmental contamination. These compounds spread in lakes, drinking water, groundwater, seawater, and soil. Unlike naturally occurring halogenated compounds, which can be used as antibiotics to treat bacterial infections, man-made halogenated compounds, which are used as degreasers, solvents, biocides, pharmaceuticals, cleaning agents, and in many other industrial applications, are dangerous when introduced to the environment (Wu et al., 2019; Kirkinci et al., 2021). This is because these compounds do not degrade easily in natural environments because of their chemical stability, resulting in their environmental accumulation. Moreover, these compounds can become concentrated and accumulate in organisms through the food chain, with carcinogenic, teratogenic, and mutagenic effects (Fan et al., 2020; Lou Y. Y. et al., 2021; Zhang C. et al., 2021). This poses a serious threat to human health and has become an issue of concern all over the world (Artabe et al., 2020; Lou Y. Y. et al., 2021).

As the main decomposers in nature, microorganisms convert complex organic compounds into simple compounds, thus maintaining the cycle of elements that are vital to life (Hellal et al., 2021; Kajla et al., 2021; Yu et al., 2021). Microorganisms growing in environments polluted by organic halogenated compounds have the potential to transform these compounds owing to the presence of enzymes that catalyze dehalogenation in their cells, called dehalogenases (Atashgahi et al., 2018; Oyewusi et al., 2020b, 2021b). Among them, 2-haloacid dehalogenases are a family of critical enzymes that hydrolytically catalyze the dehalogenation of 2-haloacids to form corresponding 2-hydroxy acids (Kurihara and Esaki, 2008; Adamu et al., 2020). They cannot only degrade toxic pollutants with low energy consumption but also have a wide substrate profile and high catalytic efficiency. They have highly chiral resolution properties, which may enable the production of optically pure 2-halogenated and 2-hydroxyl compounds (Oyewusi et al., 2020a). Hence, 2-haloacid dehalogenases are highly valuable in the field of environmental remediation and environmentally friendly manufacturing of chiral chemicals. Here, we review the isolation source, classification, molecular structure, catalytic mechanism, catalytic properties, and industrial applications of 2-haloacid dehalogenases. These will enrich the biocatalytic repertoire of haloacid dehalogenases and broaden their applications and developments in the future.

ISOLATION SOURCES AND CLASSIFICATION OF 2-HALOACID DEHALOGENASES

Microorganisms possessing 2-haloacid dehalogenase are widespread in nature, and have been explored since the beginning of the 20th century. So far, increasing numbers of bacterial and fungal species capable of degrading halogenated xenobiotic pollutants have been isolated (**Table 1**). Most of these microorganisms were isolated from terrestrial environments, with only a few from marine environments, including *Burkholderia* sp. I37C (Chiba et al., 2009), *Rhodobacteraceae* sp. (Novak et al., 2013a), *Psychromonas ingrahamii* (Novak et al., 2013b), *Pseudomonas stutzeri* DEH130 (Zhang et al., 2013), *Paracoccus* sp. DEH99 (Zhang et al., 2014), *Lysinibacillus boronitolerans* MH2 (Heidarrezaei et al., 2020), and *Bacillus megaterium* BHS1 (Wahhab et al., 2020). The marine environment is the primary and optimal sink for halogenated pollutants because of their natural release by marine macroalgae, bacteria, sponges, tunicates, corals, worms, phytoplankton, and other invertebrates (Bidleman et al., 2019). Additionally, marine environments are considered extreme owing to a combination of unique properties including high pressure, high salinity, low temperature, oligotrophy, and special lighting conditions (de Oliveira et al., 2020; Ameen et al., 2021; Zhang J. et al., 2021). Because of this, microorganisms living in this environment are diverse and specific in gene composition and ecological functions; the intracellular enzymes of these microorganisms are correspondingly diverse and specific, conferring physiological and biochemical characteristics such as barophilicity, salt tolerance, cold adaptability, hyperthermostability, chemoselectivity, stereoselectivity, and regioselectivity (Thippeswamy et al., 2021; Zhang J. et al., 2021). The marine environment is therefore expected to be an important source of novel enzymes.

TABLE 1 | The reported microorganisms degrading 2-haloalkanoic acids.

Microorganisms	Genus	References
Bacteria	*Agrobacterium*	Köhler et al., 1998
	Alcaligenes	Hill et al., 1999
	Ancylobacter	Kumar et al., 2016
	Arthrobacter	Bagherbaigi et al., 2013
	Azotobacter	Diez et al., 1996
	Bacillus	Horisaki et al., 2011; Ratnaningsih and Idris, 2018; Oyewusi et al., 2021a
	Burkholderia	Edbeib et al., 2020
	Klebsiella	Idris Ratnaningsih, 2015
	Lysinibacillus	Heidarrezaei et al., 2020
	Methylobacterium	Kurihara and Esaki, 2008
	Mesorhizobium	Zakary et al., 2021
	Moraxella	Kurihara et al., 2000
	Paracoccidioides	Satpathy et al., 2015
	Paracoccus	Zhang et al., 2014
	Pseudoalteromonas	Liao et al., 2015
	Pseudomonas	Hasan et al., 1994; Park et al., 2003; Schmidberger et al., 2008; Zhang et al., 2013
	Psychromonas	Novak et al., 2013b
	Pyrococcus	Arai et al., 2006
	Rhizobium	Adamu et al., 2016; Oyewusi et al., 2020b
	Rhodobacteraceae	Novak et al., 2013a
	Serratia	Rosland Abel et al., 2012
	Sulfolobus	Xu et al., 2004
	Xanthobacter	van der Ploeg et al., 1991
Fungi	*Beauveria*	Satpathy et al., 2016
	Botrytis	Bustillo et al., 2003
	Candida	Polnisch et al., 1991
	Dichomitus	Muzikár et al., 2011
	Fusarium	Li et al., 2011
	Metarhizium	Satpathy et al., 2016
	Phanerochaete	Wang et al., 2009
	Pycnoporus	Muzikár et al., 2011
	Trichoderma	Bagherbaigi et al., 2013

The 2-haloacid dehalogenases have been classified according to amino acid sequence conservation and substrate selectivity (Wang et al., 2018; Adamu et al., 2020). These enzymes are classified into four types according to their substrate specificities and product configurations: D-2-haloacid dehalogenase (D-DEX, EC 3.8.1.9), L-2-haloacid dehalogenase (L-DEX, EC 3.8.1.2), configuration-inverting DL-2-haloacid dehalogenase (DL-DEXi, EC 3.8.1.10), and configuration-retaining DL-2-haloacid dehalogenase (DL-DEXr, EC 3.8.1.11) (Zakary et al., 2021). D-DEX catalyzes the dehalogenation of D-2-haloalkanoic

acids, whereas L-DEX specifically acts on L-2-haloalkanoic acids. DL-DEXi and DL-DEXr act on both enantiomers of substrates, but yield different product configurations. The 2-haloacid dehalogenases in general are divided into Group I and Group II enzymes according to the amino acid sequence homology; D-DEX and DL-DEX belong to Group I and L-DEX to Group II.

STRUCTURAL AND CATALYTIC CHARACTERISTICS OF 2-HALOACID DEHALOGENASES

The structural diversity of 2-haloacid dehalogenases determines their diversity of function. The different types of 2-haloacid dehalogenases have different structures and catalytic mechanisms; an overview of this is provided in this section.

L-DEX

Structural Characteristics and Catalytic Mechanism

L-DEX specifically acts on L-2-haloalkanoic acids to produce D-2-hydroxyalkanoic acids. These enzymes are widespread in nature and their biochemical characteristics and structures have been studied extensively (Satpathy et al., 2016; Wang et al., 2016; Adamu et al., 2020). So far, the three-dimensional (3D) structures of specific L-DEXs and their substrate complexes have been analyzed, including L-DEX YL from *Pseudomonas* sp. strain YL (Hisano et al., 1996), DhlB from *Xanthobacter autotrophicus* GJ10 (Ridder et al., 1997), PH0459 from *Pyrococcus horikoshii* OT3 (Arai et al., 2006), DehIVa from *Burkholderia cepacia* MBA4 (Schmidberger et al., 2007), DehSft from *Sulfolobus tokodaii* (Rye et al., 2009) and DehRhb from *Rhodobacteraceae* (Novak et al., 2013a).

L-DEX is an α/β type hydrolase consisting of a typical Rossman-fold-like core domain and subdomain, with the active site located between the two domains (**Figure 1**), apart from DhlB, which is composed of a core domain and two subdomains. Most L-DEX molecules are dimers consisting of two identical subunits, except for PH0459, which is a monomer according to its crystal structure (Arai et al., 2006). In a typical L-DEX structure, six-stranded parallel β-sheets (in order: β5-β4-β1-β6-β7-β8) are flanked on both sides by five α-helices, forming three layers of α/β fold units together constituting a sandwich domain (Hisano et al., 1996; Poelarends and Whitman, 2010; Zhang et al., 2018). Although the core domain of L-DEX has an α/β-type structure, it does not belong to the α/β hydrolase fold family, in which the typical domains are eight-stranded β-strands (in order: β1-β2-β4-β3-β5-β6-β7-β8) with the β2-strand antiparallel to the others. Two β-strands are separated by α-helix from the third strand, forming a β/α/β unit. The first α-helix and the last α-helix are located at one side of the β-sheet, and the remaining α-helices are at the other side (Janssen, 2004; Kunka et al., 2018; Babkova et al., 2020; Mazur et al., 2021).

The dehalogenation is catalyzed by L-DEX in an S_N2 nucleophilic substitution reaction as confirmed by X-ray Crystallography, O^{18} isotope labeling, liquid chromatography–mass spectrometry (LC–MS), site-directed mutagenesis, and quantum mechanic/molecular mechanic (QM/MM) calculations (Adamu et al., 2017a,b). The carboxylic acid group of the aspartic acid residue acts as the nucleophile in the active center, which attacks the C2 atom of the L-2-haloalkanoic acid to form an ester intermediate (Schmidberger et al., 2007). This intermediate product is then hydrolyzed by a water molecule, activated by His/Glu (in DehRhb) or Asn/Ser (in DehIVa) or Lys (in L-DEX YL) (**Figure 2**). The resultant halide ions are stabilized with the assistance of Arg or Asn or Phe. Greater numbers of halide ion acceptors can cleave stronger C-X bonds (Kurihara, 2011; Kondo et al., 2014).

Biochemical Properties

L-DEXs have been isolated from both terrestrial and marine environments. Some biochemical characteristics are shared between enzymes, and some differ. For example, L-DEX exhibits high catalytic activity on chlorinated and brominated substrates, but no such activity on D-2-haloalkanoic acids. Additionally, this enzyme cannot catalyze the dehalogenation of fluorinated and C_3-substituted haloalkanoic acids. With the exception of L-DEX YL, L-DEXs only show high catalytic activity on haloalkanoic acids of two or three carbons in length, with low or no activity on haloalkanoic acids four or more carbons in length (van der Ploeg et al., 1991; Liu et al., 1994; Zhang et al., 2013, 2014).

L-DEX enzymes differ in substrate specificity; L-DEX YL is more specific to L-2-chloropropionic acid than chloroacetic acid, whereas the L-DEX from *Bacillus* strain I37C is more specific to chloroacetic acid than to 2-chloropropionic acid (Liu et al., 1994; Chiba et al., 2009). The optimal pH range for L-DEX reactions is 9–11 (alkaline). Subunit molecular weights range from 25 to 28 kDa. Natural L-DEXs exist as monomers, dimers, and tetramers (van der Ploeg et al., 1991; Liu et al., 1994; Zhang et al., 2013, 2014).

L-DEXs isolated from different bacterial species have different thermal stability: the optimum reaction temperature for L-DEX from the terrestrial *Pseudomonas putida* is 30°C−45°C, and it loses 50% activity after 15 min incubation at 55°C. *Psychromonas. ingrahamii* is isolated from the sea-ice interface (−10°C) and exhibits psychrophilic properties; the lowest temperature at which this strain is able to grow is −12°C. L-DEX Pin, from *P. ingrahamii*, has an optimum reaction temperature of 45°C, with a melting temperature of 85°C. L-DEX Pin possesses the characteristics of both psychrophilic and thermophilic enzymes. Structurally, compared with mesophilic enzymes, L-DEX Pin has more hydrophobic surfaces and more salt bridges (Novak et al., 2013b).

The optimum reaction temperature for DehRhb, isolated from marine Rhodobacteraceae, is 55°C. The activity of this enzyme remains at ∼45% after incubation for 1 h at 60°C, indicating moderate thermal stability. Its key catalytic residues are His183 and Glu21, which are different from L-DEXs from terrestrial environments, suggesting that it may catalyze the dehalogenation with a novel catalytic mechanism (Novak and Littlechild, 2013). In summary, natural dehalogenases with novel properties may be more likely to be isolated from marine and other extreme environments; a greater understanding of their structures, catalytic mechanism and catalytic properties may

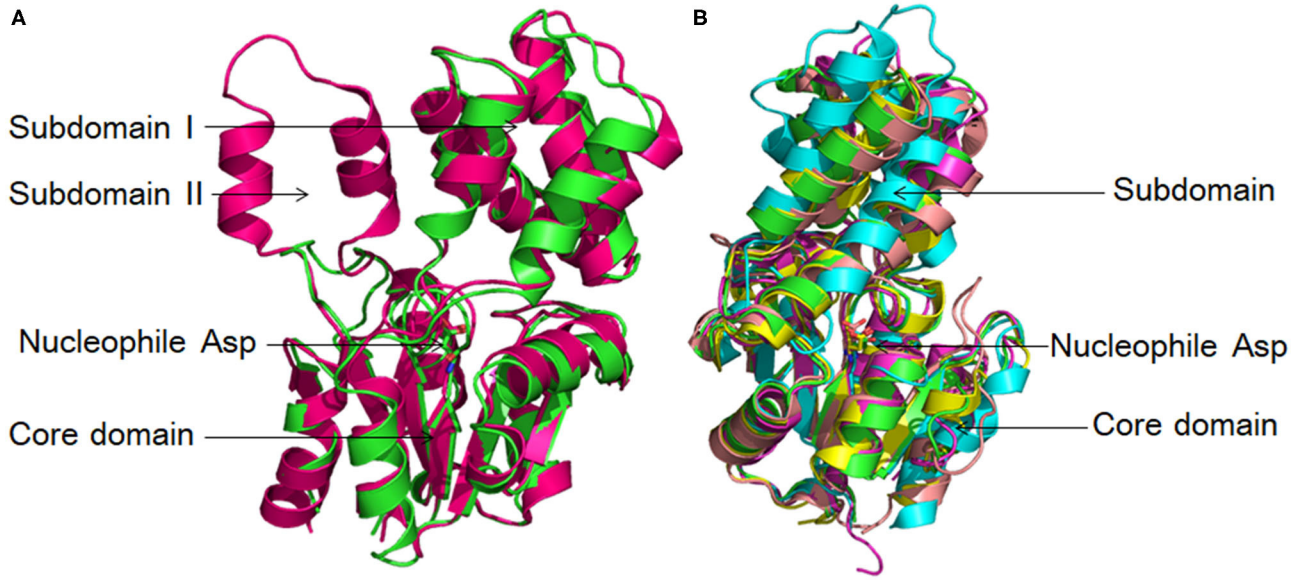

FIGURE 1 | L-DEX structures. **(A)** Structural superposition of DhlB (hotpink, PDB ID: 1qq5) and L-DEX YL (green, PDB ID: 1jud). **(B)** Structural superposition of DhlB (hotpink, PDB ID: 1qq5), L-DEX YL (green, PDB ID: 1jud), PH0459 (cyan, PDB ID: 1x42), DehIVa (magenta, PDB ID: 2no4), DehSft (yellow, PDB ID: 2w11) and DehRhb (salmon, PDB ID: 2yml).

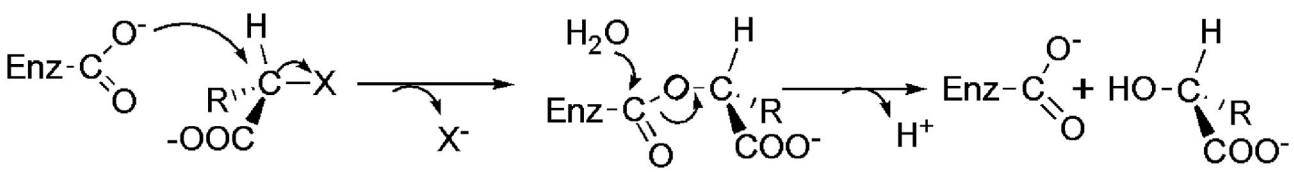

FIGURE 2 | Reaction mechanism of L-DEX (Schmidberger et al., 2007).

provide theoretical guidance for determining the direct evolution of L-DEXs and other dehalogenases.

DL-DEX

Structural Characteristics and Catalytic Mechanism

DL-DEX enzymes, which include DL-DEXi and DL-DEXr, catalyze the hydrolytic dehalogenation of both enantiomers of 2-haloalkanoic acids to produce corresponding 2-hydroxyalkanoic acids.

For DL-DEXi, the configuration of the product is opposite to the substrate: the C2 atom of the substrate configuration is inverted during dehalogenation catalyzed by DL-DEXi. Six DL-DEXi enzymes have been reported so far, including DL-DEX YL from *Pseudomonas putida* YL (Hasan et al., 1994; Soda et al., 1996), DL-DEX 113 from *Pseudomonas* sp. 113 (Nardi-Dei et al., 1999; Park et al., 2003), DehI from *Pseudomonas putida* PP3 (Park et al., 2003; Schmidberger et al., 2008), DL-DEX Mb from *Methylobacterium* sp. CPA1 (Siwek et al., 2013), DehE from *Rhizobium* sp. RC1 (Hamid et al., 2011; Zainal Abidin et al., 2019), and DhIIV from *Alcaligenes xylosoxidans* ABIV (Brokamp et al., 1996; Hamid et al., 2011). The crystal structures of DehI and DL-DEX Mb have been studied, revealing that DL-DEXi is an α-helical hydrolase, with no structural homology to L-DEX and other fold superfamilies in the hydrolases (Schmidberger et al., 2008; Siwek et al., 2013).

As shown in **Figure 3**, DehI is a homodimer according to its crystallographic structure. The N-terminus (amino acid residues 1–130) and C-terminus (residues 166–296) share 16% sequence identity in monomers, which form a pseudo-dimer. The active site is located at the interface of the pseudo-dimer, which binds D- and L- substrates (Schmidberger et al., 2008). The catalytic mechanism of DL-DEXi is different to that of L-DEX: dehalogenation catalyzed by D-DEXi is directly mediated by an activated water molecule, without involving the formation of E-S ester intermediate (**Figure 4**) (Nardi-Dei et al., 1999). The nucleophilic water molecule is likely activated by the conserved Asp and Asn residues; however, there is no relevant experimental evidence for this.

The transformation of the C_2-configuration of the substrate catalyzed by DL-DEXr is opposite to that of DL-DEXi. DL-DEXr catalyzes dehalogenation with retention of the C_2-configuration of the substrate. Therefore, the substrate and product share the same configuration. DL-DEXr has so far only been reported in *P. putida* PP3 (Weightman et al., 1982; Park et al., 2003).

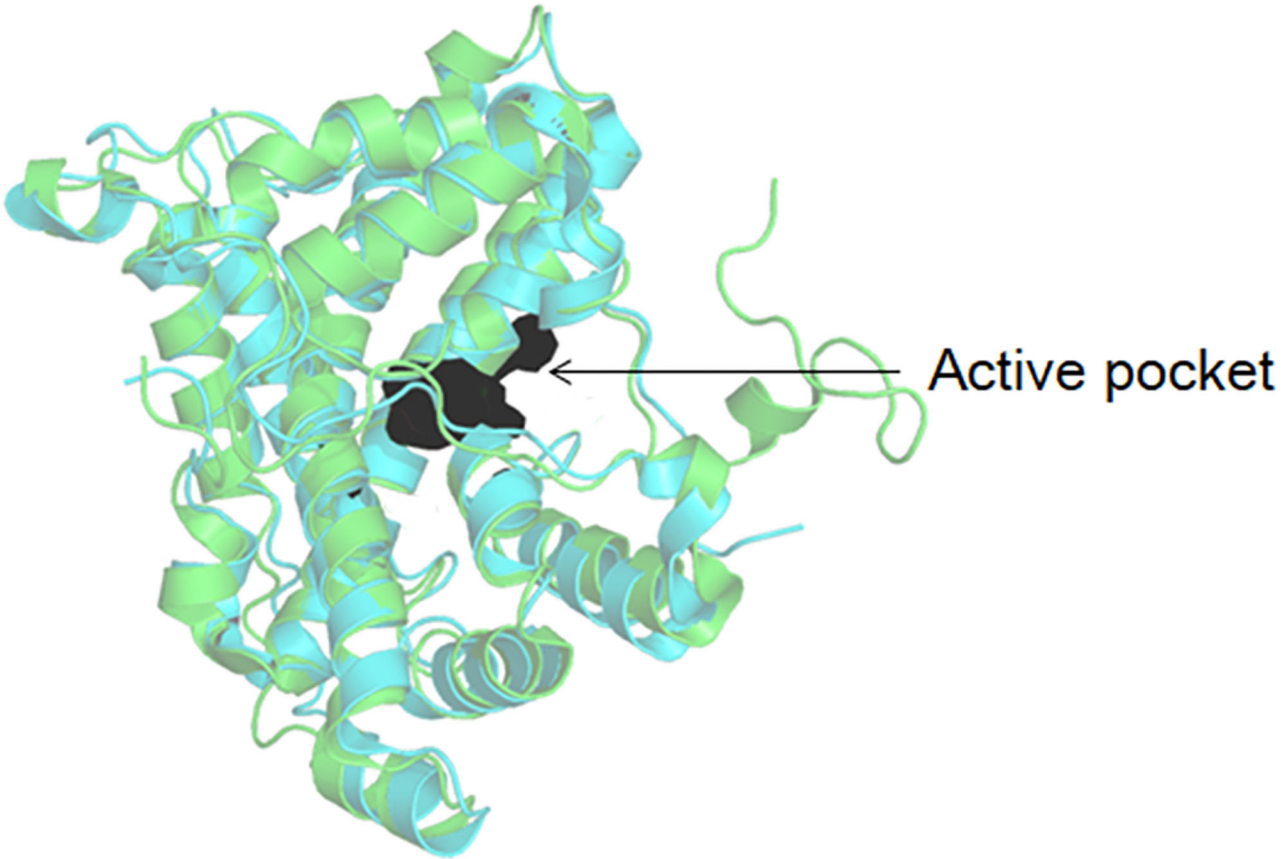

FIGURE 3 | Structural superposition of DehI (green, PDB ID: 3bjx) and DL-DEX Mb (cyan, PDB ID: 4n2x). The active pocket is shown as surface.

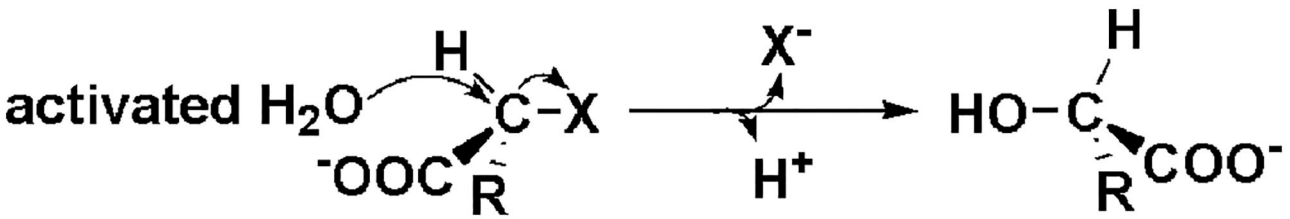

FIGURE 4 | Reaction mechanism of DL-DEXi (Nardi-Dei et al., 1999).

Gene sequence information for this enzyme is still unknown, and the reaction mechanism has not been analyzed. It is proposed that dehalogenation involves a cysteine residue, as DL-DEXr is highly sensitive to sulfhydryl reagents such as *N*-ethylmaleimide and *p*-chloromercuribenzoic acid. The reaction is thought to proceed with double inversion of the C_2-configuration of the substrate, resulting in the retention of the C_2-configuration: the first C_2-configuration inversion releases halogen ions and forms an E-S thioester intermediate; then, the intermediate is hydrolyzed under the attack of a water molecule, and the C_2-configuration is reversed again. However, there is currently no direct experimental data to confirm this hypothesis (**Figure 5**) (Weightman et al., 1982).

Biochemical Properties

In DL-DEXs, only DehI, DehE, DL-DEX 113 and DL-DEX ABIV have been characterized in terms of their enzymatic properties (Brokamp et al., 1996; Schmidberger et al., 2008). These enzymes have a greater specificity for L-2-haloalkanoic acids than D-2-haloalkanoic acids (**Table 2**). DL-DEXi can catalyze the dehalogenation of haloalkanoic acids with a carbon chain length of two to four, and catalyzes the formation of oxalate from trichloroacetate (Soda et al., 1996). Most DL-DEXi enzymes are homodimers, except for DL-DEX YL, which is a monomer. The subunit molecular weight ranges from 26 to 36 kDa (Kondo et al., 2014). DL-DEXi maximum activity levels occur at a pH of ∼9.5. The optimum reaction temperature is

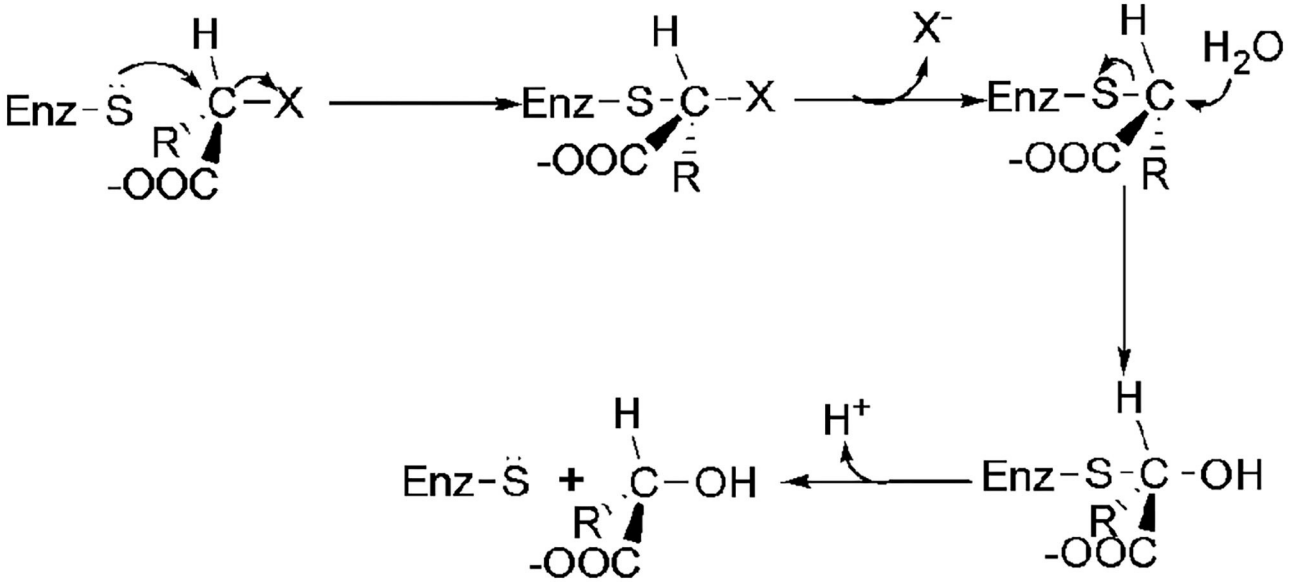

FIGURE 5 | Possible mechanism of DL-DEXr involving the retention of C_2-configuration of the substrate (Weightman et al., 1982).

TABLE 2 | Enatioselectivity of DL-DEXis from different strains.

Enzymes	Strains	L/D[a]	References
DehI	*P. putida* PP3	1.2	Park et al., 2003
DehE	*R.* sp. RC1	1.6	Hamid et al., 2011
DL-DEX 113	*P.* sp. 113	1.4	Park et al., 2003
DhlIV	*A. xylosoxidans* ABIV	1.1	Brokamp et al., 1996
DL-DEX YL	*P. putida* YL	–	
DL-DEX Mb	*M.* sp. CPA1	–	

[a] *L/D, the ratio of catalytic activity on L-2-chloropropionic acid and D-2-chloropropionic acid; -, no experimental data is available.*

between 30 and 40°C (Leigh et al., 1986; Park et al., 2003; Hamid et al., 2011). DL-DEXr is sensitive to SH-reagents; like DL-DEXi, it degrades haloalkanoic acids with a chain length of 2–4 (Weightman et al., 1982).

D-DEX

Structural Characteristics and Catalytic Mechanism

D-DEXs specifically catalyze the hydrolytic dehalogenation of D-2-haloalkanoic acids to produce L-2-hydroxyacids. So far, only four kinds of primary structure information are available for D-DEX, including DehD from *Rhizobium* sp. RC1 (Sudi et al., 2014), DehII from *Agrobacterium* sp. NHG3 (Higgins et al., 2005), HadD AJ1 from *Pseudomonas putida* AJ1 (Smith et al., 1990) and DehDIV-R from *Pseudomonas* sp. ZJU26 (Wang Y. et al., 2020). HadD AJ1 and DehDIV-R share the highest sequence homology (89%); HadD AJ1 and DehII NHG3 share 22.2% sequence homology, and HadD AJ1 and DehD share 32.6% sequence homology.

The author has extensively studied on the structure and catalytic mechanism of HadD AJ1. The crystal structure of HadD AJ1 is highly similar to that of DL-DEXi. Both types of enzymes are α-helical proteins, different from the α/β fold structure. HadD AJ1 is a homotetramer according to its crystallographic structure; each monomer comprises two repeats with 20% sequence identity (**Figure 6**). The two repeated folds are composed of N-terminal α-helices 1–6 and C-terminal α-helices 7–12, respectively, with a linker section containing 33 amino acids and a 3_{10}-helix η_1 (**Figure 6A**). These two repeats are stabilized by van der Waals forces, salt bonds, hydrogen bonds, and hydrophobic interactions. As shown in **Figure 6B**, helix α_4 and α_{10} are arranged in parallel with each other, and α_6 and α_{12} cross each other at the bulge between them. Helices α_6 and α_{12} mutually interlace at their bulges, located in the middle of the helices (Wang et al., 2018). This has been reported in many proteins with internal structural repeats, which are considered to result from genetic processes such as fusion and fission of domains and gene duplication during protein evolution (Longo et al., 2014; Berezovsky et al., 2017; Vrancken et al., 2020).

In HadD AJ1, Asp205 is the key catalytic residue, activating the water molecule with the assistance of Asn131. This was identified through an analysis of the complex structure of wildtype (WT) enzyme binding the product L-lactic acid (L-LA) and a D205N mutant binding the substrate D-2-chloropropionate (D-2-CPA) (**Figure 7A**). The dehalogenation catalyzed by D-DEX is directly mediated by activated water molecules, without forming an ester intermediate in the reaction process; this is the same process as DL-DEXi (**Figure 7B**). The activated water molecule attacks the C2 atom of the substrate from the opposite side of the halogen atom, breaking the C-X bond (**Figure 7A**). The halogen ion is released toward F281, and simultaneously, the hydroxyl group of the activated water molecule is bonded

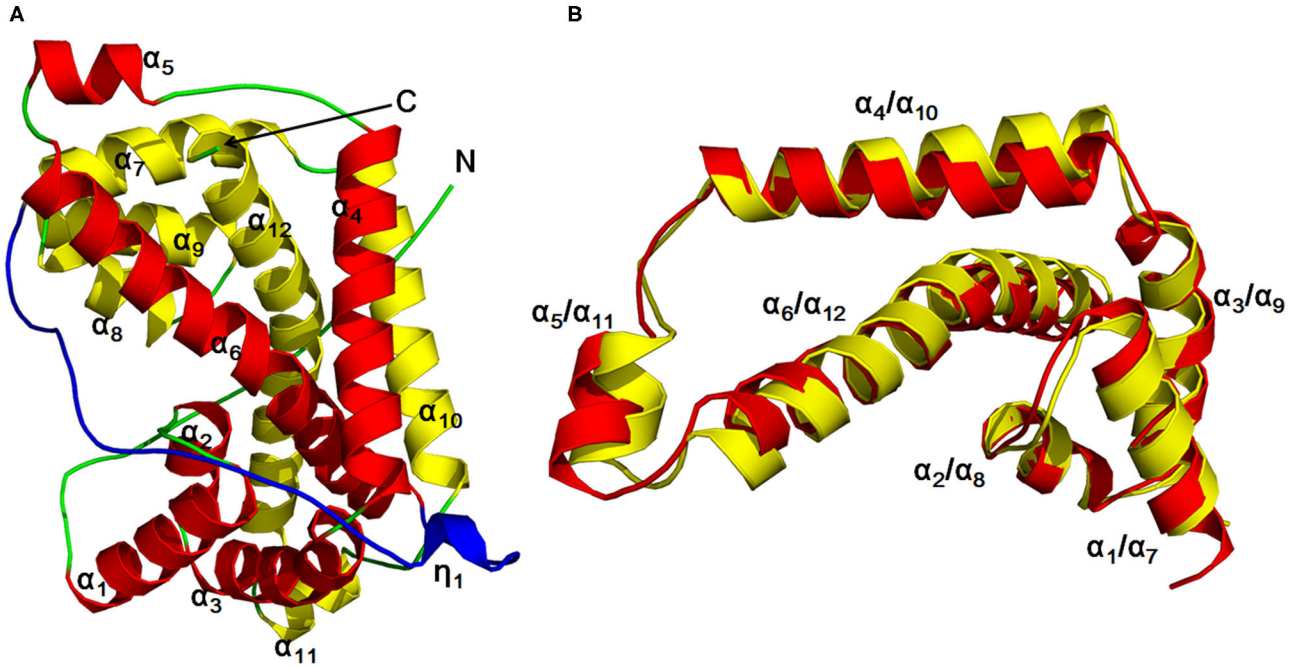

FIGURE 6 | HadD AJ1 monomer (Wang et al., 2018). **(A)** Ribbon representation of monomeric HadD AJ1 composed of two repeats (repeat 1: red; repeat 2: yellow) and a linker (cyan). **(B)** 3D superposition of repeat 1 (red) and repeat 2 (yellow).

to the C2 atom of the substrate to form L-lactic acid (Wang et al., 2018).

D-DEX and DL-DEXi share high amino acid sequence as well as structural homology. Moreover, both types of enzymes catalyze dehalogenation by the same mechanism, directly mediated by the nucleophilic water molecule; this differs from dehalogenation catalyzed by L-DEX, which is mediated by E-S ester intermediates. This suggests an evolutionarily close relationship between D-DEX and DL-DEXi.

Biochemical Properties

Currently, there are only a few studies on D-DEX enzymes, likely a result of the lack of microorganisms known to produce D-DEX. From analyses of DehD and HadD AJ1 biochemical properties, D-DEXs specifically catalyze dehalogenation of D-2-chlorinated and D-2-brominated acids with carbon chain lengths of 2–4. However, D-DEX has a higher catalytic activity on brominated than chlorinated substrates (Smith et al., 1990; Huyop and Sudi, 2012). K_m values of DehD, HadD AJ1, and DehDIV-R are 0.06, 0.94, and 2.2 mmol/L, respectively, with D-2-CPA as the substrate (Smith et al., 1990; Huyop and Sudi, 2012; Wang Y. et al., 2020). Compared with HadD AJ1 and DehDIV-R, DehD has a stronger affinity for D-2-CPA.

The natural active states of D-DEXs are different: DehD exists is a homodimer, while HadD AJ1 is a homotetramer. The optimal reaction pH of D-DEXs ranges from 9.0 to 10.0. The enzyme activity decreases rapidly when the pH falls outside the range of 8.0–10.0; under these conditions, HadD AJ1 exhibits <50% catalytic activity (Smith et al., 1990). In comparison with L-DEXs, D-DEXs are mesophilic, with an optimal reaction temperature of 50°C–60°C; however, the enzyme molecules are relatively stable between 30 and 40°C, but rapidly lose activity in a reaction temperature higher than 40°C (Smith et al., 1990).

APPLICATION

The 2-haloacid dehalogenases can detoxify halogenated pollutants by hydrolysis without the addition of other reductive agents; for this reason, their potential application in bioremediation is particularly attractive (Behbahani et al., 2018; Oyewusi et al., 2020b, 2021b; Zakary et al., 2021). The 2-haloacid dehalogenases are also highly stereoselective, and they may therefore be valuable in fine chemistry synthesis applications (Chen and Ribeiro de Souza, 2019; Adamu et al., 2020; Wang S. et al., 2020). These enzymes can be used to obtain chiral hydroxy acids and haloalkanoic acids with low molecular weights; these small organic acids generally act as intermediates for synthesizing agrochemicals, medicines, and other important chemicals (Leemans Martin et al., 2020; Gurushankara, 2021). Hence, 2-haloacid dehalogenases are promising and potentially highly valuable for their application in environmental remediation and chemical synthesis (Bommarius, 2015; Tanokura et al., 2015; Zhang et al., 2018); here, we discuss the main fields in which they could be applied.

Environmental Bioremediation

Halogenated carboxylic acids such as 2-chloropropionic acids and 2,2-chloropropionic acids are widely used as an

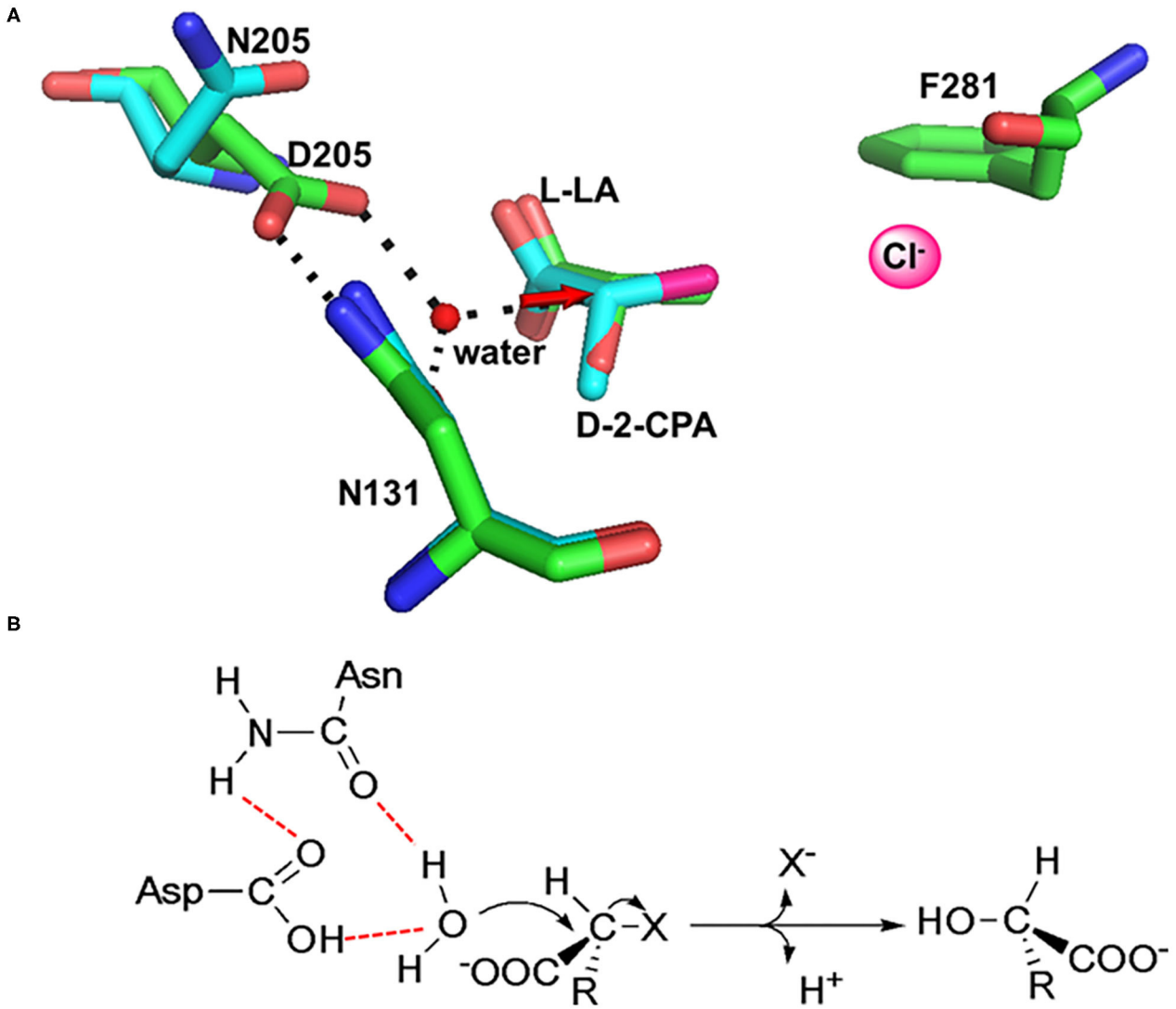

FIGURE 7 | The molecular mechanism of dehalogenation catalyzed by D-DEX. **(A)** Structural superimposition of WT/L-LA (green, PDB ID: 5gzy) and D205N/D-2-CPA (cyan, PDB ID: 5gzx) complex. **(B)** Reaction mechanism of D-DEX (Wang et al., 2018).

intermediate in the synthesis of pesticides and pharmaceuticals, especially the chirally pure 2-chloropropionic acid precursors for synthesizing many chiral drugs (Nguyen et al., 2021; Zhou et al., 2021). However, these haloacids produce chlorinated organic contaminants owing to extensive use and improper disposal. Haloacids are also intermediates in the degradation of some halogenated compounds, such as 1,2-dichloroalkane and hexachlorocyclohexane, which results in more haloacid contaminants in the environment (Hermon et al., 2018). The accumulation of these pollutants causes serious environmental problems and threats to human and other organisms' health. The 2-haloacid dehalogenase can catalyze the dehalogenation of 2-chloropropionic acids and 2,2-dichloropropionic acids to form non-toxic hydroxyl acids, which is a very promising potential tool for environmental bioremediation (Oyewusi et al., 2021b; Zakary et al., 2021). Dioxin compounds are carcinogenic byproducts originating from natural and anthropogenic sources such as herbicides, pesticides, and combustion processes; high levels of dioxin-contamination have been reported in food, soils, and blood samples of local residents in Southern Vietnam (Nguyen et al., 2021). *Burkholderia cenocepacia* strain 869T2 can degrade 0.2 mg L^{-1} of dioxin within 1 week under aerobic conditions, in which L-2-haloacid dehalogenase plays a crucial role (Nguyen et al., 2021). Haloacetic acids are the second most prominent class of disinfection by-products, and are frequently detected in surface and drinking water systems. These compounds have genotoxic, mutagenic, cytotoxic, and tumorigenic effects in humans (Kim et al., 2020; Long et al., 2021; Lou J. et al., 2021). In metabolically engineered *Burkholderia* species, the degradation activity of haloacetic acids can be increased by 4–8

times (Su et al., 2013). The bacterial degradation of haloacetic acids was found to be affected by water distribution system conditions, including pH, phosphate, total organic carbon and residual chlorine (Behbahani et al., 2018). The order of mean haloacetic acid degradation rates has been found to be di >mono >tri-halogenated acetic acids.

Phytoremediation has been attracting more attention as an environmentally friendly technology to clean up environmental contamination (Kurade et al., 2021); transgenic tobacco that produces haloalkane dehalogenase and haloacid dehalogenase, and which therefore contains a complete degradation pathway, has been reported to degrade 1,2-dichloroethane (Mena-Benitez et al., 2008).

Fine Chemical Synthesis

The growing interest in the use of 2-haloacid dehalogenases in fine chemical synthesis is due to their chiral selectivity. Optically pure compounds are generally synthesized using chemical methods; however, this is unpopular owing to the involvement of toxic reagents, as well as the low yield and low optical purity of products (Santi et al., 2021). Biocatalysis is considered as a more environmentally friendly and effective method because of the mild reaction conditions, and remarkable enantioselectivity (Novak et al., 2013b; Schober and Faber, 2013; Wang S. et al., 2020).

L-2-chloropropionic acid is an important precursor in the synthesis of herbicides and pesticides (Zhou et al., 2021). D-DEX specifically hydrolyzes D-2-chloropropionic acid in racemic 2-chloropropionic acid; L-2-chloropropane acid is therefore obtained with high enantiomeric purity by separation (Gong et al., 2018). To obtain optically active L-2-chloropropionic acid, Imperial Chemical Industries has already applied HadD AJ1 to the resolution of racemic 2-chloropropionic acid in an industrial setting, which has been the primary method for producing chiral chloropropionic acid (Taylor Stephen, 1985; Parker and Colby, 1995). It has also been used by AstraZeneca in the resolution of *rac*-2-CPA by D-DEX. This method is also suitable for the production of other short-chain chiral 2-halogenated acids, and the scale can be higher than 1,000 tons/year (Schober and Faber, 2013).

D-2-CPA is an important raw material for chemical synthesis that can be directly used to produce a variety of pharmaceutical intermediates, such as the nutritional medicine L-alanyl-L-glutamine and the anti-tuberculosis drug thiolactomycin. L-DEX can be used for the resolution of racemic 2-chloropropionic acids to obtain D-2-CPA with enantiomeric purity (Breuer et al., 2004).

Optically pure lactic acid is an important chiral intermediate in the synthesis of agrochemical, pharmaceutical, and chemical industries; it has been reported that L-lactic acid can be used to synthesize nanoparticles and nanofibers, which act as drug carriers (Chuan et al., 2020; Liu et al., 2021; Ma et al., 2021; Yavari Maroufi et al., 2021). D-lactic acid is also involved in the synthesis of important chiral drug intermediates, such as methyl D-lactate (Sengupta et al., 2020). Xie and colleagues studied the reaction conditions of L-DEX from thermophilic archaea *Sulfolobus tokodaii* in the catalytic conversion of racemic 2-chloropropionic acid to D-lactic acid (Rye et al., 2009; Xie et al., 2015); after optimizing reaction conditions with regard to substrate, buffer, and enzyme concentration, preparation of D-lactic acid was found to work best with 0.5 mol/L 2-chloropropionic acid.

D-2-bromobutyric acid is used as an intermediate for the synthesis of pharmaceuticals and agrochemicals. The fluoroacetate dehalogenase mutant H155V/W156R/Y219M is reported to catalyze the kinetic resolution of rac-2-bromobutyric acid, producing D-2-bromobutyric acid with an enantiomeric excess of 99.7% (Wang S. et al., 2020).

Agricultural Production

Herbicides with broad spectrum can effectively remove a variety of weeds, such as monochloroacetic acid, 2-chloropropionic acid, and 2-dichloropropionic acid. However, these herbicides can also damage economically valuable crops, resulting in significant losses in agricultural production. These losses can be avoided by developing herbicide-resistant crops, which requires the introduction of genes encoding dehalogenases into these crops. The *dehD* gene from *Rhizobium* sp. RCI, encoding D-2-haloacid dehalogenase, has been successfully introduced into tobacco as selective tag, constructing a transgenic variant of *Nicotiana benthamiana* with anti-monochloroacetic acid activity (Mohamed et al., 2020). This transgenic, herbicide-resistant tobacco is confirmed to be effective at various development stages, including seed germination and mature leaf stages. The dehalogenase gene is therefore likely to play an important role as a dominant, selectable marker gene for the construction of other crop species resistant to broad-spectrum halogenated compound herbicides.

Other Fields

Dehalogenases can also be used to construct biosensors for *in situ* detection of organic halogenated pollutants in the environment (Artabe et al., 2020; Gul et al., 2020a,b). By immobilizing halohydrin dehalogenase on a glass fiber membrane, detection limits of 0.06 mmol/L 1,3-dichloro-2-propanol and 0.09 mmol/L 2,3-dibromo-1-propanol have been achieved (Gul et al., 2020b). A detection limit of 1 mg/L dichlorethane has been achieved by immobilizing haloalkane dehalogenase on stacked chitosan films (Shahar et al., 2019a,b).

Dehalogenases act as tags when genetically fused to a protein of interest, termed HaloTag technology (England et al., 2015; Döbber and Pohl, 2017; Erdmann et al., 2019). This technology overcomes the current limitations of traditional protein tagging platforms, as it can be applied to protein isolation and purification, studies of protein synthesis and degradation, analyses of protein function, studies of protein–protein and protein–DNA interactions, and molecular and cellular imaging (Encell et al., 2012; Merrill et al., 2019; Cattoglio et al., 2020; Freitas et al., 2021; Minner-Meinen et al., 2021). Furthermore, novel technologies have been developed for tumor diagnosis and treatment involving the linkage of dehalogenase fused with cancer cell recognition peptides to multifunctional nanoparticles (Garbujo et al., 2020).

DISCUSSION AND PROSPECTS

A variety of 2-haloacid dehalogenases have so far been isolated and identified. Although structural information and catalytic mechanisms for L-DEX, DL-DEXi, and D-DEX have generally been well-understood, very little information on the structure and catalytic mechanism of DL-DEXr is available. Therefore, further study is necessary to understand DL-DEXr.

Enzyme stereoselectivity has been attracting a great deal of attention for asymmetric synthesis and chiral resolution. The 2-haloacid dehalogenases show typical stereoselectivity; however, little is known about the stereoselective mechanism. The enantioselective mechanism of L-DEX has been studied using quantum mechanics/molecular mechanics (QM/MM) and fragment molecular orbital calculation (Kondo et al., 2015; Adamu et al., 2019), which have confirmed that the high activation energy barrier prevents this enzyme from acting on the D-substrate. However, it is still unclear how selectivity of enzymes on chiral substrates is regulated. The stereoselective mechanism of D-DEX has been studied, and enzymatic stereoselectivity was found to be controlled by the residue Leu288, which determines the entry of L-substrate into the active site of the enzyme with steric hindrance. The mutation of residue leucine to isoleucine enables the enzyme to catalyze the dehaologenation of the L-substrate, owing to the different rotation position of Ile288 compared with Leu288. In the mutant enzyme, Ile288 functions as a wing gatekeeper, interacting with the substrate by gate-flipping during dehalogenation, allowing the L-substrate to enter the active site. However, it is still unclear how DL-DEXr and DL-DEXi recognize and interact with chiral substrates. Stereoselective properties make biocatalysts valuable in the preparation of optically pure compounds, which is an important area of environmentally friendly chemistry. An ideal industrial biocatalyst should have both high catalytic activity and specific stereoselectivity; exploring the molecular regulatory mechanisms underlying these properties forms the basis of artificial customization of dehalogenases with these properties. Reactions can be controlled using direct regulation of enzyme selectivity, forming products with high optical purity and unique structures. Further study on the stereoselectivity of 2-haloacid dehalogenase is therefore required in order to successfully manipulate this property.

Most 2-haloacid dehalogenases have a high catalytic activity with short-chain halogenated acid substrates containing fewer than four carbon atoms, while they show weak or no catalytic activity for longer-chain halogenated acids. Additionally, the low tolerance of these enzymes to organic solvents limits the range of their substrate profile. In order to obtain enantiomerically pure chiral products, enzymatic catalysis is sometimes used in enantiomeric resolution by combining with chemical convergence (Clayton et al., 2020). However, the conditions of the enzymatic reaction are incompatible with the high temperature and extreme pH required for chemical hydrolysis in the downstream separation process. Therefore, it remains necessary to identify novel 2-haloacid dehalogenases with unique properties, allowing them to function in these more extreme conditions (Marshall et al., 2021). Marine microorganisms may be the primary source of novel enzymes with extraordinary properties owing to their previously established genetic and biochemical diversity.

The birth of protein engineering technology has opened up a new route for researchers to develop excellent biocatalysts by redesigning natural enzymes (Marshall et al., 2021; Watanabe et al., 2021; Xiong et al., 2021). Many enzyme engineering design strategies have emerged, such as directed evolution, rational, semi-rational, *de novo*, computer-assisted, and artificial intelligence (Bunzel et al., 2021; Narayanan et al., 2021; Tunyasuvunakool et al., 2021; Woolfson, 2021; Wu et al., 2021). These strategies have been used to improve enzyme stability, activity, and selectivity for substrates. However, so far, only L-2-haloacid dehalogenases have been engineered to alter their substrate specificity. The mutation of residue Ser188 to Val in the enzyme DehE enables it to act on 3-chloropropionic acid (Hamid et al., 2015). Recent developments in understanding the structural and catalytic properties of 2-haloacid dehalogenases will also likely enable these enzymes to be more easily modified for commercial uses alongside L-2-haloacid dehalogenases. Given this overall direction of research, an increasing variety of 2-haloacid dehalogenases will likely be modified through protein engineering techniques to improve their properties for biotechnological applications.

AUTHOR CONTRIBUTIONS

YW and QX handled the literature collection and literature research. YW prepared the original draft. QZ, JX, and DP modified the manuscript. All authors critically reviewed, contributed to, and approved the final manuscript.

FUNDING

This work was supported by the National Natural Science Foundation of China (22078308), Innovation Leadership Program in Sciences and Technologies for Central Plains Talent Plan (214200510009), Key Scientific Research Projects in the Universities of Henan Province (20A180024), Research Project of Shangqiu Normal University (700144), Postdoctoral Science Foundation of Henan Province (50026003), Program for Science and Technology Innovative Research Team in University of Henan Province (21IRTSTHN025), and Innovation Leadership Program in Sciences and Technologies for Zhengzhou Talent Gathering Plan, Henan Academician Workstation for Industrial Technology of Dry Chilli.

ACKNOWLEDGMENTS

We would like to thank the reviewers for their constructive comments.

REFERENCES

Adamu, A., Abdul Wahab, R., Aliyu, F., Abdul Razak, F. I., Mienda, B. S., Shamsir, M. S., et al. (2019). Theoretical analyses on enantiospecificity of L-2-haloacid dehalogenase (DehL) from *Rhizobium* sp. RC1 towards 2-chloropropionic acid. *J. Mol. Graph Model.* 92, 131–139. doi: 10.1016/j.jmgm.2019.07.012

Adamu, A., Shamsir, M. S., Wahab, R. A., Parvizpour, S., and Huyop, F. (2017a). Multi-template homology-based structural model of L-2-haloacid dehalogenase (DehL) from *Rhizobium* sp. RC1. *J. Biomol. Struct. Dyn.* 35, 3285–3296. doi: 10.1080/07391102.2016.1254115

Adamu, A., Wahab, R. A., Aliyu, F., Aminu, A. H., Hamza, M. M., and Huyop, F. (2020). Haloacid dehalogenases of *Rhizobium* sp. and related enzymes: Catalytic properties and mechanistic analysis. *Process Biochem.* 92, 437–446. doi: 10.1016/j.procbio.2020.02.002

Adamu, A., Wahab, R. A., and Huyop, F. (2016). L-2-Haloacid dehalogenase (DehL) from *Rhizobium* sp. RC1. *SpringerPlus* 5:695. doi: 10.1186/s40064-016-2328-9

Adamu, A., Wahab, R. A., Shamsir, M. S., Aliyu, F., and Huyop, F. (2017b). Deciphering the catalytic amino acid residues of L-2-haloacid dehalogenase (DehL) from *Rhizobium* sp. RC1: an in silico analysis. *Comput. Biol. Chem.* 70, 125–132. doi: 10.1016/j.compbiolchem.2017.08.007

Ameen, F., AlNadhari, S., and Al-Homaidan, A. A. (2021). Marine microorganisms as an untapped source of bioactive compounds. *Saudi J. Biol. Sci.* 28, 224–231. doi: 10.1016/j.sjbs.2020.09.052

Arai, R., Kukimoto-Niino, M., Kuroishi, C., Bessho, Y., Shirouzu, M., and Yokoyama, S. (2006). Crystal structure of the probable haloacid dehalogenase PH0459 from *Pyrococcus horikoshii* OT3. *Protein Sci.* 15, 373–377. doi: 10.1110/ps.051922406

Artabe, A. E., Cunha-Silva, H., and Barranco, A. (2020). Enzymatic assays for the assessment of toxic effects of halogenated organic contaminants in water and food. A review. *Food Chem. Toxicol.* 145, 111677–111697. doi: 10.1016/j.fct.2020.111677

Atashgahi, S., Liebensteiner, M. G., Janssen, D. B., Smidt, H., Stams, A. J. M., and Sipkema, D. (2018). Microbial synthesis and transformation of inorganic and organic chlorine compounds. *Front. Microbiol.* 9:3079. doi: 10.3389/fmicb.2018.03079

Babkova, P., Dunajova, Z., Chaloupkova, R., Damborsky, J., Bednar, D., and Marek, M. (2020). Structures of hyperstable ancestral haloalkane dehalogenases show restricted conformational dynamics. *Comput. Struct. Biotechnol. J.* 18, 1497–1508. doi: 10.1016/j.csbj.2020.06.021

Bagherbaigi, S., Gicana, R., Lamis, R. J., Nemati, M., and Huyop, F. (2013). Characterisation of *Arthrobacter* sp. S1 that can degrade α and β-haloalkanoic acids isolated from contaminated soil. *Ann. Microbiol.* 63, 1363–1369. doi: 10.1007/s13213-012-0595-4

Behbahani, M., Lin, B., Phares, T. L., and Seo, Y. (2018). Understanding the impact of water distribution system conditions on the biodegradation of haloacetic acids and expression of bacterial dehalogenase genes. *J. Hazard. Mater.* 351, 293–300. doi: 10.1016/j.jhazmat.2018.02.047

Berezovsky, I. N., Guarnera, E., and Zheng, Z. (2017). Basic units of protein structure, folding, and function. *Prog. Biophys. Mol. Bio* 128, 85–99. doi: 10.1016/j.pbiomolbio.2016.09.009

Bidleman, T. F., Andersson, A., Jantunen, L. M., Kucklick, J. R., Kylin, H., Letcher, R. J., et al. (2019). A review of halogenated natural products in Arctic, Subarctic and Nordic ecosystems. *Emerg. Contam.* 5, 89–115. doi: 10.1016/j.emcon.2019.02.007

Bommarius, A. (2015). Biocatalysis: a status report. *Annu. Rev. Chem.* 6, 319–345. doi: 10.1146/annurev-chembioeng-061114-123415

Breuer, M., Ditrich, K., Habicher, T., Hauer, B., Keseler, M. D., Sturmer, R., et al. (2004). Industrial methods for the production of optically active intermediates. *Angew Chem. Int. Edit.* 43, 788–824. doi: 10.1002/anie.200300599

Brokamp, A., Happe, B., and Schmidt, F. R. (1996). Cloning and nucleotide sequence of a D,L-haloalkanoic acid dehalogenase encoding gene from *Alcaligenes xylosoxidans* ssp. denitrificans ABIV. *Biodegradation* 7, 383–396. doi: 10.1007/BF00056422

Bunzel, H. A., Anderson, J. L. R., and Mulholland, A. J. (2021). Designing better enzymes: insights from directed evolution. *Curr. Opin. Struct. Biol.* 67, 212–218. doi: 10.1016/j.sbi.2020.12.015

Bustillo, A., Aleu, J., Hernández-Galán, R., and Collado, I. (2003). Biotransformation of the fungistatic compound (R)-(+)-1-(4′-chlorophenyl) propan-1-ol by *Botrytis cinerea*. *J. Mol. Catal. B Enzym.* 21, 267–271. doi: 10.1016/S1381-1177(02)00231-X

Cattoglio, C., Darzacq, X., Tjian, R., and Hansen, A. S. (2020). Estimating cellular abundances of halo-tagged proteins in live mammalian cells by flow cytometry. *Bio Protoc.* 10, 3527–3544. doi: 10.21769/BioProtoc.3527

Chen, B. S., and Ribeiro de Souza, F. Z. (2019). Enzymatic synthesis of enantiopure alcohols: current state and perspectives. *RSC Adv.* 9, 2102–2115. doi: 10.1039/C8RA09004A

Chiba, Y., Yoshida, T., Ito, N., Nishimura, H., Imada, C., Yasuda, H., et al. (2009). Isolation of a bacterium possessing a haloacid dehalogenase from a marine sediment core. *Microbes Environ.* 24, 276–279. doi: 10.1264/jsme2.ME09123

Chuan, D., Fan, R., Wang, Y., Ren, Y., Wang, C., Du, Y., et al. (2020). Stereocomplex poly(lactic acid)-based composite nanofiber membranes with highly dispersed hydroxyapatite for potential bone tissue engineering. *Compos. Sci. Technol.* 192, 1–12. doi: 10.1016/j.compscitech.2020.108107

Clayton, A. D., Labes, R., and Blacker, A. J. (2020). Combination of chemocatalysis and biocatalysis in flow. *Curr. Opin. Green Sustain. Chem.* 26:100378. doi: 10.1016/j.cogsc.2020.100378

de Oliveira, B. F. R., Carr, C. M., Dobson, A. D. W., and Laport, M. S. (2020). Harnessing the sponge microbiome for industrial biocatalysts. *Appl. Microbiol. Biot.* 104, 8131–8154. doi: 10.1007/s00253-020-10817-3

Diez, A., Prieto, M. I., Alvarez, M. J., Bautista, J. M., Garrido, A., and Puyet, A. (1996). Improved catalytic performance of a 2-haloacid dehalogenase from *Azotobacter* sp. by ion-exchange immobilisation. *Biochem. Biophl. Res. Co* 220, 828–833. doi: 10.1006/bbrc.1996.0489

Döbber, J., and Pohl, M. (2017). HaloTag^{TM}: evaluation of a covalent one-step immobilization for biocatalysis. *J. Biotechnol.* 241, 170–174. doi: 10.1016/j.jbiotec.2016.12.004

Edbeib, M., Wahab, R., Huyop, F., Aksoy, H., and Kaya, Y. (2020). Further analysis of *Burkholderia pseudomallei* MF2 and identification of putative dehalogenase gene by PCR. *Indones J. Chem.* 20, 386–394. doi: 10.22146/ijc.43262

Encell, L. P., Friedman Ohana, R., Zimmerman, K., Otto, P., Vidugiris, G., Wood, M. G., et al. (2012). Development of a dehalogenase-based protein fusion tag capable of rapid, selective, and covalent attachment to customizable ligands. *Curr. Chem. Genomics* 6, 55–71. doi: 10.2174/1875397301206010055

England, C. G., Luo, H., and Cai, W. (2015). HaloTag technology: a versatile platform for biomedical applications. *Bioconjug. Chem.* 26, 975–986. doi: 10.1021/acs.bioconjchem.5b00191

Erdmann, R. S., Baguley, S. W., Richens, J. H., Wissner, R. F., Xi, Z., Allgeyer, E. S., et al. (2019). Labeling strategies matter for super-resolution microscopy: a comparison between HaloTags and SNAP-tags. *Cell Chem. Biol.* 26, 584–592. doi: 10.1016/j.chembiol.2019.01.003

Fan, Y., Chen, S. J., Li, Q. Q., Zeng, Y., Yan, X., and Mai, B. X. (2020). Uptake of halogenated organic compounds (HOCs) into peanut and corn during the whole life cycle grown in an agricultural field. *Envirorn. Pollut.* 263, 1–9. doi: 10.1016/j.envpol.2020.114400

Freitas, A. I., Domingues, L., and Aguiar, T. Q. (2021). Tag-mediated single-step purification and immobilization of recombinant proteins toward protein-engineered advanced materials. *J. Adv. Res.* doi: 10.1016/j.jare.2021.06.010. [Epub ahead of print].

Garbujo, S., Galbiati, E., Salvioni, L., Mazzucchelli, M., Frascotti, G., Sun, X., et al. (2020). Functionalization of colloidal nanoparticles with a discrete number of ligands based on a "HALO-bioclick" reaction. *Chem. Commun.* 56, 11398–11401. doi: 10.1039/D0CC04355A

Gong, Y., Ma, S., Wang, Y., Xu, Y., Sun, A., Zhang, Y., et al. (2018). Characterization of a novel deep-sea microbial esterase EstC10 and its use in the generation of (R)-methyl-2-chloropropionate. *J. Oceanol. Limnol.* 36, 473–482. doi: 10.1007/s00343-018-6297-4

Gul, I., Bogale, T. F., Chen, Y., Yang, X., Fang, R., Feng, J., et al. (2020a). A paper-based whole-cell screening assay for directed evolution-driven enzyme engineering. *Appl. Microbiol. Biot.* 104, 6013–6022. doi: 10.1007/s00253-020-10615-x

Gul, I., Wang, Q., Jiang, Q., Fang, R., and Tang, L. (2020b). Enzyme immobilization on glass fiber membrane for detection of halogenated compounds. *Anal. Biochem.* 609, 1–8. doi: 10.1016/j.ab.2020.113971

Gurushankara, H. P. (2021). "Chapter 13-Recent developments in biocatalysis and its influence on the pharmaceutical industry," in *Recent Developments in Applied Microbiology and Biochemistry*, ed B. Viswanath (Cambridge, MA: Academic Press), 127–139.

Hamid, A. A. A., Hamid, T. H. T. A., Wahab, R. A., Omar, M. S. S., and Huyop, F. (2015). An S188V mutation alters substrate specificity of non-stereospecific α-haloalkanoic acid dehalogenase E (DehE). *PLoS ONE* 10:e0121687. doi: 10.1371/journal.pone.0121687

Hamid, T. H. T. A., Hamid, A. A. A., and Huyop, F. (2011). A review on non-stereospecific haloalkanoic acid dehalogenases. *Afr. J. Biotechnol.* 10, 9725–9736. doi: 10.5897/AJB11.934

Hasan, A. K. M. Q., Takada, H., Koshikawa, H., Liu, J. Q., Kurihara, T., Esaki, N., et al. (1994). Two kinds of 2-halo acid dehalogenases from *Pseudomonas* sp. YL induced by 2-chloroacrylate and 2-chloropropionate. *Biosci. Biotechnol. Biochem.* 58, 1599–1602. doi: 10.1271/bbb.58.1599

Heidarrezaei, M., Shokravi, H., Huyop, F., Rahimian Koloor, S. S., and Petru, M. (2020). Isolation and characterization of a novel bacterium from the marine environment for trichloroacetic acid bioremediation. *Appl. Sci.* 10, 1–17. doi: 10.3390/app10134593

Hellal, J., Joulian, C., Urien, C., Ferreira, S., Denonfoux, J., Hermon, L., et al. (2021). Chlorinated ethene biodegradation and associated bacterial taxa in multi-polluted groundwater: insights from biomolecular markers and stable isotope analysis. *Sci. Total Environ.* 763, 1–10. doi: 10.1016/j.scitotenv.2020.142950

Hermon, L., Denonfoux, J., Hellal, J., Joulian, C., Ferreira, S., Vuilleumier, S., et al. (2018). Dichloromethane biodegradation in multi-contaminated groundwater: insights from biomolecular and compound-specific isotope analyses. *Water Res.* 142, 217–226. doi: 10.1016/j.watres.2018.05.057

Higgins, T. P., Hope, S. J., Effendi, A. J., Dawson, S., and Dancer, B. N. (2005). Biochemical and molecular characterisation of the 2,3-dichloro-1-propanol dehalogenase and stereospecific haloalkanoic dehalogenases from a versatile *Agrobacterium* sp. *Biodegradation* 16, 485–492. doi: 10.1007/s10532-004-5670-5

Hill, K. E., Marchesi, J. R., and Weightman, A. J. (1999). Investigation of two evolutionarily unrelated halocarboxylic acid dehalogenase gene families. *J. Bacteriol.* 181, 2535–2547. doi: 10.1128/JB.181.8.2535-2547.1999

Hisano, T., Hata, Y., Fujii, T., Liu, J.-Q., Kurihara, T., Esaki, N., et al. (1996). Crystal structure of L-2-haloacid dehalogenase from *Pseudomonas* sp. YL: an α/β hydrolase structure that is different from the α/β hydrolase fold. *J. Biol. Chem.* 271, 20322–20330. doi: 10.1074/jbc.271.34.20322

Horisaki, T., Yoshida, E., Sumiya, K., Takemura, T., Yamane, H., and Nojiri, H. (2011). Isolation and characterization of monochloroacetic acid-degrading bacteria. *J. Gen. Appl. Microbiol.* 57, 277–284. doi: 10.2323/jgam.57.277

Huyop, F., and Sudi, I. Y. (2012). D-specific dehalogenases, a review. *Biotechnol. Biotec. Eq.* 26, 2817–2822. doi: 10.5504/BBEQ.2011.0143

Idris and Ratnaningsih, E. (2015). Cloning of haloacid dehalogenase gene from *Bacillus cereus* local strain with the addition of restriction sites. *Procedia Chem.* 16, 314–320. doi: 10.1016/j.proche.2015.12.058

Janssen, D. B. (2004). Evolving haloalkane dehalogenases. *Curr. Opin. Chem. Biol.* 8, 150–159. doi: 10.1016/j.cbpa.2004.02.012

Kajla, S., Nagi, G. K., and Kumari, R. (2021). Microorganisms employed in the removal of contaminants from wastewater of iron and steel industries. *Rend Lincei Sci. Fis.* 32, 257–272. doi: 10.1007/s12210-021-00982-6

Kim, D.-H., Park, C. G., and Kim, Y. J. (2020). Characterizing the potential estrogenic and androgenic activities of two disinfection byproducts, monohaloacetic acids and haloacetamides, using *in vitro* bioassays. *Chemosphere* 242, 1–6. doi: 10.1016/j.chemosphere.2019.125198

Kirkinci, S. F., Edbeib, M. F., Aksoy, H. M., Marakli, S., and Kaya, Y. (2021). Identification of Dalapon degrading bacterial strain, *Psychrobacter* sp. TaeBurcu001 isolated from Antarctica. *Polar Sci.* 28, 1–9. doi: 10.1016/j.polar.2021.100656

Köhler, R., Brokamp, A., Schwarze, R., Reiting, R. H., and Schmidt, F. R. (1998). Characteristics and DNA-sequence of a cryptic haloalkanoic acid dehalogenase from *Agrobacterium tumefaciens* RS5. *Curr. Microbiol.* 36, 96–101. doi: 10.1007/s002849900286

Kondo, H., Fujimoto, K. J., Tanaka, S., Deki, H., and Nakamura, T. (2015). Theoretical prediction and experimental verification on enantioselectivity of haloacid dehalogenase L-DEX YL with chloropropionate. *Chem. Phys. Lett.* 623, 101–107. doi: 10.1016/j.cplett.2015.01.053

Kondo, H., Nakamura, T., and Tanaka, S. (2014). A significant role of Arg41 residue in the enzymatic reaction of haloacid dehalogenase L-DEX YL studied by QM/MM method. *J. Mol. Catal. B Enzym.* 110, 23–31. doi: 10.1016/j.molcatb.2014.09.006

Kumar, A., Pillay, B., and Olaniran, A. O. (2016). L-2-haloacid dehalogenase from *Ancylobacter aquaticus* UV5: sequence determination and structure prediction. *Int. J. Biol. Macromol.* 83, 216–225. doi: 10.1016/j.ijbiomac.2015.11.066

Kunka, A., Damborsky, J., and Prokop, Z. (2018). "Chapter Seven - Haloalkane Dehalogenases From Marine Organisms," in *Methods in Enzymology*, ed B. S. Moore (Cambridge, MA: Academic Press), 203–251.

Kurade, M. B., Ha, Y. H., Xiong, J. Q., Govindwar, S. P., Jang, M., and Jeon, B. H. (2021). Phytoremediation as a green biotechnology tool for emerging environmental pollution: a step forward towards sustainable rehabilitation of the environment. *Chem. Eng. J.* 415, 1–19. doi: 10.1016/j.cej.2021.129040

Kurihara, T. (2011). A mechanistic analysis of enzymatic degradation of organohalogen compounds. *Biosci. Biotechnol. Biochem.* 75, 189–198. doi: 10.1271/bbb.100746

Kurihara, T., and Esaki, N. (2008). Bacterial hydrolytic dehalogenases and related enzymes: occurrences, reaction mechanisms, and applications. *Chem. Rec.* 8, 67–74. doi: 10.1002/tcr.20141

Kurihara, T., Esaki, N., and Soda, K. (2000). Bacterial 2-haloacid dehalogenases: structures and reaction mechanisms. *J. Mol. Catal. B Enzym.* 10, 57–65. doi: 10.1016/S1381-1177(00)00108-9

Kurumbang, N. P., Dvorak, P., Bendl, J., Brezovsky, J., Prokop, Z., and Damborsky, J. (2014). Computer-assisted engineering of the synthetic pathway for biodegradation of a toxic persistent pollutant. *ACS Synth. Biol.* 3, 172–181. doi: 10.1021/sb400147n

Leemans Martin, L., Peschke, T., Venturoni, F., and Mostarda, S. (2020). Pharmaceutical industry perspectives on flow chemocatalysis and biocatalysis. *Curr. Opin. Green Sustain* 25:100350. doi: 10.1016/j.cogsc.2020.04.011

Leigh, J. A., Skinner, A. J., and Cooper, R. A. (1986). Isolation and partial characterisation of dehalogenase-deficient mutants of a *Rhizobium* sp.. *FEMS Microbiol. Lett.* 36, 163–166. doi: 10.1111/j.1574-6968.1986.tb01688.x

Li, J., Cai, W., and Zhu, L. (2011). The characteristics and enzyme activities of 4-chlorophenol biodegradation by *Fusarium* sp. *Bioresource Technol.* 102, 2985–2989. doi: 10.1016/j.biortech.2010.10.006

Liao, L., Sun, X., Zeng, Y., Luo, W., Yu, Y., and Chen, B. (2015). A new L-haloacid dehalogenase from the Arctic psychrotrophic *Pseudoalteromonas* sp. BSW20308. *Polar Biol.* 38, 1161–1169. doi: 10.1007/s00300-015-1674-3

Liu, J., Zhai, H., Sun, Y., Wu, S., and Chen, S. (2021). Developing high strength poly(L-lactic acid) nanofiber yarns for biomedical textile materials: a comparative study of novel nanofiber yarns and traditional microfiber yarns. *Mater. Lett.* 300:130229. doi: 10.1016/j.matlet.2021.130229

Liu, J. Q., Kurihara, T., Hasan, A. K., Nardi-Dei, V., Koshikawa, H., Esaki, N., et al. (1994). Purification and characterization of thermostable and nonthermostable 2-haloacid dehalogenases with different stereospecificities from *Pseudomonas* sp. strain YL. *Appl. Environ. Microbiol.* 60, 2389–2393. doi: 10.1128/aem.60.7.2389-2393.1994

Long, K., Sha, Y., Mo, Y., Wei, S., Wu, H., Lu, D., et al. (2021). Androgenic and teratogenic effects of iodoacetic acid drinking water disinfection byproduct *in vitro* and *in vivo*. *Environ. Sci. Technol.* 55, 3827–3835. doi: 10.1021/acs.est.0c06620

Longo, L. M., Kumru, O. S., Middaugh, C. R., and Blaber, M. (2014). Evolution and design of protein structure by folding nucleus symmetric expansion. *Structure* 22, 1377–1384. doi: 10.1016/j.str.2014.08.008

Lou, J., Wang, W., and Zhu, L. (2021). Transformation of emerging disinfection byproducts Halobenzoquinones to haloacetic acids during chlorination of drinking water. *Chem. Eng. J.* 418, 129326. doi: 10.1016/j.cej.2021.129326

Lou, Y. Y., Fontmorin, J.-M., Amrane, A., Fourcade, F., and Geneste, F. (2021). Metallic nanoparticles for electrocatalytic reduction of halogenated organic compounds: A review. *Electrochim. Acta* 377, 138039. doi: 10.1016/j.electacta.2021.138039

Ma, F., He, L., Lindner, E., and Wu, D. Y. (2021). Highly porous poly(L-lactic) acid nanofibers as a dual-signal paper-based bioassay platform for in vitro diagnostics. *Appl. Surf. Sci.* 542:148732. doi: 10.1016/j.apsusc.2020.148732

Marshall, J. R., Mangas-Sanchez, J., and Turner, N. J. (2021). Expanding the synthetic scope of biocatalysis by enzyme discovery and protein engineering. *Tetrahedron* 82:131926. doi: 10.1016/j.tet.2021.131926

Mazur, A., Prudnikova, T., Grinkevich, P., Mesters, J. R., Mrazova, D., Chaloupkova, R., et al. (2021). The tetrameric structure of the novel haloalkane dehalogenase DpaA from Paraglaciecola agarilytica NO_2. *Acta Crystallogr. D Struct. Biol.* 77, 347–356. doi: 10.1107/S2059798321000486

Mena-Benitez, G. L., Gandia-Herrero, F., Graham, S., Larson, T. R., McQueen-Mason, S. J., French, C. E., et al. (2008). Engineering a catabolic pathway in plants for the degradation of 1,2-dichloroethane. *Plant Physiol.* 147, 1192–1198. doi: 10.1104/pp.108.119008

Merrill, R. A., Song, J., Kephart, R. A., Klomp, A. J., Noack, C. E., and Strack, S. (2019). A robust and economical pulse-chase protocol to measure the turnover of HaloTag fusion proteins. *J. Biol. Chem.* 294, 16164–16171. doi: 10.1074/jbc.RA119.010596

Minner-Meinen, R., Weber, J. N., Albrecht, A., Matis, R., Behnecke, M., Tietge, C., et al. (2021). Split-HaloTag® imaging assay for sophisticated microscopy of protein-protein interactions in planta. *Plant Commun.* 2:100212. doi: 10.1016/j.xplc.2021.100212

Mohamed, E., Mohamed, J., Huyop, F., Wahab, R., and Abdul-Hamid, H. (2020). Developing herbicide tolerant transgenic plants for sustainable weed management. *Int. J. Emerg. Trends Eng. Res.* 8, 60–66. doi: 10.30534/ijeter/2020/0981.22020

Muzikár, M., Kresinová, Z., Svobodová, K., Filipová, A., Cvančarová, M., Cajthamlová, K., et al. (2011). Biodegradation of chlorobenzoic acids by ligninolytic fungi. *J. Hazard. Mater.* 196, 386–394. doi: 10.1016/j.jhazmat.2011.09.041

Narayanan, H., Dingfelder, F., Butt,é, A., Lorenzen, N., Sokolov, M., and Arosio, P. (2021). Machine Learning for biologics: opportunities for protein engineering, developability, and formulation. *Trends Pharmacol. Sci.* 42, 151–165. doi: 10.1016/j.tips.2020.12.004

Nardi-Dei, V., Kurihara, T., Park, C., Miyagi, M., Tsunasawa, S., Soda, K., et al. (1999). DL-2-Haloacid dehalogenase from *Pseudomonas* sp. 113 is a new class of dehalogenase catalyzing hydrolytic dehalogenation not involving enzyme-substrate ester intermediate. *J. Biol. Chem.* 274, 20977–20981. doi: 10.1074/jbc.274.30.20977

Nguyen, B. T., Hsieh, J. L., Lo, S. C., Wang, S. Y., Hung, C. H., Huang, E., et al. (2021). Biodegradation of dioxins by *Burkholderia cenocepacia* strain 869T2: role of 2-haloacid dehalogenase. *J. Hazard. Mater.* 401:123347. doi: 10.1016/j.jhazmat.2020.123347

Novak, H., and Littlechild, J. (2013). "Marine enzymes with applications for biosynthesis of fine chemicals," in *Marine Enzymes for Biocatalysis*, ed A. Trincone (Sawston: Woodhead Publishing), 89–106.

Novak, H. R., Sayer, C., Isupov, M. N., Paszkiewicz, K., Gotz, D., Spragg, A. M., et al. (2013a). Marine *Rhodobacteraceae* L-haloacid dehalogenase contains a novel His/Glu dyad that could activate the catalytic water. *FEBS J.* 280, 1664–1680. doi: 10.1111/febs.12177

Novak, H. R., Sayer, C., Panning, J., and Littlechild, J. A. (2013b). Characterisation of an L-haloacid dehalogenase from the marine psychrophile *Psychromonas ingrahamii* with potential industrial application. *Mar. Biotechnol.* 15, 695–705. doi: 10.1007/s10126-013-9522-3

Oyewusi, H. A., Huyop, F., and Wahab, R. A. (2020a). Molecular docking and molecular dynamics simulation of *Bacillus thuringiensis* dehalogenase against haloacids, haloacetates and chlorpyrifos. *J. Biomol. Struct. Dyn.* 38, 1–16. doi: 10.1080/07391102.2019.1580616

Oyewusi, H. A., Huyop, F., Wahab, R. A., and Hamid, A. A. A. (2021a). *In silico* assessment of dehalogenase from Bacillus thuringiensis H2 in relation to its salinity-stability and pollutants degradation. *J. Biomol. Struct. Dyn.* 39, 1–15. doi: 10.1080/07391102.2021.1927846

Oyewusi, H. A., Wahab, R. A., and Huyop, F. (2020b). Dehalogenase-producing halophiles and their potential role in bioremediation. *Mar. Pollut. Bull.* 160:111603. doi: 10.1016/j.marpolbul.2020.111603

Oyewusi, H. A., Wahab, R. A., and Huyop, F. (2021b). Whole genome strategies and bioremediation insight into dehalogenase-producing bacteria. *Mol. Biol. Rep.* 48, 2687–2701. doi: 10.1007/s11033-021-06239-7

Park, C., Kurihara, T., Yoshimura, T., Soda, K., and Esaki, N. (2003). A new DL-2-haloacid dehalogenase acting on 2-haloacid amides: purification, characterization, and mechanism. *J. Mol. Catal. B Enzym.* 23, 329–336. doi: 10.1016/S1381-1177(03)00096-1

Parker, K., and Colby, J. (1995). Immobilisation of the D-2-haloacid dehalogenase from *Pseudomonas putida* strain AJ1/23. *Biodegradation* 6, 191–201. doi: 10.1007/BF00700457

Poelarends, G. J., and Whitman, C. P. (2010). "Mechanistic and structural studies of microbial dehalogenases: How nature cleaves a carbon–halogen bond," in *Comprehensive Natural Products II*, ed H. W. Liu and L. Mander (Oxford: Elsevier), 89–123.

Polnisch, E., Kneifel, H., Franzke, H., and Hofmann, K. H. (1991). Degradation and dehalogenation of monochlorophenols by the phenol-assimilating yeast *Candida maltosa*. *Biodegradation* 2, 193–199. doi: 10.1007/BF00124493

Ratnaningsih, E., and Idris, I. (2018). Cloning and expression of haloacid dehalogenase gene from *Bacillus cereus* IndB1. *Indones. J. Biotechnol.* 22, 55–60. doi: 10.22146/ijbiotech.27338

Ridder, I. S., Rozeboom, H. J., Kalk, K. H., Janssen, D. B., and Dijkstra, B. W. (1997). Three-dimensional structure of L-2-haloacid dehalogenase from *Xanthobacter autotrophicus* GJ10 complexed with the substrate-analogue formate. *J. Biol. Chem.* 272, 33015–33022. doi: 10.1074/jbc.272.52.33015

Rosland Abel, S., Ibrahim, N., and Huyop, F. (2012). Identification of *Serratia marcescens* SE1 and determination of its herbicide 2,2-dichloropropionate (2,2-DCP) degradation potential. *Malays. J. Microbiol.* 8, 259–265. doi: 10.21161/mjm.44412

Rye, C. A., Isupov, M. N., Lebedev, A. A., and Littlechild, J. A. (2009). Biochemical and structural studies of a L-haloacid dehalogenase from the thermophilic archaeon *Sulfolobus tokodaii*. *Extremophiles* 13, 179–190. doi: 10.1007/s00792-008-0208-0

Santi, M., Sancineto, L., Nascimento, V., Braun Azeredo, J., Orozco, E. V. M., Andrade, L. H., et al. (2021). Flow biocatalysis: a challenging alternative for the synthesis of apis and natural compounds. *Int. J. Mol. Sci.* 22:990. doi: 10.3390/ijms22030990

Satpathy, R., Konkimalla, V. S. B., and Ratha, J. (2015). *In-silico* gene co-expression network analysis in *Paracoccidioides brasiliensis* with reference to haloacid dehalogenase superfamily hydrolase gene. *J. Pharm. Bioallied Sci.* 7, 212–217. doi: 10.4103/0975-7406.160023

Satpathy, R., Konkimalla, V. S. B., and Ratha, J. (2016). *In silico* phylogenetic analysis and molecular modelling study of 2-haloalkanoic acid dehalogenase enzymes from bacterial and fungal origin. *Adv. Bioinform.* 2016, 8701201–8701201. doi: 10.1155/2016/8701201

Schmidberger, J. W., Wilce, J. A., Tsang, J. S. H., and Wilce, M. C. J. (2007). Crystal structures of the substrate free-enzyme, and reaction intermediate of the HAD superfamily member, haloacid dehalogenase DehIVa from *Burkholderia cepacia* MBA4. *J. Mol. Biol.* 368, 706–717. doi: 10.1016/j.jmb.2007.02.015

Schmidberger, J. W., Wilce, J. A., Weightman, A. J., Whisstock, J. C., and Wilce, M. C. (2008). The crystal structure of DehI reveals a new alpha-haloacid dehalogenase fold and active-site mechanism. *J. Mol. Biol.* 378, 284–294. doi: 10.1016/j.jmb.2008.02.035

Schober, M., and Faber, K. (2013). Inverting hydrolases and their use in enantioconvergent biotransformations. *Trends Biotechnol.* 31, 468–478. doi: 10.1016/j.tibtech.2013.05.005

Sengupta, S., Das, P., and Datta, S. (2020). "Fermentative production of optically pure lactic acid from renewable materials," in *Encyclopedia of Renewable and Sustainable Materials*, ed S. Hashmi and I. A. Choudhury (Oxford: Elsevier), 447–453.

Shahar, H., Tan, L. L., Ta, G. C., and Heng, L. Y. (2019a). Detection of halogenated hydrocarbon pollutants using enzymatic reflectance biosensor. *Sensors Actuat. B Chem.* 281, 80–89. doi: 10.1016/j.snb.2018.10.076

Shahar, H., Tan, L. L., Ta, G. C., and Heng, L. Y. (2019b). Optical enzymatic biosensor membrane for rapid in situ detection of organohalide in water samples. *Microchem. J.* 146, 41–48. doi: 10.1016/j.microc.2018.12.052

Siwek, A., Omi, R., Hirotsu, K., Jitsumori, K., Esaki, N., Kurihara, T., et al. (2013). Binding modes of DL-2-haloacid dehalogenase revealed by crystallography, modeling and isotope effects studies. *Arch. Biochem. Biophys.* 540, 26–32. doi: 10.1016/j.abb.2013.09.012

Smith, J. M., Harrison, K., and Colby, J. (1990). Purification and characterization of D-2-haloacid dehalogenase from *Pseudomonas putida* strain AJ1/23. *J. Gen. Microbiol.* 136, 881–886. doi: 10.1099/00221287-136-5-881

Soda, K., Kurihara, T., Liu, J. Q., NardiDei, V., Park, C., Miyagi, M., et al. (1996). Bacterial 2-haloacid dehalogenases: structures and catalytic properties. *Pure Appl. Chem.* 68, 2097–2103. doi: 10.1351/pac199668112097

Su, X., Deng, L., Kong, K. F., and Tsang, J. S. (2013). Enhanced degradation of haloacid by heterologous expression in related Burkholderia species. *Biotechnol. Bioeng.* 110, 2687–2696. doi: 10.1002/bit.24917

Sudi, I. Y., Hamid, A. A., Shamsir, M. S., Jamaluddin, H., Wahab, R. A., and Huyop, F. (2014). Insights into the stereospecificity of the D-specific dehalogenase from *Rhizobium* sp. RC1 toward D- and L-2-chloropropionate. *Biotechnol. Biotechnol. Equip.* 28, 608–615. doi: 10.1080/13102818.2014.937907

Tanokura, M., Miyakawa, T., Guan, L., and Hou, F. (2015). Structural analysis of enzymes used for bioindustry and bioremediation. *Biosci. Biotech. Biochem.* 79, 1391–1401. doi: 10.1080/09168451.2015.1052770

Taylor Stephen, C. (1985). *D-2-haloalkanoic acid halidohydrolase. US19850789765*. U.S. Patent.

Thippeswamy, M., Rajasrerlatha, V., Shubha, D., and Niveditha, B. T. (2021). "Chapter 24- Metagenomics and future perspectives in discovering pollutant degrading enzymes from soil microbial communities," in *Recent Developments in Applied Microbiology and Biochemistry*, ed B. Viswanath (Cambridge, MA: Academic Press), 257–267.

Tunyasuvunakool, K., Adler, J., Wu, Z., Green, T., Zielinski, M., Žídek, A., et al. (2021). Highly accurate protein structure prediction for the human proteome. *Nature* 596, 1–9. doi: 10.1038/s41586-021-03828-1

van der Ploeg, J., van Hall, G., and Janssen, D. B. (1991). Characterization of the haloacid dehalogenase from *Xanthobacter autotrophicus* GJ10 and sequencing of the dhlB gene. *J. Bacteriol.* 173, 7925–7933. doi: 10.1128/jb.173.24.7925-7933.1991

Vrancken, J. P. M., Tame, J. R. H., and Voet, A. R. D. (2020). Development and applications of artificial symmetrical proteins. *Comput. Struct. Biotechnol. J.* 18, 3959–3968. doi: 10.1016/j.csbj.2020.10.040

Wahhab, B., Anuar, N., Wahab, R., Al-Nimer, M., Samsulrizal, N., Abdul Hamid, A., et al. (2020). Characterization of a 2,2-dichloropropionic acid (2,2-DCP) degrading alkalotorelant *Bacillus megaterium* strain BHS1 isolated from blue lake in turkey. *J. Trop. Life Sci.* 10, 245–252. doi: 10.11594/jtls.10.03.08

Wang, C., Xi, J., Hu, H. Y., and Wen, X. (2009). Biodegradation of gaseous chlorobenzene by white-rot fungus *Phanerochaete chrysosporium*. *Biomed. Environ. Sci.* 21, 474–478. doi: 10.1016/S0895-3988(09)60005-2

Wang, S., Cheng, Z., Xu, Y., Yang, L., Wang, J. B., Tian, Z., et al. (2020). Structure-guided protein design of fluoroacetate dehalogenase for kinetic resolution of *rac*-2-bromobutyric acid. *Green Synth. Catal.* 1, 60–65. doi: 10.1016/j.gresc.2020.05.004

Wang, Y., Cao, X., Feng, Y., and Xue, S. (2016). Environment-induced conformational and functional changes of L-2-haloacid dehalogenase. *J. Biosci. Bioeng.* 121, 491–496. doi: 10.1016/j.jbiosc.2015.09.008

Wang, Y., Feng, Y., Cao, X., Liu, Y., and Xue, S. (2018). Insights into the molecular mechanism of dehalogenation catalyzed by D-2-haloacid dehalogenase from crystal structures. *Sci. Rep.* 8:1454. doi: 10.1038/s41598-017-19050-x

Wang, Y., Xue, S., Zhou, Q., and Pei, D. (2020). Recent progress in 2-haloacid dehalogenases. *Chin. J. Biotechnol.* 36, 868–878. doi: 10.13345/j.cjb.190370

Watanabe, S., Ito, M., and Kigawa, T. (2021). DiRect: Site-directed mutagenesis method for protein engineering by rational design. *Biochem. Biophys. Res. Co* 551, 107–113. doi: 10.1016/j.bbrc.2021.03.021

Weightman, A. J., Weightman, A. L., and Slater, J. H. (1982). Stereospecificity of 2-monochloropropionate dehalogenation by the two dehalogenases of *Pseudomonas putida* PP3: evidence for two different dehalogenation mechanisms. *Microbiology* 128, 1755–1762. doi: 10.1099/00221287-128-8-1755

Woolfson, D. N. (2021). A brief history of *de novo* protein design: minimal, rational, and computational. *J. Mol. Biol.* doi: 10.1016/j.jmb.2021.167160. [Epub ahead of print].

Wu, L., Qin, L., Nie, Y., Xu, Y., and Zhao, Y.-L. (2021). Computer-aided understanding and engineering of enzymatic selectivity. *Biotechnol. Adv.* doi: 10.1016/j.biotechadv.2021.107793. [Epub ahead of print].

Wu, Q., Bouwman, H., Uren, R. C., van der Lingen, C. D., and Vetter, W. (2019). Halogenated natural products and anthropogenic persistent organic pollutants in chokka squid (*Loligo reynaudii*) from three sites along the South Atlantic and Indian Ocean coasts of South Africa. *Environ. Pollut.* 255:113282. doi: 10.1016/j.envpol.2019.113282

Xie, G., Pan, D., He, W., and Gao, G. (2015). Application of L-2-haloacid dehalogenase from thermophilic Archaea Sulfolobus tokodaii in the production of D-lactic acid. *Chem. J. Chinese Univ.* 36, 698–703. doi: 10.7503/cjcu20140739

Xiong, W., Liu, B., Shen, Y., Jing, K., and Savage, T. R. (2021). Protein engineering design from directed evolution to *de novo* synthesis. *Biochem. Eng. J.* 174:108096. doi: 10.1016/j.bej.2021.108096

Xu, S., Qin, S., and Pan, X.-M. (2004). Thermal and conformational stability of Ssh10b protein from archaeon Sulfolobus shibattae. *Biochem. J.* 382, 433–440. doi: 10.1042/BJ20040191

Yavari Maroufi, L., Ghorbani, M., Mohammadi, M., and Pezeshki, A. (2021). Improvement of the physico-mechanical properties of antibacterial electrospun poly lactic acid nanofibers by incorporation of guar gum and thyme essential oil. *Colloid Surface A* 622:126659. doi: 10.1016/j.colsurfa.2021.126659

Yu, F., Li, Y., Wang, H., Peng, T., Wu, Y. R., and Hu, Z. (2021). Microbial debromination of hexabromocyclododecanes. *Appl. Microbiol. Biot.* 105, 4535–4550. doi: 10.1007/s00253-021-11095-3

Zainal Abidin, M. H., Abd Halim, K. B., Huyop, F., Tengku Abdul Hamid, T. H., Abdul Wahab, R., and Abdul Hamid, A. A. (2019). The mechanistic role of active site residues in non-stereo haloacid dehalogenase E (DehE). *J. Mol. Graph. Model.* 90, 219–225. doi: 10.1016/j.jmgm.2019.05.003

Zakary, S., Oyewusi, H., and Huyop, F. (2021). Genomic analysis of mesorhizobium loti strain tono reveals dehalogenases for bioremediation. *J. Trop. Life Sci.* 11, 67–77. doi: 10.11594/jtls.11.01.09

Zhang, C., Allen, K. N., and Dunawaymariano, D. (2018). Mechanism of substrate recognition and catalysis of the haloalkanoic acid dehalogenase family member α-phosphoglucomutase. *Biochemistry* 57, 4504–4517. doi: 10.1021/acs.biochem.8b00396

Zhang, C., Yuan, Z., Liu, Y., Zhang, Q., Chen, Y., Saleem, S., et al. (2021). The online detection of halogenated hydrocarbon in the atmosphere. *Opt Laser Eng* 142:106586. doi: 10.1016/j.optlaseng.2021.106586

Zhang, J., Cao, X., Xin, Y., Xue, S., and Zhang, W. (2013). Purification and characterization of a dehalogenase from *Pseudomonas stutzer*i DEH130 isolated from the marine sponge Hymeniacidon perlevis. *World J. Microbiiol. Biotechnol.* 29, 1791–1799. doi: 10.1007/s11274-013-1340-2

Zhang, J., Jiang, L., Chen, X., Lv, K., Basiony, M., Zhu, G., et al. (2021). Recent advances in biotechnology for marine enzymes and molecules. *Curr. Opin. Biotechnol.* 69, 308–315. doi: 10.1016/j.copbio.2021.05.009

Zhang, J., Xin, Y., Cao, X., Xue, S., and Zhang, W. (2014). Purification and characterization of 2-haloacid dehalogenase from marine bacterium *Paracoccus* sp. DEH99, isolated from marine sponge *Hymeniacidon perlevis*. *J. Ocean Univ. China* 13, 91–96. doi: 10.1007/s11802-014-2357-3

Zhang, M., Shi, Q., Song, X., Wang, H., and Bian, Z. (2019). Recent electrochemical methods in electrochemical degradation of halogenated organics: a review. *Environ. Sci. Pollut. Res. Int.* 26, 10457–10486. doi: 10.1007/s11356-019-04533-3

Zhou, H., Li, Y., Jiang, R., Wang, X., Wang, Y., Xue, Y., et al. (2021). An efficient route towards R-2-phenoxypropionic acid synthesis for biotransformative production of R-2-(4-hydroxyphenoxy) propionic acid. *Chinese J. Chem. Eng.* 32, 315–323. doi: 10.1016/j.cjche.2020.06.013

Conflict of Interest: JX is an employee of Zhengzhou Tuoyang Industrial Co., Ltd.

The remaining authors declare that the research was conducted in the absence of any commercial or financial relationships that could be construed as a potential conflict of interest.

Publisher's Note: All claims expressed in this article are solely those of the authors and do not necessarily represent those of their affiliated organizations, or those of the publisher, the editors and the reviewers. Any product that may be evaluated in this article, or claim that may be made by its manufacturer, is not guaranteed or endorsed by the publisher.

frontiers in Microbiology

ORIGINAL RESEARCH
published: 25 October 2021
doi: 10.3389/fmicb.2021.742300

Characterization and Application of a New β-Galactosidase Gal42 From Marine Bacterium *Bacillus* sp. BY02

Zihan Zhou[1†], Ningning He[1†], Qi Han[1], Songshen Liu[1], Ruikun Xue[1], Jianhua Hao[2,3] and Shangyong Li[1]**

[1] School of Basic Medicine, Qingdao University, Qingdao, China, [2] Key Laboratory of Sustainable Development of Polar Fishery, Ministry of Agriculture and Rural Affairs, Yellow Sea Fisheries Research Institute, Chinese Academy of Fishery Sciences, Qingdao, China, [3] Jiangsu Collaborative Innovation Center for Exploitation and Utilization of Marine Biological Resource, Lianyungang, China

β-Galactosidase plays an important role in medicine and dairy industry. In this study, a new glycoside hydrolase family 42 (GH42) β-galactosidase-encoding gene, *gal42*, was cloned from a newly isolated marine bacterium *Bacillus* sp. BY02 and expressed in *Escherichia coli*. Structural characterization indicated that the encoding β-galactosidase, Gal42, is a homotrimer in solution, and homology modeling indicated that it retains the zinc binding sites of the Cys cluster. The reaction activity of Gal42 was significantly increased by Zn^{2+} (229.6%) and other divalent metal ions (Mn^{2+}, Mg^{2+}, and Co^{2+}), while its activity was inhibited by EDTA (53.9%). Meanwhile, the thermo-stability of the Gal42 was also significantly enhanced by 5 and 10 mM of zinc ion supplement, which suggested that the "Cys-Zn" motif played important roles in both structural stability and catalytic function. Furthermore, Gal42 showed effective lactose hydrolysis activity, which makes the enzyme hydrolyze the lactose in milk effectively. These properties make Gal42 a potential candidate in food technology.

Keywords: β-galactosidase, glycoside hydrolase family 42, *Bacillus* sp. BY02, lactose hydrolysis, zinc ion

OPEN ACCESS

Edited by:
Benwei Zhu,
Nanjing Tech University, China

Reviewed by:
Carlos Vera Vera,
Universidad de Santiago de Chile, Chile
Xinjun Yu,
Zhejiang University of Technology, China

***Correspondence:**
Jianhua Hao
haojh@ysfri.ac.cn
Shangyong Li
lisy@qdu.edu.cn

[†]These authors have contributed equally to this work

Specialty section:
This article was submitted to Microbiotechnology, a section of the journal Frontiers in Microbiology

Received: *16 July 2021*
Accepted: *16 September 2021*
Published: *25 October 2021*

Citation:
Zhou Z, He N, Han Q, Liu S, Xue R, Hao J and Li S (2021) Characterization and Application of a New β-Galactosidase Gal42 From Marine Bacterium Bacillus sp. BY02. Front. Microbiol. 12:742300. doi: 10.3389/fmicb.2021.742300

INTRODUCTION

Currently, lactose intolerance is one of the most common nutritional disorders, with 70% of the world's population affected by it (Horner et al., 2011; Di Costanzo and Berni Canani, 2018). The undigested lactose is fermented by colonic bacteria to produce gas and other by-products, leading to bloating cramps and diarrhea (Silberman and Jin, 2019). Removal of lactose from milk by the conversion of lactose to D-glucose and D-galactose is of great value for lactose-intolerant people.

β-Galactosidase (EC 3.2.1.23), also referred to as lactase, is an important member of glycosyl hydrolase, which can hydrolyze *O*-glycosidic bonds of lactose by hydrolysis reaction, resulting in the production of glucose and galactose (Vera et al., 2017; Singh et al., 2019). Treating dairy products with β-galactosidase through pre-hydrolyzation that can reduce lactose concentration offers a promising solution (Li et al., 2020). Thus far, numerous β-galactosidases were purified, cloned, and characterized from bacteria (Mavromatis et al., 2010; Tian et al., 2013), fungi (Rico-Díaz et al., 2017), yeast (de Freitas et al., 2020), plants (Deng et al., 2019), and mammals (He et al., 2008). Among all sources, microbial β-galactosidases have drawn extensive attraction due to their high yields, high activity, and abundance (Oliveira et al., 2011). In our previous research, a new β-galactosidase gene (*gal2A*) was cloned from the marine bacterium *Alteromonas* sp. QD01

and can be expressed in *Escherichia coli* (Li et al., 2020). According to the specific features of the sequence and reaction mechanism, β-galactosidases are classified as glycoside hydrolase (GH) families 1, 2, 35, 39, 42, 59, 147, and 165 in carbohydrate-active enzyme families.[1] Among them, GH families 1, 2, and 35 contain many different types of polysaccharide-degrading enzymes, which can degrade different substrates. However, most of the enzymes belonging to GH family 42 (GH42) are β-galactosidase. Structurally, the GH family 42 representatives consist of three domains (Maksimainen et al., 2012). The first domain is a catalytic domain containing (α/β) eight barrels and two glutamic acid residues. The two highly conserved residues in all GH42 β-galactosidases act as an acid/base catalyst and a nucleophilic site (Barrangou et al., 2009). The second domain involves the trimer formation. The third domain forms a small β-barrel, and the function of domain C is unknown. In many cases, the applications of GH42 β-galactosidases are limited by their low activity, low thermal stability, or high inhibition by reaction products (Panesar et al., 2010; Zhang et al., 2018).

In this study, a new β-galactosidase encoding gene, *gal42*, was cloned from marine bacterium *Bacillus* sp. BY02 and expressed in *E. coli*. The recombinant β-galactosidase, Gal42, is a potential candidate in the production of lactose-free foods.

MATERIALS AND METHODS

Materials

The *E. coli* strains, BL21 (DE3), and expression vector, pET28a(+), were purchased from Takara (Dalian, China). *O*-Nitrophenol (ONP) and *o*-nitrophenyl-β-D-galactopyranoside (ONPG) were purchased from Sangon Biotech (Shanghai, China). Lactose, glucose, and galactose used for this study were supplied by Solarbio (Beijing, China). The thin-layer chromatography (TLC) silica gel plates were purchased from Merck (Darmstadt, Germany). All other materials used were of the analytical degree.

Isolation and Identification of *Bacillus* sp. BY02

The seawater samples were isolated and obtained from the surface of Yellow Sea sediment (depth 20 m, 120.16° E 35.01° N). They were diluted to 10 times then spread and cultured on Zobell 2216E medium (5.0 g of peptone, 1.0 g of yeast extract, 0.01 g of iron phosphate, 16.0 g of agar, and 1,000 ml of natural seawater were placed in the dark for several weeks, and the pH was adjusted to 7.6–7.8). A few strains that were positive were isolated after incubation at 25°C for 7 days. In order to identify which one can produce β-galactosidase, the selective medium [1% (w/v) peptone, 1% (w/v) yeast extract, 0.5% (w/v) lactose, 2% (w/v) NaCl, 0.004% (w/v) X-gal, and 1.5% (w/v) agar, pH 7.0] was used to culture and screen the strain. Among them, strain BY02 with high activity was collected and used for a further study. According to the 16S rRNA gene sequence analysis, strain BY02 was identified as a member of genus *Bacillus*. In order to evaluate the influence of lactose and glucose on the expression of β-galactosidase, strain BY02 was cultured on three kinds of medium (with 2% glucose, 2% lactose, 2% glucose, and lactose) for 3 days at 25°C.

Sequence Analysis

The gene for β-galactosidase was amplified from the genome of *Bacillus* sp. BY02. The open reading frame (ORF) finder in the National Center for Biotechnology Information (NCBI)[2] was used to identify the ORFs. SignalP-5.0 server was used to analyze the signal peptide of the amino acid sequence.[3] ExPASy was used to calculate the theoretical isoelectric point (pI) and molecular weight (Mw) of Gal42.[4] Conserved Domain Database (CDD) was used to improve the phylogenetic analysis. In addition, a BLAST algorithm program was performed to search similar sequences for Gal42. The ESPript[5] and ClustalX program were used for multiple comparison analysis of Gal42 and BCA-β-Gal (PDB ID: 3TTS). MEGA 7.0 software was used to construct the evolutionary tree.

Molecular Modeling

The three-dimensional (3D) structure of Gal42 was built by homology modeling using the SWISS MODEL.[6] The crystalline structure of β-galactosidase from *Bacillus circulans* sp. *alkalophilus* (PDB ID: 3TTS) with sequence identity of 64.36% was chosen as the template. The Global Model Quality Estimation (GMQE) and Qualitative Model Energy Analysis (QMEAN) values for the homology model were calculated to evaluate the model quality and reliability. Pymol (version 2.4.1) was used to visualize the 3D structure, build organization graphics, and draw illustrations.

Expression and Purification of Recombinant β-Galactosidase

gal42 gene was synthesized by Synbio Technologies (Suzhou, China) and inserted into corresponding sites of plasmid pET-28a(+) between the recognition sites *Nco*I and *Xho*I. After the recombination, the plasmid was expressed in *E. coli* BL21 (DE3), which was cultured in Terrific Broth (TB) medium containing 30 μg/ml of kanamycin at 37°C until the optical density at 600 nm ($OD_{(600)}$) reached 0.6–0.8. Afterward, the addition of 0.1 mM of isopropyl β-D-thiogalactoside (IPTG) was performed to induce the expression of the target protein at 20°C and 200 rpm for 36 h. The target β-galactosidase was purified and harvested in AKTA150 FPLC system using Ni-NTA Sepharose affinity column (5 ml His-Trap™ High Performance, GE Healthcare, Madison, WI, United States). The supernatant that was obtained by the crude enzyme incubated in 50 mM of phosphate buffer (pH 7.6) was centrifuged for 10 min at 12,000 rpm. After sonication at ice condition (150 W, 2-s burst, and 2-s stop, 30 min), the obtained supernatant was loaded into the previously equilibrated affinity column. Then, the washing

[1] www.cazy.org

[2] https://www.ncbi.nlm.nih.gov/orffinder/

[3] http://www.cbs.dtu.dk/services/SignalP/

[4] https://web.expasy.org/cgibin/protparam/protparam

[5] http://espript.ibcp.fr/ESPript/ESPript/

[6] https://swissmodel.expasy.org/

buffer (20 mM of imidazole, 20 mM of phosphate buffer, and 500 mM of NaCl, pH 7.6) was used to deplete proteins other than target proteins. The target protein was eluted by elution buffer (150 mM of imidazole, 20 mM of phosphate buffer, and 500 mM of NaCl, pH 7.6). Mw and purity of the enzymes were assayed by 10% sodium dodecyl sulfate–polyacrylamide gel electrophoresis (SDS-PAGE), and the protein concentration was determined by the bicinchoninic acid (BCA) protein assay kit (Beyotime Biotechnology, Shanghai, China). In brief, protein samples (2 μg) were resolved by 10% SDS-PAGE (the voltage of 75 V for concentrated glue and 120 V for separating glue), and Coomassie brilliant blue was used for staining.

Activity Assay

The activity of β-galactosidase can be reflected by the production of ONP using ONPG as substrate. Briefly, 50 μl of diluted enzyme sample was mixed with 450 μl of 10 mM ONPG solution (20 mM of phosphate buffer, pH 7.0). Then, the reaction system was incubated at 40°C for 10 min and stopped by adding 500 μl of Na_2CO_3 (1 M). Furthermore, the released ONP was measured at 420 nm. Under the experimental conditions, one unit (U) of β-galactosidase activity was defined as the amount of enzyme required to release 1 μmol of ONP per minute (Li et al., 2019).

Effect of Temperature, pH, Metal Ions, and Chelators on β-Galactosidase Activity

In order to determine the optimal temperature of the Gal42, substrate reactions for Gal42 and ONPG were carried out at different temperature ranging from 0 to 70°C. To determine the thermal stability of Gal42, the residual activity was measured after incubation at 0–70°C for 60 min. To examine the optimal pH, substrates for Gal42 and ONPG were carried out in Britton–Robinson buffers at pH 5.11–10.42. To determine the pH stability of Gal42, the residual enzyme activity was measured after Gal42 was cultured in buffers with different pH values at 4°C for 12 h. By monitoring the enzyme activity in the presence of different cations [using 1 mM of $BaCl_2$, $FeSO_4$, $CaCl_2$, $CuSO_4$, $FeCl_3$, KCl, $MnCl_2$, $Al_2(SO_4)_3$, $CoCl_2$, NaCl, $(NH_4)_2SO_4$, NiCl, $MgSO_4$, Li_2SO_4, and $ZnSO_4$ in 20 mM of phosphate buffer] or chelating agents (1 mM of ethylenediamine tetraacetic acid (EDTA) and SDS), the effects of metal ions and chelating agents on Gal42 activity were determined as previously. Meanwhile, the effects of different concentrations of zinc ions (1, 5, and 10 mM) on optimal temperature and thermal stability were also detected according to the above conditions.

Reaction Product Analysis

The reaction product of Gal42 in lactose and milk was determined by TLC. Briefly, 900 μl of lactose (5 mg/ml) and 100 μl of Gal42 were mixed and incubated under pH 8.0 at 40°C for 480 min. The reaction products were collected and boiled for 10 min at different time points (0, 1, 10, 30, 60, 360, and 480 min) to inactivate the enzyme. After that, 4 μl of sample from each time point was spotted in a horizon line on the silica gel TLC plate, and the plate was developed with a 3:2:5 (by vol.) mixture of glacial acetic acid, water, and 1-butanol. Later, after drying, the plate was treated with a 9:1 mixture of atomized ethanol and sulfuric acid. Heat the plate for 30 min at a temperature of 80°C, and the hydrolyzed products could be observed. The hydrolyzed products of lactose in drinking milk (4.2–5.0% lactose) (Inner Mongolia Mengniu Dairy Group Co., Ltd., Hohhot, China) was also observed by using the method described above. The diluted milk was mixed with enzymes, sampled at the same point, and then analyzed by TLC method, with galactose as the standard. Negative-ion electrospray ionization–mass spectrometry (ESI-MS) system (Thermo Fisher Scientific™ Q Exactive™ Hybrid Quadrupole-Orbitrap™, Waltham, MA, United States) was employed to further investigate the composition of the reaction products. The instrument conditions were syringe pump injection-flow rate 50 μl/min, sheath gas 15 L/min, auxiliary gas 5 L/min, auxiliary gas temperature 150°C, capillary temperature 300°C, and S-lens voltage 50 V.

Nucleotide Sequence Accession Numbers

The β-galactosidase gene (*gal42*) of strain *Bacillus* sp. BY02 was deposited in GenBank under accession number MW246571.

RESULTS AND DISCUSSION

Isolation and Sequence Analysis

Thus far, several β-galactosidases have been purified and identified from bacteria (Mavromatis et al., 2010; Tian et al., 2013) and fungi (Rico-Díaz et al., 2017), including genus of *Bacillus* (Boon et al., 2000), *Bifidobacterium* (Hsu et al., 2007), and *Aspergillus* (Saqib et al., 2017). However, the productivity of β-galactosidases from natural microbial cells hardly meets the needs of industrial application due to the low yield (Park and Oh, 2010; Oliveira et al., 2011). Boosting the reaction efficiency of β-galactosidases is a precondition for achieving its industrial application. In a previous study, Becerra et al. (2001) has improved the partial secretion percentage of β-galactosidases in the culture medium through directing mutations at the N-terminus of the protein. Gutshall et al. (1995) reported that the β-galactosidase LacG isolated from *Arthrobacter* sp. B7 has a high specific activity. Thus far, the main industrial sources of β-galactosidase are *Aspergillus* sp. and *Kluyveromyces* (de Freitas et al., 2020).

In this study, the marine bacterium *Bacillus* sp. BY02 showed high intracellular β-galactosidase activity (19 U/ml) when grown in the 2216E medium containing 2% lactose. As shown in **Supplementary Figure 1**, it can produce β-galactosidase in the presence of lactose on 2216E X-Gal agar. The genome sequence analysis of *Bacillus* sp. BY02 showed that it contains a putative galactosidase-encoding gene, *gal42*, which consists of an ORF of 2,010 bp. The prepared β-galactosidase Gal42 contains 669 amino acid residues. The predicted Mw and theoretical pI of the expressed β-galactosidase were 78.38 kDa and 4.46, respectively.

A phylogenetic tree was constructed containing Gal42 and other reported β-galactosidases in GH families 1, 2, 35, and 42 (**Figure 1**). In this neighbor-joining tree, Gal42 formed a monophyletic cluster with the β-galactosidase from GH42. In order to further explore the conserved and catalytic domains of Gal42, a multiple sequence alignment was established among Gal42 and other three β-galactosidase, Bca-β-gal from *Bacillus* (GenBank code: QCG73672), BI Gal42A from *Bifidobacterium animalis* subsp. (GenBank code: ACS45863), Bbg II from *Bifidobacterium bifidum* S17 (GenBank code: ADO53518), β-gal II from *Bifidobacterium adolescentis* (GenBank code: AAR2413), and A4-β-Gal from *Thermus thermophilus* A4 (GenBank code: BAA28362) (**Supplementary Figure 2**). According to multiple sequence alignment analysis, the acid/base catalyst site (Glu148) and the nucleophilic site (Glu305) conserved in the GH42 β-galactosidases were also present in the amino acid sequence of Gal42. The further BLAST analysis and comparison with the NCBI CDD clarified Gal42 as a GH42 enzyme, which showed the highest homology with the β-galactosidase from *Neobacillus bataviensis* (GenBank code: TWE08672, 80.45% identity) and the β-galactosidase from *Mesobacillus foraminis* (GenBank code: TCN25424, 79.10% identity). These results indicated that Gal42 is a new member of the GH42 β-galactosidase.

Three-Dimensional Structure Analysis

The structural characterization indicated that the encoding β-galactosidase, Gal42, is a homotrimer in solution. As shown in **Figure 2A**, the 3D structure of Gal42 was constructed using SWISS-MODEL on the basis of homologs of known structure (Bca-β-gal, PDB ID: 3TTS). The GMQE and QMEAN values for the homology model were 0.87 and −3.05, respectively, indicating good model quality and high reliability. The homologous modeling result showed that Gal42 preserved the catalytic sites (Asn147, Glu148, Met304, and Glu305) and zinc binding sites of Cys cluster (Cys11, Cys153, Cys155, and Cys158). According to the sequence logo analysis (**Figure 2B**), two regions, "NEY" (Asn147-Glu148-Tyr149) and "ME" (Met304-Glu305), were conserved in the catalytic cave (Maksimainen et al., 2012). The catalytic residues Glu148 and Glu305 are highly conserved in all GH42 β-galactosidases, which play a role as an acid/base catalyst and a nucleophilic site, respectively (Barrangou et al., 2009). In addition, the Asn147 and Met304

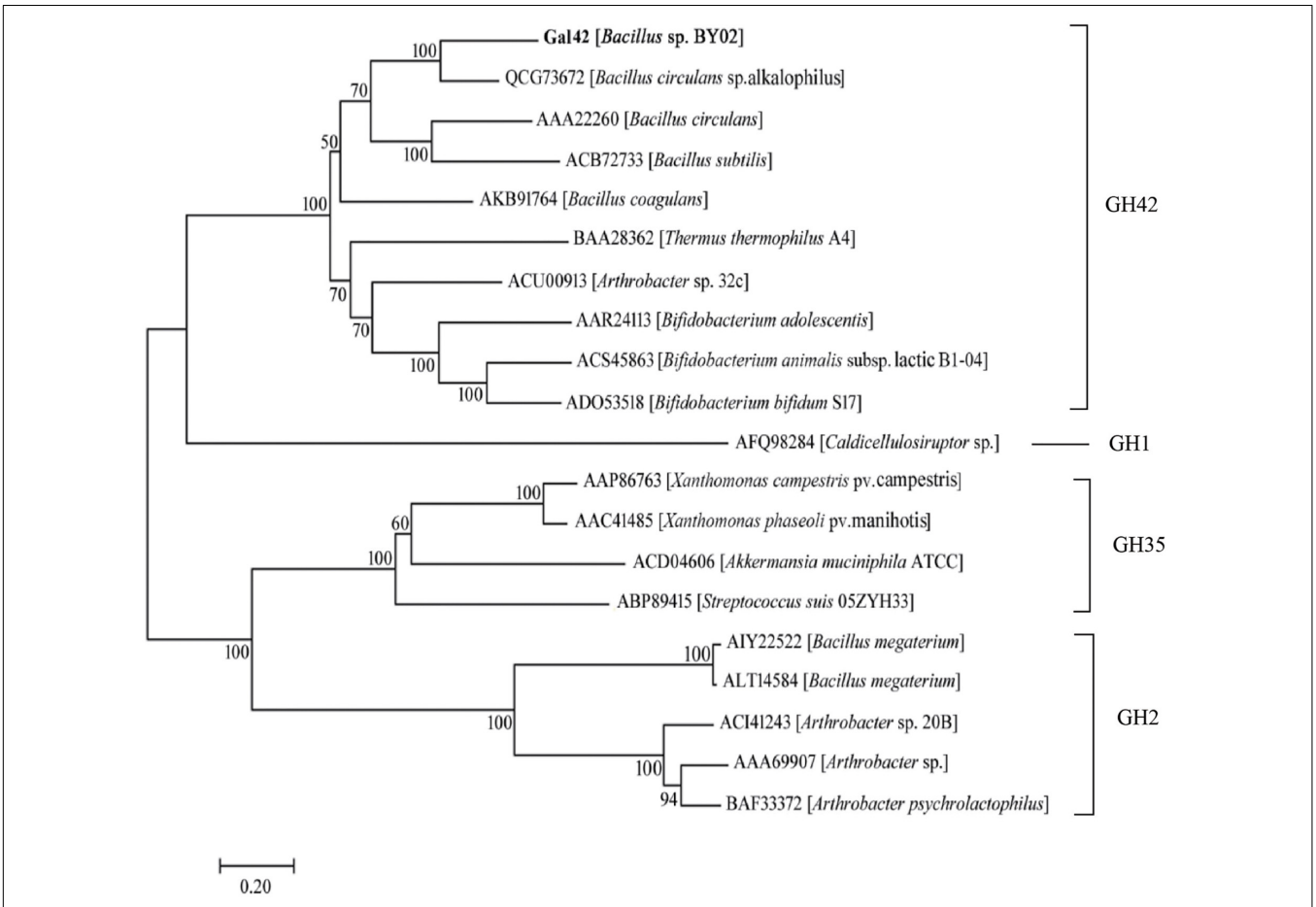

FIGURE 1 | Evolutionary analysis of β-galactosidases. The phylogenetic tree of Gal42 and other β-galactosidases was constructed using the ClustalX program based the reference 16S rDNA sequences, which were collected from the National Center for Biotechnology Information (NCBI) database. The phylogenetic tree (1,000 bootstraps) was constructed using the MEGA 7.0 program *via* neighbor-joining method.

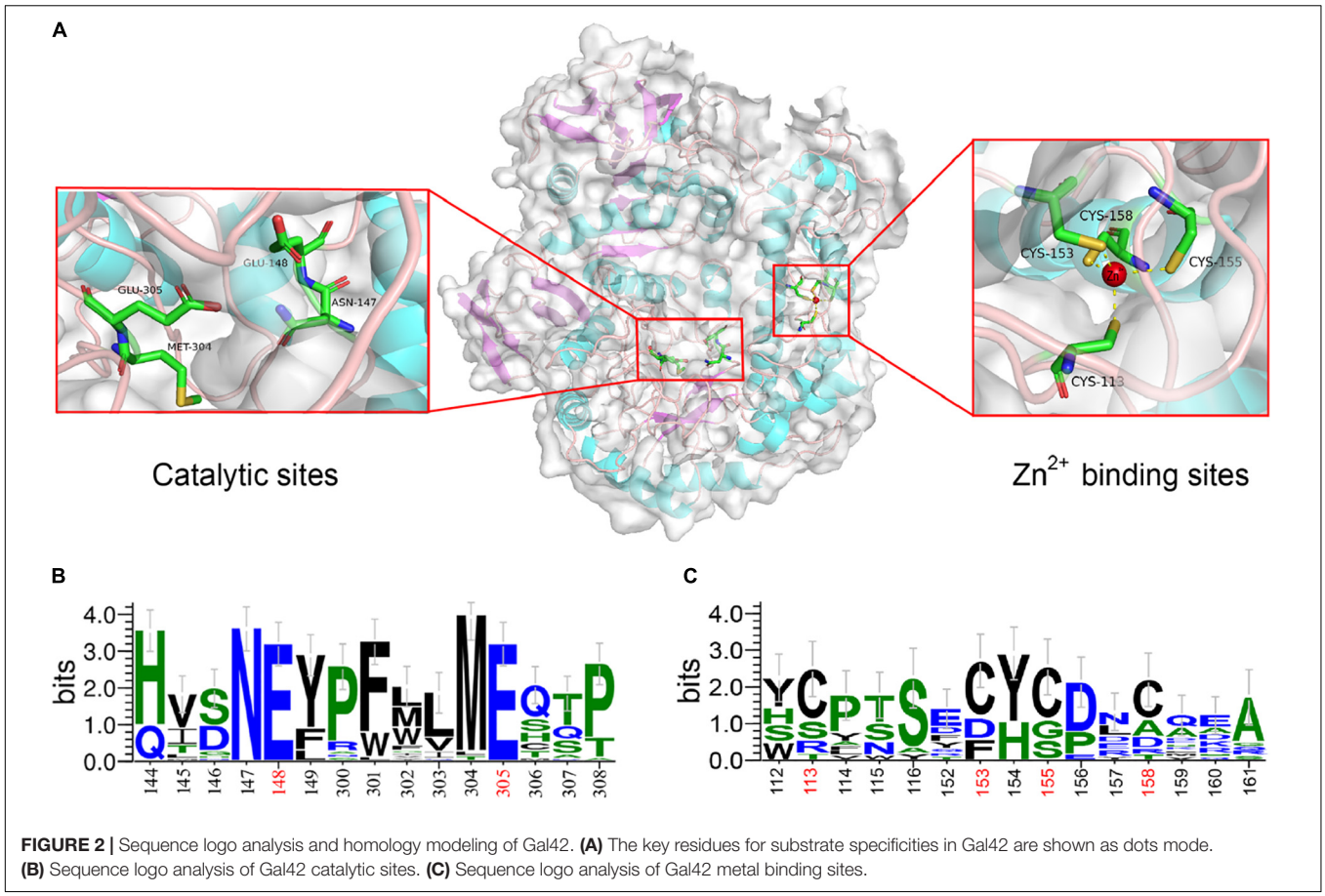

FIGURE 2 | Sequence logo analysis and homology modeling of Gal42. **(A)** The key residues for substrate specificities in Gal42 are shown as dots mode. **(B)** Sequence logo analysis of Gal42 catalytic sites. **(C)** Sequence logo analysis of Gal42 metal binding sites.

preceding the two sites are also highly conserved. Tyr275, which is invariant in GH42, forms a hydrogen bond with the catalytic nucleophile Glu305, consistent with its proposed role as regulator. Trp313 provides aromatic stacking in GH42 and may modulate specificity by adopting different conformations (Hinz et al., 2004). The Zn^{2+} binding sites of Gal42 maintain its zinc coordination function in the Gal42 structure (**Figure 2A**). Meanwhile, as shown in **Figure 2C**, Cys cluster was not conserved in GH42 β-galactosidases, which illustrated that possession of metal binding sites was not a commonality in β-galactosidases.

Purification and Biochemical Characterization

gal42 gene was cloned and overexpressed in *E. coli* BL21(DE3) through the pET28a(+) plasmid. The formed *E. coli* BL21-pET28a-gal42 strain was cultured in Luria Bertani (LB) broth for proliferation and then in TB medium for enzyme production with IPTG. As shown in **Figure 3A**, the β-galactosidases activity of purified Gal42 was up to 217 U/ml, with biomass of 27 g/L at 60 h. The Mw of the purified Gal42 was analyzed by SDS-PAGE and showed to be about 74 kDa with a dominating band (**Figure 3B**), which is consistent with its theoretical Mw (78.38 kDa).

As shown in **Figure 4A**, the optimal reaction temperature of the purified Gal42 was 40°C. In the thermal stability assays, Gal42 was kept stable at 0–30°C (**Figure 4B**). The enzyme remained approximately 50% activity even after 40°C incubation. The optimal pH of Gal42 in Britton–Robinson buffers was determined to be 7.44 (**Supplementary Figure 3A**), which is similar to that of other GH42 β-galactosidases (Hu et al., 2007; Hildebrandt et al., 2009). Additionally, after a 12-h pretreatment in Britton–Robinson buffers at pH 5.11–10.42, the enzyme remained stable at pH 6.0–8.5, with an activity exceeding 60% (**Supplementary Figure 3B**). Especially, the residual activity of Gal42 was nearly 100% of its maximum activity at pH range 7.0–8.0. Compared with a pH-stable β-galactosidase BgaL from *Paracoccus* sp. 32d (Wierzbicka-Woś et al., 2011), Gal42 has shown wider pH-stability range. Considering the neutral pH of milk, β-galactosidase Gal42 was easily utilized and suitable in producing lactose-free milk with its properties mentioned above.

Effect of Zinc Ions on Biochemical Characterization

β-Galactosidase Gal42 contained a zinc binding site of the Cys cluster. Herein, the effect of zinc ions on biochemical characterization of Gal42 was determined (**Figure 4**). In the presence of Zn^{2+}, the enzyme activity of Gal42 was significantly increased at the temperature of 10–60°C. At 40°C, the enzyme activity of Gal42 increased to 119 and 126% with 5 and 10 mM

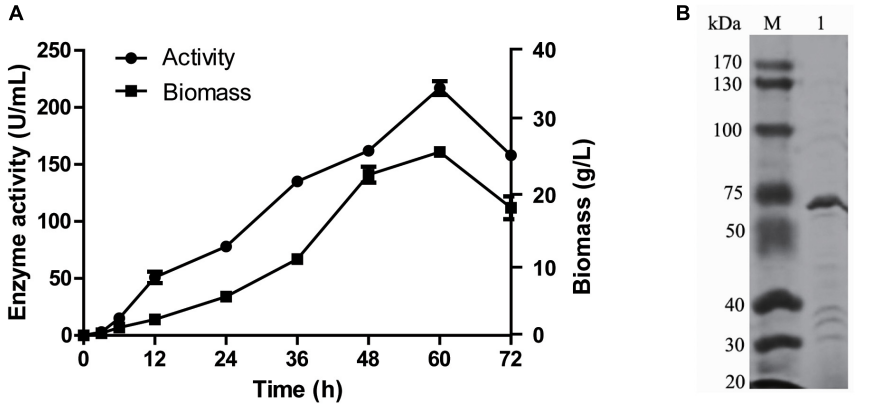

FIGURE 3 | Expression and purification of recombinant Gal42. **(A)** Time curve of Gal42 activity secreted into culture medium. **(B)** Sodium dodecyl sulfate–polyacrylamide gel electrophoresis (SDS-PAGE) analysis of the Gal42. The protein samples were separated by 10% SDS-PAGE gel and stained with Coomassie Blue G-250. Lane M, protein marker; Lane 1, the purified Gal42.

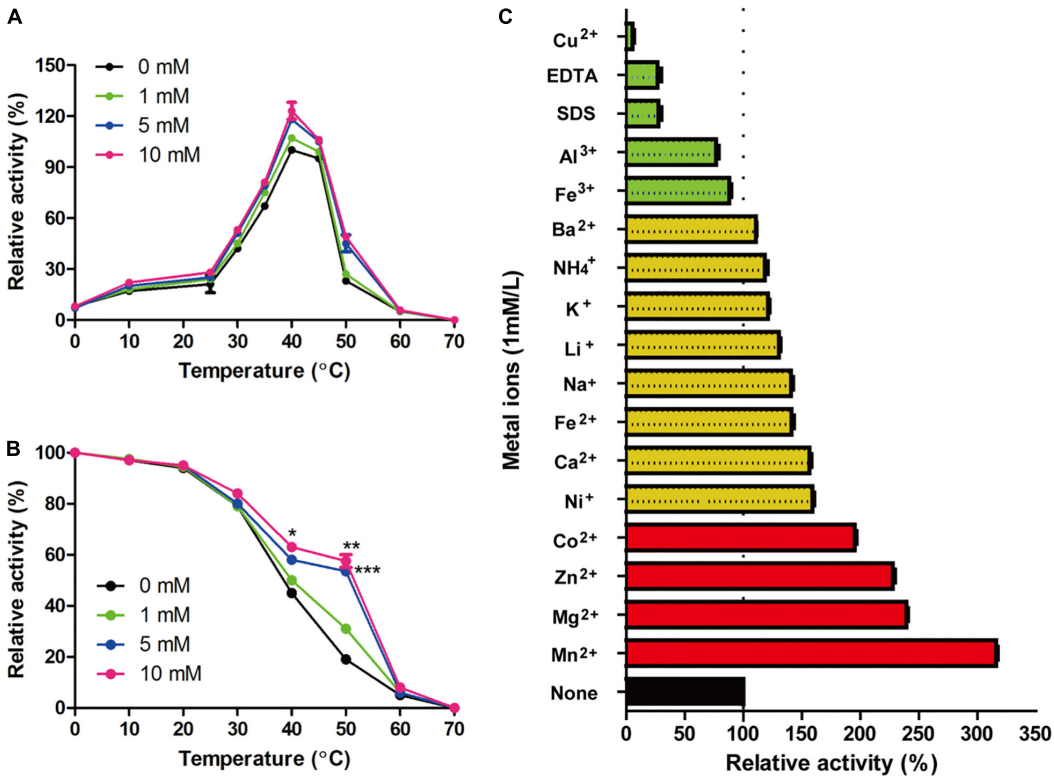

FIGURE 4 | Effect of zinc ions and other metal ions on enzymatic activity of Gal42. **(A)** Effect of zinc ions and temperature on the activity of Gal42. **(B)** Effect of zinc ions on thermo-stability of Gal42. **(C)** Effects of metal ions, EDTA, and SDS on the activity of Gal42. Activity without addition of chemicals was defined as 100%. The values are the mean values ± standard deviations of three experiments in three replicates. $^{*}p < 0.05$; $^{**}p < 0.01$; and $^{***}p < 0.001$.

of zinc ions, respectively. However, the optimal temperature of the Gal42 was not affected by Zn^{2+} (**Figure 4A**). In the presence of 1 mM of Zn^{2+}, the thermo-stability of Gal42 was slightly increased; and in the presence of 5 mM of Zn^{2+}, the thermo-stability of Gal42 was significantly increased on 40 and 50°C ($p < 0.001$). Meanwhile, by increasing the concentration of Zn^{2+} to 10 mM, the activity of Gal42 was not significantly increased anymore (**Figure 4B**). As shown in **Figure 4C**, Cu^{2+}, EDTA, and SDS showed significant inactivation effects on the activity of Gal42. The activity of Gal42 can be activated by Li^{+}, Ba^{2+}, Fe^{2+}, Ca^{2+}, K^{+}, NH_4^{+}, Ni^{+}, and Na^{+}; while it was slightly inhibited by Fe^{3+} and Al^{3+}. More interestingly, Gal42 can be activated not only by Zn^{2+} but also by divalent metal ions (Co^{2+}, Mn^{2+}, and Mg^{2+}). As shown in previous studies,

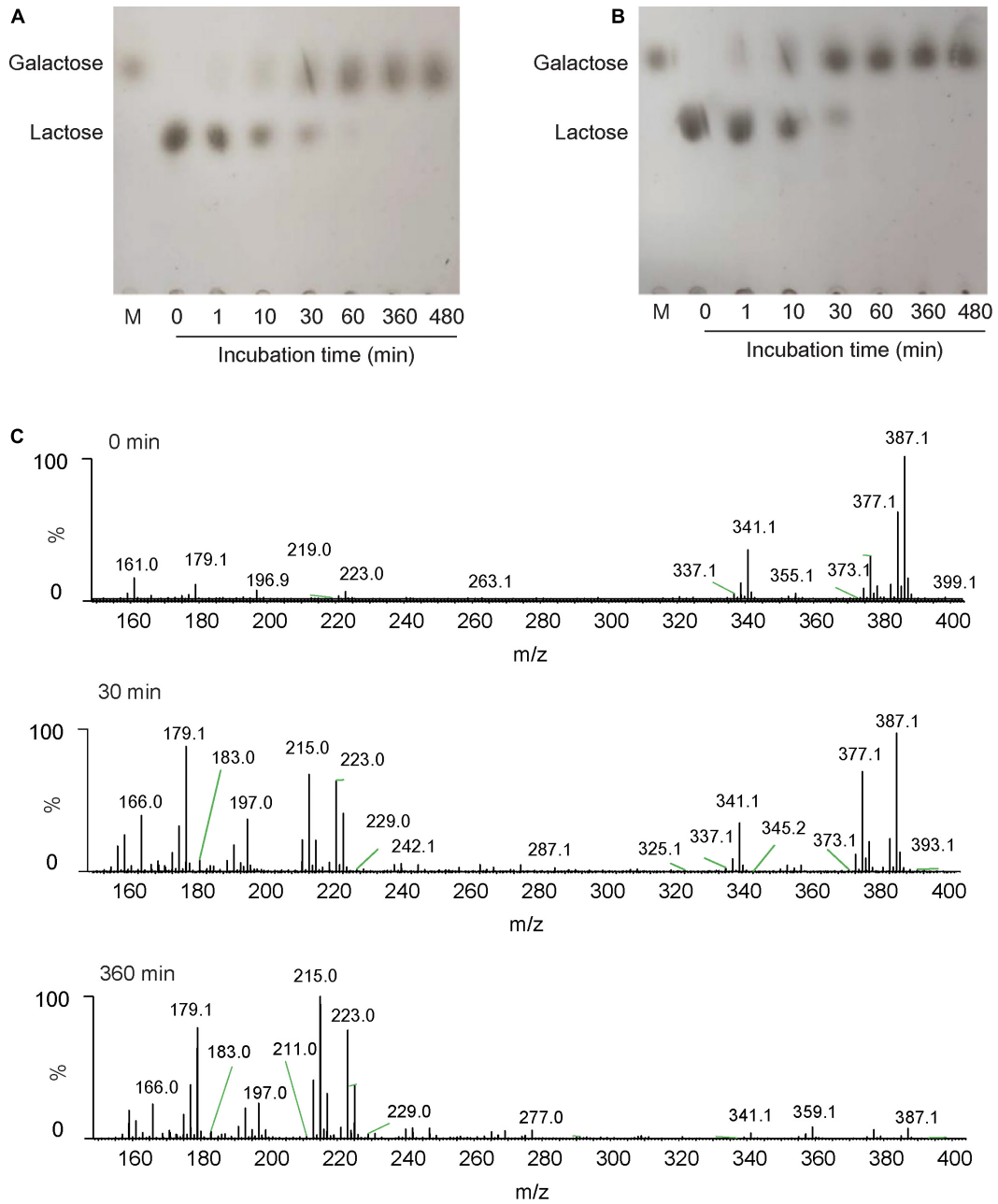

FIGURE 5 | The analysis of action patterns and reaction products for Gal42. **(A)** Thin-layer chromatography (TLC) analysis of Gal42-hydrolyzed lactose. **(B)** TLC analysis of Gal42-hydrolyzed milk. Lane M, standard galactose. **(C)** Electrospray ionization–mass spectrometry (ESI-MS) analysis of reaction products for Gal42 after 0-, 30-, and 360-min incubation.

the metal ions of Mn^{2+}, Mg^{2+}, Zn^{2+}, and Ni^{+} could greatly inhibit the activity of a β-galactosidase from *Alteromonas* sp. ML52 over 32.4% (Sun et al., 2018). The results further showed that zinc ion plays an important role in Gal42, and it is a novel enzyme with different characteristics from other enzymes belonging to GH42.

The presence of ions often affects the activity and stability of β-galactosidase. The β-galactosidase obtained from bacterial strain *Erwinia* sp. E602 (Xia et al., 2018) was also obviously inactivated by Cu^{2+} with about 5% activity. Mg^{2+} and Na^{+} are both required to achieve the maximal activity of the β-galactosidase (Juers et al., 2001). The active site of Mg^{2+} can be substituted by Mn^{2+} without many differences in activity. In this study, Gal42 showed obviously enhancing activity when Mn^{2+} and Mg^{2+} presented, and the presence of Na^{+} also increases the activity of Gal42. Mn^{2+} and Mg^{2+} are beneficial to many reported β-galactosidase activities, such as enzymes from *Pediococcus pentosaceus* and *Pediococcus acidilactici*

(Lee et al., 2017; Chanalia et al., 2018). In the aspect of structural analysis, Mg^{2+} binds to each subunit and has the largest influence on the nearest substrate binding site. It also can modulate the chemistry of active site components (Lo et al., 2010). Another important role of Mg^{2+} is that it can stabilize a mobile loop at the active site through interacting with Glu residue (Sutendra et al., 2007). What is more interesting is, in the presence of Zn^{2+}, the activity and thermo-stability of Gal42 were significantly increased. There are three types Zn^{2+} binding sites in proteins: catalytic, co-catalytic, and structural. Among them, the Zn^{2+} binding is coordinated by four amino acid side chains, including either four cysteines or two histidines in combination with two cysteines (Shumilina et al., 2014). Maksimainen et al. (2012) have demonstrated that Zn^{2+} does not play a role in the catalytic cycle in Bca-β-gal; however, the binding of Zn^{2+} stabilized the structure of the catalytic domain. In the same sense, our experimental results showed that the activity and thermal stability of Gal42 were improved in the presence of zinc ion (**Figure 4**). The improved thermo-stability of Gal42 with the presence of Zn^{2+} may be due to the greatly increased stability of Zn^{2+} binding site (Cys113, Cys153, Cys155, and Cys158) (**Figure 2**).

Analysis of Hydrolysates From Lactose and Milk

In this study, lactose and milk were used as the substrates, and the reaction was carried out for a certain time under the catalysis of Gal42 to detect and analyze the decomposition of lactose. TLC was used to analyze its reaction product. As shown in **Figure 5A**, monosaccharides are formed by hydrolysis of lactose during the reaction. After 360 min, lactose had been fully hydrolyzed into monosaccharides. The reaction products were further identified by negative ESI-MS. As shown in **Figure 5C**, the main peak at 341.1 and 377.1 *m/z* corresponded to lactose, and 179.1 and 223.0 *m/z* corresponded to galactose. These results indicated that the lactose almost fully hydrolyzed into galactose within 360 min.

According to the properties of Gal42, the enzyme activity can be relatively stable in a certain range of pH (covers the pH range of milk). Therefore, it was completely feasible to use Gal42 to hydrolyze lactose in milk in industrial application. In this study, it could be observed that the lactose content in milk can decreased with the enzyme reaction of Gal42. The reaction was completed within 60 min, and all lactose was decomposed into monomers (**Figure 5B**). In conclusion, this characteristic indicates that Gal42 may have a good application prospect in dairy industry.

CONCLUSION

Herein, a new GH42 β-galactosidase-encoding gene was cloned and overexpressed. The recombinant β-galactosidase showed high yield, pH stability, and thermal stability. The "Cys-Zn" motif played important roles in both structural stability and catalytic function. With the present Zn^{2+}, thermo-stability of Gal42 was improved. Furthermore, Gal42 showed high lactose hydrolysis activity, which enables the enzyme to effectively hydrolyze the lactose in milk. These biochemical properties make Gal42 a potential candidate for food technology applications.

DATA AVAILABILITY STATEMENT

The datasets presented in this study can be found in online repositories. The names of the repository/repositories and accession number(s) can be found in the article/ **Supplementary Material**.

AUTHOR CONTRIBUTIONS

ShL and JH designed the experiments. ZZ, NH, QH, and ShL analyzed the data and wrote the main manuscript text. RX and NH carried out three-dimensional modeling and analysis. All authors have read and agreed to the published version of the manuscript.

FUNDING

This research was funded by the National Natural Science Foundation of China (NSFC) (grant number 31900031), the Central Public-interest Scientific Institution Basal Research Fund CAFS (grant number 2020TD67), and the Shandong Provincial Natural Science Foundation (grant number ZR2019BD027).

SUPPLEMENTARY MATERIAL

The Supplementary Material for this article can be found online at: https://www.frontiersin.org/articles/10.3389/fmicb.2021.742300/full#supplementary-material

Supplementary Figure 1 | Effects of glucose and lactose on the expression of β-galactosidase of *Bacillus* sp. BY02. *E. coli* strain BL21(DE3) was used as a control. **(A)** β-galactosidase selective medium with 2% glucose. **(B)** β-galactosidase selective medium with 2% lactose. **(C)** β-galactosidase selective medium with 2% glucose and lactose.

Supplementary Figure 2 | Sequence comparison of Gal42 with related β-galactosidase from GH family 42 and a β-galactosidase (PDB: 3TTS) from *Bacillus circulans* sp. alkalophilus. Identical residues are shaded in red. β-Gal II from *Bifidobacterium adolescentis* (Genbank code: AAR24113); Bca-β-gal from Bacillus *circulans* sp. alkalophilus (Genbank code: QCG73672); Bbg II from *Bifidobacterium bifidum* S17 (Genbank code: ADO53518); BI Gal42a from *Bifidobacterium animalis* subsp. (Genbank code: ACS45863) and A4-β-Gal from *Thermus thermophilus* A4 (Genbank code: BAA28362). The catalytic sites and metal binding sites are labeled in red and black pentagrams, respectively. The black arrows domain structure **(A–C)**.

Supplementary Figure 3 | Effect of pH on Gal42 enzymatic activity. **(A)** Effect of pH on the activity of Gal42 in Britton-Robinson buffers (pH 5.11–10.42); **(B)** pH-stability of Gal42. Gal42 pH stability was incubated at 4°C for 12 h in Britton-Robinson buffers (pH 5.11–10.42), and then residual activity was assayed under normal assay conditions. Values are the mean values ± standard deviations of three experiments in three replicates.

REFERENCES

Barrangou, R., Briczinski, E. P., Traeger, L. L., Loquasto, J. R., Richards, M., Horvath, P., et al. (2009). Comparison of the complete genome sequences of *Bifidobacterium animalis* subsp. Lactis dsm 10140 and bl-04. *J. Bacteriol.* 191, 4144–4151. doi: 10.1128/jb.00155-09

Becerra, M., Prado, S. D., Siso, M. I., and Cerdán, M. E. (2001). New secretory strategies for kluyveromyces lactis beta-galactosidase. *Protein Eng.* 14, 379–386. doi: 10.1093/protein/14.5.379

Boon, M. A., Janssen, A. E., and van 't Riet, K. (2000). Effect of temperature and enzyme origin on the enzymatic synthesis of oligosaccharides. *Enzyme Microb. Technol.* 26, 271–281. doi: 10.1016/s0141-0229(99)00167-2

Chanalia, P., Gandhi, D., Attri, P., and Dhanda, S. (2018). Purification and characterization of β-galactosidase from probiotic pediococcus acidilactici and its use in milk lactose hydrolysis and galactooligosaccharide synthesis. *Bioorg. Chem.* 77, 176–189. doi: 10.1016/j.bioorg.2018.01.006

de Freitas, M. F. M., Hortêncio, L. C., de Albuquerque, T. L., Rocha, M. V. P., and Gonçalves, L. R. B. (2020). Simultaneous hydrolysis of cheese whey and lactulose production catalyzed by β-galactosidase from *kluyveromyces lactis* NRRL Y1564. *Bioprocess. Biosyst. Eng.* 43, 711–722. doi: 10.1007/s00449-019-02270-y

Deng, Z., Pei, Y., Wang, S., Zhou, B., Li, J., Hou, X., et al. (2019). Carboxymethylpachymaran entrapped plant-based hollow microcapsules for delivery and stabilization of β-galactosidase. *Food Funct.* 10, 4782–4791. doi: 10.1039/c9fo00649d

Di Costanzo, M., and Berni Canani, R. (2018). Lactose intolerance: common misunderstandings. *Ann. Nutr. Metab.* 73(Suppl. 4), 30–37. doi: 10.1159/000493669

Gutshall, K. R., Trimbur, D. E., Kasmir, J. J., and Brenchley, J. E. (1995). Analysis of a novel gene and beta-galactosidase isozyme from a psychrotrophic arthrobacter isolate. *J. Bacteriol.* 177, 1981–1988. doi: 10.1128/jb.177.8.1981-1988.1995

He, T., Priebe, M. G., Zhong, Y., Huang, C., Harmsen, H. J., Raangs, G. C., et al. (2008). Effects of yogurt and bifidobacteria supplementation on the colonic microbiota in lactose-intolerant subjects. *J. Appl. Microbiol.* 104, 595–604. doi: 10.1111/j.1365-2672.2007.03579.x

Hildebrandt, P., Wanarska, M., and Kur, J. (2009). A new cold-adapted beta-d-galactosidase from the antarctic arthrobacter sp. 32c - gene cloning, overexpression, purification and properties. *BMC Microbiol.* 9:151. doi: 10.1186/1471-2180-9-151

Hinz, S. W., van den Brock, L. A., Beldman, G., Vincken, J. P., and Voragen, A. G. (2004). Beta-galactosidase from bifidobacterium adolescentis dsm20083 prefers beta(1,4)-galactosides over lactose. *Appl. Microbiol. Biotechnol.* 66, 276–284. doi: 10.1007/s00253-004-1745-9

Horner, T. W., Dunn, M. L., Eggett, D. L., and Ogden, L. V. (2011). B-galactosidase activity of commercial lactase samples in raw and pasteurized milk at refrigerated temperatures. *J. Dairy Sci.* 94, 3242–3249. doi: 10.3168/jds.2010-3742

Hsu, C. A., Lee, S. L., and Chou, C. C. (2007). Enzymatic production of galactooligosaccharides by β-galactosidase from *Bifidobacterium longum* bcrc 15708. *J. Agric. Food Chem.* 55, 2225–2230. doi: 10.1021/jf063126+

Hu, J. M., Li, H., Cao, L. X., Wu, P. C., Zhang, C. T., Sang, S. L., et al. (2007). Molecular cloning and characterization of the gene encoding cold-active beta-galactosidase from a psychrotrophic and halotolerant planococcus sp. L4. *J. Agric. Food Chem.* 55, 2217–2224. doi: 10.1021/jf062910r

Juers, D. H., Heightman, T. D., Vasella, A., McCarter, J. D., Mackenzie, L., Withers, S. G., et al. (2001). A structural view of the action of *escherichia coli* (lacz) beta-galactosidase. *Biochemistry* 40, 14781–14794. doi: 10.1021/bi011727i

Lee, J. Y., Kwak, M. S., Roh, J. B., Kim, K., and Sung, M. H. (2017). Microbial β-galactosidase of pediococcus pentosaceus id-7: isolation, cloning, and molecular characterization. *J. Microbiol. Biotechnol.* 27, 598–609. doi: 10.4014/jmb.1611.11015

Li, D., Li, S., Wu, Y., Jin, M., Zhou, Y., Wang, Y., et al. (2020). Cloning and characterization of a new β-galactosidase from alteromonas sp. Qd01 and its potential in synthesis of galacto-oligosaccharides. *Mar. Drugs* 18:312. doi: 10.3390/md18060312

Li, S., Zhu, X., and Xing, M. (2019). A new β-galactosidase from the antarctic bacterium alteromonas sp. Ant48 and its potential in formation of prebiotic galacto-oligosaccharides. *Mar. Drugs* 17:599. doi: 10.3390/md17110599

Lo, S., Dugdale, M. L., Jeerh, N., Ku, T., Roth, N. J., and Huber, R. E. (2010). Studies of glu-416 variants of beta-galactosidase (e. Coli) show that the active site mg(2+) is not important for structure and indicate that the main role of mg (2+) is to mediate optimization of active site chemistry. *Protein J.* 29, 26–31. doi: 10.1007/s10930-009-9216-x

Maksimainen, M., Paavilainen, S., Hakulinen, N., and Rouvinen, J. (2012). Structural analysis, enzymatic characterization, and catalytic mechanisms of β-galactosidase from bacillus circulans sp. Alkalophilus. *FEBS J.* 279, 1788–1798. doi: 10.1111/j.1742-4658.2012.08555.x

Mavromatis, K., Sikorski, J., Lapidus, A., Glavina Del Rio, T., Copeland, A., Tice, H., et al. (2010). Complete genome sequence of alicyclobacillus acidocaldarius type strain (104-ia). *Stand Genomic Sci.* 2, 9–18. doi: 10.4056/sigs.591104

Oliveira, C., Guimarães, P. M., and Domingues, L. (2011). Recombinant microbial systems for improved β-galactosidase production and biotechnological applications. *Biotechnol. Adv.* 29, 600–609. doi: 10.1016/j.biotechadv.2011.03.008

Panesar, P. S., Kumari, S., and Panesar, R. (2010). Potential applications of immobilized β-galactosidase in food processing industries. *Enzyme Res.* 2010:473137. doi: 10.4061/2010/473137

Park, A. R., and Oh, D. K. (2010). Galacto-oligosaccharide production using microbial beta-galactosidase: current state and perspectives. *Appl. Microbiol. Biotechnol.* 85, 1279–1286. doi: 10.1007/s00253-009-2356-2

Rico-Díaz, A., Ramírez-Escudero, M., Vizoso-Vázquez, Á, Cerdán, M. E., Becerra, M., and Sanz-Aparicio, J. (2017). Structural features of aspergillus niger β-galactosidase define its activity against glycoside linkages. *FEBS J.* 284, 1815–1829. doi: 10.1111/febs.14083

Saqib, S., Akram, A., Halim, S. A., and Tassaduq, R. (2017). Sources of β-galactosidase and its applications in food industry. *3 Biotech.* 7:79. doi: 10.1007/s13205-017-0645-5

Shumilina, E., Dobrovolska, O., Del Conte, R., Holen, H. W., and Dikiy, A. (2014). Competitive cobalt for zinc substitution in mammalian methionine sulfoxide reductase b1 overexpressed in e. Coli: structural and functional insight. *J. Biol. Inorg. Chem.* 19, 85–95. doi: 10.1007/s00775-013-1064-7

Silberman, E. S., and Jin, J. (2019). Lactose intolerance. *JAMA* 322:1620. doi: 10.1001/jama.2019.9608

Singh, D., Lee, S., and Lee, C. H. (2019). Fathoming aspergillus oryzae metabolomes in formulated growth matrices. *Crit. Rev. Biotechnol.* 39, 35–49. doi: 10.1080/07388551.2018.1490246

Sun, J., Yao, C., Wang, W., Zhuang, Z., Liu, J., Dai, F., et al. (2018). Cloning, expression and characterization of a novel cold-adapted β-galactosidase from the deep-sea bacterium alteromonas sp. Ml52. *Mar. Drugs* 16:469. doi: 10.3390/md16120469

Sutendra, G., Wong, S., Fraser, M. E., and Huber, R. E. (2007). Beta-galactosidase (*escherichia coli*) has a second catalytically important mg2+ site. *Biochem. Biophys. Res. Commun.* 352, 566–570. doi: 10.1016/j.bbrc.2006.11.061

Tian, J., Zhang, Y., Liu, B., Zuo, D., Jiang, T., Guo, J., et al. (2013). Presep: predicting the propensity of a protein being secreted into the supernatant when expressed in pichia pastoris. *PLoS One* 8:e79749. doi: 10.1371/journal.pone.0079749

Vera, C., Guerrero, C., Wilson, L., and Illanes, A. (2017). Synthesis of propyl-β-d-galactoside with free and immobilized β-galactosidase from *Aspergillus oryzae*. *Process Biochem.* 53, 162–171. doi: 10.1016/j.procbio.2016.11.024

Wierzbicka-Woś, A., Cieśliński, H., Wanarska, M., Kozłowska-Tylingo, K., Hildebrandt, P., and Kur, J. (2011). A novel cold-active β-d-galactosidase from the paracoccus sp. 32d–gene cloning, purification and characterization. *Microb. Cell Fact.* 10:108. doi: 10.1186/1475-2859-10-108

Xia, Y., He, L., Mao, J., Fang, P., Ma, X., and Wang, Z. (2018). Purification, characterization, and gene cloning of a new cold-adapted β-galactosidase from erwinia sp. E602 isolated in northeast china. *J. Dairy Sci.* 101, 6946–6954. doi: 10.3168/jds.2018-14605

Zhang, Z., Zhang, F., Song, L., Sun, N., Guan, W., Liu, B., et al. (2018). Site-directed mutation of β-galactosidase from aspergillus candidus to reduce galactose

inhibition in lactose hydrolysis. *3 Biotech*. 8:452. doi: 10.1007/s13205-018-1418-5

Conflict of Interest: The authors declare that the research was conducted in the absence of any commercial or financial relationships that could be construed as a potential conflict of interest.

Publisher's Note: All claims expressed in this article are solely those of the authors and do not necessarily represent those of their affiliated organizations, or those of the publisher, the editors and the reviewers. Any product that may be evaluated in this article, or claim that may be made by its manufacturer, is not guaranteed or endorsed by the publisher.

frontiers in Microbiology

ORIGINAL RESEARCH
published: 29 November 2021
doi: 10.3389/fmicb.2021.781138

Heterologous Expression and Characterization of a High-Efficiency Chitosanase From *Bacillus mojavensis* SY1 Suitable for Production of Chitosan Oligosaccharides

Jianrong Wang[1,2†], Xiaoming Li[3†], Hao Chen[1,2], Bilian Lin[1,2] and Liangzhong Zhao[1,2*]*

[1] College of Food and Chemical Engineering, Shaoyang University, Shaoyang, China, [2] Hunan Provincial Key Laboratory of Soybean Products Processing and Safety Control, Shaoyang, China, [3] Bioengineering Research Center, Guangzhou Institute of Advanced Technology, Guangzhou, China

OPEN ACCESS

Edited by:
Benwei Zhu,
Nanjing Tech University, China

Reviewed by:
Nan Peng,
Huazhong Agricultural University, China
Shuji Tani,
Osaka Prefecture University, Japan

***Correspondence:**
Hao Chen
spgc13@163.com
Liangzhong Zhao
sys169@163.com

[†] These authors have contributed equally to this work

Specialty section:
This article was submitted to Microbiotechnology, a section of the journal Frontiers in Microbiology

Received: 22 September 2021
Accepted: 26 October 2021
Published: 29 November 2021

Citation:
Wang J, Li X, Chen H, Lin B and Zhao L (2021) Heterologous Expression and Characterization of a High-Efficiency Chitosanase From Bacillus mojavensis SY1 Suitable for Production of Chitosan Oligosaccharides. Front. Microbiol. 12:781138. doi: 10.3389/fmicb.2021.781138

Chitosanase plays an important role in enzymatic production of chitosan oligosaccharides (COSs). The present study describes the gene cloning and high-level expression of a high-efficiency chitosanase from *Bacillus mojavensis* SY1 (CsnBm). The gene encoding CsnBm was obtained by homologous cloning, ligated to pPICZαA, and transformed into *Pichia pastoris* X33. A recombinant strain designated X33-C3 with the highest activity was isolated from 120 recombinant colonies. The maximum activity and total protein concentration of recombinant strain X33-C3 were 6,052 U/ml and 3.75 g/l, respectively, which were obtained in fed-batch cultivation in a 50-l bioreactor. The optimal temperature and pH of purified CsnBm were 55°C and 5.5, respectively. Meanwhile, CsnBm was stable from pH 4.0 to 9.0 and 40 to 55°C. The purified CsnBm exhibited high activity toward colloidal chitosan with degrees of deacetylation from 85 to 95%. Furthermore, CsnBm exhibited high efficiency to hydrolyze different concentration of colloidal chitosan to produce COSs. The result of this study not only identifies a high-efficiency chitosanase for preparation of COSs, but also casts some insight into the high-level production of chitosanase in heterologous systems.

Keywords: *Bacillus mojavensis*, chitosanase, high efficiency, *Pichia pastoris*, Chitosan oligosaccharides

INTRODUCTION

As the second abundant polysaccharide on earth, chitin is composed of N-acetylglucosamine linked by β-1,4 glycoside bonds, and the lack of solubility limits its industrial application (Kaczmarek et al., 2019; Schmitz et al., 2019). Chitosan, the derivative products from deacetylation of chitin, exhibits better commercial value than chitin owing to its better solubility (Romanazzi et al., 2018). Chitosan is soluble in diluted acid and applied in some fields, but high viscosity and poor water solubility limit further industrial application. Chitosan oligosaccharides (COSs) are oligomers with the degree of polymerization (DP) 2-20 and mainly from hydrolysis of chitosan. Compared with

chitin or chitosan, COSs have many advantages such as excellent water solubility, low viscosity, and biodegradability (Li et al., 2016; Yuan et al., 2019). Meanwhile, many researches demonstrated that COSs display various bioactivities such as anti-tumor (Xu et al., 2017), positive effects on host gut health (Zhang et al., 2018; Wu et al., 2019), and immune activation (Kim et al., 2006). Because of the excellent water solubility and various biological activities, COSs have attracted increasing interest in many industries. The preparation methods of COSs mainly include chemical, physical, and enzymatic method. Among these three methods, the enzymatic production of COSs has received more attention due to its environmental friendliness, high identification of hydrolysis sites, non-toxicity, and controllability (Yuan et al., 2019). However, the high production cost limits the enzymatic method as the main choice for industrial-scale preparation of COSs (Yuan et al., 2019). Therefore, the isolation and high-level expression of high-efficiency chitosan degrading enzymes can provide a basis for the enzymatic production of COSs.

Chitosanases belong to glycoside hydrolase (GH) and catalyze hydrolysis of β-1,4 glycoside bonds of chitosan to produce COSs. Based on the sequence similarity, chitosanases are grouped into seven GH families by CAZy database, which include GH3, GH5, GH7, GH8, GH46, GH75, and GH80. Among these seven GH families, chitosanases from GH46 have been characterized extensively (Viens et al., 2015). The GH46 chitosanases are mainly derived from bacterial sources, especially from *Bacillus* and *Streptomyces* (Viens et al., 2015). As an important member of GH46, chitosanases from *Bacillus* exhibit excellent catalytic properties and the end products of chitosan hydrolyzed by *Bacillus* chitosanases are mainly composed of chitobiose, chitotriose, and chitotetraose (Qin et al., 2018b; Yang et al., 2020; Cui et al., 2021). Chitosanases from *Bacillus* exhibit great potential value to preparation of COSs, but low-level production of chitosanases in wild-type strain limits further industrial-scale application (Thadathil and Velappan, 2014). Therefore, it is crucial to improve the production of *Bacillus* chitosanases. Heterologous expression is an effective method to improve the production of recombinant proteins. For chitosanases, the most used host is *Escherichia coli* (*E. coli*), followed by *Pichia pastoris* (*P. pastoris*). The results of previous studies demonstrated that *P. pastoris* is more suitable for production of chitosanases than *E. coli* (Peng et al., 2013; Ding et al., 2019; Zhou J. L. et al., 2020; Zheng et al., 2021). Compared with *E. coli*, *P. pastoris* has many advantages such as high expression level, extracellular secretion of target recombinant protein, low secretion level of endogenous protein, and mature fermentation process. Therefore, high-level expression of chitosanases in *P. pastoris* could cut the cost and provide foundation for its application in industrial-scale production of COSs.

In this study, a high-efficiency chitosanase (named CsnBm) was cloned from *Bacillus mojavensis* SY1 (*B. mojavensis* SY1) and expressed in *P. pastoris*. The properties of purified CsnBm were characterized. Furthermore, hydrolytic pattern and preparation of COSs were investigated. The results of this study will provide a high-efficiency chitosanase for production of COSs.

MATERIALS AND METHODS

Materials

The *P. pastoris* X33, vector pPICZαA, and zeocin were purchased from Invitrogen (Carlsbad, CA, United States). The *E. coli* strain Top 10 was used to propagate plasmids. *B. mojavensis* SY1 was isolated from shrimp and crab shell waste and conserved in our laboratory. Restriction enzymes (*Eco*RI, *Sac*I, and *Xba*I), T_4-DNA ligase, and DNA polymerase (PrimeSTAR^{TM} HS) were purchased from Takara Biotechnology (Beijing, China). Endo-glycosidase H_f (Endo H_f) was purchased from New England Biolabs (NEB, Ipswich, MA, United States). TIANprep Midi Plasmid and TIANamp Bacteria DNA Kit were purchased from Tiangen Biotech (Beijing, China). Powdery chitosan with 85 to 95% degrees of deacetylation (DA) and glucosamine were purchased from Yuanye Biotechnology (Shanghai, China). Chitobiose, chitotriose, chitotetraose, chitopentaose, and chitohexaose were obtained from Long Dragon Bio (Huizhou, China). Furthermore, GlcN, $(GlcN)_2$, $(GlcN)_3$, $(GlcN)_4$, $(GlcN)_5$, and $(GlcN)_6$ were short for glucosamine, chitobiose, chitotriose, chitotetraose, chitopentaose, and chitohexaose, respectively.

Media for *E. coli* and *P. pastoris* include LBZ (LB with 25 μg/ml zeocin), YPDZ (yeast extract peptone dextrose medium with 100 μg/ml zeocin), BMGY (buffered glycerol complex medium), and BMMY (buffered methanol complex medium). Media for high cell density fermentation was BSM. LBZ, YPDZ, BMGY, BMMY, and BSM were prepared according to a previous study (Wang et al., 2013).

Gene Cloning and Bioinformatics Analysis

Genomic DNA from *B. mojavensis* SY1 was extracted by using the TIANamp Bacteria DNA Kit. Two primers (*csnbm*-fw, 5′-ATGAAAATCAGTTTGGAGAAA-3′ and *csnbm*-rev, 5′-TTATTT GATTACGAAATCACC-3′) based on the sequence of *B. mojavensis* strain UCMB5075 chromosome (GenBank: CP051464.1, 1279715-1280551) were designed for PCR amplification. The cloned fragment was ligated into the pMD20T vector and then sequenced. The obtained sequence was first analyzed *via* online BLASTn and BLASTx provided by the National Center for Biotechnology Information (NCBI). Sequence identity of CsnBm against different chitosanases was performed by DNAman 6.0. The signal peptide was analyzed by SignalP 5.0 server. Modeler 10.1 was used for homology modeling of CsnBm and the crystal structure of chitosanase from *Bacillus subtilis* (*B. subtilis*) MY002 was chosen as template (PDB deposition: 7C6D). PyMOL was used to analyze the obtained model.

Heterologous Expression of CsnBm in *Pichia pastoris* X33

The process for heterologous expression of CsnBm in *P. pastoris* X33 was the same as previous studies (Peng et al., 2013; Wang et al., 2019b). Two primers were designed (*csnbm-Eco*RI-fw, 5′-AGCGAATTCGCCGGACTGAACAAGGATCAA-3′ and

*csnbm-Not*I-fw, 5′-AGCTGGCGGCCG CTTTGATTACGAAA TCACCGT-3′) for PCR amplification. The resulting PCR product without the native signal sequence was cloned into the *P. pastoris* expression vector pPICZαA at *Xba*I and *Eco*RI sites to generate pPICZαA-*csnbm*. The expression vector pPICZαA-*csnbm* was linearized with *Sac*I and electrotransformed into *P. pastoris* X33 competent cell. After transformation, cells were screened on YPDZ plates with different concentrations of zeocin (from 100 to 500 μg/ml). The method for screening transformants was the same as the previously described method (Wang et al., 2019a). The detailed protocol is provided in the **Supplementary Material**.

The recombinant strain with the highest activity was further cultivated in 7- and 50-l bioreactors. The cultivation conditions and medium composition of high cell density fermentation are provided in the **Supplementary Material**. The enzyme activity, cell density (wet cell weight), and total protein concentration were monitored throughout the fermentation. The chitosanase activity was measured according to the previous methods (Guo et al., 2019). Chitosan (0.5 g) with 90% DA was dissolved in 100 ml of acetic acid-sodium acetate buffer (pH 5.5, 0.2 mM) and used as substrate. After 2 min preheating at 55°C, 50 μl of diluted enzyme was added to 350 μl 0.5% (w/v) colloidal chitosan. In addition, the reaction mixture was incubated at 55°C for 10 min, and then 600 μl of 3,5-dinitrosalicylic acid (DNS) was added to end the reaction. The reducing sugars released from the substrates were determined with DNS method. One unit of enzyme activity was defined as the amount of enzyme that releases 1 μmol reducing sugars/min. The concentration of total protein was detected by the Bradford method using BSA as standard. Wet cell weight (WCW) was obtained by centrifuging 10-ml samples in a pre-weighted centrifuge tube at 8,000 × *g* for 10 min and discarding supernatant.

Purification, Substrate Specificity, and Kinetic Parameters

The method for purification of recombinant CsnBm was the same as the previously described method (Wang et al., 2015). The supernatant without cell was harvested by centrifuging fermented broth at 10,000 × *g* for 10 min at 8°C, and then concentrated by ultrafiltration with a membrane of 10 kDa cutoff. The supernatant containing recombinant CsnBm was purified by Ni^{2+}-nitrilotriacetate (NTA) resin chromatography (Sangon Biotech, China). The purified recombinant CsnBm was analyzed by SDS-PAGE.

For deglycosylation, the purified CsnBm was deglycosylated using 300 U of Endo H_f for 3 h at 37°C according to the manufacturer's instructions (NEB, United States). The deglycosylated and untreated samples were analyzed by SDS-PAGE. For substrate specificity, chitosan with different DA (85, 90, and 95%), colloidal chitin, xylan, and microcrystalline cellulose were used as substrate. The kinetic parameters were detected using different concentrations of chitosan with 90% DA (1, 1.5, 2, 2.5, 3, 4, 5, 6, and 8 mg/ml) as substrate. The values of V_{max} and K_m were calculated by program Graft.

Characterization of CsnBm

The optimal pH of CsnBm was assayed in different 50 mM buffer from pH 3.5 to 7 (acetic acid-sodium acetate for pH 3.5 to 6 and Na_2HPO_4-NaH_2PO_4 for pH 6.5 to 7.0). The relative activity at different pH was calculated by setting pH 5.5 as 100%. For pH stability, CsnBm was incubated at 25°C in 50 mM buffer with different pH from 4.0 to 11.0 for 6 h (acetic acid-sodium acetate for pH 3.0 to 6.0, Na_2HPO_4-NaH_2PO_4 for pH 6.0 to 8.0, Tris-HCl for pH 7.0 to 9.0, and Gly-NaOH for pH 9.0 to 10.0), and then the residual activity was determined. The enzyme activity of the sample treated with distilled water was considered as 100%, and other values were recorded as a percentage of the highest value. All measurements were carried out in triplicate.

The optimal temperature of CsnBm was measured at different temperatures from 30 to 70°C. The relative activities at different temperature were calculated by setting 55°C as 100%. The thermal stability of CsnBm was studied by incubating at temperatures from 40 to 70°C for 20, 40, and 60 min, and the residual activity was determined at pH 5.5 and 55°C. The residual activity was calculated by taking the activity of non-heated CsnBm as 100%. All measurements were carried out in triplicate.

The effect of different metal ions on the stability of CsnBm was analyzed by incubating enzyme samples for 4 h at room temperature in 50 mM Tris-HCl buffer (pH 7.0), containing 1 and 5 mM of Ca^{2+}, Mg^{2+}, Na^{+}, K^{+}, Li^{+}, Zn^{2+}, Mn^{2+}, Co^{2+}, Hg^{2+}, Ag^{+}, and Fe^{2+}. The residual activity was determined as described previously.

Hydrolytic Pattern of CsnBm

The hydrolytic properties of CsnBm were determined and analyzed according to a previous study (Guo et al., 2019). The 0.5% (w/v) colloidal chitosan with 90% DA, $(GlcN)_2$, $(GlcN)_3$, $(GlcN)_4$, $(GlcN)_5$, and $(GlcN)_6$ were used as substrate to investigate the hydrolytic properties of CsnBm. Purified CsnBm was added to 0.5% (w/v) colloidal chitosan (sodium acetate buffer pH 5.5, 0.2 mM) and 0.3% (w/v) COSs (dissolved in distill water), and then incubated at 55°C for 2 h. Samples withdrawn at different times were immediately incubated at 90°C for 10 min and centrifuged at 10,000 × *g* for 5 min. The samples withdrawn at different times were analyzed by thin-layer chromatography (TLC) method. Samples were spotted on a TLC plate, developed in isopropanol:water:ammonium hydroxide (15:1:7.5, v/v) as solvent, and sprayed with 0.2% ninhydrin (dissolved in ethanol). The hydrolysis products were visualized by heating the plate at 100°C for 10 min.

Production of Chitosan Oligosaccharides by CsnBm

During the process of production of COSs by CsnBm, the colloidal chitosan with 90% DA was used as substrate. The supernatant of crude CsnBm from 50-L high-density fermentation was used for the preparation of COSs. Reactions were carried out in a 50-ml flask containing 10 ml of different concentrations of colloidal chitosan (1, 2, 3, and 4%, w/v) with different amounts of the crude CsnBm (3, 6, 9, 12, and 15 U/ml). The flasks were incubated at 55°C and 100 rpm for 1 h and

the reaction was stopped by incubating at 90°C for 10 min, and then 1 M NaOH was added to adjust the pH to 8.5 and finally centrifuged at 10,000 × *g* for 5 min. The hydrolytic products were analyzed by TLC and high-performance liquid chromatography (HPLC) method. The HPLC system (Thermo Fisher Scientific, United States) was equipped with a refractive index detector and a Zorbax carbohydrate analysis column (4.6 × 250 mm, 5 μm) (Agilent, United States). The mobile phase was composed of acetonitrile and water (70:30, v/v) and the flow rate was 0.8 ml/min. The concentrations of different COSs were quantified by integrating peak areas according to the respective standard curve (Qin et al., 2018b). The method for calculation of total COSs yield is provided in the **Supplementary Material**. Furthermore, the concentrations of different COSs and total COSs yield at different reaction time were studied. The reaction was carried out in a 500-ml flask containing 200 ml of 4% colloidal chitosan (w/v) with 9 U/ml of CsnBm. The flasks were incubated at 55°C and 100 rpm, the reaction samples (1 ml) were withdrawn at 5, 10, 15, 20, 25, 30, 40, 50, and 60 min. The methods for sample treatment and analysis were the same as abovementioned. The effects of different CsnBm additions on the production of the same COS were analyzed. Experiments were conducted in triplicate, and measurements were presented with their means and SD. Data were subjected to one-way ANOVA analysis by SPSS (version 24.0) and Duncan's multiple range tests ($p < 0.05$) to compare the mean value of different treatments.

RESULTS AND DISCUSSION

Gene Cloning and Bioinformatics Analysis

Sequence analysis showed that the open reading frame of CsnBm was 837 bp (Accession No, OK172330), which encoded 278 amino acid residues. The molecular weight and the theoretical pI of the deduced amino acid sequence (named CsnBm) were

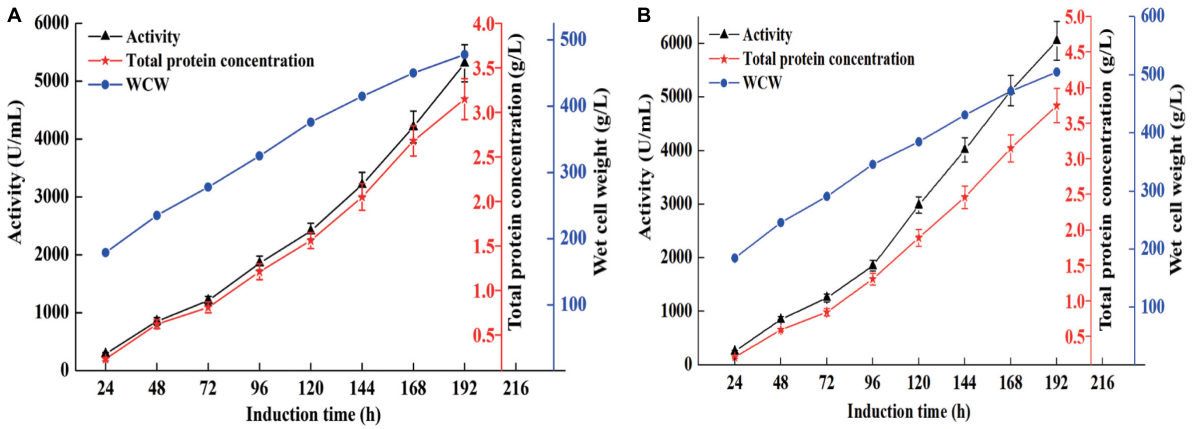

FIGURE 1 | The chitosanase activity, total protein concentration, and cell growth of the recombinant strain X33-C3 during fed-batch fermentation in 7-L **(A)** and 50-L **(B)** bioreactors.

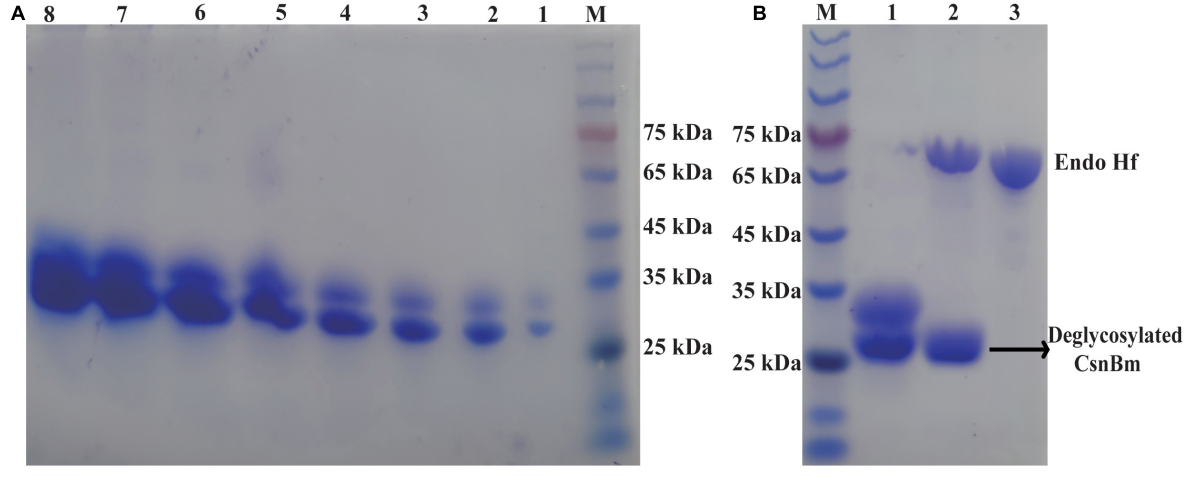

FIGURE 2 | SDS-PAGE analysis of CsnBm. **(A)** Supernatant from different induction time in 50-L bioreactors. M, marker, lanes 1–8 represent supernatant from 24 to 192 h. **(B)** Purified and EndoH_f treatment CsnBm. M marker, lane 1: purified CsnBm, lane 2: Deglycosylated CsnBm and Endo H_f, lane 3: Endo H_f.

31.3 kDa and 7.68, respectively, predicted by ProtParam. The first 36 amino acid residues of CsnBm were signal peptide. The results of NCBI blastp revealed that CsnBm shared 98.1% identity to chitosanase from *B. mojavensis* UCMB5075 (Accession No. WP_168747460.1), followed by chitosanase *Bacillus halotolerans* (96.3% identity, Accession No. WP_059336147.1). Multiple alignment of CsnBm with previous reported chitosanases showed that Glu19 and Asp35 were catalytic active sites. In addition, a conservative motif (DGRGYT) was found among these different chitosanases (**Supplementary Figure 1**).

The tertiary structure of CsnBm was obtained by homology modeling using chitosanase from *B. subtilis* MY002 as template (PDB deposition: 7c6c.1). The identity of tertiary structure between CsnBm and chitosanase from *B. subtilis* MY002 was 91.74%, and the overall structure of CsnBm is also close to previously reported GH46 members (**Supplementary Figure 2A**). The molecular structure of CsnBm can be divided into upper and lower domains, which contains nine α-helices and two β-strands (**Supplementary Figure 2B**). The predicted substrate binding region of CsnBm was a closed tunnel that is different from other GH46 chitosanases with open clefts (Marcotte et al., 1996; Saito et al., 1999; Lyu et al., 2015; Wang et al., 2020). The substrate binding region of CsnBm was highly negatively charged that is suitable for binding the cationic chitosan (**Supplementary Figure 2C**). The hydrogen bonds were the main force to stabilize the network between $(GlcN)_6$ and substrate binding region of CsnBm. As shown in **Supplementary Figure 2D**, several residues play an important role in binding substrate, which is similar to previous studies (Takauka et al., 2014; Li et al., 2021).

Heterologous Expression of CsnBm in *Pichia pastoris* X33

The 726-bp PCR product (named *csnbm*) without the native signal sequence was integrated in frame with the *Saccharomyces cerevisiae* α-factor secretion signal sequence under the control of the AOX1 promoter in plasmid pPICZαA to obtain the expression vector pPICZαA-*csnbm*. The expression vector pPICZαA-*csnbm* was linearized and transformed into *P. pastoris* X33. After transformation, many colonies were formed on the YPDZ plates. For initial screening, a total of 120 recombinant colonies were screened. Among these 120 recombinant colonies, six recombinant colonies (named recombinant strain X33-C1 to X33-C6) with higher activity (from 13 to 21 U/ml) were selected and cultivated in shaking flask. The results of shaking flask fermentation are shown in **Supplementary Figure 3**. The recombinant strain X33-C3 exhibited the highest activity (121 U/ml) among these six recombinants. Therefore, the recombinant strain X33-C3 was chosen for high cell density fermentation.

High cell density fermentation was carried out in 7- and 50-l bioreactors. As shown in **Figure 1A**, the maximum activity and total protein concentration produced by recombinant strain X33-C3 in the 7-l bioreactor reach 5,310 U/ml and 3.15 g/L, respectively. Meanwhile, the maximum activity and total protein concentration produced by recombinant strain X33-C3 in the 50-l bioreactor were 6,052 U/ml and 3.75 g/l, respectively (**Figure 1B**). In this study, the maximum activity of recombinant strain X33-C3 in the 50-l bioreactor was about 50-fold to that in shake flask cultivation (121 U/ml). Based on the results of this and previous studies, we can make a conclusion that high cell density fermentation is an effective method to improve the production of chitosanase in *P. pastoris*. The production of recombinant chitosanase from *Bacillus amyloliquefaciens* (*B. amyloliquefaciens*) is almost improved by 35.91-fold from the shake flask to the 5-l bioreactor (Luo et al., 2020). The study of Zhou R. et al. (2020) also reported that the enhancement of recombinant chitosanase from *Aspergillus oryzae* NKY2017 is almost 70-fold by high cell density fermentation.

According to the previous studies, we found that *E. coli* is the most favorite host for heterologous expression of chitosanase, followed by *P. pastoris*. Compared with *E. coli*, *P. pastoris* has some advantages such as extracellular expression and very low secretion levels of endogenous proteins, which are suitable for large-scale preparation of recombinant chitosanase. In this study, the production of CsnBm was 3.75 g/l and the recombinant CsnBm is the main protein of supernatant (**Figure 2A**). The result of this study is similar with previous works; some recombinant chitosanases were overexpressed at high level during methanol induction in *P. pastoris*. The expression level of chitosanases from *Mitsuaria* sp. 141, *B. amyloliquefaciens*, *Aspergillus oryzae* NKY2017, and *Streptomyces* sp. N174 is almost 1.6, 4.5, 3.1, and 8.5 g/l, respectively (Peng et al., 2013; Ding et al., 2019; Luo et al., 2020; Zhou R. et al., 2020). Furthermore, all of these recombinant chitosanases are approximately free from contaminating proteins, which facilitates downstream processing.

Purification, Kinetic Parameters, and Substrate Specificity

The recombinant CsnBm from the culture supernatant was purified by Ni^{2+}-NTA resin chromatography (**Supplementary Table 1**). After ultrafiltration and affinity chromatography, the specific activity of CsnBm was 2,663 U/mg. The purified CsnBm showed two bands on SDS-PAGE, which were approximately 33 and 27 kDa, respectively (**Figure 2A**). The band with 33 kDa was larger than the calculated molecular mass of CsnBm that may probably due to glycosylation. CsnBm was found to have one N-glycosylation site (N20GTT) by N-glycosylation site analysis

TABLE 1 | The substrate specificity of CsnBm.

Substrate	Relative activity (%)
Colloidal chitosan with 85% DA	91
Colloidal chitosan with 90% DA	100
Colloidal chitosan with 95% DA	93
Microcrystalline cellulose	ND
Colloidal chitin	ND
Xylan	ND

ND represents the enzyme activity was not detected.

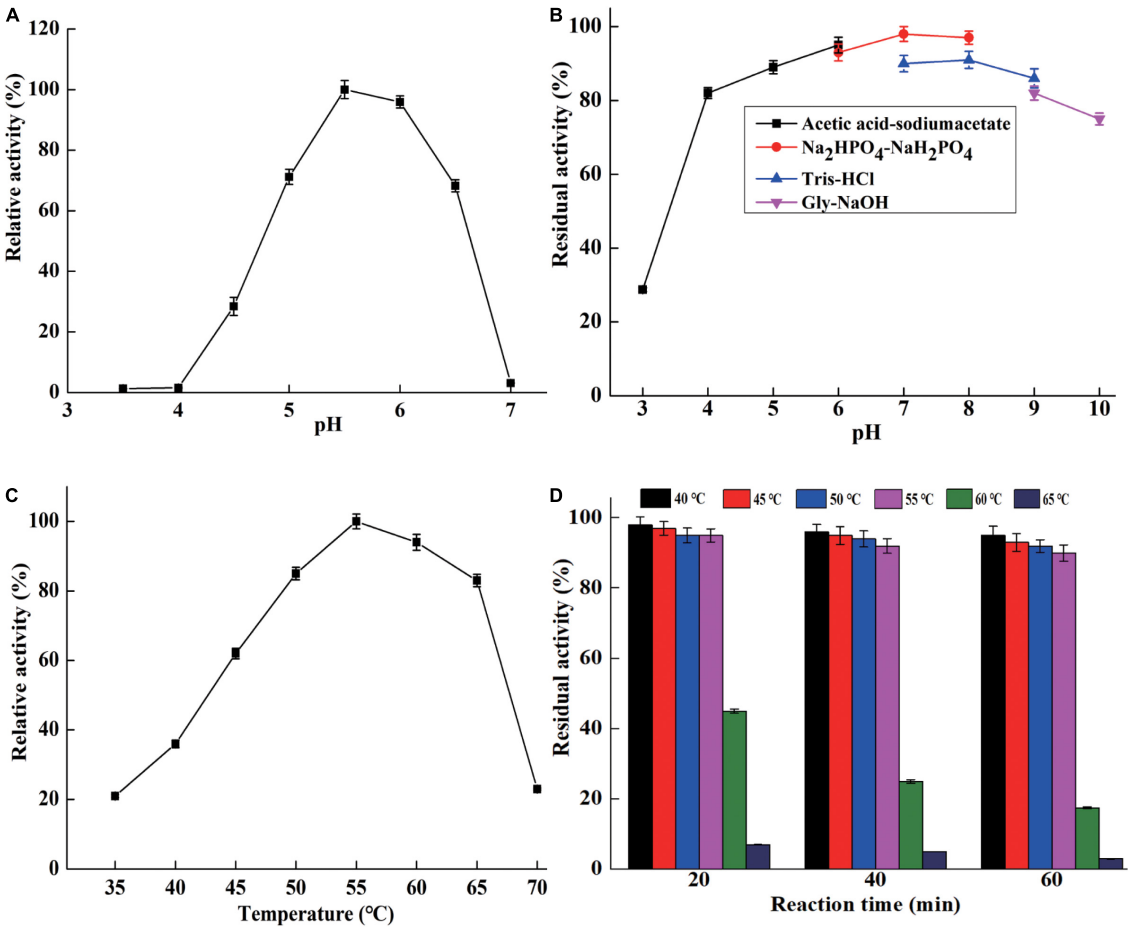

FIGURE 3 | The characterization of purified CsnBm. Optimum pH **(A)**, pH stability **(B)**, optimum temperature **(C)**, and thermostability **(D)**.

TABLE 2 | Effects of different metal cations on CsnBm activity.

Metal cations	Residual activity (%)	
	1 mM	5 mM
Control	100	100
Co^{2+}	92	86
Cu^{2+}	62	30
Fe^{2+}	9	6
Na^{+}	96	95
Ca^{2+}	112	109
K^{+}	96	93
Mn^{2+}	180	153
Mg^{2+}	115	112
Zn^{2+}	121	111

(NetNGlyc 1.0 Server).[1] After deglycosylation using EndoH_f, there was only a single band about 27 kDa, suggesting that the 33-kDa band was a glycoprotein (**Figure 2B**).

[1]http://www.cbs.dtu.dk/services/NetNGlyc/

Kinetic parameters of CsnBm were determined, and the values of K_m and V_{max} of CsnBm were 0.71 mg/ml and 2,802 μM/min/mg, respectively (**Supplementary Table 2**). The CsnBm with very low K_m and high V_{max} revealed that it has high substrate affinity and catalytic efficiency. CsnBm exhibited the highest activity toward colloidal chitosan with 90% DA, followed by colloidal chitosan with 95 and 85% DA, respectively (**Table 1**). Similar to other chitosanases from the GH46 family, CsnBm exhibited no activity toward microcrystalline cellulose, xylan, and colloidal chitin.

Characterization of CsnBm

CsnBm exhibited maximum activity at pH 5.5 and remained active at a pH range from 5 to 6.5 (**Figure 3A**). The optimal pH of CsnBm is similar to chitosanase from *Gynuella sunshinyii* (*G. sunshinyii*) and *Aspergillus fumigatus* (*A. fumigatus*) CJ22-326 (Qin et al., 2018a; Zhou J. L. et al., 2020). CsnBm was stable from pH 4.0 to 9.0, and the residual activity was above 80% after 4 h of incubating at 25°C (**Figure 3B**). The solubility of chitosan is a key factor on hydrolysis efficiency of chitosan. CsnBm was active and stable from pH 4.5 to 6.0, which is suitable for production of COSs, since chitosan

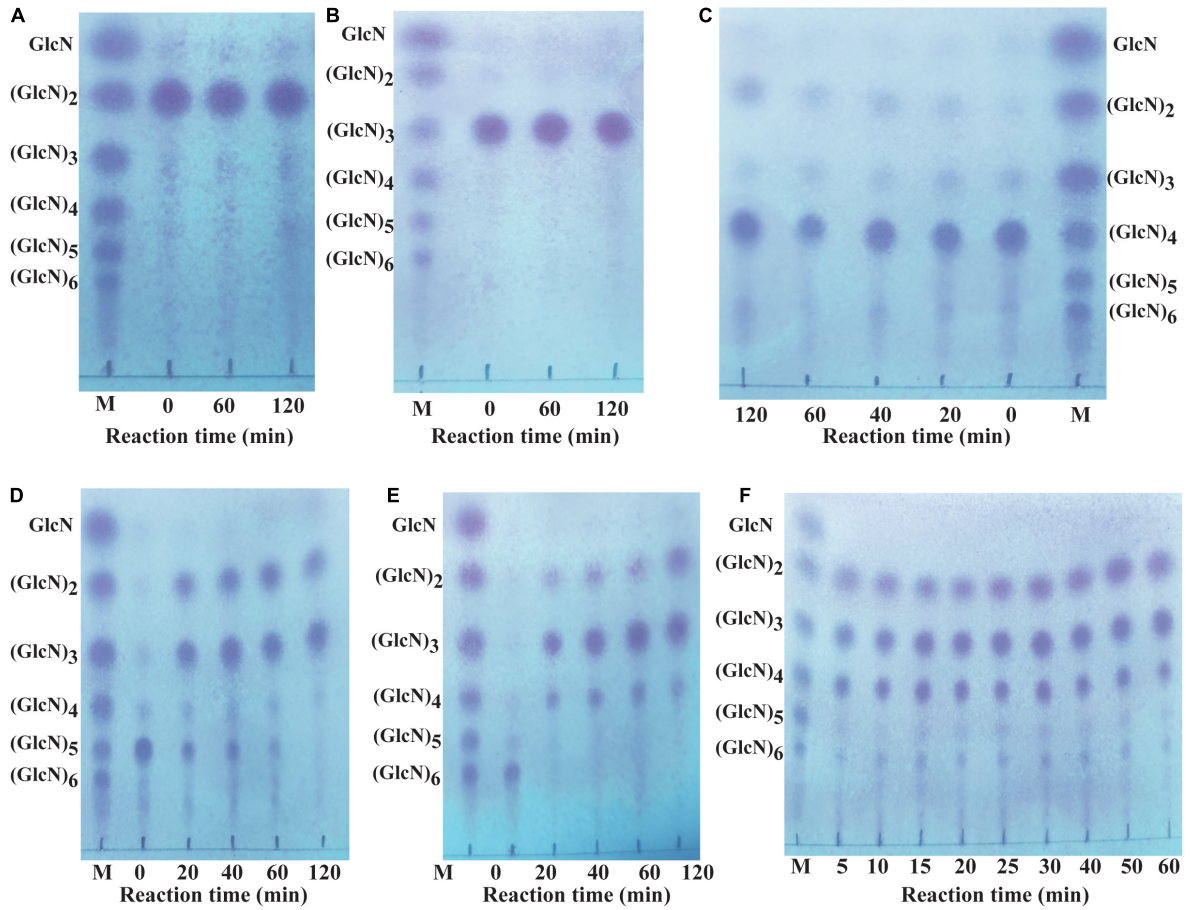

FIGURE 4 | Analysis of the hydrolytic process of CsnBm toward COSs and 0.5% colloidal chitosan. Chitobiose **(A)**, Chitotriose **(B)**, Chitotetraose **(C)**, Chitopentaose **(D)**, Chitohexaose **(E)**, and 0.5% colloidal chitosan **(F)**. M, marker sugars containing GlcN, $(GlcN)_2$, $(GlcN)_3$, $(GlcN)_4$, $(GlcN)_5$, and $(GlcN)_6$.

has better solubility below pH 6.0. The optimal temperature of CsnBm was 55°C and the relative activities from 50 to 65°C were above 80% (**Figure 3C**). CsnBm was stable from 45 to 55°C, the residual activities of CsnBm were above 90% after heat treatment for 20 to 60 min (**Figure 3D**). CsnBm decreased dramatically when the temperature was higher than 55°C, and the residual activities of CsnBm were only 45, 25, and 15%, respectively, after 20 to 60 min incubation at 60°C. For 65°C, CsnBm exhibited only 7% residual activity after 20 min incubation. The thermal stability of CsnBm is better than chitosanase Csn-SH from *Bacillus atrophaeus* (*B. atrophaeus*), BaCsn46A and BaCsn46B from *B. amyloliquefaciens*, and CsnQ from *Bacillus* sp. Q1098 (Qin et al., 2018b; Luo et al., 2020; Ma et al., 2020; Cui et al., 2021). The possible reason for CsnBm with better thermal stability was N-glycosylation, which is a common post-translational modification in *P. pastoris* (Bretthauer and Castellino, 1999). Some previous works revealed that glycosylation is helpful for the thermal stability and catalytic activity of recombinant proteins (Fonseca-Maldonado et al., 2013; Cheng et al., 2015). The temperature properties of CsnBm revealed that it is suitable for preparation of COSs at 55°C. Reaction temperature at high temperature is helpful for improving hydrolysis efficiency and reducing risk of microbial contamination (Botha et al., 2018).

CsnBm was activated by Ca^{2+}, Zn^{2+}, Mg^{2+}, and Mn^{2+}, which were 1.09- to 1.8-fold than that of the control, when the concentration of these metal ions was 1 or 5 mM (**Table 2**). CsnBm was inhibited by Fe^{2+} and Cu^{2+}, especially when Fe^{2+} was 5 mM, and the residual activity was only 6% (**Table 2**). K^{+} and Co^{2+} had little effect on the activity of CsnBm. Based on the results of this study and some previous researches, we found that metal ions are activators or inhibitors mainly depending on the specific target chitosanases. In some previous studies, Mn^{2+} has a positive effect on improving the activity of chitosanase. For example, the activities of chitosanase from *A. fumigatus* CJ22-326, *Bacillus* sp. MD-5, and *Chromobacterium violaceum* are improved by 3. 0-, 1. 2-, and 2.8-fold, respectively, in the presence of Mn^{2+} (Azevedo et al., 2020; Yang et al., 2020; Zhou J. L. et al., 2020). However, the chitosanase from *Streptomyces roseolus*, *Acinetobacter calcoaceticus* TKU024, and *Serratia marcescens* TKU011 are inhibited by Mn^{2+} (Wang et al., 2008, 2011; Jiang et al., 2012). In this study, the relative activity of CsnBm was increased by 10% in the presence of Zn^{2+}, similar to the chitosanases from *Staphylococcus capitis* and *Streptomyces*

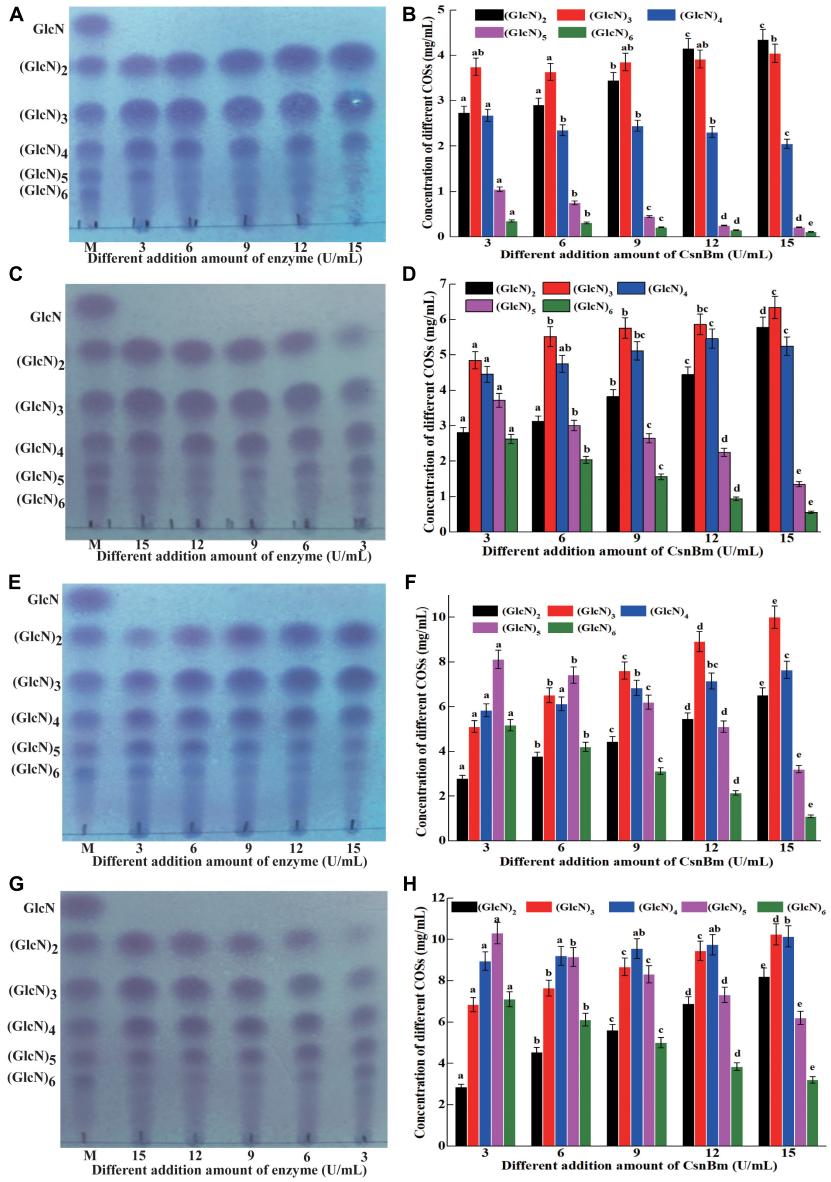

FIGURE 5 | Analysis of hydrolysates from different concentration of colloidal chitosan addition with different amounts of CsnBm. TLC analysis of hydrolysates from 1% **(A)**, 2% **(C)**, 3% **(E)**, and 4% colloidal chitosan **(G)**. M, marker sugars containing GlcN, $(GlcN)_2$, $(GlcN)_3$, $(GlcN)_4$, $(GlcN)_5$, and $(GlcN)_6$. HPLC analysis of hydrolysates from 1% **(B)**, 2% **(D)**, 3% **(F)**, and 4% colloidal chitosan **(H)**. The effects of different CsnBm additions on the production of the same COS were analyzed. Different lowercase superscripts in the columns with same color indicated statistical difference ($p < 0.05$). Experiments were conducted in triplicate, and measurements were presented with their means and SD. Data were subjected to one-way ANOVA analysis by SPSS (version 24.0) and Duncan's multiple range tests ($p < 0.05$) to compare the mean value of different treatments.

niveus (Sun et al., 2018; Chen et al., 2021). On the contrary, the chitosanase from *Aspergillus* sp. W-2 and *Aquabacterium* sp. A7-Y is inhibited by Zn^{2+} (Zhang et al., 2015; Wang et al., 2021).

Hydrolytic Pattern of CsnBm

Different COSs and 0.5% colloidal chitosan with 90% DA were selected as substrate to analyze the hydrolytic pattern of CsnBm. CsnBm exhibited no activity toward $(GlcN)_2$ and $(GlcN)_3$; even the reaction time prolonged to 2 h (**Figures 4A,B**). As shown in **Figure 4C**, a little $(GlcN)_4$ is cleaved and converted to $(GlcN)_2$ after 2 h incubation, indicating that CsnBm hardly hydrolyzed the β-1,4 linkage in $(GlcN)_4$. CsnBm showed high efficiency for $(GlcN)_5$ and $(GlcN)_6$, and most of $(GlcN)_5$ was cleaved into $(GlcN)_2$ and $(GlcN)_3$ after 20 min incubation (**Figure 4D**). CsnBm completely hydrolyzed $(GlcN)_6$ to yield $(GlcN)_2$, $(GlcN)_3$, and $(GlcN)_4$ only after 20 min incubation (**Figure 4E**). The products of 0.5% colloidal chitosan hydrolyzed by CsnBm are shown in **Figure 4F**. The main products were $(GlcN)_2$, $(GlcN)_3$, and $(GlcN)_4$, incubated for 5 to 60 min.

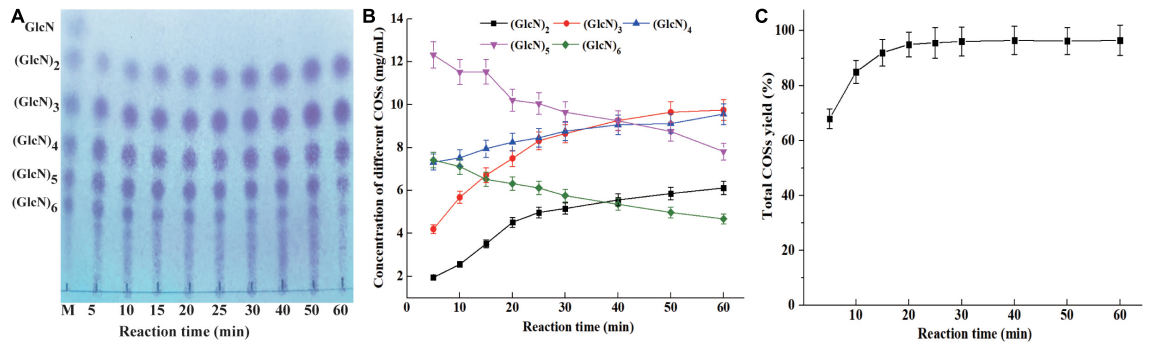

FIGURE 6 | Analysis of hydrolysates of 4% colloidal chitosan with 9 U/ml crude CsnBm at different reaction times. **(A)** TLC analysis of hydrolysates from different reaction time. M, marker sugars containing GlcN, $(GlcN)_2$, $(GlcN)_3$, $(GlcN)_4$, $(GlcN)_5$, and $(GlcN)_6$. **(B)** The concentrations of COSs at different reaction time. **(C)** Total COSs yield of 4% colloidal chitosan at different reaction time.

TABLE 3 | Enzymatic conversion of chitosan to COSs by chitosanases.

Microorganism source	Amount of enzyme (U/ml)	Concentration of chitosan (%)	Reaction time (Min)	Total COSs yield (%)	Major products	References
A. fumigatus CJ22-326	30	2	480	97.3	$(GlcN)_2$ to $(GlcN)_6$	Zhou J. L. et al. (2020)
P. barengoltzii	5	5	240	79.3	$(GlcN)_2$ to $(GlcN)_4$	Jiang et al. (2021)
B. amyloliquefaciens	3	3	180	86.9	$(GlcN)_2$ to $(GlcN)_6$	Qin et al. (2018b)
B. atrophaeus BSS	20	4	40	80.6	$(GlcN)_2$ to $(GlcN)_6$	Cui et al. (2021)
B. mojavensis SY1	9	4	15	92.3	(GlcN)2 to (GlcN)6	This study

No GlcN was detected during the hydrolytic process of COSs and 0.5% colloidal chitosan in this study. These results showed that CsnBm is an endo-type chitosanase. Furthermore, based on the hydrolytic process of $(GlcN)_6$, we deduced that CsnBm may have two binding and cutting modes. One cutting mode of CsnBm was the "4 + 2" splitting mode that CsnBm hydrolyzed $(GlcN)_6$ to produce $(GlcN)_2$ and $(GlcN)_4$. The other was the "3 + 3" splitting mode that hydrolyzed $(GlcN)_6$ to produce $(GlcN)_3$. A previous study found that chitosanase interacts with $(GlcN)_6$ in three ways, which are related to subsites −2 to + 4, −3 to + 3, and −4 to + 2, respectively (Pechsrichuang et al., 2018). The hydrolytic pattern of CsnBm is similar to previous reported chitosanases. The chitosanases from *B. amyloliquefaciens*, *G. sunshinyii*, *Bacillus* sp. MD-5, and marine *Bacillus* sp. exhibit no activity toward $(GlcN)_2$ and $(GlcN)_3$ and the final hydrolysis products are mainly composed of $(GlcN)_2$, $(GlcN)_3$, and $(GlcN)_4$ (Qin et al., 2018a,b; Ma et al., 2020; Yang et al., 2020).

Production of Chitosan OligosaccharidesCOSs by CsnBm

Previous reports have shown that COSs with different degrees of polymerization (DP) exhibit different biological activities (Li et al., 2016; Yuan et al., 2019). Li et al. (2012) found that COS with DP 2 to 6 showed obvious scavenging activity against hydroxyl radical and COS with low DP exhibits better reducing power. In addition, Li et al. (2014) also investigated the antimicrobial activity against *Staphylococcus aureus* of COSs with DP 2 to 12 and found that the COS exhibits antibacterial activity with a DP of at least 5. Previous studies found that COSs with DP 2 to 7 could improve the chilling tolerance of wheat seedlings and COS with DP7 shows the best effect (Zou et al., 2017). Therefore, it is necessary to investigate the process of preparation of COSs by CsnBm. The hydrolysis reactions were carried out with different concentrations of colloidal chitosan (1 to 4%, w/v) and different amounts of CsnBm (3, 6, 9, 12, and 15 U/ml). The results of different hydrolysis reactions are shown in **Figure 5**. The hydrolysis of 1% colloidal chitosan mainly produced $(GlcN)_2$, $(GlcN)_3$, and $(GlcN)_4$ as final products (**Figures 5A,B**). As shown in **Figures 5C,D**, the hydrolysates of 2% colloidal chitosan mainly include $(GlcN)_2$, $(GlcN)_3$, $(GlcN)_4$, and $(GlcN)_5$, when the amounts of CsnBm were 3, 6, and 9 U/ml, respectively. As the amount of CsnBm increased to 12 and 15 U/ml, the hydrolysates were mainly composed of $(GlcN)_2$, $(GlcN)_3$, and $(GlcN)_4$. For 3% colloidal chitosan addition with 3, 6, and 9 U/ml of CsnBm, the end products mainly contained $(GlcN)_2$, $(GlcN)_3$, $(GlcN)_4$, $(GlcN)_5$, and $(GlcN)_6$ (**Figures 5E,F**). With the increased addition of CsnBm to 12 and 15 U/ml,

the end products were mainly composed of $(GlcN)_2$, $(GlcN)_3$, $(GlcN)_4$, and $(GlcN)_5$. The hydrolysates 4% colloidal chitosan added with 3 and 6 U/ml were predominantly composed of $(GlcN)_3$, $(GlcN)_4$, $(GlcN)_5$, and $(GlcN)_6$ (**Figures 5G,H**). As the amount of CsnBm increased to 9, 12, and 15 U/ml, the hydrolysis of 4% colloidal chitosan produced $(GlcN)_2$, $(GlcN)_3$, $(GlcN)_4$, and $(GlcN)_5$ as the main end products (**Figures 5G,H**). The HPLC charts of all reactions are shown in **Supplementary Figure 4**. The total COSs yields of all reactions were above 91.2% (**Supplementary Figure 5**).

The concentration of different COSs and total COSs yields under different reaction times with 4% colloidal chitosan addition with 9 U/ml CsnBm were further studied. As shown in **Figures 6A,B**, the COSs mixture mainly include $(GlcN)_2$, $(GlcN)_3$, $(GlcN)_4$, $(GlcN)_5$, and $(GlcN)_6$ after 5 min reaction and the total COSs yield was 68.2% (**Figure 6C**). After 10 min of reaction, the total COS yield increased from 68.2 to 85.3%, and the concentrations of $(GlcN)_2$, $(GlcN)_3$, $(GlcN)_4$, $(GlcN)_5$, and $(GlcN)_6$ increased gradually. The total COSs yield reached 92.3% when the reaction time was 15 min and the concentrations of $(GlcN)_2$, $(GlcN)_3$, $(GlcN)_4$, $(GlcN)_5$, and $(GlcN)_6$ were 3.52, 6.72, 7.95, 11.53, and 6.52 g/L (**Figure 6B**). During the hydrolysis time from 20 to 60 min, the COSs with higher DP (6 and 5) were gradually cleaved into $(GlcN)_2$, $(GlcN)_3$, and $(GlcN)_4$ (**Figures 6A,B**). The total COSs yields of reactions from 20 to 60 min were in the range from 95.1 to 96.5% (**Figure 6C**). The HPLC charts of all reactions are shown in **Supplementary Figure 6**. CsnBm exhibited high hydrolytic activity on chitosan and the above results demonstrated that CsnBm is suitable for the controllable production of COSs.

Up to now, many chitosanases have been used to prepare COSs (**Table 3**). Zhou J. L. et al. (2020) reported that the total COSs yield reaches 97.29% after 8 h reaction with 2% chitosan addition with 30 U/ml of *A. fumigatus* CJ22-326 chitosanase. The bifunctional chitosanase PbCsn8 from *Paenibacillus barengoltzii* could cleave 5% chitosan into $(GlcN)_2$, $(GlcN)_3$, and $(GlcN)_4$ in the presence of 5 U/ml PbCsn8 after 4 h reaction and the total COSs yield is 79.3% (Jiang et al., 2021). The work of Qin et al. (2018b) found that the total COSs yield of 3% chitosan is 86.85% after the addition of 100 U/g chitosanases from *B. amyloliquefaciens* for 3 h hydrolysis reaction. In this study, after 15 min reaction in the presence of 9 U/ml CsnBm, the total COSs yield of 4% chitosan was 92.3%, which is more efficient than previously reported chitosanases.

CONCLUSION

In this study, the high-efficiency chitosanase CsnBm from *B. mojavensis* SY1 was high-level heterologously expressed and biochemically characterized. The maximum activity and total protein concentration of CsnBm were 6,052 U/ml and 3.75 g/l, respectively. The purified CsnBm was most active at 55°C and pH 5.5. The K_m and V_{max} of CsnBm were 0.71 mg/ml and 2,802 μM/min/mg, respectively. CsnBm exhibited high efficiency hydrolysis of chitosan to produce COSs. The excellent properties and high-level production of CsnBm will provide a basis for its application in industrial-scale preparation of COSs.

DATA AVAILABILITY STATEMENT

The data presented in the study are deposited in the NCBI, accession number OK172330.

AUTHOR CONTRIBUTIONS

JW contributed to gene clone, construct recombinant strain, and bioinformatics analysis of CsnBm. XL contributed to analysis of COSs by TLC and HPLC. HC contributed to the analysis of the hydrolytic properties of CsnBm. BL contributed to high-density fermentation and purification of CsnBm. LZ contributed to experiment planning. All authors contributed to the article and approved the submitted version.

FUNDING

This work was supported by the National Nature Science Fund of China 31971338 and the Science and Technology Innovation Program of Hunan Province (2019TP1028, 2019SK2122, 2019NK4229 and S2021GCZDYF0535).

SUPPLEMENTARY MATERIAL

The Supplementary Material for this article can be found online at: https://www.frontiersin.org/articles/10.3389/fmicb.2021.781138/full#supplementary-material

REFERENCES

Azevedo, M. I. G., Oliveira, S. T., Silva, C. F. B., Carneiro, R. F., Nagano, C. S., Gadelha, A. C. S., et al. (2020). Secretory production in *Escherichia coli* of a GH46 chitosanase from *Chromobacterium violaceum*, suitable to generate antifungal chitooligosaccharides. *Int. J. Biol. Macromol.* 165, 1482–1495. doi: 10.1016/j.ijbiomac.2020.09.221

Bretthauer, R. K., and Castellino, F. J. (1999). Glycosylation of *Pichia pastoris*-derived proteins. *Biotechnol. Appl. Biochem.* 30, 193–200.

Botha, J., Mizrachi, E., Myburg, A. A., and Cowan, D. A. (2018). Carbohydrate active enzyme domains from extreme thermophiles: components of a modular toolbox for lignocellulose degradation. *Extremophiles* 22, 1–12. doi: 10.1007/s00792-017-0974-7

Cheng, Y. S., Chen, C. C., Huang, J. W., Ko, T. P., Huang, Z., and Guo, R. T. (2015). Improving the catalytic performance of a GH11 xylanase by rational protein engineering. *Appl. Microbiol. Biotechnol.* 99, 9503–9510.

Chen, T., Cheng, G., Jiao, S., Ren, L., Zhao, C., Wei, J., et al. (2021). Expression and biochemical characterization of a novel marine chitosanase from *Streptomyces*

niveus suitable for preparation of chitobiose. *Mar. Drugs* 19:300. doi: 10.3390/md19060300

Cui, D., Yang, J., Lu, B., and Shen, H. (2021). Efficient preparation of chitooligosaccharide with a potential chitosanase Csn-SH and its application for fungi disease protection. *Front. Microbiol.* 12:682829. doi: 10.3389/fmicb.2021.682829

Ding, M., Zhang, T., Sun, C., Zhang, H., and Zhang, Y. (2019). A Chitosanase mutant from *Streptomyces* sp. *Int. J. Biol. Macromol.* 151, 1091–1098. doi: 10.1016/j.ijbiomac.2019.10.151

Fonseca-Maldonado, R., Vieira, D. S., Alponti, J. S., Bonneil, E., Thibault, P., and Ward, R. J. (2013). Engineering the pattern of protein glycosylation modulates the thermostability of a GH11 xylanase. *J. Biol. Chem.* 288, 25522–25534. doi: 10.1074/jbc.M113.485953

Guo, N., Sun, J., Wang, W., Gao, L., Liu, J., Liu, Z., et al. (2019). Cloning, expression and characterization of a novel chitosanase from *Streptomyces albolongus* ATCC 27414. *Food Chem.* 286, 696–702. doi: 10.1016/j.foodchem.2019.02.056

Jiang, X., Chen, D., Chen, L., Yang, G., and Zou, S. (2012). Purification, characterization, and action mode of a chitosanase from *Streptomyces roseolus* induced by chitin. *Carbohydr. Res.* 355, 40–44. doi: 10.1016/j.carres.2012.05.002

Jiang, Z., Ma, S., Guan, L., Yan, Q., and Yang, S. (2021). Biochemical characterization of a novel bifunctional chitosanase from *Paenibacillus barengoltzii* for chitooligosaccharide production. *World J. Microbiol. Biotechnol.* 37:83. doi: 10.1007/s11274-021-03051-0

Kim, H. M., Hong, S. H., Yoo, S. J., Baek, K. S., Jeon, Y. J., and Choung, S. Y. (2006). Differential effects of chitooligosaccharides on serum cytokine levels in aged subjects. *J. Med. Food* 9, 427–430. doi: 10.1089/jmf.2006.9.427

Kaczmarek, M. B., Struszczyk-Swita, K., Li, X., Szczęsna-Antczak, M., and Daroch, M. (2019). Enzymatic modifications of chitin, chitosan, and chitooligosaccharides. *Front. Bioeng. Biotechnol.* 7:243. doi: 10.3389/fbioe.2019.00243

Li, K., Xing, R., Liu, S., Li, R., Qin, Y., Meng, X., et al. (2012). Separation of chito-oligomers with several degrees of polymerization and study of their antioxidant activity. *Carbohydr. Polym.* 88, 896–903. doi: 10.1016/j.carbpol.2012.01.033

Li, K., Xing, R., Liu, S., Qin, Y., Yu, H., and Li, P. (2014). Size and pH effects of chitooligomers on antibacterial activity against *Staphylococcus aureus*. *Int. J. Biol. Macromol.* 64, 302–305. doi: 10.1016/j.ijbiomac.2013.11.037

Lyu, Q., Shi, Y., Wang, S., Yang, Y., Han, B., Liu, W., et al. (2015). Structural and biochemical insights into the degradation mechanism of chitosan by chitosanase OU01. *Biochim. Biophys. Acta* 50, 1953–1961. doi: 10.1016/j.bbagen.2015.06.011

Li, K., Xing, R., Liu, S., and Li, P. (2016). Advances in preparation, analysis and biological activities of single chitooligosaccharides. *Carbohydr. Polym.* 139, 178–190. doi: 10.1016/j.carbpol.2015.12.016.

Luo, S., Qin, Z., Chen, Q., Fan, L., Jiang, L., and Zhao, L. (2020). High level production of a *Bacillus amlyoliquefaciens* chitosanase in *Pichia pastoris* suitable for chitooligosaccharides preparation. *Int. J. Biol. Macromol.* 149, 1034–1041. doi: 10.1016/j.ijbiomac.2020.02.001

Li, Y., Gou, Y., Liu, Z., Xie, T., and Wang, G. (2021). Structure-based rational design of chitosanase CsnMY002 for high yields of chitobiose. *Colloids Surf. B. Biointerfaces* 202:111692. doi: 10.1016/j.colsurfb.2021.111692

Marcotte, E. M., Monzingo, A. F., Ernst, S. R., Brzezinski, R., and Robertus, J. D. (1996). X-ray structure of an anti-fungal chitosanase from *streptomyces* N174. *Nat. Struct. Biol.* 3, 155–162. doi: 10.1038/nsb0296-155

Ma, C., Li, X., Yang, K., and Li, S. (2020). Characterization of a new chitosanase from a marine *Bacillus* sp. and the anti-oxidant activity of its hydrolysate. *Mar. Drugs* 18:126. doi: 10.3390/md18020126

Peng, N., Xu, W., Wang, F., Hu, J., Ma, M., Hu, Y., et al. (2013). Mitsuaria chitosanase with unrevealed important amino acid residues: characterization and enhanced production in *Pichia pastoris*. *Appl. Microbiol. Biotechnol.* 97, 171–179. doi: 10.1007/s00253-012-3901-y

Qin, Z., Chen, Q., Lin, S., Luo, S., Qiu, Y., and Zhao, L. (2018a). Expression and characterization of a novel cold-adapted chitosanase suitable for chitooligosaccharides controllable preparation. *Food Chem.* 253, 139–147. doi: 10.1016/j.foodchem.2018.01.137

Qin, Z., Luo, S., Li, Y., Chen, Q., Qiu, Y., Zhao, L., et al. (2018b). Biochemical properties of a novel chitosanase from *Bacillus amyloliquefaciens* and its use in membrane reactor. *Lwt-food Sci. Technol.* 97, 9–16. doi: 10.1016/j.lwt.2018.06.027

Pechsrichuang, P., Lorentzen, S. B., Aam, B. B., Tuveng, T. R., Hamre, A. G., Eijsink, V. G. H., et al. (2018). Bioconversion of chitosan into chito-oligosaccharides (CHOS) using family 46 chitosanase from *Bacillus subtilis* (BsCsn46A). *Carbohydr. Polym.* 186, 420–428. doi: 10.1016/j.carbpol.2018.01.059

Romanazzi, G., Feliziani, E., and Sivakumar, D. (2018). Chitosan, a biopolymer with triple action on postharvest decay of fruit and vegetables: eliciting, antimicrobial and film-forming properties. *Front. Microbiol.* 9:2745. doi: 10.3389/fmicb.2018.02745

Saito, J., Kita, A., Higuchi, Y., Nagata, Y., Ando, A., and Miki, K. (1999). Crystal structure of chitosanase from *Bacillus circulans* MH-K1 at 1.6-A resolution and its substrate recognition mechanism. *J. Biol. Chem.* 274, 30818–30825. doi: 10.1074/jbc.274.43.30818

Sun, H., Cao, R., Li, L., Zhao, L., and Liu, Q. (2018). Cloning, purification and characterization of a novel GH46 family chitosanase. *Process Biochem.* 75, 146–151. doi: 10.1016/j.procbio.2018.09.021

Schmitz, C., Auza, L. G., Koberidze, D., Rasche, S., Fischer, R., and Bortesi, L. (2019). Conversion of chitin to defined chitosan oligomers: current status and future prospects. *Mar. Drugs* 17:452. doi: 10.3390/md17080452

Thadathil, N., and Velappan, S. P. (2014). Recent developments in chitosanase research and its biotechnological applications: a review. *Food Chem.* 150, 392–399. doi: 10.1016/j.foodchem.2013.10.083

Takauka, T. E., Bianchetti, C. M., Tobimatsu, Y., Bergeman, L. F., Ralph, J., and Fox, B. G. (2014). Structure-guided analysis of catalytic specificity of the abundantly secreted chitosanase SACTE_5457 from *Streptomyces* sp. SirexAA-E. *Proteins* 82, 1245–1257. doi: 10.1002/prot.24491

Viens, P., Lacombe-Harvey, M. È, and Brzezinski, R. (2015). Chitosanases from family 46 of glycoside hydrolases: from proteins to phenotypes. *Mar. Drugs* 13, 6566–6587. doi: 10.3390/md13116566

Wang, S. L., Peng, J. H., Liang, T. W., and Liu, K. C. (2008). Purification and characterization of a chitosanase from *Serratia marcescens* TKU011. *Carbohydr. Res.* 343, 1316–1323.

Wang, S. L., Tseng, W. N., and Liang, T. W. (2011). Biodegradation of shellfish wastes and production of chitosanases by a squid pen-assimilating bacterium, *Acinetobacter calcoaceticus* TKU024. *Biodegradation* 22, 939–948. doi: 10.1007/s10532-011-9453-5

Wang, J. R., Li, Y. Y., Xu, S. D., Li, P., Liu, J. S., and Liu, D. N. (2013). High-level expression of pro-form lipase from *Rhizopus oryzae* in *Pichia pastoris* and its purification and characterization. *Int. J. Mol. Sci.* 15, 203–217. doi: 10.3390/ijms15010203

Wang, J. R., Li, Y. Y., and Liu, D. (2015). Gene cloning, high-level expression, and characterization of an alkaline and thermostable lipase from *Trichosporon coremiiforme* V3. *J. Microbiol. Biotechnol.* 25, 845–855. doi: 10.4014/jmb.1408.08039

Wang, J., Zhang, T., Li, Y., Li, L., Wang, Y., Yang, B., et al. (2019b). High-level expression of Thermomyces dupontii thermo-alkaline lipase in *Pichia pastoris* under the control of different promoters. *3 Biotech* 9:33. doi: 10.1007/s13205-018-1531-5

Wang, J., Wu, Z., Zhang, T., Wang, Y., and Yang, B. (2019a). High-level expression of *Thermomyces dupontii* thermophilic lipase in *Pichia pastoris* via combined strategies. *3 Biotech* 9:62. doi: 10.1007/s13205-019-1597-8

Wu, M., Li, J., An, Y., Li, P., Xiong, W., Li, J., et al. (2019). Chitooligosaccharides prevents the development of colitis-associated colorectal cancer by modulating the intestinal microbiota and mycobiota. *Front. Microbiol.* 10:2101. doi: 10.3389/fmicb.2019.02101

Wang, Y., Qin, Z., Fan, L., and Zhao, L. (2020). Structure-function analysis of *Gynuella sunshinyii* chitosanase uncovers the mechanism of substrate binding in GH family 46 members. *Int. J. Biol. Macromol.* 165, 2038–2048. doi: 10.1016/j.ijbiomac.2020.10.066

Wang, Y. X., Li, D., Liu, M. X., Xia, C. Y., Fan, Q. W., Li, X., et al. (2021). Preparation of active chitooligosaccharides with a novel chitosanase AqCoA and their application in fungal disease protection. *J. Agr. Food Chem.* 69, 3351–3361. doi: 10.1021/acs.jafc.0c07802

Xu, Q., Wang, W., Yang, W., Du, Y., and Song, L. (2017). Chitosan oligosaccharide inhibits EGF-induced cell growth possibly through blockade of epidermal growth factor receptor/mitogen-activated protein kinase pathway. *Int. J. Biol. Macromol.* 98, 502–505. doi: 10.1016/j.ijbiomac.2017.02.021

Yuan, X., Zheng, J., Jiao, S., Cheng, G., Feng, C., and Du, Y. (2019). A review on the preparation of chitosan oligosaccharides and application to human health, animal husbandry and agricultural production. *Carbohydr. Polym.* 220, 60–70. doi: 10.1016/j.carbpol.2019.05.050

Yang, G., Sun, H., Cao, R., Liu, Q., and Mao, X. (2020). Characterization of a novel glycoside hydrolase family 46 chitosanase, Csn-BAC, from *Bacillus* sp. MD-5. *Int. J. Biol. Macromol.* 146, 518–523. doi: 10.1016/j.ijbiomac.2020.01.031

Zhang, J., Cao, H., Li, S., Zhao, Y., Wang, W., Xu, Q., et al. (2015). Characterization of a new family 75 chitosanase from *Aspergillus* sp. W-2. *Int. J. Biol. Macromol.* 81, 362–369. doi: 10.1016/j.ijbiomac.2015.08.026

Zou, P., Tian, X., Dong, B., and Zhang, C. (2017). Size effects of chitooligomers with certain degrees of polymerization on the chilling tolerance of wheat seedlings. *Carbohydr. Polym.* 160, 194–202. doi: 10.1016/j.carbpol.2016.12.058

Zhang, C., Jiao, S., Wang, Z. A., and Du, Y. (2018). Exploring effects of chitosan oligosaccharides on mice gut microbiota in vitro fermentation and animal model. *Front. Microbiol.* 9:2388. doi: 10.3389/fmicb.2018.02388

Zhou, J. L., Liu, X. B., Yuan, F., Deng, B., and Yu, X. B. (2020). Biocatalysis of heterogenously-expressed chitosanase for the preparation of desirable chitosan oligosaccharides applied against phytopathogenic fungi. *ACS. Sustain. Chem. Eng.* 8, 4781–4791.

Zhou, R., Liao, X., Liu, F., Dong, Q., Chen, W., Wang, Y., et al. (2020). High-level expression of an acidic and thermostable chitosanase in *Pichia pastoris* using multi-copy expression strains and high-celldensity cultivation. *Biotechnol. Bioproc. Eng.* 25, 562–570.

Zheng, Q., Meng, X., Cheng, M., Li, Y., Liu, Y., and Chen, X. (2021). Cloning and characterization of a new chitosanase from a deep-sea bacterium *serratia* sp. QD07. *Front. Microbiol.* 12:619731. doi: 10.3389/fmicb.2021.619731

Conflict of Interest: The authors declare that the research was conducted in the absence of any commercial or financial relationships that could be construed as a potential conflict of interest.

Publisher's Note: All claims expressed in this article are solely those of the authors and do not necessarily represent those of their affiliated organizations, or those of the publisher, the editors and the reviewers. Any product that may be evaluated in this article, or claim that may be made by its manufacturer, is not guaranteed or endorsed by the publisher.

frontiers | Frontiers in Microbiology

ORIGINAL RESEARCH
published: 25 April 2022
doi: 10.3389/fmicb.2022.783155

Variation in Bacterial Community Structures and Functions as Indicators of Response to the Restoration of *Suaeda salsa*: A Case Study of the Restoration in the Beidaihe Coastal Wetland

Changfei He[1,3†], Li Zheng[1,2†], Jinfeng Ding[4], Wei Gao[1], Qian Li[1], Bin Han[1,2] and Jingxi Li[1]*

[1] Key Laboratory of Marine Eco-Environmental Science and Technology, First Institute of Oceanography, Ministry of Natural Resources, Qingdao, China, [2] Laboratory for Marine Ecology and Environmental Science, Pilot National Laboratory for Marine Science and Technology, Qingdao, China, [3] Institute of Marine Science and Technology, Shandong University, Qingdao, China, [4] Institute of Coastal Environmental Pollution Control, Ministry of Education Key Laboratory of Marine Environment and Ecology, College of Environmental Science and Engineering, Ocean University of China, Qingdao, China

OPEN ACCESS

Edited by:
Xiaoke Hu,
Yantai Institute of Coastal Zone Research (CAS), China

Reviewed by:
Zhao Wang,
University of California, Irvine, United States
Hui Wang,
Shantou University, China

***Correspondence:**
Li Zheng
zhengli@fio.org.cn

† These authors have contributed equally to this work

Specialty section:
This article was submitted to Microbiotechnology, a section of the journal Frontiers in Microbiology

Received: *25 September 2021*
Accepted: *14 March 2022*
Published: *25 April 2022*

Citation:
He C, Zheng L, Ding J, Gao W, Li Q, Han B and Li J (2022) Variation in Bacterial Community Structures and Functions as Indicators of Response to the Restoration of Suaeda salsa: A Case Study of the Restoration in the Beidaihe Coastal Wetland. Front. Microbiol. 13:783155. doi: 10.3389/fmicb.2022.783155

Microbes play an essential role in the restoration of degraded coastal wetlands. However, few studies have focused on the role of key bacteria in the restoration process. Here, *Suaeda salsa* was planted to recover the biodiversity in the degraded Beidaihe coastal wetland. We monitored omics and soil environmental factors to understand the complex relationship between the bacterial community and wetland health during the restoration period. After planting *S. salsa* in the degraded area, the soil quality was improved in the later stage of restoration (LPR). Bacterial α-diversity increased with restoration and was positively correlated with TOC. Proteobacteria is the dominant bacterial phylum during the restoration period, and Bacteroidetes, Planctomycetes, Gemmatimonadetes, and Acidobacteria were sensitive to the planting restoration. Random forest analysis picked 30 key OTUs, showing the key bacterial variation of successful restoration. The result indicated that the sum of the relative abundances of key bacterial OTUs was more than 2% in the health wetland. The β-diversity showed that the growth of *S. salsa* reshaped the soil bacterial community structure and function in the LPR, which recovered to the level in the control area. Putative biogeochemical functions showed that symbionts and aromatic compound degradation were dominant bacterial functions in the growth period of *S. salsa*. Our study proposed a new indicator to assess wetland health and the planting restoration of *S. salsa* increased bacteria groups with the ability of symbionts and aromatic compound degradation in the Beidaihe coastal wetland. This study expanded our knowledge of coastal wetland restoration and its ecological contributions.

Keywords: wetland restoration, bacterial community, biogeochemical functions, environmental factors, biological indicator

INTRODUCTION

Coastal wetlands are transitional gradients between terrestrial and oceanic ecosystems and play essential roles in biogeochemical cycles and biodiversity (Mcleod et al., 2011). Due to high primary production, coastal wetlands can produce 40% more plant biomass annually than the same area of forest (Bertness et al., 2008; Hopkinson et al., 2012). This means that coastal plants play an essential ecological role in response to carbon cycling in the world. Recently, an increasing number of coastal wetlands have undergone degradation and shrinkage due to marine pollution, such as oil spills and wastewater discharge. More than 50% of coastal wetlands are on the edge of degradation worldwide (Davidson, 2014). Wetland degradation causes the death of coastal vegetation (Dai et al., 2013), which dramatically decreases the net primary productivity and accelerates the salinization or barren of coastal soil. Replanting coastal vegetation is an efficient way to recover wetland health (Williams and Faber, 2001; Zou et al., 2014). For example, replanting mangroves in the degraded or damaged wetlands successfully recovered the ecological function of the coasts of southern Louisiana (Madison et al., 2013).

Due to a limited understanding of wetland restoration, it is still a challenge to restore degraded wetlands. Since the 1960's, scientists have paid attention to coastal ecosystem degradation, and great efforts have been made to restore and recreate damaged ecosystems (Daily, 1995; Zhao et al., 2016). Although many coastal wetland restoration projects are conducted every year, wetland degradation has not been retarded worldwide (Kentula, 2000; Lv and Liu, 2008). Bacteria play a crucial role in the restoration process of degraded coastal wetlands. Understanding the bacterial roles in the restoration period enables us to understand further the degradation and restoration of coastal wetlands.

The bacterial community is sensitive in response to the variation of the habitat environment. In coastal wetland ecosystems, the soil is an important medium for interacting bacteria and various habitats (Mitsch et al., 2013). Bacteria grow in the soil, and any soil property will influence the community structure, such as salinity, total organic carbon (TOC), and heavy metals (Dupont et al., 2014; Beattie et al., 2018; Jílková et al., 2021). Heavy metals, usually toxic environmental pollutants, decrease biodiversity in a coastal wetland. In addition, coastal plants can absorb salts from the soil to decrease the salinization of coastal soil (Bernstein, 1975), or provide a carbon source for soil bacteria via phytodetritus and root exudates (Giere, 2009; Geisseler et al., 2011). Chaudhary et al. (2018) reported that the growth of halophytes increased the bacterial diversity and shaped the bacterial community structure in salt marshes.

The bacteria community is a potential biological indicator to assess the restoration effect and wetland health since they play mainly ecological roles in the material cycles, energy flow, and ecosystem stability during the restoration period (Yu et al., 2012; Lv et al., 2016; Ma et al., 2016). The abundance of *Desulfovibrio* decreased with the planting restoration in the Yellow River Delta, China (Ma et al., 2016). Biological indices, such as richness, minor populations of soil microbial communities, and abundance of microbes, have also been used to evaluate the restoration effects of wetlands in the coastal wetlands (Wortley et al., 2013; Zhang et al., 2015; Ma et al., 2017; Lee et al., 2020).

Thousands of different operational taxonomic units (OTUs) can be obtained, and the changes of the complex bacterial communities were illuminated by 16S rRNA sequencing analysis (Ma et al., 2016; Chaudhary et al., 2018; Jílková et al., 2021). Random forest (RF) models are an ensemble learning method for classification and regression that operates by constructing a multitude of decision trees at training time and outputting the class (Ließ et al., 2012). The key bacterial OTUs that responded to planting restoration might be picked using the machine learning method to assess the restoration effect. For example, the key bacterial OTUs were studied by RF modules to predict the plant ages during the rice life cycle (Edwards et al., 2018).

Since the Penglai 19–3 oil spill event occurred in 2011, half the *S. salsa* wetland had gradually degraded in the Beidaihe coastal wetland after a few years. In 2017, the planting restoration project was performed in the degraded area by the local government. We monitored the variation of soil environmental factors and bacterial community composition and functions at different time points during the restoration period. This study aims to: (i) understand the effects of planting restoration on soil environmental variables, bacterial diversity, composition, and function. (ii) establish new bioindicators via the soil bacterial community to assess or diagnose the health of coastal wetlands. (iii) explore the relationship between bacterial community composition and function and environmental factors during the restoration period.

MATERIALS AND METHODS

Research Site

The Beidaihe coastal wetland is located west of Bohai Bay, China, in a temperate monsoon climate zone, and the average annual precipitation is 530–630 mm, with 70% rainfall during the summer (May–July). *Suaeda salsa* is the dominant native vegetation, which begins to germinate in March, elongates in May, and flourishes in August. Owing to the oil spill contamination in 2011, half of the coastal wetland had degraded in our restoration area (approximately 7.3 hectares). *Suaeda salsa* was planted to restore the vegetation in the degradation area. Four sites (R1–R4) were established to research the soil bacterial community during the restoration period. The other half of the coastal wetland was not degraded, in which the *S. salsa* has been growing well, as the control area. Five sites (C1–C5) were set up to study the soil bacterial diversity (**Figure 1**).

Abbreviations: EPC, the early period in the control area. Samples include EPC1 to EPC5 in March; EPR, the early period of planting restoration in the degraded area. Samples includes EPR1 to EPR4 in March; PC, the planting period in the control area. Samples includes PC1 to PC5 in May; PR, the planting period in the restoration area. Samples includes PR1 to PR4 in May; LPC, the later period of in the control area. Samples includes LPC1 to LPC5 in August; LPR, the later period of in the restoration area. Samples includes LPR1 to LPR5 in August.

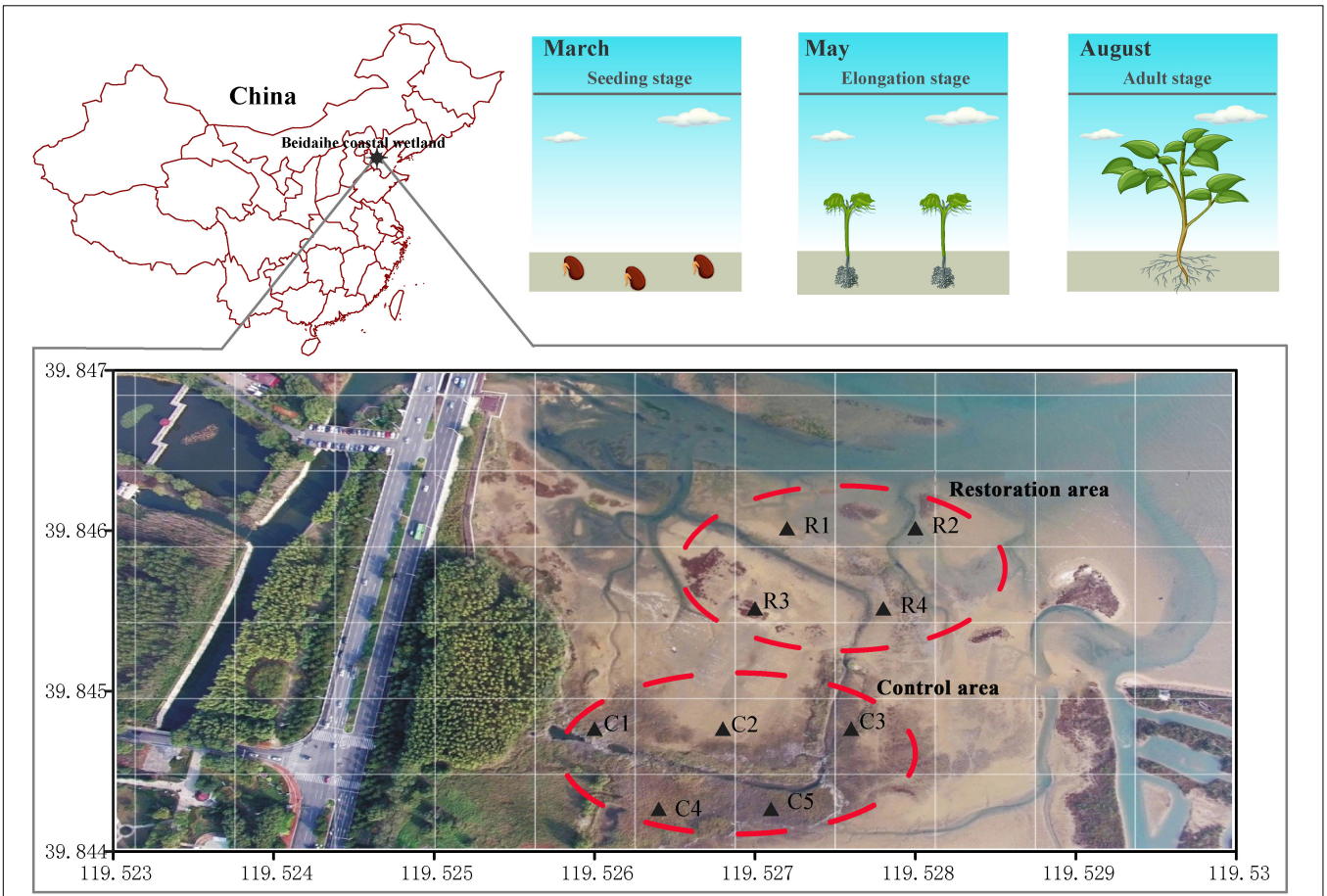

FIGURE 1 | Geographic location of sampling area in the Beidaihe coastal wetland. The aerial picture was taken in August 2016. *Suaeda salsa* barely grew in the restoration area and was dense in the control area. We sowed *S. salsa* seeds in March 2017 in the restoration area. The control area did not suffer degradation.

In the restoration area (R1–R4), *S. salsa* was planted seeds in March. To improve the density of *S. salsa* in the restoration area, *S. salsa* seedlings was replanted in May again. In August, *S. salsa* grew exuberantly in the restoration area and the *S. salsa* coverage reached approximately 80% compared to the control area.

Sample Collection

There are nine trial sites to collect the samples. Three replicates of surface soil (0–5 cm) were randomly collected at each site to be assemble as a mixed sample, which was used to extract genomic DNA and detect environmental parameters. A total of 27 soil samples were collected in March, May, and August, respectively (**Supplementary Table 1**). Based on sampling sites and collection time, 27 samples were divided into six subsamples, including EPR (Early Period of Restoration, the soil samples in the restoration area in March before restoration started), EPC (Early Period of Control, the soil samples in the control area in March), PR (Period of Restoration, the soil samples in the restoration area in May), PC (Period of Control, the soil samples in the control area in May), LPR (Later Period of Restoration, the soil samples in the restoration area in August), and LPC (Later Period of Control, the soil samples in the control area in August).

DNA Extraction, PCR Amplification, and Sequencing

According to the manufacturer's instructions, DNA was extracted from 0.5 g of soil sample using a PowerSoil DNA isolation kit (MoBio, Carlsbad, CA, United States). Extracted DNA was quantified using a spectrophotometer (Nanodrop, PeqLab, Germany). The V3-V4 region of bacterial 16S rRNA genes was amplified from the total DNA by PCR, using the specific primers 341F: CCTACGGGNGGCWGCAG and 806R:GGACTACHVGGGTATCTAAT (Guo et al., 2017). with sample-specific barcodes. The Illumina PE250 library was constructed and sequenced at Novogene Bio-Technologies Co., Ltd., Tianjin, China.

The 16S rRNA gene sequences were processed using QIIME 1.9.1, USEARCH (Caporaso et al., 2010; Bokulich et al., 2013). Raw reads with an average phred score of < 20 were discarded, and a 10-bp window from the first base with a 1-bp step length was used to filter. The detailed results showed in **Supplementary Table 2**. The rarefaction plots were presented in **Supplementary Figure 1**. The clean paired-end Illumina reads were joined, extracted by the join_paired_ends.py and extract_barcodes.py scripts. Based on the high-quality 16S representative sequences

at 97% identify level, an OTU table was generated by USEARCH (Edgar, 2010). The representative sequences were conducted using the RDP classifier (Version 2.2) and annotated with the SILVA 138.1 (Pruesse et al., 2007; Wang Q. et al., 2007; Quast et al., 2013). Functional annotation of prokaryotic taxa (FAPROTAX) is a manually constructed database that maps prokaryotic taxa to putative functions based on the literature on cultured representatives (Louca et al., 2016). A Python script, collapse_table.py,[1] can convert the OTU tables into putative functional tables based on the taxa identified in a sample and their functional annotations in the FAPROTAX database. The bacterial taxon of each function was obtained from a report file.

Statistical Analysis

All statistical analyses and plots were performed using R software (version 3.6[2]) (Ginestet, 2011). The Shannon and Simpson diversity was calculated using the "diversity" function, and the "rda" function conducted redundancy analysis (RDA) for linking bacterial communities to environmental variables using the Vegan package (Oksanen et al., 2013). The Monte Carlo permutation test (permu = 999) was performed to detect the significance of the environmental variables. Analysis of differential phylum abundance was performed using a linear model in the Performance Analytics package (Peterson et al., 2014). Analysis of variance (ANOVA) was performed using the "aov" function from the Stats package (R Core Team, 2018). A "cor" function calculated the Spearman correlation coefficient, and the p-value was adjusted with "p.adjust" (method = "bonferoni") in the R.

Generation of Sparse Random Forest Models

To model the health of wetland soil as a function of the bacterial community, we developed full RF models for soil samples by regressing the relative abundance of all OTUs against the healthy state of coastal wetland soil from which the samples were collected. For the training data, we selected eight samples from March and August in the degradation region. From the model, we ranked individual OTUs by their importance in contributing to the accuracy of wetland health prediction by the model. This process was performed by permuting the relative abundance levels for an OTU and calculating the increase in the mean squared error of the model. When permuted yield increased errors in the model, the OTU abundance was essential to the model's accuracy. The step was performed using the "importance" command from the random Forest R package (Liaw and Wiener, 2002). Because not all OTUs in the RF model contributed to the accuracy of the model, we next performed 10-fold cross validation to evaluate model performance using the "replicate" function in the randomForest R package. We found a minimal increase in accuracy when including more than 30 of the most important OTUs (**Supplementary Figure 2**). The top 30 important OTUs from the full RF model were used as input for sparse RF models for each phase.

Measurements of Environmental Parameters

Soil salinity was measured according to the method of Gartley (2011). Briefly, aqueous extract (mix 50 mL water with 10 g air-dried soil) of soil sample was prepared by shaking the mixture for 5 min and then allowed to settle for 4 h. The extraction was used to detect soil salinity with a conductivity meter (YSI Incorporated Ohio). 15 g of soil was weighed and dried to constant weight using a vacuum freeze drier (24 h) to detect the soil water content. A gas chromatography-mass spectrometer (GC-MS) was utilized to detect the polycyclic aromatic hydrocarbon (PAHs) concentration, according to Lin et al. (2018). Briefly, a total of 5 g air-dried soil (filtered through 100 mesh screen) was extracted twice with N-hexane/dichloromethane solution (1:1, v/v). The extract solution was dehydrated by anhydrous sodium carbonate and filtered through a cellulose acetate membrane (0.2 μm). The solution was used to detect the PAH concentration with 5973N GC-MS (Agilent, United States). Total organic carbon (TOC) in the soil samples was detected with a Vario Micro Cube Elemental Analyzer (Elementar, Germany) (Sun et al., 2014). The heavy metal contents were determined using ICP-MS (Agilent ICP-MS 7500a) (Li et al., 2017). The steps were as follows: the soil samples were ground to a fine powder using a pestle in an agate mortar after drying. Powdered samples weighing 0.1 g were digested by a microwave system. The digestion solution was fixed to 25 g with ultrapure water to detect the concentration of heavy metals. Meanwhile, 5 μg/L Re element was considered as the internal standard element. The heavy metal contents in certified reference materials (Yellow Sea marine sediments, GBW07333) were measured to verify the accuracy and precision of the analytical method.

RESULTS

The Alpha Diversity of Bacteria and Soil Physicochemical Properties

During the restoration time in the Beidaihe coastal wetland, a total of 10386 different OTUs were identified. In the restoration area, bacterial richness gradually increased with restoration (EPR: 0.17, PR: 0.21, LPR: 0.41). The richness slightly increased with time in the control area (EPC: 0.23, PC: 0.23, LPC: 0.33). In the later period of restoration (LPR and LPC), the bacterial diversity was significantly high compared to other periods (**Supplementary Figure 3**). A similar trend was shown in OTU numbers, shannon index and simpson in the Beidaihe coastal wetland (**Table 1** Part A).

The soil environmental factors and heavy metal concentrations are shown in **Table 1** Part B and Part C in the restoration period of Beidaihe coastal wetland. The soil water content ranged from 18 to 22%, slightly high in PC and PR (May). The soil salinity decreased slightly during the growth of *S. salsa*. The highest soil salinity (2.45 ± 0.67 g/kg)

[1]http://www.loucalab.com/archive/FAPROTAX/lib/php/index.php?section=Download

[2]https://cran.r-project.org/

TABLE 1 | Alpha-diversity and environmental factors in different restoration periods between degradation and non-degradation regions.

Site	OTUs	Shannon	Simpson	Water Content (%)	Salinity (g/kg)	PAHs (ng/g)	TOC (%)	Cr (mg/Kg)	Cu (mg/Kg)	Zn (mg/Kg)	As (mg/Kg)	Cd (mg/Kg)	Pb (mg/Kg)
	Part A					Part B		Part C					
EPR	^{b}3614	^{b}5.72	0.989	0.18 ± 0.01	2.45 ± 0.67	^{b}1875.29 ± 310.24	^{b}0.17 ± 0.01	10.4 ± 1.09	4.51 ± 0.81	13.20 ± 2.46	^{a}1.96 ± 0.3	0.06 ± 0.01	10.13 ± 0.71
EPC	^{b}5318	^{b}6.00	0.992	0.18 ± 0.01	2.4 ± 0.45	^{b}1606.3 ± 130.31	^{b}0.23 ± 0.04	11.6 ± 1.77	4.28 ± 0.85	12.04 ± 1.53	^{a}2.01 ± 0.28	0.03 ± 0.01	11.45 ± 2.34
PR	^{b}4528	^{b}6.00	0.993	0.21 ± 0.02	1.63 ± 1.09	^{b}1490.61 ± 165.3	^{b}0.26 ± 0.11	11 ± 2.08	5.51 ± 0.94	14.23 ± 2.67	^{b}1.67 ± 0.14	0.06 ± 0.01	9.54 ± 0.92
PC	^{b}5648	^{b}6.04	0.987	0.22 ± 0.01	2.16 ± 0.54	^{b}1435.63 ± 382.15	^{a}0.48 ± 0.11	10.72 ± 0.6	5.08 ± 0.77	12.75 ± 1.82	^{b}1.82 ± 0.1	0.03 ± 0.01	10.14 ± 2.32
LPR	^{a}6935	^{a}6.69	0.994	0.19 ± 0.04	1.23 ± 0.39	^{a}694.95 ± 8.83	^{a}0.52 ± 0.11	9.20 ± 2.4	4.44 ± 0.76	12.71 ± 1.24	^{b}1.44 ± 0.09	0.03 ± 0.01	9.56 ± 2.31
LPC	^{a}6608	^{a}6.46	0.993	0.18 ± 0.03	1.79 ± 0.25	^{a}1016.62 ± 169.10	^{a}0.55 ± 0.11	9.82 ± 1.9	3.81 ± 0.86	10.80 ± 1.92	^{b}1.80 ± 0.13	0.02 ± 0.01	7.63 ± 0.47

Part A, Alpha-diversity of bacteria in different groups. Part B, the environmental parameters in different groups. Part C, the heavy metal concentration in different groups. The Kruskal–Wallis test was used to determine the significant difference: ^{a,b} the different letters represent the significant difference ($p < 0.05$) among all soils.

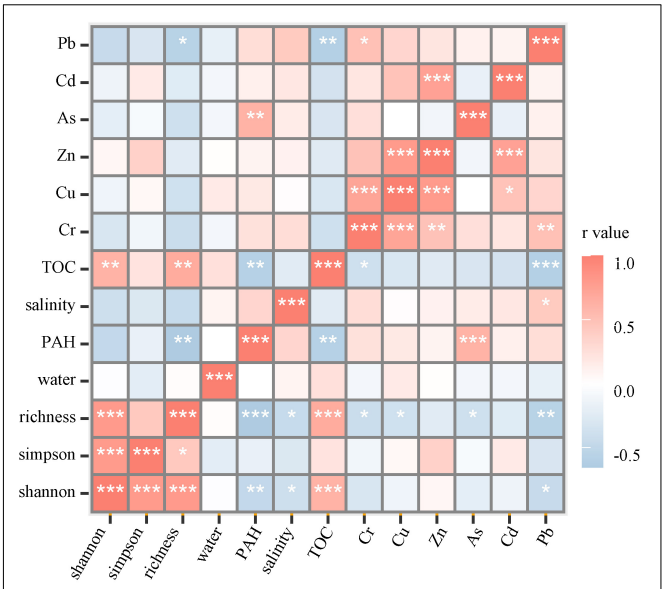

FIGURE 2 | The spearman correlation in bacterial diversity and soil environmental factors. The * stands for the p value. *, $p < 0.05$; **, $p < 0.01$; ***, $p < 0.001$.

was measured in the EPR, and the lowest (1.23 ± 0.39 g/kg) was measured in the LPR. The PAH concentration in LPR (694.95 ± 8.83 ng/g) and LPC (1016.62 ± 169.10 ng/g) was significantly lower than that in EPR (1875.29 ± 310.24 ng/g), EPC (1606.3 ± 130.31 ng/g), PR (1490.61 ± 165.3 ng/g), and PC (1435.63 ± 382.15 ng/g). The TOC concentration was significantly higher in PC, LPR, and LPC than in EPC, EPR, and PR, showing that the growth of *S. salsa* introduced the organic carbon to coastal soil. Among the heavy metals, the order of concentration was Zn (10.8 – 14.23 mg/kg) > Cr (9.2 – 11.6 mg/kg) > Pb (7.63 – 11.45 mg/kg) > Cu (3.81 – 5.51 mg/kg) > As (1.44 – 2.01 mg/kg) > Cd (0.02 – 0.06 mg/kg). In general, the concentration of all heavy metals showed a slight decrease during the wetland restoration process. The heavy metal, As decreased significantly in PR, PC, LPR, and LPC.

The spearman correlation showed that bacterial richness and the shannon index significantly positive correlated with the TOC concentration and negatively correlated with heavy metals, PAHs, and salinity. A significantly negative correlation was shown between TOC concentration and some contaminants, such as PAHs and heavy metals, Cr and Pb (**Figure 2**). The relationship illustrated that bacterial diversity increased in response to the high TOC concentration but decreased due to the high PAH, heavy metal concentration, and salinity in the soil.

Bacterial Community Composition During the Restoration Time

A total of sixty-nine different phyla were discovered during the restoration time. The bacterial communities were dominated by the phylum Proteobacteria, followed by Bacteroidetes, Planctomycetes, Firmicutes, Actinobacteria,

Gemmatimonadetes, Chloroflexi, Acidobacteria, and Verrucomicrobia, which accounted for 94% of all bacterial reads (**Figure 3**). Correlation analysis showed that the relative abundance of Bacteroides presented a significantly negative correlation with that of Planctomycetes, Gemmatimonadetes, and Acidobacteria (**Supplementary Figure 4**).

Proteobacteria were dominant in restoration period, and the relative abundance decreased slightly with the growth of *S. salsa* (**Figure 3**). Gammaproteobacteria, Alphaproteobacteria, and Deltaproteobacteria were the abundant classes of Proteobacteria. Deltaproteobacteria were more abundant in the restoration area than that in the control area. Epsilonproteobacteria were the most abundant in EPR, and the relative abundance decreased with the growth of *S. salsa* in the restoration area (**Supplementary Figure 5**). In Bacteroidetes, its relative abundance was lower in the PC, LPC, and LPR compared to that in EPC, EPR, and PR, showing that the growth of *S. salsa* likely decreased the relative abundance of Bacteroidetes. The dominant classes were Flavobacteriia, Bacteroidia, and Sphingobacteriia in the Bacteroidetes. The relative abundance of Flavobacteriia decreased gradually with restoration time in the degradation area and had highest abundance in the EPR. Bacteroidia and Sphingobacteriia were dominant in the control areas (**Supplementary Figure 6**). Relative abundance of Planctomycetes in LPC, PC, and LPR were higher than in EPC, EPR, and PR. Dominated classes, Planctomycetaceae and Phycisphaeraceae, accounted for more than 72% of the total reads in Planctomycetes (**Supplementary Figure 7**). For the Acidobacteria, its relative abundance was high in LPC, PC, and LPR. Holophagae was most abundant in Acidobacteria and mostly distributed in EPR and PR (**Supplementary Figure 8**).

The bacteria community varied at the genus level during the restoration time. The top ten genera in each sample were chosen to analyze the bacterial community (**Supplementary Figure 9**). These genera account for approximately 45% to 67% of all bacterial OTUs. In the restoration area, *Desulfosarcina*, *Ilumatobacter*, *Loktanella,* and *Actibacter* were dominant genera in EPR and PR and the abundances of these genera were significantly higher than those in other periods. The growth of *S. salsa* shaped the distribution of dominant genera at the restoration area. These genera include *Planctomyces*, *Exiguobacterium*, *Citrobacter*, *Rhodopirellula*, *Pir4_lineage*, *Urania-1B-19_marine_sediment_group*, *Blastopirellula*, *Acinetobacter*, *unidentified bacterium wb1_A18*, and *Pseudomonas*, were dominant bacteria in LPR and were consistent with the predominant genera in PC and LPC. It is worth noting that the bacterial community in EPC had uniquely dominant genera, *Gramella*, *Roseovarius*, and *Marinobacter*, the relative abundances of which were significantly higher than those in the other groups.

The Key Bacterial Operational Taxonomic Units During the Restoration Time

Operational taxonomic units (OTUs) are the basic taxonomic units for bacterial community structure and are sensitive to the variation of *S. salsa* growth and environmental factors (Edwards et al., 2018; Liu et al., 2019). Based on the random forest (RT) model, a total of 30 different key bacterial OTUs were identified during the restoration time, which could successfully predict 73.7% of the test samples (**Supplementary Table 3**), showing that these key OTUs can be used to represent the variation of the bacterial community during the restoration process.

The relative abundance of the key OTUs in different groups is shown in **Figure 4A**. Many key OTUs were abundant in LPR, ECP, PC, and LPC. Based on V3-V4 sequences, the phylogenetic analysis found that these key OTUs were divided into 11 different clusters, including Gammaproteobacteria, Alphaproteobacteria, Acidobacteria, Firmicutes, SBR1093, Gemmatimonadetes, Chloroflexi, Planctomycetes, Bacteroidetes and Deltaproteobacteria (**Figure 4B**). Most key OTUs belonged to Proteobacteria, Planctomycetes, and Bacteroidetes. The detailed annotation results of each key OTU are shown in **Supplementary Table 4**. For example, OTU_391, OTU_143, OTU_132, OTU_39, and OTU_35 were annotated into *Winogradskyella*, *Marinobacter*, *Fusibacter*, *Sediminicola*, and *Halioglobus,* respectively, and these genera were most abundant in EPR and PR. OTU 13 belonged to Planctomyces and was the dominant OTU in LPR, EPC, PC, and LPC.

Among the relative abundance of key bacterial OTUs in the whole bacterial community, the sum of the relative abundances of all key bacterial OTUs was a potential biological indicator to evaluate the restoration effect and health (**Figure 4C**). The sum of the relative abundance of all key bacterial OTUs ranged from 0.8 to 5.7% during restoration time. However, it ranged from 2 to 5.7% in LPR, PC, and LPC, significantly higher than in EPR and PR ($< 2\%$). It was noteworthy that the sum of the relative abundance of all key bacterial OTUs in EPC was not significantly different from that in the other groups.

The Distribution of the Bacterial Community and Function During Restoration Time

The β-diversity of the bacterial community and function are shown in **Figure 5**. PCA results showed that the bacterial community in LPR was most similar to that in the control area, indicating that the growth of *S. salsa* shaped the bacterial community in the restoration area (**Figure 5A**). And the bacterial community function represented a similar variation with the community (**Figure 5B**). In the degraded periods (EPR and PR), bacterial community function was most related to the respiration of inorganic sulfur compounds, such as sulfur respiration, sulfate respiration, respiration of sulfur compounds, and thiosulfate respiration. However, the dominant bacterial functions included aromatic compound degradation, symbionts, hydrocarbon degradation, nitrate reduction, phototrophy, and photoautotrophy in the health periods (control and LPR) (**Figure 5B**). The β-Diversity analysis showed that the growth of *S. salsa* shaped the bacterial community in the soil and affected the bacterial community's function.

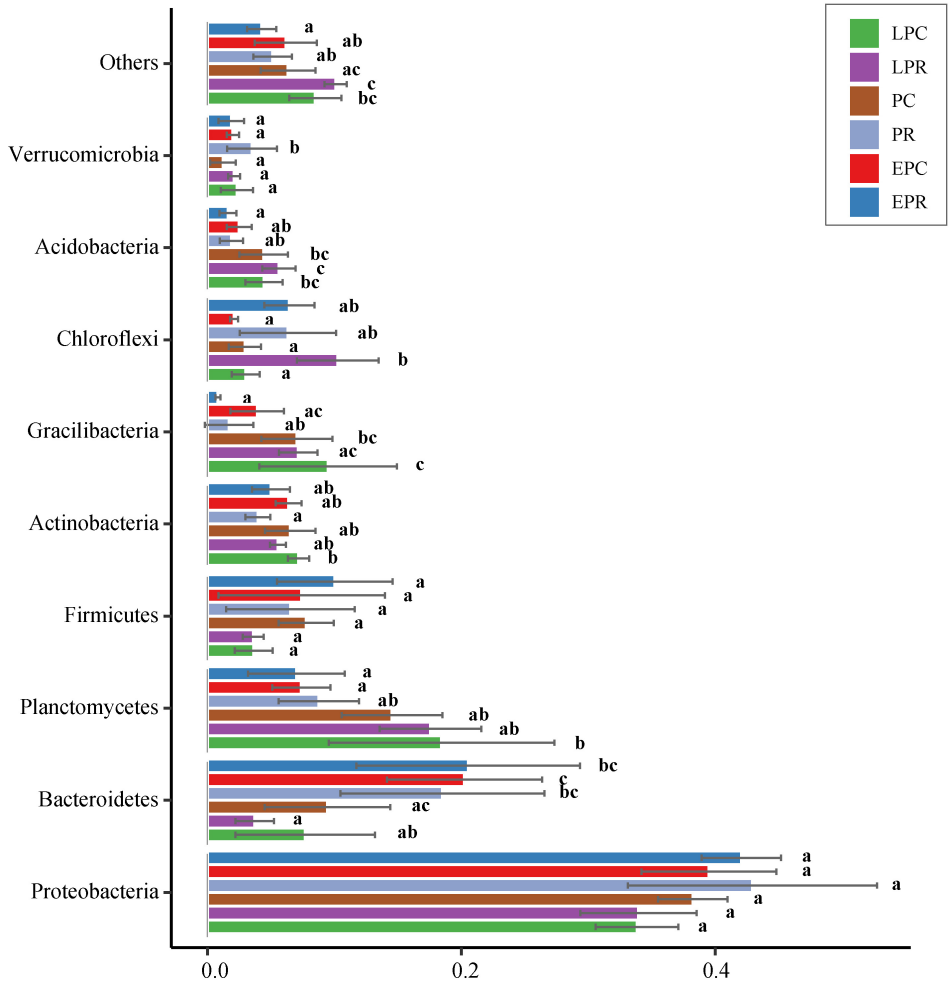

FIGURE 3 | Bar plots of the top 9 phyla abundances during different restoration periods in the degraded and non-degraded wetland. [a,b,c]The different letters represent the significant difference ($p < 0.05$) between different groups.

Bacterial Community Connects With Soil Environmental Factors During the Restoration Time

To study the relationship between the bacterial community and soil environmental factors, redundancy analysis (RDA) was performed, and the first two axes explained 39.86 and 17.24% of the total variance, respectively (**Figure 6A**). The first axis was driven by soil properties (TOC, PAHs) and some heavy metals Cu/Zn/Cd, while the second axis was driven by salinity and As. The TOC concentration correlated significantly with the bacterial community structure in LPR, PC, and LPC. The concentrations of heavy metals and PAH significantly affected the community structure in EPR and PR. The bacterial community in EPCs could be affected by salinity and heavy metals (As).

As a biological indicator, the sum of the relative abundance of 30 key bacterial OTUs correlated closely to the variation in soil environmental factors. We found that the sum of the relative abundance of all key bacterial OTUs was significantly positively correlated with the TOC concentration (**Figure 6B**) and negatively correlated with the PAH concentration in the soil (**Figure 6C**). This showed that the sum of the relative abundance of all key bacterial OTUs was most sensitive in response to the various environmental factors.

Bacterial Community Function and Association With Soil Environmental Factors During the Restoration Process

Bacteria are involved in diverse ecological roles, including chemoheterotrophy, aerobic chemoheterotrophy, respiration of different S-containing substances, symbionts, hydrocarbon degradation, fermentation, aromatic compound degradation, and phototrophy (**Figure 7**). Among them, the respiration of inorganic sulfur compounds, such as sulfate respiration, sulfur respiration, respiration of sulfur compounds, and thiosulfate respiration, was significantly dominant in the restoration area compared to that in the control area, and the relative abundance decreased slightly in the LPR of the restoration area. Deltaproteobacteria and Firmicutes were involved in

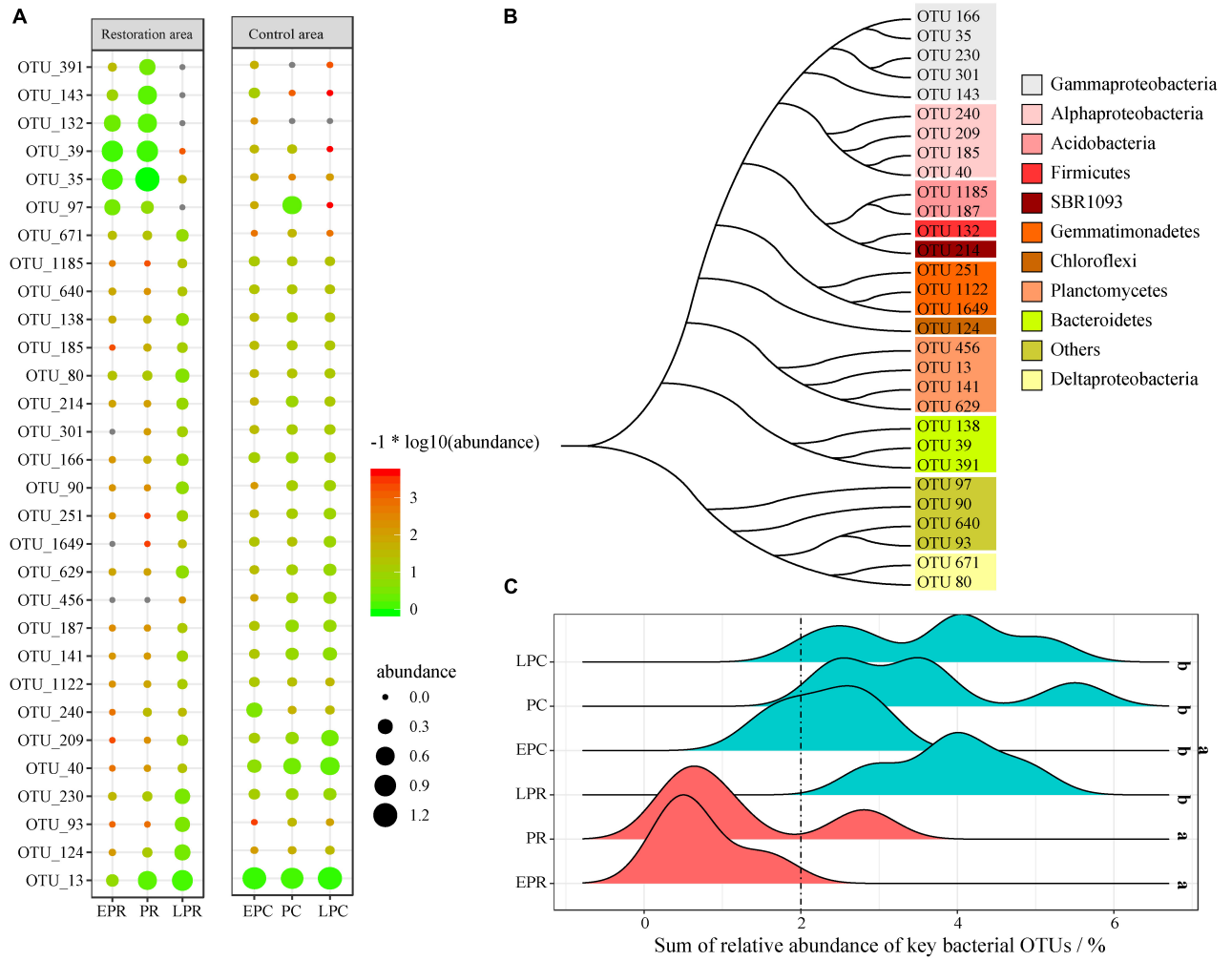

FIGURE 4 | The random forest (RF) model detects the key operational taxonomic units (OTUs) during the restoration time. **(A)** The fingerprint spectrum of key OTUs in different groups; **(B)** phylogenetic analysis of key OTUs; **(C)** the sum of relative abundance of key OTUs in different groups. [a,b]The different letters represent the significant difference ($p < 0.05$). OrangeRed represents the samples during the degradation period. Cyan stands for samples of restoration success and control area.

the respiration of inorganic sulfur compounds during the restoration time (**Figure 7B**). The ecological function of symbionts and aromatic compound degradation was determined via Gammaproteobacteria, Bacteroidetes, and Firmicutes. Theirs relative abundances were significantly higher in LPR, PC, and LPC than in EPR, PR, and EPC. Chemoheterotrophy and aerobic chemoheterotrophy were the most abundant bacterial community roles during the restoration time, showing that heterotrophic bacteria played an essential role in the material cycle of coastal wetlands.

Spearman correlation was applied to study the relationship between bacterial community function and soil environmental factors (**Figure 7C**). Bacterial diversity (richness), the sum of key OTUs, and TOC were positively correlated with symbionts and aromatic compound degradation functions and negatively related to the respiration of inorganic sulfur compounds during the restoration time. The PAH concentration and some pollutants were significantly positively correlated with the bacterial chemoheterotrophy and negatively associated with the symbionts and aromatic compound degradation. The relationship showed that the restoration of *S. salsa* promoted the growth of bacteria with symbionts and aromatic compound degradation functions to improve the soil TOC. Among the degraded area, bacteria with the respiration of inorganic sulfur compound function were abundant, negatively correlated to soil TOC to hold back organic carbon storage.

DISCUSSION

The degradation of coastal wetlands is an environmental problem worldwide. An increasing number of scientists are trying their best to treat this "environmental disease" (Williams and Faber, 2001; Zou et al., 2014; Sapkota and White, 2020). *Suaeda salsa* is a salt-tolerant plant (Lynum et al., 2020) and serves as the dominant native plant in Beidaihe coastal wetland, which is a

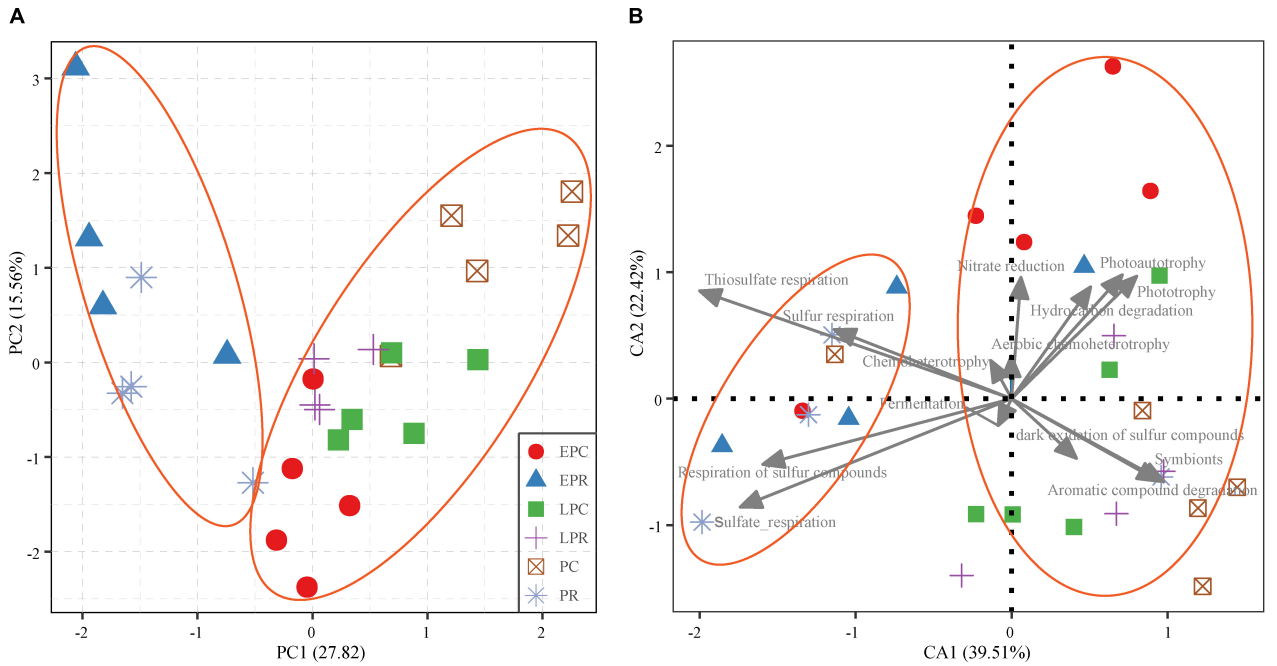

FIGURE 5 | The β-diversity of the bacterial community **(A)** and bacterial community function **(B)**. The shape and color of the point stand the different groups. The gray line is the dominant bacterial function (the relative abundance > 1%).

suitable species to restore the degraded wetland in our restoration project. Previous restoration projects have successfully recovered the ecological function by planting *S. salsa* in China's Yellow River Delta (YRD) (Ma et al., 2017). In our study, we traced the process of planting restoration and explored the soil environmental factors and bacterial community and function to understand the relationship between soil bacteria and *S. salsa* restoration.

The restoration of planting *S. salsa* improved the soil organic carbon concentration and changed the bacterial community in coastal wetlands. Bacteria can decompose the particulate matter to produce organic carbon in the soil, such as biological carbon pump theory in the ocean (Coleman, 1994; Jiao et al., 2018; Lian et al., 2021). In our study, soil TOC concentration was significantly higher in the LPR than in the EPR and PR (**Table 1**), indicating that the growth of *S. salsa* potentially provided the organic matter for soil microbial activities and shaped community structure and function. PCA analysis found that the bacterial community in LPR was more similar to that in the control area (**Figure 5**). In addition, *S. salsa* was a primary net primary productivity in Beidaihe coastal wetland, which can fix the carbon dioxide into organic carbon to be delivered into the soil by root exudates (Giere, 2009; Geisseler et al., 2011; Chaudhary et al., 2018; Ward, 2020). Our study showed that the growth of *S. salsa* increased the symbiotic function of the soil bacterial community. Symbiosis was any close and long-term biological interaction between two different biological organisms (Brinkman et al., 2002), suggesting a close exchange between bacteria and *S. salsa*.

Due to its biotoxicity, PAHs are an important and typical pollutant of oil contaminants (Vane et al., 2014). The Beidaihe wetland has been damaged by oil pollution since the Bohai 19–3 oil spill accident occurred in 2011. Lin et al. (2018) conducted a survey and ecological risk assessment of PAHs in this wetland in 2016. It was found that the ecological risk of PAHs in degraded regions reached a medium level. In our study, the PAH concentrations decreased gradually with restoration. Biological degradation was the main process of PAH transformation in the coastal wetlands (Bourceret et al., 2018). The aromatic compound degradation functions were abundant in LPR, PC, and LPC, suggesting that the growth of *S. salsa* promotes the microbial degradation of PAH, which can be explained by the soil priming effect (Bastida et al., 2019).

In addition, heavy metal elements (As, Cd, Cr, Zn, and Cu) affected the bacterial community structure due to a toxic effect, particularly at high concentrations (Wang Y. et al., 2007; Li et al., 2020). In our study, heavy metals decreased slightly with restoration, affected the bacterial community in EPR and PR, and were negatively related to bacterial richness and the Shannon index. Some studies have proven that *S. salsa* can absorb heavy metals from soil (Lutts and Lefèvre, 2015; Zhang et al., 2018). A previous study showed that some heavy metals negatively affected microbial biomass accumulation and productivity even at low concentrations, such as 1 ppm for Pb, 2 ppm for Cd and 5 ppm for Zn (Beattie et al., 2018).

The biological and chemical parameters had profitably changed in LPR, suggesting a successful restoration in the Beidaihe coastal. For example, the respiration of inorganic sulfur compounds was more abundant in the restoration area, and their relative abundance decreased slightly in LPR (**Figure 7**). Bacteria utilize the inorganic sulfur compounds as electron acceptors to

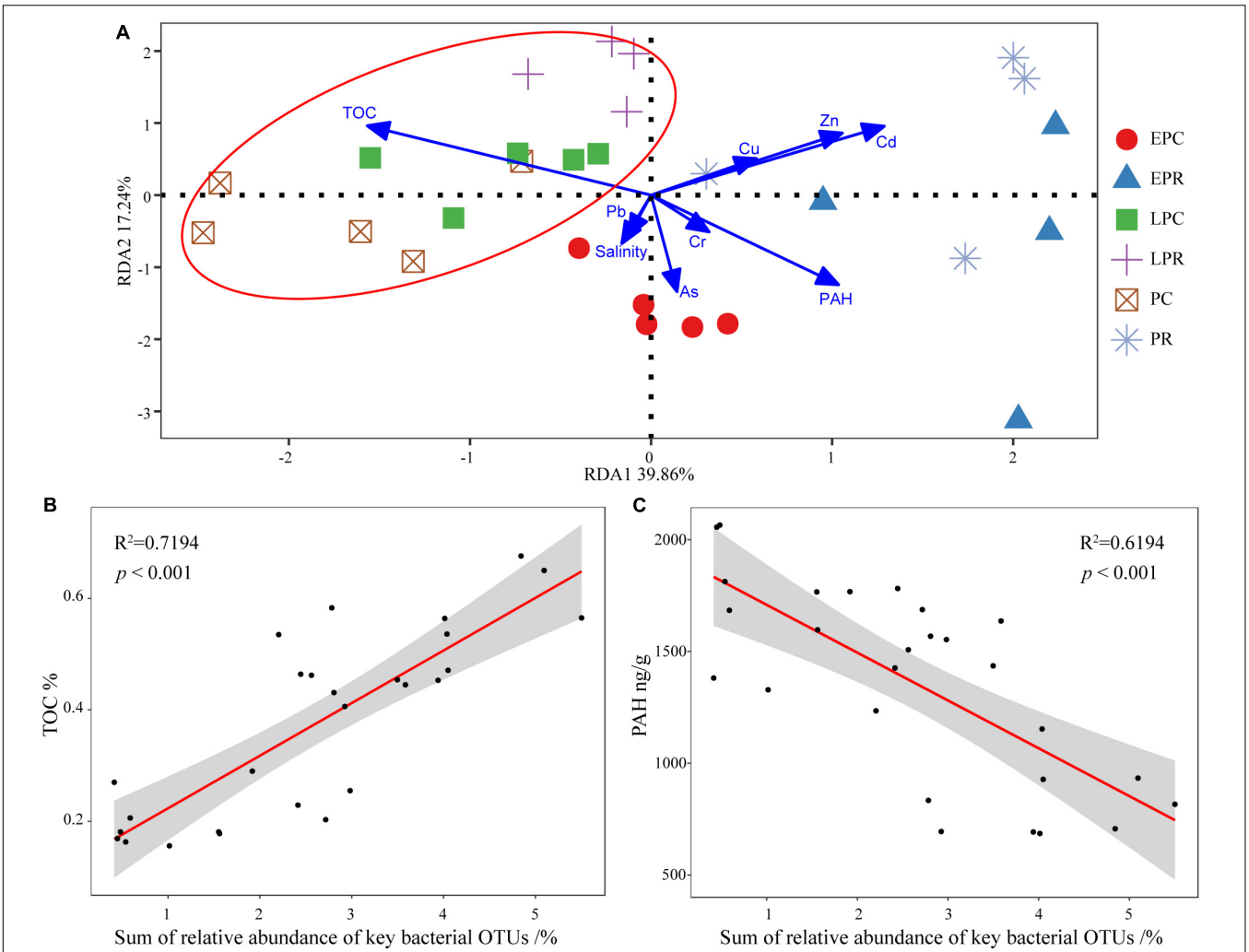

FIGURE 6 | The relationship between bacterial community structure and environmental factors. **(A)** Redundancy analysis (RDA) analyze the relationship between bacterial community and environmental factors in different groups. The shape and color of the point stands for different groups. Linear-regression analysis between the sum of relative abundance of key operational taxonomic units (OTUs) and total organic carbon (TOC) **(B)**, and polycyclic aromatic hydrocarbon (PAH) **(C)** concentration.

produce reduced sulfur, such as hydrogen sulfide, via respiration (Hedderich et al., 1998; Florentino et al., 2016). Hydrogen sulfide is a broad-spectrum poison (Lindenmann et al., 2010), suggesting a wetland health threat of respiration of inorganic sulfur compounds in the restoration area.

The assessment and diagnosis of coastal wetland health are the most important for efficient management. In our study, the soil environmental parameters, bacterial community structure, diversity, and function shifted after the restoration of *S. salsa*, which were good indicators to evaluate the restoration effect. High TOC (Ruiz-Jaen and Aide, 2005; Milton and Finlayson, 2018) and low pollutant concentrations (Chen et al., 2019) indicated healthy soil quality, similar to the soil parameters in LPR (**Table 1**). Due to the limited information on monitoring data, these parameters lack efficiency and accuracy to define the restoration effect in coastal wetlands (Suding, 2011). Urakawa and Bernhard (2017) reported that the evaluation of restoration could not be met effectively by a single physical and chemical parameter, but a combination of multiple attributes is effective for robust wetland assessment and management. Therefore, bacterial populations serve as the most sensitive and rapid bioindicator in response to various environmental changes, which is suitable to evaluate wetland health. A study showed that bacterial richness could be applied to assess coastal wetland health (high richness was considered a healthy wetland) (Delgado-Baquerizo et al., 2016; Urakawa and Bernhard, 2017). In our study, the bacterial richness in LPR and LPC was significantly higher than that in EPR and PR but was not significantly different from that in PC and EPC, suggesting a low efficiency and accuracy to assess wetland health. Notably, the sum of key OTUs showed a significantly different in PC period, suggesting a higher accuracy compared to richness (**Figure 4C**). The sum of key OTUs closely related to the soil parameters (TOC and PAH concentration) and bacterial function (decreasing respiration of inorganic sulfur compounds

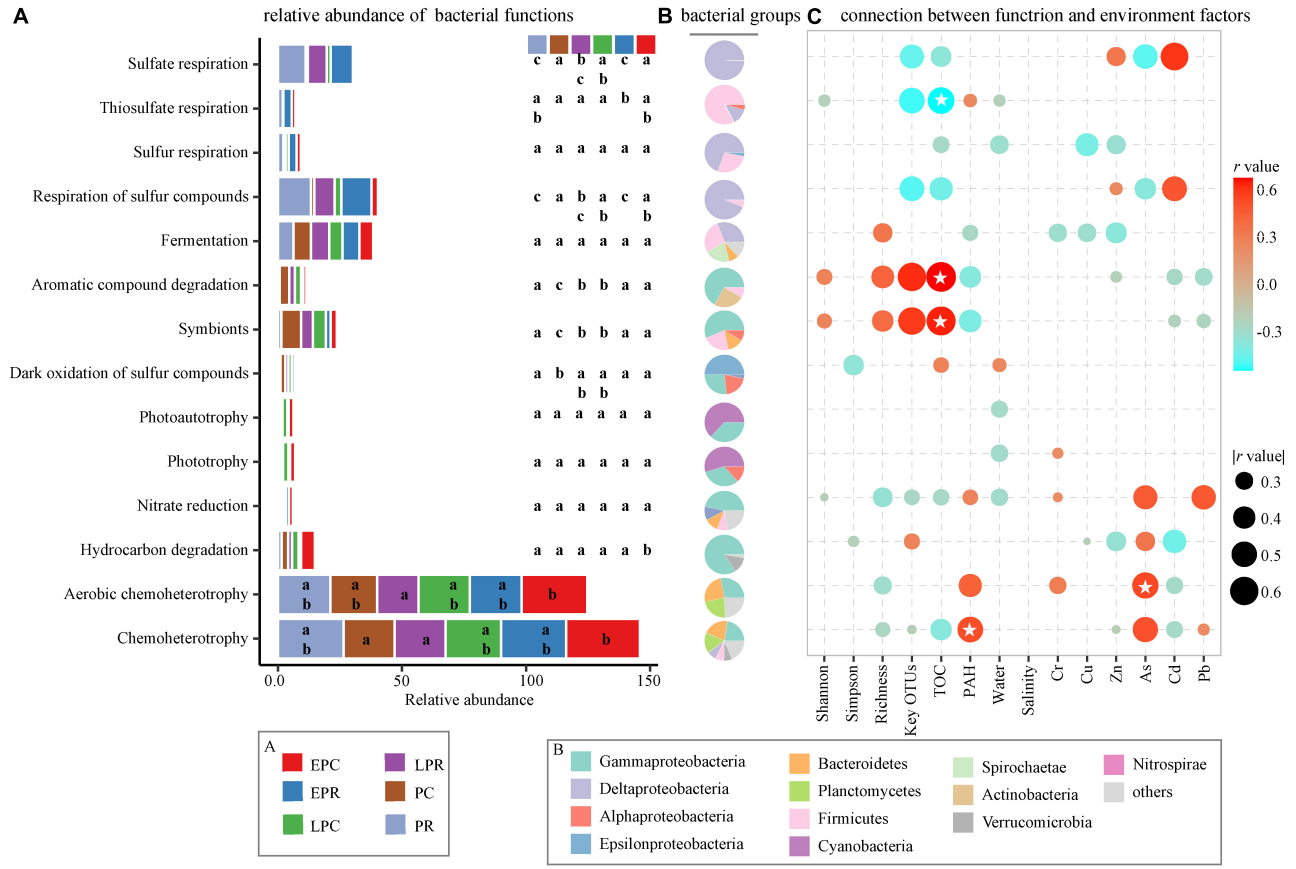

FIGURE 7 | Bacterial ecological roles during the restoration time. **(A)** The relative abundance of different bacterial functions. The color presents different groups, consistent with the color in **Figures 3**, **5**, **6**. **(B)** The main bacterial phylum contributed to the ecological functions. The different colors stand for the bacterial taxon. **(C)** The connection between bacterial function and soil environmental factors. $|r| > 0.3$, * stands for $p < 0.05$.

and increasing symbionts and aromatic compound degradation during the restoration time), indicating that the sum of key OTUs was a synthetic attribute of multiple attributes in chemistry and biology. This presented a new bioindicator to assess or diagnose coastal wetland health, which was more efficient and accurate than other parameters.

In this study, our results provided a good reference for the health assessment of wetlands by key bacterial OTUs. Among the RF modules, it is difficult to control the inner workings of the model, like a "black box." It is more helpful to improve the RF module by the large-scale samples and more attempts between different parameters and random seeds. In the future, Large-scale studies in the coastal wetland degradation will provide sufficient evidence for the key bacterial OTUs by RF modules as bioindicator to assess the restoration effect and wetland health. Meanwhile, the absolute abundance of key OTUs is necessary to understand the variation of key OTUs in the quantity level.

CONCLUSION

The degraded Beidaihe coastal wetland was restored by planting native vegetation *S. salsa*. Based on the restoration processes, we found that the soil TOC and bacterial diversity increased, and pollutant concentrations, such as PAHs and heavy metals, decreased after the restoration of *S. salsa*. This indicated that restoration could potentially improve the carbon storage ability in the soil. In addition, variations in biological and chemical parameters can be applied to predict soil health, such as high soil TOC and bacterial diversity and low pollutant concentrations. Interestingly, we found that the sum of key OTUs is closely related to the soil TOC, PAH, and bacterial functions, and it can accurately evaluate the effect of the restoration. This case study is the first time to propose an accurate biological indicator to assess or diagnose coastal wetland health. Although our research was focused on northern China's coastal wetlands, it provides a good reference for the health assessment of other wetlands.

DATA AVAILABILITY STATEMENT

The datasets presented in this study can be found in online repositories. The names of the repository/repositories and accession number(s) can be found below: https://www.ncbi.nlm.nih.gov/bioproject/PRJNA767015.

AUTHOR CONTRIBUTIONS

LZ and CH conceived the study. CH wrote the manuscript and performed the statistical analyses. LZ revised the manuscript. JD, WG, and QL involved in the field investigation and soil sampling. BH and JL performed PAHs and heavy mental analysis. All authors discussed the results and commented in the manuscript.

FUNDING

This research was supported by the National Natural Science Foundation of China (Nos. 41776176 and 41806201), the National Natural Science Foundation of China-Shandong Joint Funded Project (No. U1606404), Bohai 19-3 Platform Oil Spill Compensation Project: Ecological Restoration of Coastal Wetland in Beidaihe and Open Fund of Key Laboratory of Biotechnology and Bioresources Utilization (Dalian Minzu University), and Ministry of Education (No. KF202006), China.

SUPPLEMENTARY MATERIAL

The Supplementary Material for this article can be found online at: https://www.frontiersin.org/articles/10.3389/fmicb.2022.783155/full#supplementary-material

REFERENCES

Bastida, F., García, C., Fierer, N., Eldridge, D. J., Bowker, M. A., Abades, S., et al. (2019). Global ecological predictors of the soil priming effect. *Nat. Commun.* 10;3481. doi: 10.1038/s41467-019-11472-7

Beattie, R. E., Henke, W., Campa, M. F., Hazen, T. C., McAliley, L. R., and Campbell, J. H. (2018). Variation in microbial community structure correlates with heavy-metal contamination in soils decades after mining ceased. *Soil Biol. Biochem.* 126, 57–63. doi: 10.1016/j.soilbio.2018.08.011

Bernstein, L. (1975). Effects of salinity and sodicity on plant growth. *Ann. Rev. Phytopathol.* 13, 295–312. doi: 10.1146/annurev.py.13.090175.001455

Bertness, M. D., Crain, C., Holdredge, C., and Sala, N. (2008). Eutrophication and consumer control of new England salt marsh. *Conserv. Biol.* 22, 131–139. doi: 10.1111/j.1523-1739.2007.00801.x

Bokulich, N. A., Subramanian, S., Faith, J. J., Gevers, D., Gordon, J. I., Knight, R., et al. (2013). Quality-filtering vastly improves diversity estimates from Illumina amplicon sequencing. *Nat. Methods* 10, 57–59. doi: 10.1038/nmeth.2276

Bourceret, A., Leyval, C., Faure, P., Lorgeous, C., and Cébron, A. (2018). High PAH degradation and activity of degrading bacteria during alfalfa growth where a contrasted active community developed in comparison to unplanted soil. *Environ. Sci. Pollut. Res.* 25, 29556–29571. doi: 10.1007/s11356-018-2744-1

Brinkman, F. S., Blanchard, J. L., Cherkasov, A., Av-Gay, Y., Brunham, R. C., Fernandez, R. C., et al. (2002). Evidence that plant-like genes in chlamydia species reflect an ancestral relationship between Chlamydiaceae, cyanobacteria, and the chloroplast. *Genome Res.* 12, 1159–1167. doi: 10.1101/gr.341802

Caporaso, J. G., Kuczynski, J., Stombaugh, J., Bittinger, K., Bushman, F. D., Costello, E. K., et al. (2010). QIIME allows analysis of high-throughput community sequencing data. *Nat. Methods* 7, 335–336. doi: 10.1038/nmeth.f.303

Chaudhary, D. R., Kim, J., and Kang, H. (2018). Influences of different halophyte vegetation on soil microbial community at temperate salt marsh. *Microb. Ecol.* 75, 729–738. doi: 10.1007/s00248-017-1083-y

Chen, W., Cao, C., Liu, D., Tian, R., Wu, C., Wang, Y., et al. (2019). An evaluating system for wetland ecological health: case study on nineteen major wetlands in Beijing-Tianjin-Hebei region China. *Sci. Total Environ.* 666, 1080–1088. doi: 10.1016/j.scitotenv.2019.02.325

Coleman, D. C. (1994). The microbial loop concept as used in terrestrial soil ecology studies. *Microb. Ecol.* 28, 245–250. doi: 10.1007/BF00166814

Dai, X., Ma, J., Zhang, H., and Xu, W. (2013). Evaluation of ecosystem health for the coastal wetlands at the Yangtze Estuary. Shanghai. *Wetl. Ecol. Manag.* 21, 433–445. doi: 10.3390/ijerph182111642

Daily, G. C. (1995). Restoring value to the world's degraded lands. *Science* 269, 350–354. doi: 10.1126/science.269.5222.350

Davidson, N. C. (2014). How much wetland has the world lost? Long-term and recent trends in global wetland area. *Mar. Freshw. Res.* 65, 934–941. doi: 10.1071/mf14173

Delgado-Baquerizo, M., Maestre, F. T., Reich, P. B., Jeffries, T. C., Gaitan, J. J., Encinar, D., et al. (2016). Microbial diversity drives multifunctionality in terrestrial ecosystems. *Nat. Commun.* 7:10541. doi: 10.1038/ncomms10541

Dupont, C. L., Larsson, J., Yooseph, S., Ininbergs, K., Goll, J., Asplund-Samuelsson, J., et al. (2014). Functional tradeoffs underpin salinity-driven divergence in microbial community composition. *PLoS One* 9:e89549. doi: 10.1371/journal.pone.0089549

Edgar, R. C. (2010). Search and clustering orders of magnitude faster than BLAST. *Bioinformatics* 26, 2460–2461. doi: 10.1093/bioinformatics/btq461

Edwards, J. A., Santos-Medellín, C. M., Liechty, Z. S., Nguyen, B., Lurie, E., Eason, S., et al. (2018). Compositional shifts in root-associated bacterial and archaeal microbiota track the plant life cycle in field-grown rice. *PLoS Biol.* 16:e2003862. doi: 10.1371/journal.pbio.2003862

Florentino, A. P., Weijma, J., Stams, A. J., and Sánchez-Andrea, I. (2016). "Ecophysiology and application of acidophilic sulfur-reducing microorganisms," in *Biotechnology of Extremophiles*, ed. P. H. Rampelotto (New York, NY: Springer, Cham), 141–175. doi: 10.1007/978-3-319-13521-2_5

Gartley, K. L. (2011). "Recommended methods for measuring soluble salts in soils," in *Recommended Soil Testing Procedures for the Northeastern United States. Northeastern Regional Publication*, Vol. 493, eds J. T. Sims and A. Wolf (Newark, DE: Agricultural Experiment Station, University of Delaware).

Geisseler, D., Horwath, W. R., and Scow, K. M. (2011). Soil moisture and plant residue addition interact in their effect on extracellular enzyme activity. *Pedobiologia* 54, 71–78. doi: 10.1016/j.pedobi.2010.10.001

Giere, O. (2009). "The biotope: factors and study methods," in *Meiobenthology: The Microscopic Motile Fauna of Aquatic Sediments*, ed. A. de Leon Oliver (Berlin: Springer), 7–62. doi: 10.1007/978-3-540-68661-3_2

Ginestet, C. (2011). ggplot2: elegant graphics for data analysis. *J. R. Stat. Soc.* A 174, 245–246. doi: 10.1111/j.1467-985X.2010.00676_9.x

Guo, M., Wu, F., Hao, G., Qi, Q., Li, R., Li, N., et al. (2017). *Bacillus subtilis* improves immunity and disease resistance in rabbits. *Front. Immunol.* 8:354. doi: 10.3389/fimmu.2017.00354

Hedderich, R., Klimmek, O., Kröger, A., Dirmeier, R., Keller, M., and Stetter, K. O. (1998). Anaerobic respiration with elemental sulfur and with disulfides. *FEMS Microbiol. Rev.* 22, 353–381. doi: 10.1111/j.1574-6976.1998.tb00376.x

Hopkinson, C. S., Cai, W. J., and Hu, X. (2012). Carbon sequestration in wetland dominated coastal systems—a global sink of rapidly diminishing magnitude. *Curr. Opin. Environ. Sustain.* 4, 186–194. doi: 10.1016/j.cosust.2012.03.005

Jiao, N., Cai, R., Zheng, Q., Tang, K., Liu, J., Jiao, F., et al. (2018). Unveiling the enigma of refractory carbon in the ocean. *Natl. Sci. Rev.* 5, 459–463. doi: 10.1093/nsr/nwy020

Jílková, V., Jandová, K., and Kukla, J. (2021). Responses of microbial activity to carbon, nitrogen, and phosphorus additions in forest mineral soils differing in organic carbon content. *Biol. Fertil. Soils* 57, 513–521. doi: 10.1007/s00374-021-01545-5

Kentula, M. E. (2000). Perspectives on setting success criteria for wetland restoration. *Ecol. Eng.* 15, 199–209. doi: 10.1016/s0925-8574(00)00076-8

Lee, H., Heo, Y. M., Kwon, S. L., Yoo, Y., Lee, A. H., Kwon, B. O., et al. (2020). Recovery of the benthic bacterial community in coastal abandoned saltern requires over 35 years: a comparative case study in the Yellow Sea. *Environ. Int.* 135:105412. doi: 10.1016/j.envint.2019.105412

Li, J., Sun, C., Zhang, L., Ding, J., Jiang, F., Wang, Z., et al. (2020). Current distribution characteristics of trace elements in the coral-reef systems of Xisha Islands China. *Mar. Pollut. Bull.* 150:110737. doi: 10.1016/j.marpolbul.2019.110737

Li, J., Sun, C., Zheng, L., Yin, X., Chen, J., and Jiang, F. (2017). Geochemical characteristics of rare earth elements in the surface sediments from the Spratly Islands of China. *Mar. Pollut. Bull.* 114, 1103–1109. doi: 10.1016/j.marpolbul.2016.10.016

Lian, J., Zheng, X., Zhuo, X., Chen, Y. L., He, C., Zheng, Q., et al. (2021). Microbial transformation of distinct exogenous substrates into analogous composition of recalcitrant dissolved organic matter. *Environ. Microbiol.* 23, 2389–2403. doi: 10.1111/1462-2920.15426

Liaw, A., and Wiener, M. (2002). Classification and regression by randomForest. *R News* 2, 18–22.

Ließ, M., Glaser, B., and Huwe, B. (2012). Uncertainty in the spatial prediction of soil texture: comparison of regression tree and random forest models. *Geoderma* 170, 70–79. doi: 10.1016/j.geoderma.2011.10.010

Lin, F., Han, B., Ding, Y., Li, Q., Gao, W., and Zheng, L. (2018). Distribution characteristics, sources, and ecological risk assessment of polycyclic aromatic hydrocarbons in sediments from the qinhuangdao coastal wetland China. *Mar. Pollut. Bull.* 127, 788–793. doi: 10.1016/j.marpolbul.2017.09.054

Lindenmann, J., Matzi, V., Neuboeck, N., Ratzenhofer-Komenda, B., Maier, A., and Smolle-Juettner, F. M. (2010). Severe hydrogen sulphide poisoning treated with 4-dimethylaminophenol and hyperbaric oxygen. *Diving Hyperb. Med.* 40, 213–217.

Liu, M., Huang, H., Bao, S., and Tong, Y. (2019). Microbial community structure of soils in Bamenwan mangrove wetland. *Sci. Rep.* 9, 1–11. doi: 10.1038/s41598-019-44788-x

Louca, S., Parfrey, L. W., and Doebeli, M. (2016). Decoupling function and taxonomy in the global oceanmicrobiome. *Science* 353, 1272–1277. doi: 10.1126/science.aaf4507

Lutts, S., and Lefèvre, I. (2015). How can we take advantage of halophyte properties to cope with heavy metal toxicity in salt-affected areas? *Ann. Bot.* 115, 509–528. doi: 10.1093/aob/mcu264

Lv, X., Ma, B., Yu, J., Chang, S. X., Xu, J., Li, Y., et al. (2016). Bacterial community structure and function shift along a successional series of tidal flats in the yellow river Delta. *Sci. Rep.* 6:36550. doi: 10.1038/srep36550

Lv, X. G., and Liu, X. H. (2008). Wetland research progresses in China – dedicated to the 50th anniversary of northeast institute of geography and agroecology CAS. *Sci. Geogr. Sin.* 28, 301–308.

Lynum, C. A., Bulseco, A. N., Dunphy, C. M., Osborne, S. M., Vineis, J. H., and Bowen, J. L. (2020). Microbial community response to a passive salt marsh restoration. *Estuaries Coasts* 43, 1439–1455. doi: 10.1007/s12237-020-00719-y

Ma, B., Wang, H. Z., Dsouza, M., Lou, J., He, Y., Dai, Z. M., et al. (2016). Geographic patterns of co-occurrence network topological features for soil microbiota at continental scale in eastern China. *ISME* 10, 1891–1901. doi: 10.1038/ismej.2015.261

Ma, Z., Zhang, M., Xiao, R., Cui, Y., and Yu, F. (2017). Changes in soil microbial biomass and community composition in coastal wetlands affected by restoration projects in a Chinese delta. *Geoderma* 289, 124–134. doi: 10.1016/j.geoderma.2016.11.037

Madison, M. J., Mack, S. K., Lane, R. R., and Day, J. W. (2013). "Wetland restoration using mangroves in southern Louisiana," in *Paper Presented at the SPE Americas E&P Health, Safety, Security and Environmental Conference*, Galveston TX. doi: 10.2118/163789-MS

Mcleod, E., Chmura, G. L., Bouillon, S., Salm, R., Björk, M., Duarte, C. M., et al. (2011). A blueprint for blue carbon: toward an improved understanding of the role of vegetated coastal habitats in sequestering CO2. *Front. Ecol. Environ.* 9:552–560. doi: 10.1890/110004

Milton, G. R., and Finlayson, C. M. (2018). "Freshwater ecosystem types and extents," in *Freshwater Ecosystems in Protected Areas*, eds F. Max, A. H. Arthington, and A. Pittock (London: Routledge), 17–33. doi: 10.4324/9781315226385-2

Mitsch, W. J., Bernal, B., Nahlik, A. M., Mander, Ü, Zhang, L., Anderson, C. J., et al. (2013). Wetlands, carbon, and climate change. *Landsc. Ecol.* 28, 583–597.

Oksanen, J., Blanchet, F. G., Kindt, R., Legendre, P., Minchin, P. R., O'hara, R. B., et al. (2013). *Package 'Vegan'. Community Ecology Package, Version*, Vol. 2. 1–295.

Peterson, B. G., Carl, P., Boudt, K., Bennett, R., Ulrich, J., Zivot, E., et al. (2014). *Performance Analytics: Econometric tools for Performance and risk Analysis. R package Version*, Vol. 1. 107.

Pruesse, E., Quast, C., Knittel, K., Fuchs, B. M., Ludwig, W., Peplies, J., et al. (2007). SILVA: a comprehensive online resource for quality checked and aligned ribosomal RNA sequence data compatible with ARB. *Nucleic Acids Res.* 35, 7188–7196. doi: 10.1093/nar/gkm864

Quast, C., Pruesse, E., Yilmaz, P., Gerken, J., Schweer, T., Yarza, P., et al. (2013). The SILVA ribosomal RNA gene database project: improved data processing and web-based tools. Opens external link in new windowNucl. *Acids Res.* 41, D590–D596. doi: 10.1093/nar/gks1219

R Core Team (2018). *R: A Language and Environment for Statistical Computing*. Vienna: R Foundation for Statistical Computing.

Ruiz-Jaen, M. C., and Aide, T. M. (2005). Restoration success: how is it being measured? *Restor. Ecol.* 13, 569–577. doi: 10.1111/j.1526-100x.2005.00072.x

Sapkota, Y., and White, J. R. (2020). Carbon offset market methodologies applicable for coastal wetland restoration and conservation in the united states: a review. *Sci. Total Environ.* 701:134497. doi: 10.1016/j.scitotenv.2019.134497

Suding, K. N. (2011). Toward an era of restoration in ecology: successes, failures, and opportunities ahead. *Annu. Rev. Ecol. Evol. Syst.* 42:465. doi: 10.1146/annurev-ecolsys-102710-145115

Sun, X., Song, J. M., Yu, Y., and Sun, L. L. (2014). A rapid method for determing the total organic carbon and total nitrogen in marine sediments with an elemental analyzer. *Mar. Sci.* 38, 14–19.

Urakawa, H., and Bernhard, A. E. (2017). Wetland management using microbial indicators. *Ecol. Eng.* 108, 456–476. doi: 10.1016/j.ecoleng.2017.07.022

Vane, C. H., Kim, A. W., Beriro, D. J., Cave, M. R., Knights, K., Moss-Hayes, V., et al. (2014). Polycyclic aromatic hydrocarbons (PAH) and polychlorinated biphenyls (PCB) in urban soils of Greater London UK. *Appl. Geochem.* 51, 303–314. doi: 10.1016/j.apgeochem.2014.09.013

Wang, Q., Garrity, G. M., Tiedje, J. M., and Cole, J. R. (2007). Naive bayesian classifier for rapid assignment of rRNA sequences into the new bacterial taxonomy. *Appl. Environ. Microbiol.* 73, 5261–5267. doi: 10.1128/AEM.00062-07

Wang, Y., Shi, J., Wang, H., Lin, Q., Chen, X., and Chen, Y. (2007). The influence of soil heavy metals pollution on soil microbial biomass, enzyme activity, and community composition near a copper smelter. *Ecotoxicol. Environ. Saf.* 67, 75–81. doi: 10.1016/j.ecoenv.2006.03.007

Ward, R. D. (2020). Carbon sequestration and storage in Norwegian Arctic coastal wetlands: impacts of climate change. *Sci. Total Environ.* 748:141343. doi: 10.1016/j.scitotenv.2020.141343

Williams, P., and Faber, P. (2001). Salt marsh restoration experience in San Francisco Bay. *J. Coast. Res.* 27, 203–211.

Wortley, L., Hero, J. M., and Howes, M. (2013). Evaluating ecological restoration success: a review of the literature. *Restor. Ecol.* 21, 537–543. doi: 10.1111/rec.12028

Yu, Y., Wang, H., Liu, J., Wang, Q., Shen, T., Guo, W., et al. (2012). Shifts in microbial community function and structure along the successional gradient of coastal wetlands in Yellow River Estuary. *Eur. J. Soil Biol.* 49, 12–21. doi: 10.1016/j.ejsobi.2011.08.006

Zhang, S., Bai, J., Wang, W., Huang, L., Zhang, G., and Wang, D. (2018). Heavy metal contents and transfer capacities of phragmites australis and suaeda salsa in the yellow river Delta China. *Phys. Chem. Earth.* 104, 3–8. doi: 10.1016/j.pce.2018.02.011

Zhang, Y. R., Wang, R. Q., Kaplan, D., and Liu, J. (2015). Which components of plant diversity are most correlated with ecosystem properties? A case study in a restored wetland in northern China. *Ecol. Indic.* 49, 228–236. doi: 10.1016/j.ecolind.2014.10.001

Zhao, Q., Bai, J., Huang, L., Gu, B., Lu, Q., and Gao, Z. (2016). A review of methodologies and success indicators for coastal wetland restoration. *Ecol. Indic.* 60, 442–452. doi: 10.1016/j.ecolind.2015.07.003

Zou, Y., Liu, J., Yang, X., Zhang, M., Tang, C., and Wang, T. (2014). Impact of coastal wetland restoration strategies in the chongming dongtan wetlands, China: waterbird community composition as an indicator. *Acta Zool. Hung.* 60, 185–198.

Conflict of Interest: The authors declare that the research was conducted in the absence of any commercial or financial relationships that could be construed as a potential conflict of interest.

Publisher's Note: All claims expressed in this article are solely those of the authors and do not necessarily represent those of their affiliated organizations, or those of the publisher, the editors and the reviewers. Any product that may be evaluated in this article, or claim that may be made by its manufacturer, is not guaranteed or endorsed by the publisher.

Advantages of publishing in Frontiers

OPEN ACCESS
Articles are free to read for greatest visibility and readership

FAST PUBLICATION
Around 90 days from submission to decision

HIGH QUALITY PEER-REVIEW
Rigorous, collaborative, and constructive peer-review

TRANSPARENT PEER-REVIEW
Editors and reviewers acknowledged by name on published articles

Frontiers
Avenue du Tribunal-Fédéral 34
1005 Lausanne | Switzerland

Visit us: www.frontiersin.org
Contact us: frontiersin.org/about/contact

REPRODUCIBILITY OF RESEARCH
Support open data and methods to enhance research reproducibility

DIGITAL PUBLISHING
Articles designed for optimal readership across devices

FOLLOW US
@frontiersin

IMPACT METRICS
Advanced article metrics track visibility across digital media

EXTENSIVE PROMOTION
Marketing and promotion of impactful research

LOOP RESEARCH NETWORK
Our network increases your article's readership